Desulfurization and Denitrogenation of Liquid Fuels: Oxidation and Adsorption Technologies

Ph.D. Thesis

PRERANA SIKARWAR
ID No. 2015RCH9503

DEPARTMENT OF CHEMICAL ENGINEERING
MALAVIYA NATIONAL INSTITUTE OF TECHNOLOGY JAIPUR
AUGUST, 2019

Desulfurization and Denitrogenation of Liquid Fuels: Oxidation and Adsorption Technologies

Submitted in

fulfillment of the requirements for the degree of

Doctor of Philosophy

by

PRERANA SIKARWAR
ID: 2015RCH9503

Under the Supervision of

Dr. V. SUBBARAMAIAH
Assistant Professor

DEPARTMENT OF CHEMICAL ENGINEERING
MALAVIYA NATIONAL INSTITUTE OF TECHNOLOGY JAIPUR
AUGUST, 2019

DECLARATION

I, **Prerana Sikarwar**, declare that this thesis titled, "**Desulfurization and Denitrogenation of Liquid Fuels: Oxidation and Adsorption Technologies**" and the work presented in it, are my own. I confirm that:

- This work was done wholly or mainly while in candidature for a research degree at this university.
- Where any part of this thesis has previously been submitted for a degree or any other qualification at this university or any other institution, this has been clearly stated.
- Where I have consulted the published work of others, this is always clearly attributed.
- Where I have quoted form the work of others, the source is always given. With the exception of such quotations, this is entirely my own work.
- I have acknowledged all main sources of help.
- Where the thesis is based on work done by myself, jointly with others, I have made clear exactly what was done by others and what I have contributed myself.

Date:

Prerana Sikarwar
(2015RCH9503)

CERTIFICATE

This is to certify that the thesis entitled "**Desulfurization and Denitrogenation of Liquid Fuels: Oxidation and Adsorption Technologies**" being submitted by **Prerana Sikarwar (**2015RCH9503**)** is a bonafide research work carried out under my supervision and guidance in fulfillment of the requirement for the award of the degree of **Doctor of Philosophy** in the Department of **Chemical Engineering**, Malaviya National Institute of Technology, Jaipur, India. The matter embodied in this thesis is original and has not been submitted to any other University or Institute for the award of any other degree.

Place: Jaipur
Date:

Dr. V. Subbaramaiah
Assistant Professor
Supervisor
Department of Chemical Engineering
MNIT, Jaipur

ACKNOWLEDGEMENT

My research journey has been fascinating as well as challenging at times but I was fortunate enough to have brightest of minds & souls around me throughout this period and without their technical and emotional aid, the completion of this mammoth assignment has not been achievable. I would like to take advantage of this opportunity to acknowledge and extend my huge appreciation to everyone, who so generously contributed to the study presented in this thesis.

At the outset, I bow to the almighty GOD for giving me strength, audacity, motivation, enthusiasm and displaying the right path to accomplish this research work. Equally, I express my earnest and cordial gratitude to the person who made this happen, my supervisor, my mentor, Dr V. Subbaramaiah, Assistant Professor Department of Chemical Engineering, MNIT, Jaipur (Raj.). He has been a living role model; brightest of mind I ever came across; extremely hard working and it's his hungriness and determination towards perfection, which has encouraged me to advance for excellence and nothing less. Over the past three and half year he was right there all the time, advising, reassuring & inspiring every bit of me to overcome from daily hurdles and to progressively achieve my objectives. His expertise, invaluable observations and healthy criticism educated me to do experiments with utmost perfection, investigate in depth and to keep the research on the right track. It's an honour working with him and I feel blessed to have the opportunity to be a part of his Laboratory. Thank You SIR!

I owe my most sincere thanks to Dr. U.K. Arun for his constant motivation and providing necessary laboratory facilities during my doctoral research endeavor. My special word of thanks also goes to Dr. Vijayalakshmi Gosu for being with me as a family member throughout. Her scientific inputs, invaluable guidance and emotional support have always kept me going ahead. I am grateful to the members of Department Research Evaluation Committee: Dr. Prabhat Pandit, Dr. U.K. Arun, & Dr. Abbas Raja Naziruddin for their detailed critique, valuable suggestions and insightful comments during my research journey.

I also sincerely express my gratitude to Prof. Udaykumar R Yaragatti, Director, MNIT, Jaipur for making all the facilities available for charring out my doctoral

research. My sincere gratitude goes to Dr. Kailash Singh (HOD) and other faculties of Chemical Engineering department, MNIT, Jaipur for their unstinted support and innumerable help during the course of entire study. I would also like to thank technical staff, Mr. Uttam Singh & S. N. Reddy for their technical support and administrative staff for helping me with their respective roles.

My acknowledgement will never be complete without the special mention of my lab mates Sudanshu Singh, Shivali Arora, Rohitash Kumar and Archana Dhakad for always being there for any personal and professional help, sharing their resources, keeping a healthy atmosphere and most importantly bearing me during ups and downs of my fascinating journey of this research work.

Now, I would like to acknowledge the people who mean world to me, MY FAMILY. I would like to dedicate this thesis to my parents, Mr. R.S. Sikarwar, Mrs. Saroj Sikarwar and my in-laws, Dr. V.S. Sengar, Mrs. Keshar Sengar for their unconditional love and support throughout my life and during this study. I owe special thanks to my sisters, Anjana Tomar & Shivani Sikarwar, my brother, Himanshu S Sikarwar, my brother in law, Gaurav Tomar and my sister in laws, Nisha Sengar & Dr. Neelam Sikarwar for their constant encouragement, supporting me spiritually and giving me the strength to work through all these years.

Last, but not the least, I am greatly indebted to my soul mate, my husband, Ashish Singh Sengar. Thank you for standing behind me all the time, showing faith in me and offering me the liberty to choose what I desired.

Prerana Sikarwar

ABSTRACT

Ultra-deep desulfurization and denitrogenation of liquid fuels has recently gained considerable attention owing to the strict environmental rules and regulations. The demand for ultralow- level sulfur and nitrogen fuels has increased globally in the past years and will continue to increase in the upcoming years, and that might put immense pressure on refineries. Currently, hydrotreating is industrially employed to reduce the concentration of sulfur & nitrogen compounds in transportation fuels. This process requires severe operating conditions along with large amount of hydrogen and catalyst. Further, this process is not efficient enough to remove organosulfur sulfur and heterocyclic nitrogen compounds from liquid fuels. To remove these compounds approximately 4 times more active catalyst is required than conventional along with more severe operating conditions. Implementation of these conditions will lead to the dramatic rise in capital and operational cost along with the loss of octane number due to the undesired saturation of aromatic compounds present in the fuel. In order to overcome these drawbacks, two alternative technologies (oxidation and adsorption) have been explored in the present work to reduce refractory sulfur and nitrogen compounds from transportation fuels.

In the oxidation process, catalyst plays a very crucial role since it is responsible for the activation of oxidant. Mesoporous supported catalyst, especially MCM-41 has gained considerable attention in recent years owing to its huge surface area, ordered structure, and uniform pore size. Researchers have employed various silica precursors such as n-alkyl amines, aerosol, n-alkoxysilanes, TEOS and water glass for the preparation of MCM-41. Nevertheless, the synthesis of MCM-41 by using the above precursors suffered a major drawback due to its high production cost. Therefore, in the present work, an alternate silica source from coal fly ash (CFA) was utilized for the synthesis of MCM-41. In the present work, two mesoporous silica catalysts (Mo/MCM-41 & ExtMCM-41) derived from CFA were employed for the reduction of sulfur and nitrogen content in liquid fuels. For the synthesis of Mo/MCM-41, firstly catalytic support material (MCM-41) was synthesized from CFA, and then molybdenum species were incorporated into the framework of it by using wet impregnation technique. Characterization results revealed that MCM-41 was

successfully synthesized from CFA, and Mo species were dispersed well on the MCM-41 framework. As synthesized Mo/MCM-41 was tested for the batch oxidative desulfurization (ODS) of dibenzothiophene (DBT) containing model oil, and approximately 94 % removal of DBT was achieved under optimum operating conditions (DBT concentration = 600 mg/L, temperature = 363 K, catalyst dose = 6 g/L, time = 3 h). The oxidative reaction of DBT follows the pseudo-first-order reaction kinetics. The effect of nitrogen compounds on ODS of DBT containing model oil was also studied under optimized conditions achieved from the ODS process. In order to improve the performance of mesoporous silica, solvent extraction route was explored rather than conventional calcination method. X-Ray Diffraction (XRD) results showed that ExtMCM-41 exhibited highly ordered hexagonal mesoporous structure, and possesses high surface area (691 m^2/g) as compared to MCM-41(606 m^2/g). ExtMCM-41 exhibits significantly higher catalytic activity than Mo/MCM-41. At optimum conditions (Dibenzithiophene (DBT) concentration = 1000 mg/L, temperature = 363 K, catalyst dose = 0.75 g/L, time = 3 h), approximately 93 % of DBT removal was achieved. The optimized ODS system was able to remove neutral as well as basic nitrogen compound from model oil. The effect of nitrogen compounds on ODS was also studied, and it was found that presence of nitrogen compounds inhibited the ODS process. Reusability study of spent catalyst was also studied, and it showed stable performance upto four cycles. The ODS results proved that both Mo/MCM-41 and ExtMCM-41 could be the potential catalysts for reduction of the refractory sulfur compounds from liquid fuels. The explored catalytic systems were also able to remove nitrogen compounds from liquid fuels.

In the present work, the adsorption process was also investigated to remove refractory sulfur and nitrogen compounds from liquid fuel. The major challenge associated with the adsorption process is to develop adsorbent that can specifically adsorb sulfur compounds from the fuel, easily available, and possesses significant adsorption capacity. Activated carbon-based adsorbents have gained much attention owing to their high specific area and their controllable functional groups on their surface. However, mere activated carbon performance is not that satisfactory due to limiting adsorption capacity, which may hinder the industrial application. Therefore, in the present work, modification of granular activated carbon (GAC) was carried out to enhance its adsorption capacity. GAC was firstly treated with an organic acid (rather

than conventionally used inorganic acid) to increase its pore volume and surface area and then modified with metal species (cobalt/molybdenum) to enhance the adsorption of sulfur and nitrogen compounds from model oil. The synthesized adsorbents were characterized by using Fourier transform infrared spectroscopy (FTIR), Scanning electron microscope (SEM), XRD, X-ray photoelectron spectroscopy (XPS), and Brunauer–Emmett–Teller (BET). Cobalt loaded acid treated GAC and molybdenum loaded acid treated GAC was employed for the batch adsorptive desulfurization (ADS) of model oil and batch adsorptive denitrogenation (ADN) of model oil. For the ADS of model oil 1 wt % Co/ATGAC and 1 wt % Mo/ATGAC were found as optimum adsorbents whereas for the ADN of model oil 2 wt % Co/ATGAC and 1 wt % Mo/ATGAC were found to be optimum. Adsorption isotherms and kinetic models were investigated to better understand the mechanism of the adsorption process. Thermodynamic parameters were also assessed to determine the feasibility and nature of the adsorption process. Regeneration ability of spent adsorbents was also tested. The operating parameters for simultaneous removal of DBT and indole were optimized with the aid of central composite design. For Co/ATGAC, the maximum removal of DBT and indole was achieved at a temperature of 30 °C, a dosage of 19 g/L, with an initial concentration of 223 mg/L, and with an initial concentration of indole 50 mg/L. For Mo/ATGAC, maximum removal of DBT and indole was achieved at a temperature of 25.5 °C, a dosage of 32 g/L, 186 mg/L DBT concentration and 50 mg/L indole concentration. The results obtained from adsorption studies showed that synthesized adsorbents can be successfully employed for the reduction of sulfur and nitrogen content of liquid fuel.

TABLE OF CONTENTS

LIST OF FIGURES

LIST OF TABLES

NOMENCLATURE

List of Abbreviations

AC	Activated carbon
ADN	Adsorptive denitrogenation
ADS	Adsorptive desulfurization
ATGAC	Acetic acid treated granular activated carbon
BDN	Biodenitrogenation
BDS	Biodesulfurization
BET	Brunauer, Emmett and Teller
BR	Batch reactor
BT	Benzothiophene
CCD	Central composite design
CFA	Coal fly ash
CFFBR	Continuous-flow fixed-bed reactor
CHP	Cumene hydroperoxide
Co/ATGAC	Cobalt impregnated acetic acid treated GAC
CTAB	Cetyl trimethyl ammonium bromide
CYHPO	Cyclohexanone peroxide
DBT	Dibenzothiophene
DESs	Deep eutectic solvents
DMDBT	4,6-dimethyl dibenzothiophene
EDN	Extractive denitrogenation
EDS	Extractive desulfurization
FBFR	Fixed bed flow reactor
FBR	Fixed bed reactor
FTIR	Fourier transform infrared spectroscopy
GAC	Granular activated carbon
HDN	Hydrodenitrogenation
HDS	Hydrodesulphurization
ILs	Ionic liquids
MAR	Micro-autoclave reactor

Mo/ATGAC	Molybdenum impregnated acetic acid treated GAC
MOFs	Metal-organic frameworks
ODN	Oxidative denitrogenation
ODS	Oxidative desulfurization
PM	Particulate matter
POM	Polyoxometalate
RSM	Response surface methodology
SBR	Slurry batch reactor
SEM	Scanning electron microscopy
TBHP	tert-Butyl hydroperoxide
TEM	Transmission electron microscopy
Th	Thiophene
USEPA	United States Environmental Protection agency
XPS	X-ray photoelectron spectroscopy
XRD	X-ray powder diffraction

List of mathematical symbols

A_T	Temkin isotherm binding constant
B_T	Temkin constant related to the heat of adsorption
C_e	equilibrium concentration
q_e	adsorption capacity at equilibrium
K_L	Langmuir constant
q_m	Langmuir adsorption capacity
$\Delta G°$	Standard free energy change
$\Delta S°$	Standard entropy change
$\Delta H°$	Standard enthalpy change
q_t	Adsorption capacity at time t
K_R	Redlich-Peterson adsorption isotherm constant.
α_R	Redlich-Peterson adsorption isotherm constants
β	Redlich-Peterson adsorption isotherm constants
k_2	Pseudo second order rate constant
k1	Pseudo first order rate constant
Δx_i	Step change value

x_i	Actual value of independent variable
x_o	Actual value at the center point
X_i	Coded value
R	Universal gas constant
T	Temperature
K_D	Desorption constant
C_{oD}	Initial concentration of DBT in the model oil
C_{eD}	Equilibrium concentration of DBT in the model oil
C_{oI}	Initial concentration of indole in the model oil
C_{eI}	Equilibrium concentration of indole in the model oil.
m	Amount of adsorbent
V	Volume of model oil
K_F	Freundlich constant (adsorption capacity)
1/n	Freundlich constant (intensity)

LIST OF PUBLICATIONS

1) Sikarwar P, Kumar UA, Gosu V, Subbaramaiah V. Catalytic oxidative desulfurization of DBT using green catalyst (Mo/MCM-41) derived from coal fly ash. J Environ Chem Eng 2018; 6: 1736-1744.
2) Sikarwar P, Kumar UA, Gosu V, Subbaramaiah V. Synergetic effect of cobalt-incorporated acid-activated GAC for adsorptive desulfurization of DBT under mild conditions. J Chem Eng Data 2018; 63: 2975-2985.
3) Sikarwar P, Kumar UA, Gosu V, Subbaramaiah V. An overview of conventional and alternative technologies for the production of ultra-low-sulfur fuels. Rev Chem Eng (DOI: https://doi.org/10.1515/revce-2017-0082).

CHAPTER 1 INTRODUCTION

In today's modern world, energy consumption is increasing day by day, and one of the major sources of energy is fossil fuels, which satisfy the requirement of energy demand. Hydrocarbon fuels derived from fossil fuels are indispensable elements of today's progressive world, and also persist for forthcoming decades. These are used for generation of the electricity and driving of vehicles. Further, approximately 95 % of motorized transportation is dependent on fossil fuels (Pawelec, 2011). However, an increase in usage of hydrocarbon fuels due to its wide applications in the transportation sector enhances release of harmful materials such as carbon monoxide, volatile organic compounds, particulate matter, NO_x, and SO_x. Sulfur and nitrogen compounds are the most obnoxious contaminants present in the fuel. The amount of sulfur in crude oil is represented as a percent of sulfur by weight and it generally varies from less than 0.1% to more than 5%. Sulfur compounds present in crude oil can be categorized into two categories, namely aliphatic and aromatic sulfur compounds. Aliphatic organosulfur compounds such as mercaptans, sulfides, and disulfides are usually present in low boiling point fractions. Aromatic organosulfur compounds usually present in fossil fuels are thiophene (Th), benzothiophene (BT), dibenzothiophene (DBT) and their alkylated derivatives. Nitrogen compounds available in liquid fuels can also be categorized into two categories, namely basic and neutral nitrogen compounds. Amount of nitrogen compound present in fuel is very much low when compared with sulfur compounds. Basic nitrogen compound includes 6 membered ring such as quinoline, pyridine, and acridines while neutral nitrogen compounds includes 5-membered ring such as indole, pyrrole, and carbazole.

1.1 Need of desulfurization & denitrogenation

Sulfur and nitrogen compounds are the main contaminants present in transportation fuels such as gasoline, diesel and jet fuel. The combustion of these compounds releases toxic gases into the atmosphere (Palomino et al., 2014), which causes both environmental pollution and serious health hazards. During combustion, sulfur and nitrogen compounds

are converted into oxides, and thereby transform to acid rain, and other airborne particulates which are detrimental to the environment and manmade structures (Bhutto et al., 2016). Moreover, a higher level of sulfur and nitrogen content in fuels is responsible for corrosion of the combustion engine and deactivation of the catalyst present in the catalytic converter, which is responsible for reducing emissions of CO, NO_x, and thus affecting the overall performance of engine (Dasgupta et al., 2013; Campos-Martin et al., 2010). It has been also found from several studies that the quantity of sulfur compounds in diesel is directly proportional to the particulate matter (PM) emissions (Ristovski et al., 2006). PM emissions from a diesel engine can cause adverse effects on human health owing to their potential of penetrating deeply into the human lungs, causes various respiratory problems, and also it is known to be carcinogenic (Stanislaus et al., 2010). In addition, sulfur and nitrogen compounds tend to deactivate the catalysts used in various refinery operations (Gary and Handwerk, 2001). Consequently, it is mandatory to remove these hazardous compounds before exposing the fuel or its combustion. Due to the harmful effect of sulfur and nitrogen compounds on the human health and environment, strict legislation has been enforced worldwide to reduce the content of sulfur in the liquid fuel.

Production of ultra-low level transportation fuels by reducing the sulfur content in diesel, gasoline, and jet fuel has gained more attention in recent years owing to the stringent legal requirements as well as the intense demand for liquid hydrocarbon fuels with less than 1ppmw sulfur content for their application as a fuel in fuel cells (Sentorun-Shalaby et al., 2011). A fuel cell is a device, which converts hydrocarbons into electricity without any emission of pollutants, and it will be a potential alternative for the purpose of on-board electricity supply in aircraft, transport vehicles and ships (Aicher et al., 2006). The current flexible infrastructure of hydrocarbons storage, transportation, and their special features such as high energy density and readily availability made them a promising candidate for their usage as a fuel in fuel cells (Hernández-Maldonado and Yang, 2004a). The application of fuel cell-based auxiliary power units in navigation and aircraft can decrease the emissions when the airplanes are on the ground, and ships are on the port as driving engine is not in operating mode (Wang et al., 2012). However, hydrocarbon fuels such as natural gas, naphtha, methane etc. contain the sulfur compounds, which are very

harmful to the catalysts used in the fuel cell system, and also tend to deactivate the electrode in fuel cell stack (Ma et al., 2002). Therefore, the amount of sulfur in fuel should be very less (< 0.1 ppm) in order to protect the electrodes and catalyst of the fuel cell system from deactivation (Petzold et al., 2012).

1.2 Environmental standards

Due to the harmful effect of sulfur and nitrogen compounds on the human health and environment, strict legislation has been enforced worldwide to reduce the content of sulfur and nitrogen in the liquid fuel. As per the World Health Organization, the annual emission of NO_2 in the air should not be more than 40 $\mu g/m^3$ (Ahmed and Jhung, 2016). Table 1.1 depicts the upper limit of sulfur content in various countries due to stringent legislations. In Europe, Germany imposed a limit of 10 ppm on sulfur content since 2001 (Babich and Moulijn, 2003). In 2006, The United States Environmental Protection Agency (USEPA) has decreased the amount of sulfur in gasoline and diesel from 300 to 30 parts per million by weight (ppmw) and 500 to 15 ppmw respectively (Ma et al., 2002). In India, BS IV is implemented since April 2010 in 13 major cities, according to which sulfur content in diesel and petrol has been reduced from 350 to 50 ppm and 150 ppm to 50 ppm respectively, since then it has been expanded to 26 more cities. In the rest of the nation, BS III is implemented from September 2011 (Ministry of Petroleum and Natural gas, 2014).

1.3 Removal technologies

Stringent environmental rules & regulations, as well as the application of cleaner fuels in refinery operations and fuel cells, are putting immense pressure on refineries to produce fuels of lower sulfur and nitrogen content (Sarda et al., 2012). The following section briefly discusses all the existing technologies for the removal of sulfur and nitrogen compounds in liquid fuels. A comprehensive literature review on all available technologies is presented in the next chapter (Literature review).

Currently, conventional technology, hydrodesulfurization (HDS) and hydrodenitrogenation (HDN) are used for the removal of sulfur and nitrogen compounds from transportation fuels. In this process, sulfur and nitrogen compounds present in crude

oil and refinery streams convert into hydrogen sulfide, ammonia, and corresponding hydrocarbons at higher temperatures and partial pressure of hydrogen in presence of the catalyst (Srivastava, 2012). In refineries, both HDS and HDN takes place simultaneously, and the process is known as catalytic hydrotreating. This process requires high temperature (300–400 °C), high pressure (3-6 MPa) and a large amount of hydrogen in the presence of the catalyst (Sentorun-Shalaby et al. 2011). Further, more than 30 bar pressure is required for the production of light oil such as jet fuel or diesel (Song and Ma, 2003). Hence, both HDS and HDN are an expensive choice for desulfurization and denitrogenation of liquid fuels. Further, these techniques are not efficient enough to remove aromatic sulfur and nitrogen compounds from liquid fuels.

To overcome the drawbacks of HDS and HDN, various alternative technologies have been explored in recent years. These techniques include biodesulfurization (BDS) and bio-denitrogenation (BDN), extractive desulfurization (EDS) and denitrogenation (EDN), adsorptive desulfurization (ADS) and denitrogenation (ADN) oxidative desulfurization (ODS) and denitrogenation (ODN), In the BDS and BDN process, sulfur and nitrogen contaminants are removed with the aid of microorganisms at moderate temperature and pressure. In this process, microorganisms use sulfur and nitrogen compounds as a significant element for their physiological activities, and as a growth factor (Boniek et al., 2014). BDS is not commercialized yet; therefore most of the recent work is focused on the development of effective biocatalyst for treating the large volume of liquid fuels. In extractive desulfurization and denitrogenation process, sulfur and nitrogen compounds are specifically extracted from the fuel with the help of a solvent. Previously, researchers have focused on EDS/EDN with organic solvents. Nowadays, a new class of solvents including ionic liquids and deep eutectic solvents has been investigated for the efficient extractive process. In ADS and ADN process, sulfur and nitrogen compounds are specifically adsorbed on the adsorbent, both surface area and the functional group present on the surface of adsorbent plays a significant role in the adsorption of sulfur and nitrogen molecules (Ruthven, 1984). Therefore, it is considered as an economical alternative for the deep desulfurization of fuels owing to its simplicity in operation and mild operating conditions. Most of the research work in last two decades is dedicated on the development of adsorbents which exhibit high surface area, high selectivity, and easy to

regenerate. In ODS and ODN technique, organosulfur and nitrogen compounds are oxidized to their corresponding sulfoxides, sulfones, and nitrogen oxides and thereby removal of these compounds with the aid of extraction, adsorption or distillation (Fraile et al., 2016). In recent years, enormous research has been carried out on the usage of both oil soluble and insoluble oxidants and to the synthesized highly active catalyst for the oxidation process.

Among all the alternative technologies, oxidative and adsorptive processes for removal of sulfur and nitrogen compounds have gained immense attraction of researchers worldwide. These processes have the advantage of employing mild operating conditions i.e. low temperature and atmospheric pressure. Moreover, both oxidative and adsorptive processes are effective to remove aromatic sulfur and nitrogen compounds which are difficult to remove by HDS and HDN process. Both processes involve low operating and capital cost as compared to the conventional process. However, there are some limitations which are faced by both technologies. Adsorption faces two major challenges; the first challenge is to develop low-cost adsorbent with a large surface area and porosity. The second hurdle is to find adsorbents that selectively adsorb the sulfur and nitrogen compounds, which are mainly aromatic compounds that have not been removed in the hydrotreating process in refinery over the other aromatic and olefin compounds present in hydrocarbon fuel. Another limitation is the regeneration of adsorbent. Adsorbents are often difficult to regenerate, and adsorption capacity diminished severely after the regeneration process. ODS/ODN also exhibited some limitations such as oxidation of compounds present in fuel other than sulfur and nitrogen, and post-treatment of oxidized compounds. Many researchers have used hydrogen peroxide as an oxidant in the process since it is cheap and readily available. But hydrogen peroxide is immiscible with oil, which forms a biphasic system, and causes mass transfer limitation between oil and oxidant, and gives water as a byproduct which degrades the quality of the oil.

1.3.1 Role of mesoporous catalyst in oxidation process

In the oxidation process, catalyst plays a very important role as it is responsible for the activation of oxidant. Both homogeneous and heterogeneous catalysts have been used in the oxidation process (Ali et al., 2009; Green et al., 2007). Heterogeneous catalyst,

particularly the supported catalysts have received more attention as compared to homogenous catalyst due to difficulty in its separation from the reaction media. Therefore, a high surface area support material is needed for the dispersion of active metal on it. Support plays a significant role in enhancing the catalyst's activity, selectivity, stability, and also aids in its segregation from the organic phase. Mesoporous supported catalyst, especially MCM-41 for oxidation has gained considerable attention in recent years owing to its huge surface area, ordered structure, and uniform pore size (Wang et al., 2004; Zhou et al., 2015). Researchers have employed various silica precursors such as n-alkyl amines, aerosol, n-alkoxysilanes, TEOS and a water glass for the preparation of MCM-41. Nevertheless, the synthesis of MCM-41 by using the above precursors suffered a major drawback due to its high production cost. In order to make the process economic, cheap silica source should be used for the synthesis of MCM-41. In the present work, the alternate silica source derived from coal fly ash (CFA) was used for the synthesis of MCM-41. CFA contains a large amount of silica and alumina in it, and this silica can be utilized as a silica precursor for the synthesis of MCM-41. CFA is a by-product of coal combustion in the thermal power station and rich in silica content. In India, a huge quantity of fly ash produced every year (176 million tons of fly ash generated in 2015-16), only 50 to 60% of it has been utilized for various application and its disposal management is one of the major concern owing to its potential to pollute water and air (Sikarwar et al., 2018b). The major constituents of CFA are silica, alumina, and iron oxides with a small content of CaO, MgO, SO_3, and unburnt carbon. The use of CFA as a silica source for the synthesis of MCM-41 will not only make the oxidation process economic but also aids in disposal management of CFA.

1.3.2 Role of granular activated carbon in adsorption process

Activated carbon has been widely used in adsorption process due to its high surface area, good porosity, and easy functionalization with different types of functional groups. Adsorption capacities of activated carbon are directly connected to the surface area and functional group. The adsorptive phenomenon depends on textural as well as on surface properties of activated carbon (Triantafyllidis and Deliyanni, 2014). However, mere activated carbon performance is not that satisfactory in adsorption process due to its

limited adsorption capacity which may hinder its industrial application (Shi et al., 2014). In order to improve its capacity, various modifications of activated carbon have been done by researchers. It has been found from the literature data that the treatment of activated carbon with acid or base can improve the adsorption capacity of activated carbon, and the acid treated activated carbon shows more adsorption capacity as compared to base treated activated carbon and virgin activated carbon (Jung and Jhung, 2015). In addition, modification of activated carbon with metal species and metal oxides have been also studied in order to enhance the adsorption capacity of activated carbon (Thaligari et al., 2015; Saleh et al., 2017).

1.4 Thesis organization

In order to better understand the present research work, the whole thesis is divided into five chapters, and the highlights of these chapters are shown below.

Chapter 1: This chapter gives an introduction to the origin of the problem and its need. It also includes the objectives of the present work along with the outline of the research work conducted.

Chapter 2: This chapter provides a comprehensive review of all the technologies available for the reduction of sulfur and nitrogen content in liquid fuels along with their advantages and limitations. This chapter also covers the identified research gaps on the basis of literature review.

Chapter 3: This chapter gives valuable information about all the chemicals, materials, and solutions employed in the present study. It also provides aluable insight into the methodology adopted to carry out the research work.

Chapter 4: This chapter demonstrates the results of characterization studies of a synthesized catalyst and adsorbent. It includes the results of the application of synthesized catalyst and adsorbent for the removal of sulfur and nitrogen compounds in model oil in batch mode via oxidation and adsorption technologies.

Chapter 5: This chapter provides an overview of the research work conducted along with recommendations for future work.

1.5 Objectives of research

Desulfurization and denitrogenation of liquid fuels is a major concern of researchers worldwide owing to its harmful effect on the environment and stringent environmental rules and regulations. The conventional technique for the removal of these compounds is not efficient enough to reduce organosulfur and heterocyclic nitrogen compounds from liquid fuels. Consequently, various alternative techniques have been explored in recent years. Among them, oxidation and adsorption have gained immense attention of researchers globally since the process occurs under mild operating conditions i.e. low temperature and atmospheric pressure. Catalyst and adsorbents play a very crucial role in oxidation process and adsorption process, respectively. The present research work focuses on the synthesis of catalysts and adsorbents which can effectively remove refractory sulfur and nitrogen compounds from liquid fuels. The major objectives of the present work are shown below:

1) To synthesize low cost material (MCM-41 derived from coal fly ash and GAC derived from agricultural waste), for the removal of sulfur and nitrogen compounds from model fuel oil.
2) To perform physico-chemical characterization of synthesized catalysts/adsorbents (Mo/MCM-41, ExtMCM-41, Co/ATGAC and Mo/ATGAC) by N_2 adsorption-desorption, Fourier transform infrared spectroscopy (FTIR), X-ray diffraction (XRD), high resolution transmission electron microscopy (HR-TEM), X-ray photo electron spectroscopy (XPS), and field emission scanning electron microscopy (FE-SEM) techniques.
3) To evaluate the catalytic activity of Mo/MCM-41 & ExtMCM-41 for desulfurization and denitrogenation using batch oxidative technique.
4) To evaluate the performance of synthesized adsorbents (Co/ATGAC and Mo/ATGAC) for desulfurization and denitrogenation using the batch adsorptive technique.
5) To evaluate the reusability of the spent adsorbent/catalyst using solvent regeneration technique.

Table 1.1 Current sulfur specification for diesel and gasoline in some countries and their year of implementation (Sikarwar et al., 2018a)

Country	2005	2007	2008	2009	2010	2011	2012	2013	2014	2015	2016	2017
US[a]		30 ppm										
US[b]		15 ppm										
EU[a]				10 ppm								
EU[b]				10 ppm								
Japan[a]			10 ppm									
Japan[b]			10 ppm									
Australia[a]				10 ppm								
Australia[b]				10 ppm								
China[a]								10 ppm				
China[b]									10 ppm			
Korea[a], Republic of				10 ppm								
Korea[b] , Republic of				10 ppm								
India[a] (selected cities)					50 ppm							
India[a] (rest of the nation)						150 ppm						
India[b] (selected cities)					350 ppm							
India[b] (rest of the nation)						50 ppm						
Brazil[a]									500 ppm			
Brazil[b]									50 ppm			
Singapore[a]								50 ppm				
Singapore[b]								10 ppm				
Thailand[a]							50 ppm					
Thailand[b]							50 ppm					

[a] Sulfur content in gasoline
[b] Sulfur content in diesel

CHAPTER 2 LITERATURE REVIEW

Environmental concerns have given a great deal of attention for the production of ultra-low sulfur and nitrogen fuels. This chapter provides a review on various technologies available for the removal of sulfur and nitrogen compounds in liquid fuels. The comprehensive information on the basic principle, reaction mechanism, workability, advantages, and disadvantages of conventional and alternative technologies is included in this chapter. The objective of this chapter is to provide valuable insight into the recent advances made in conventional processes and alternative techniques. The following sections contained detailed information on available technologies for the reduction of sulfur and nitrogen content in liquid fuels.

2.1 Hydrodesulfurization (HDS) and Hydrodentitrogenation (HDN)

HDS and HDN are used in refineries to convert sulfur and nitrogen compounds present in crude oil and refinery streams into hydrogen sulfide, ammonia and corresponding hydrocarbons at higher temperatures and partial pressure of hydrogen in the presence of the catalyst (Srivastava, 2012). These two processes occur simultaneously in the refineries, and the process is known as catalytic hydrotreating. Desulfurization is the prime concern of researchers because the amount of sulfur present in crude oil is very high as compared to the nitrogen. In addition, enforcement of stringent environmental rules is putting immense pressure on refiners to produce fuel with sulfur content less than 10 ppm. However, the reduction of sulfur content to such a low level is dependent on the type and amount of nitrogen compounds present in liquid fuel (Rabarihoela-Rakotovao et al., 2004). Further, the conventional hydrotreating process is not effective in removing organosulfur and hetrocycle nitrogen compounds from liquid fuels.

2.1.1 Catalyst used in hydrotreating process

Production of ultraclean fuels with desired sulfur and nitrogen content mainly depends either on the severity of the operating conditions or the type of catalyst used in the process. In order to get the ultraclean fuel, it is very necessary to enhance the catalytic

properties of catalyst used in hydrotreating process. HDS technique has a high activation barrier for the hydrogenolysis of the C-S bond, and this barrier can be reduced by employing higher reaction temperature (>275 °C), higher-pressure (>30 bars) and a potent catalyst (Singh et al., 2016).

Typically, hydrotreating catalyst is composed of transition metals with vacant d orbitals such as cobalt ($3d^7$), nickel ($3d^8$), rhodium ($4d^8$), palladium ($4d^{10}$), and platinum ($5d^9$) on various supports and modified with the help of promoters (Petzold et al., 2012). Conventional hydrotreating process employs Co(Ni)Mo supported on alumina or silica as a catalyst. It has been demonstrated in previous studies that Ni containing catalysts are best for the HDN process whereas CoMo catalyst are preferred for HDS over NiMo and NiW catalysts (Furimsky and Massoth, 2005). The conventional catalyst suffers difficulty in removing alkyl-substituted DBTs because interaction between sulfur atom and active site is hindered due to the steric hindrance of alkyl groups (Pawelec et al., 2008). Therefore, these catalysts are not sufficient enough to produce fuels with sulfur content of less than 15 ppm.

Transition metal sulfides exhibit unique properties that are beneficial in hydrotreating process and are found to be the known class of active phases (Wajnert et al., 2008). Generally, catalyst is composed of Mo(W) sulfides supported on alumina and promoted with the aid of Co(Ni) (Guo et al., 2018). Pecoraro and Chianelli (1981) conducted the first organized study on catalytic activity transition metal sulfides for HDS of DBT, and found the relationship between the activity and position of the corresponding metal in the periodic table of elements. The catalytic activity of iridium sulfide phase as an active component and a mixed system of magnesium oxide and magnesium fluoride as a support showed higher catalytic activity in comparison to $CoMo/Al_2O_3$ catalyst (used in industry) for HDS of thiophenes (Wajnert et al., 2008). The synthesis process of the catalyst consists of two steps namely, precipitation and post-sulfidation. The synthesis process results in the formation of catalysts with active sites of low density along with disapproving nanostructure. In addition, sulfidation process leads to the formation of both oxides and sulfides simultaneously in the catalyst. Various research efforts have been made to upgrade this transition metal sulfide catalyst (Guo et al., 2018). It has been

demonstrated in several studies that unsupported transition metal sulfides performed better as a hydrotreating catalyst than supported transition metal sulfides (Yoosuk et al., 2010). Liu et al. (2015) studied on unsupported Ni/Zn/Mo sulfide catalysts for HDS of DBT. In their observation, 9.5Ni0.5Zn10Mo catalyst gave higher HDS activity for DBT as compared to other synthesized nickel – zinc - molybdenum catalysts, and this higher activity may be contributed to the complete sulfidation of Mo species, and effortless reduction of oxide precursors as well as sulfide catalyst. For preparation of unsupported transition metal sulfides, one step synthesis procedure was adopted which involves either the direct sulfidation of active metal salts or the decomposition of thiosalts (Guo et al., 2018).

In 2001, a new generation of commercial bulk catalyst known as NEBULA (New Bulk Activity) was introduced by ExxonMobil, Akzo Nobel and Nippon Ketjen. It is a trimetallic (Mo-W-Ni) unsupported catalyst, and possesses superior HDS activity in comparison with other catalysts available for HDS (Gochi et al., 2005). Nevertheless, these trimetallic catalysts are very costly owing to their high metal content and high consumption of hydrogen (Morales-Ortu˜no et al., 2016). In order to replace expensive bulk catalyst researchers have also explored catalyst with low metal content and better textural properties. Most of the refineries employed catalyst based on BRIM^{TM} hydroprocessing technology developed by Haldor and Topsøe while others used NEBULA (Saleh, 2015).

Nanostructured materials have drawn considerable attention during the last decade owing to their distinctive physical and chemical characteristics and better textural properties. Various types of nanostructure material have been explored for the hydrotreating process. For example, nano-structured titania powder and nanotubes were used as a support material for the HDS of DBT. Titania powder showed two times higher HDS activity than commercially available $CoMo/Al_2O_3$ catalyst (Escobar et al., 2005). Titania nanotubes supported NiW showed better HDS activity in comparison with alumina and titania supported NiW (Palcheva et al., 2013). Few researchers have also investigated combined/ hybrid materials with different properties to use as a support of active phase for hydrotreating. An example, titanium incorporated SBA-15 and alumina were combined

together and used as a support material in order to obtain benefits of both material (Morales-Ortuño and Klimova, 2017). Hybrid catalyst showed higher HDS activity for alkylated DBT in comparison with NiMo/γ-Al_2O_3. Transition metal phosphides are novel class of HDS and HDN catalysts with superior activity. It was reported that among all metal phosphides, nickelphosphide is highly active and showed better HDS activity than commercially available sulfide catalyst (Lee and Oyama, 2017).

Researchers have also studied the influence of catalyst's synthesis procedure on HDS activity, and it has been found that catalyst's synthesis procedure has an immense effect on the catalytic activity. For example, Singh et al. (2016) reported the synthesis of γ-alumina supported NiMo (ultrasmall), NiMo bimetallic metal oxide (nanoclusters) for HDS technique by two different procedures, namely colloidal synthesis and conventional wet impregnation method. They observed that the nanoclusters prepared using colloidal synthesis showed enhanced catalytic activity for HDS of DBT in comparison with the catalyst synthesized using conventional wet impregnation technique. A series of CoMo/γ-Al_2O_3 catalysts were prepared by using various techniques such as equilibrium deposition filtration (EDF), wet impregnation, dry impregnation, successive dry impregnations (Papadopoulou et al., 2003). Among these, catalyst synthesized through EDF method shown higher activity in HDS.

2.1.2 Effects of support

Effects of support have been investigated by many researchers to better understand the importance of support in the dispersion of active components or promoters, and metal-support interaction for altering the catalytic functionalities and stability. Numerous support materials such as Al_2O_3 (Miller and Hineman, 1984; Liu et al., 2007), zeolites (Lee et al., 2007), mesoporous materials (MCM-41 and SBA-15)(Deepa et al., 2012), TiO_2, ZrO_2, SiO_2 (Okamoto et al., 2002), mixed metal oxides (Trejo et al., 2008, Vázquez-Garrido et al., 2019) have been utilized in order to enhance the hydrotreating efficiency.

Many HDS and HDN studies utilized the oxides as a support material, which includes titania, alumina, silica, zirconia. γ - Alumina was used as a support in many HDS studies

due to its chemical, mechanical, and thermal stability (Xia et al., 2003). Alumina with different crystal structures (γ - Alumina, θ - Alumina, δ - Alumina) were also used to study the effect of crystal structure on HDS process (Zhang et al., 2017). δ- Alumina gave highest percentage removal of sulfur compounds. Details of the process conditions can be seen from Table 2.1. This higher removal rate is contributed to the concentrated pore size distribution, adequate interaction between support and active species, and superior sulfidation degree. It can be seen from Table 2.1 that researchers have employed δ-Alumina for HDS of both model oil and FCC diesel. Catalytic activities of the catalyst can be influenced by the morphology as well. For example, use of nanorod γ-alumina can give bimodal mesoporous structure to enhance the HDS activity of CoMo-based catalysts (Liu et al., 2012), and the catalysts supported with lath-like mesostructured γ-alumina provides the good dispersion of active phase, which aids in increasing the conversion of DBT in HDS (Hicks et al., 2003). Surface acidity is also one of the significant properties of support, which affect the dispersion of active phases and adjust the interaction of metal and support (Chen et al., 2013). The active species supported on zeolites and silica-alumina illustrate high acidity and high hydrotreating activity (Ding et al., 2007). Commercial usage of some oxides (titania and zirconia) is expelled because of their unfavorable characteristics such as inappropriate mechanical properties, low surface area, and limited thermal stability. In order to overcome these drawbacks combination of mixed oxides with γ-aluminas were used as supports to take benefit of favorable features of both systems.

Nanostructured molecular sieves such as MCM-41 and MCM-48 were first developed by the scientists of Mobil Oil Corporation. These molecular sieves have attracted the attention of many researchers for use as a support material in HDS owing to their good thermal stability, high surface area, novel morphology, and fascinating texture, uniform pore size, and pore volume (Subbaramaiah et al., 2013). SBA-15 and SBA-16 are mesoporous forms of silica. Table 2.1 shows the HDS performance of both SBA-15 and phosphorous incorporated SBA-16. SBA-15 exhibits higher pore diameter and surface area than the conventional γ-alumina (Mouli et al., 2011). Application of mesoporous silica is limited to some extent owing to the shortage of active sites. This problem can be

overcome by incorporation of Ti and Al in the framework of mesoporous silica. For example, a series of Al containing mesoporous SBA-15 with various Si/Al ratio (50, 30, 20, and 10) was synthesized by employing chemical grafting technique (Klimova et al., 2008). It was observed that catalytic activity was enhanced by incorporating aluminum in the structure of support. Ledesma et al. (2018) modified the SBA-15 with gallium and aluminum and use it as a support material for the dispersion of iridium species. The as-synthesized catalyst was used for the HDN of quinoline, and it was found that HDN activity enhanced significantly owing to the generation of Lewis and Bronsted active sites due to the incorporation of Ga and Al in SBA-15 framework.

2.1.3 Effect of nitrogen compounds on HDS process

Nitrogen compounds act as an inhibitor in HDS process by competing with sulfur compounds to get adsorbed on active sites of catalyst. The extent of inhibition in HDS is influenced by both type and concentration of nitrogen compounds. HDS is not only affected by the presence of non-heterocyclic nitrogenous compounds but severely inhibited by the presence of heterocyclic compounds such as pyridine, quinoline, indole etc. The heterocyclic nitrogen compounds can be divided into two categories, namely basic (quinoline, pyridine), and neutral (carbazole, indole). It was reported in the literature that basic nitrogen compounds strongly inhibited the HDS process as compared to neutral nitrogen compound. For example, Kwak et al. (2001) studied the inhibition effect of nitrogen compounds (quinoline and carbazole) on HDS of DBT and alkylated DBT, and it was reported that quinoline acts as a strong inhibiting agent as compared to carbazole. Farag et al. (2014) also reported that the addition of quinoline strongly inhibited the HDS of DBT in initial stages, and this poisonous effect continued to remain until the concentration of quinoline became very low. The HDS of straight-run diesel fraction over CoMoP/γ-Al_2O_3 catalyst was inhibited even by a trace quantity of nitrogen (García-Gutiérrez et al., 2014).

Table 2.1 HDS and HDN of organosulfur and nitrogen compounds under optimum reaction conditions.

Model oil	Contaminant	Catalyst	C_o (ppm)	Reactor	Temperature (°C)	Pressure (MPa)	% Removal	Reference
Decaline	Quinoline,	MoP-Ti(5)/MCM-41	1000	FBR	300-360	4	-	Duan et al. (2010)
Decalin	DMDBT	Pd/USY	500	FBR	230	5	85	Zhang et al. (2012)
Hexadecane, dodecane	DBT, DMDBT	NiMoW/P-SBA-16	500,300	BR	320	5	79,77	Guzmán et al. (2013)
Hexadecane	DBT, DMDBT	NiMoW/SBA-15	1300,500	BR	300	7.3	88,77	Mendoza-Nieto et al. (2013)
Dodecane +p-xylene+Decane	Carbazole	$Co_{0.1}Ni_{1.9}P/SiO_2$	1000	CFFBR	350	3	98	Bowker et al. (2014)
o-xylene	Carbazole	NiB	100	Micro reactor	350	6	100	Lewandowski et al. (2015)
FCC gasoline, FCC diesel	Th, BT,DBT	NiY/Carbonnanotubes	259,1126	FBR	360	2.5	99,99	Xu et al. (2015)
Hexadecane	DBT	$CoMo/Al_2O_3MgOLi$	2400	SBR	320	5.59	73	Solís-Casados et al. (2016)
Cyclohexane	DBT, DMDBT	NiMo / δ-Al_2O_3	500	CFFBR	340	4	99, 65	Wang et al. (2016)
Dodecane	Quinoline	Ir-Ga-SBA-15	200	BR	300	1.52	95	Ledesma et al. (2018)

2.2 Biodesulfurization (BDS) and Biodenitrogenation (BDN)

BDS and BDN are environmentally friendly technique, where the removal of refractory sulfur and nitrogen compounds takes place by biological activity under mild operating conditions. It is one of the low cost alternatives to HDS and HDN, and offers various advantages over conventional hydrotreating process such as lower operating cost, capital cost, and lesser greenhouse gas emissions (Labana et al., 2005). In nature, various microorganisms are present which are capable of altering organic sulfur and nitrogen molecules for usage of either the sulfur/nitrogen or the carbon skeleton (Le Borgne and Ayala, 2010), and therefore can be used as efficient source to remove organosulfur and hetrocyclic nitrogen compounds from refinery streams. In this method, microogansisms either biotransform sulfur/nitrogen compounds or utilize sulfur/nitrogen containing compounds as a sole source for growing purpose under ambient pressure and tempertaure.

2.2.1 Mechanism of BDS

Generally, the metabolic pathways for BDS of DBT and alkyl substituted DBTs can be classified into two categories, namely ring destructive and sulfur specific. Among them, the sulfur specific pathway has gained more attention.

2.2.1.1 Ring destructive metabolic pathway

Biodesulfurization which employs this metabolic pathway is known as destructive biodesulfurization as sulfur is not specifically detached from the parental organic sulfur molecules. This biocatalytic route constitutes of following major steps hydroxylation, ring cleavage, and hydrolysis (Gupta et al., 2005). The most common pathway for the metabolism of DBT is Kodama Pathway. Several bacterial genera such as *Rhizobium, Pseudomonas* have been reported in the literature which degrades DBT via Kodama metabolic pathway (Hou et al., 2005). This biological pathway hasn't gained much attention due to unwanted breakage of C-C bonds which leads to the decrease in the calorific value of the fuel.

2.2.1.2 Specific oxidative pathway (SOP)

In Specific oxidative metabolic route, carbon skeleton of DBT remains intact which results into no loss of calorific value of the fuel. This metabolic route is also known as 4S pathway, and it involves four consecutive reaction steps,and in the first step DBT is oxidized to DBTO, further converted into $DBTO_2$, thereafter it is transformed into sulfinate, and finally into hydroxybiphenyl (Kilbane, 1989). This metabolic route requires four enzymes for the transformation of DBT into 2-hydroxybiphenyl (Ohshiro and Izumi ,1999). Four enzymes, which includes two monooxygenases (DszC and DszA), one desulphinase (DszB), and one NADH: FMN oxidoreductase (DszD). The conversion of DBT into DBTO and further in to $DBTO_2$ is catalyzed by DszC, and these two steps need $FMNH_2$ and oxygen for activity (Mohebali and Ball, 2016). Finally, the fourth enzyme HPBS desulfinase (DszB, encoded by the dszB), an aromatic sulphinic acid hydrolase, is required to complete the reaction sequence (Gray et al., 2003), base activated water molecule stages a nuclophillic attack on HPBS, which transform it in to the 2-HBP. The consumption rate of HPBS to 2-HBP, which is catalyzed by dszB, is very slow (1/5 times) as compared to its production rate. Hence, the conversion of HPBS to 2-HBP is considered as the slowest step in this metabolic pathway. SOP requires approximately 4 mol of NADH to desulfurize 1 mol of DBT, which make it an energy demanding process (Oldfield et al., 1997). The mechanism of SOP for DBT is shown in Figure 2.1 .

2.2.2 Mechanism of BDN

Carbazole is found to be very difficult to degrade by microbial attack. However, several researchers have described the degradation of carbazole with the aid of few microorganisms. Metabolic degradation of carbazole by most of the microorganisms follows a similar degradation route. The metabolic route is initiated by cleavage of nitrogen compound containing ring to form anthranilic acid followed by its mineralization. The metabolic route for degradation of carbazole and products formed during the degradation was firstly reported by Ouchiyama et al. (1993). It was reported that carbazole was degraded to anthranilate and 2-hydroxypenta- 2,4-dienoate through angular dioxygenation followed by meta-cleavage and hydrolysis. Most of the isolated species transform quinoline in to 2-oxo-1,2-dihydroquinoline, first intermediate product

during the metabolic degradation of quinoline. Afterwards, metabolic route may proceed through two different routes (Kaiser et al., 1996). In the first metabolic route, cleavage of benzene ring takes place whereas in the second route nitrogen compound containing ring cleaved before benzene ring cleavage (Sun et al., 2009). Lin and Jianlong (2010) proposed metabolic route for degradation of quinoline via *Pseudomonas putida*. They proposed that the 2-hydroxy-quinoline was formed as first intermediate product due to the hydroxylation. Subsequently, the obtained intermediate product was oxidized to 2,8-dihydroxyquinoline and 8-hydroxycoumarin.

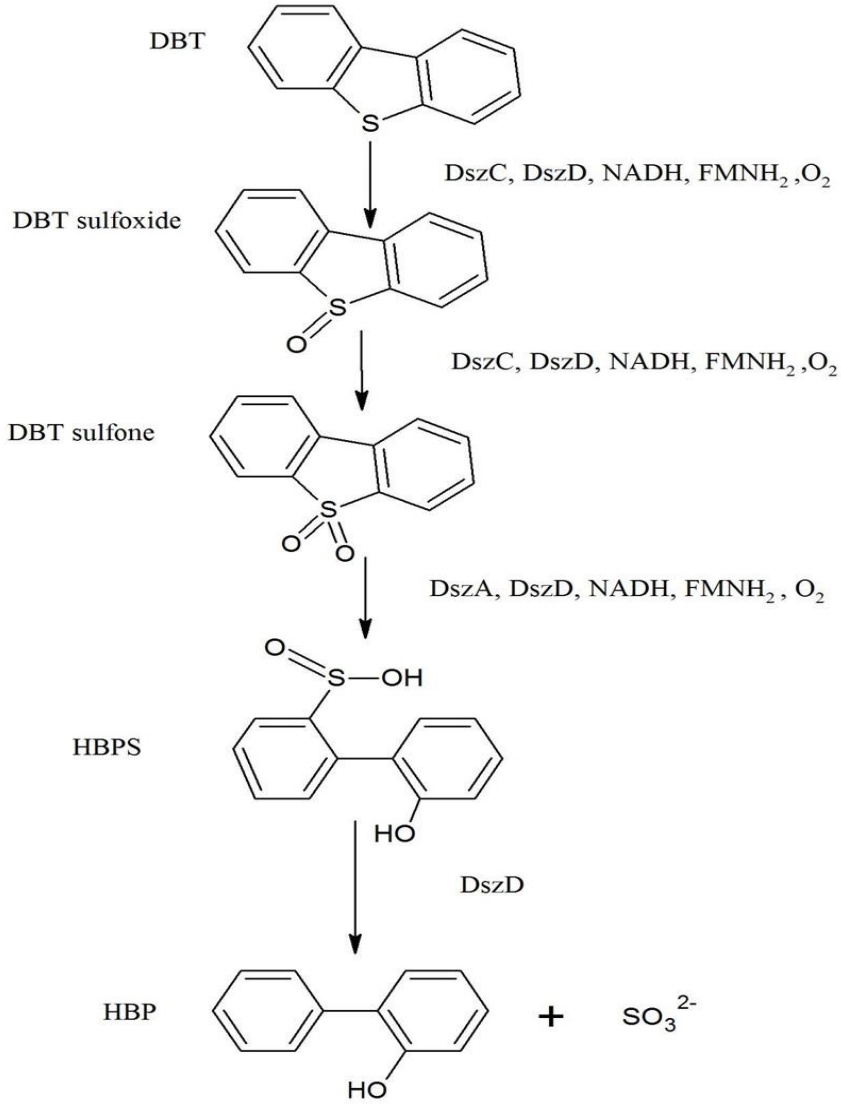

Figure 2.1 The 4S metabolic route for desulfurization of DBT (Alcon et al., 2005)

2.2.3 BDS and BDN at a glance

The BDS and BDN systems constitute of three main components, namely aqueous, oil, and cellular. Further, the cells are dispersed into three regions: cells in aggregates in the aqueous phase, free cells in the aqueous phase, oil – drop - adhered cells (Abin-Fuentes et al., 2013). It is a two-phase system in which the oil phase interacts with whole cell (biocatalyst) in the aqueous phase (Takada et al., 2005). BDS and BDN of liquid fuels is usually accompanied by employing the entire cell as a biocatalyst, which facilitates the industrialization of BDS and BDN (Honda et al., 1998). Various desulfurizing and denitrogenating microorganisms have been used as a biocatalyst in BDS/BDN process such as *Rhodococcus* sp. IGTS8 (Oldfield et al., 1997), *Rhodococcus erythropolis* H-2 (Ohshiro et al., 1996), *Mycobacterium* sp. G3 (Nekodzuka et al., 1997), *Gordonia* sp. CYKS1 (Rhee et al., 1998), *Pseudomonas delafieldii* R-8 (Luo et al., 2003), *Lysinibacillus sphaericus* (Bahuguna et al., 2011), *Burkeholderia picketti* (Jianlong et al., 2002), *Nocardia* sp. (Shukla and Kaul, 1986), *Bacillus* sp. (Uma et al., 2002). However, *Rhodococcus* sp. bacteria have been used widely by the researchers for the BDS process since they utilize 4S metabolic route to degrade DBT. Moreover, *Rhodococcus* sp. possesses hydrophobic properties which help in increasing the contact between the cell and the organosulfur compounds, and eventually increases the sulfur removal (Monticello, 2000). The high desulfurization ability of newly isolated *Rhodococcus* sp. P32C1 was reported by Maghsoudi et al. (2001) for desulfurization of middle distillate fractions like diesel oils and model oil (n-hexadecane) containing DBT. Desulfurization ability of *Rhodococcus* sp. with model oil and real oil system is shown in Table 2.2. Pseudomonas species were employed by the various researchers for the degradation of quinoline, and most of the studies were focused on the degradation pathway and the identification of products formed during the metabolic route. *Pseudomonas* strain, BC001, was utilized to degrade quinoline with removal rate in the range of 96-98 % (Sun et al., 2009). Tuo et al. (2012) isolated *Bacillus* sp. from petroleum-contaminated soil and employed it for the degradation of quinoline. Several researchers have employed both Gram-positive and Gram-negative bacteria for the removal of carbazole. Singh et al. (2013) reported the isolation and characterization of *Pseudomonas* sp., capable of utilizing carbazole. Zhao et al. (2011) isolated a series of carbazole consuming bacteria

from the activated sludge, and identified them as *Pseudomonas* sp. strains (LSSE-H2), all bacterial strains showed excellent denitrogenation efficiency. Li et al. (2008) isolated a *Klebsiella* sp. strain from dye-contaminated soil and utilize it to degrade carbazole. It was reported that combination of LSSE-H2 and *Pseudomonas delafieldii* R-8 strains can remove around 92% of carbazole and 94% of DBT from model fuel.

Conventional HDS process is carried out at elevated temperature, and in order to incorporate microbial desulfurization and denitrogenation in petroleum refining process, it is desirable to perform BDS and BDN at higher temperature with microorganisms which are able to withstand higher temperatures (Campos-Martin et al., 2010). Higher temperature offers various benefits such as decrease in oil viscosity which enables the displacement of molecules easier, enhances enzymic rates, and reduced contamination of bacteria (Gray et al. 2003; Campos-Martin et al., 2010). Few researchers have studied the desulfurization capability of various thermophilic microorganisms such as *Paenibacillus* sp. A11-2, *Klebsiella* sp. and a thermophilic bacterium (Konishii et al., 2000; Torkamani et al., 2008; Bhatia and Sharma 2012). Ishii et al. (2000) firstly studied the desulfurization abilities of isolated *Paenibacillus* sp. A11-2 thermophilic strain. Bhatia and Sharma (2012) reported the isolation of a thermophilic bacterium *Klebsiella* sp. 13T, and tested its desulfurization ability for different petroleum oils. They found that *Klebsiella* sp. 13T was capable of removing 22–53% of sulfur from different petroleum oils, and the highest sulfur was obtained for light crude oil.

Immobilized microbial cells as a biocatalyst have been used in microbial desulfurization and denitrogenation owing to their better operational stability, high oil/water volumetric ratios, continuous use, less contamination, better efficiency in catalysis in comparison to free cells, easier separation from the reaction mixture, and good storage ability (Shan et al., 2005). The free dispersion of microbial cells with hydrocarbons minimizes the mass transfer resistance in BDS and BDN process, but the separation of microbial cells from the reaction mixture become difficult. Entrapment and adsorption method have been used by the many researchers for the immobilization of cells. Naito et al. (2001) studied BDS using immobilized *Rhodococcus erythropolis* KA2-5-1 on photo-cross linkable resin prepolymers (ENT-4000 and ENTP-4000), urethane prepolymers, calcium alginate, and

agar for removal of DBT in n-tetradecane. They reported the highest desulfurization activity was achieved with ENT-4000 immobilized cells with no loss of cells from the support. It was found that recovery of biocatalyst from oil was easy. Immobilization of microbial cells on inorganic support enhances the interaction between reactants present in thr two-phase system (Feng et al., 2006). It has been found in the literature data that immobilization of microbial cells by using adsorption technique possessses more advantages than cell entrapment technique as it aids in reducing the mass transfer and the steric hindrance effect (Shan et al., 2005). Researchers have also studied BDS and BDN by decorating the surface of bacterial cells with magnetic nanoparticles to tackle the difficulties arises in conventional adsorption method such as loss of cells, mass transfer problems (Shan et al., 2005). For example, Ansari et al. (2009) and Karimi et al. (2016) decorated the surface of *Rhodococcus erythropolis* IGTS8 by magnetic Fe_3O_4 nanoparticles. They reported that decorated cells showed higher desulfurization activity (56%) than non-decorated cells in the basic salt medium. Zhuang et al. (2015) used bamboo-carbon supported Fe_3O_4 nanoparticles as an immobilizing carrier for the quinoline consuming microbial strain (*Streptomyces* sp. N01).

Table 2.2 BDS and BDN of organosulfur and nitrogen compounds under optimum reaction conditions.

Model oil	Contaminant	Microorganism	Reactor	C_o (ppm)	Temperature (°C)	Time (h)	Pressure (atm)	% removal	Reference
HDS diesel Sample diesel	-	*Rhodococcus* sp. P32C1	BR	303,1000	30	24	-	48, 23	Maghsoudi et al. (2001)
HDS diesel	DBT, Alkylated DBT	*Mycobacterium* sp. X7B	BR	535	45	24	-	86	Li et al. (2003)
HDS diesel	DBT and alkyl substituted DBTs	*Rhodococcus* sp. 1awq,	BR	200	30	-	-	78	Ma et al. (2006)
Hexadecane	DBT	RIPI-22	BR	-	30	7	-	77	Rashtchi et al. (2006)
HDS diesel, Hexadecane	DBT	*Rhodococcus erythropolis* NCC-1	BR	554, 150		96	-	50,86	Li et al. (2007)
Mineral salt medium	Quinoline	*Pseudomonas* sp. strains (BW003)	BR	192–911	30	3–8	-	96-98	Sun et al. (2009)
Hexane, Petroleum oils	DBT	*Pantoea agglomerans* D23W3,	BR	100	30	24, 120	-	93, 26–71	Bhatia and Sharma (2010)
DMSO	Carbazole	*Pseudomonas* sp. strains	BR	500	30	36	-	91-97	Zhao et al.(2011)
Diesel	BT,DBT	*Desulfobacterium indolicum*	-	166.037	30	72	1	79	Kareem et al. (2012)
Mineral salt medium	Quinoline	*Bacillus* sp. (Q2)	BR	500	30	30	-	100	Tuo et al. (2012)
HDS diesel	Alkylated DBT, BT	*Achromobacter* sp.	BR	420	37	24	-	95	Bordoloi et al. (2014)
Mineral salt medium	Quinoline	*Streptomyces* sp. N01	BR	300	45	24	-	93.5	Zhuang et al. (2015)

2.3 Extractive desulfurization (EDS) and Extractive denitrogenation (EDN)

In EDS and EDN process, sour fuel is kept in contact with a solvent to extract the organosulfur and nitrogen compounds by liquid-liquid extraction. It has several benefits over conventional method such as mild operating conditions and low energy consumptions. However, the feasibility and economic efficiency of selective extraction process strongly depends on the selection of solvent, i.e., it should be cheap, highly miscible with sulfur/nitrogen compounds, readily available, and must possess different boiling temperature than that of sulfur/nitrogen compounds present in fuel (Babich and Moulijin, 2003). Various solvents such as acetone, acetonitrile, 1-methyl-2-pyrrolidinon, methanol, ethanol, N-methylformamide, dimethylformamide, dimethyl sulfoxide, and polyethylene glycol have been successfully utilized for the extraction of sulfur and nitrogen containing molecules from liquid fuels (Funakoshi and Aida, 1998; Forte, 1996; Won et al., 2002; Hwang et al., 2007; Hwang et al., 2008; Ban et al., 2013; Kianpour and Azizian, 2014).

Bailes (1981) studied extraction capability of acetonitrile, dimethyl sulfoxide, and tetramethylene sulfone for extraction of organosulfur and aromatic compounds from light oil at room temperature. Petkov et al. (2004) achieved 7 fold reduction (from 0.2 % to .029 %) of sulfur content from hydrotreated middle distillate fuel, and the aromatic content was also reduced 3 times when extraction was performed with following solvents methanol, furfural, and ethylene glycol. Toteva et al. (2007) conducted EDS study for distillate gas oil cuts by using dimethylformamide as a selective solvent. It was reported that sulfur content of fuel can be lowered from 2 % to 0.33 % by employing two-stage extraction, in addition, aromatics content also reduced by 5 fold. However, these conventional solvents are not able to produce ultralow-sulfur fuels, and moreover, the co-extraction of lot of aromatics hydrocarbon compounds leads to degradation of the quality of fuel (Stanislaus et al., 2010). Moreover, these solvents are volatile, poisonous, flammable, and harmful to the environment.

2.3.1 Extraction through ionic liquids

Ionic liquids (ILs) are salts of low melting point and composed of an organic cation and an inorganic anion. ILs are promising alternatives to traditional volatile organic solvent since it can overcome the loss of solvent, and hard recovery problems which are associated with usage of volatile solvents. These liquids have gained the attention of many researchers because of their special characteristics such as thermal and chemical stability, low vapor pressure, recyclability, good solubility (Dharaskar et al., 2015; Kurnia et al., 2015). ILs possess structural features reminiscent of molten salts, ionic surfactants, ionic crystals and molecular liquids; and they exhibits solvent properties which are similar to polar protic liquids, molten salts, or bicontinuous microemulsions (Hayes et al., 2015). Infinite varieties of organic ions present in ionic liquids can be arranged in numerous ways, and combined together to obtain different varieties of ionic liquids (Freemantle, 2004). Extraction capability of the ionic liquid is influenced by various factors such as its size and structure of both cations and anions. The main cations are imidazolium, ammonium, pyridinium, isoquinolonium, phosphonium, and sulfonium (Bhutto et al., 2016). ILs have been studied for the extraction of sulfur oxides, organic sulfur, and nitrogen compounds from liquid fuel (Zhang and Zhang, 2002; Salleh et al., 2018).

ILs were first employed for the selective extraction of sulfur-containing sulfur molecules from fuels in 2001 by Wassercheid and co-workers (Bösmann et al., 2001). DBT extraction was investigated by using 1-3-dialkyl imidazolium alkyl sulfate ionic liquids, and found that the ion size is a significant parameter for extractive desulfurization. The most common mechanisms for extraction of sulfur-containing molecules are the π–π interaction between rings of sulfur molecules and the aromatic rings of ILs (imidazolium, phosphonium) and formation of liquid clathrates (Forsyth et al., 2004). The length of alkyl groups present in ILs also played a significant role in determining the extraction ability of it. The long chain of alkyl group results into a strong π–π interaction between the sulfur molecules and the imidazolium or pyridinium ring of the ionic liquid. For example, four nitrate based ILs were investigated for the DBT removal through extraction

(Safa et al., 2016). It was reported that ILs with cation of longer alkyl groups exhibited enhanced desulfurization capability.

Imidazolium and pyridinium based ILs were employed for the extraction of nitrogen compounds from liquid fuels, and all these ILs have shown good extraction capability for extracting basic as well as neutral compounds from model oil (Xie et al., 2008; Zhang et al., 2004). Salleh et al. (2018) studied the extraction ability of ([Emim][$MeSO_3$]) for the removal of basic and neutral nitrogen containing compounds from model oil. They demonstrated that the neutral compounds were removed better from model oil than basic nitrogen compounds. Lewis acidic ILs were successfully employed for the extraction of organosulfur and heterocyclic nitrogen compounds from model oil, and it was demonstrated that ILs showed better extraction efficiency for basic nitrogen compounds than sulfur and neutral nitrogen compounds. Phosphonium and pyrrolidinium-based ionic liquids were studied for extractive desulfurization,and [B_4P][$MeSO_4$] showed highest sulfur removal with the yields of 61, 62, and 69 % for Th, BT, DBT respectively (Ahmed et al., 2015). Non-halogen ILs such as [BMIM][HSO_4], [BMIM][CH_3COO], [BMIM][DBP], [OMIM][HSO_4], [OMIM][CH_3COO] were also utilized for extraction of sulfur compounds from liquid fuel. Among these, [OMIM][CH_3COO] showed best extracting ability towards DBT under identical operating conditions. Furthermore, the structure of imidazolium cation resembles with thiophene due to which it offered better selectivity in comparison with the six-membered cation families of pyridinium (Le Bui et al., 2017). Commercialization of EDS through ILs is not feasible due to certain drawbacks such as the unexplored effect on the ecosystem, high cost, high mutual solubility of ILs with oil, and a large amount of ILs are required for high desulfurization efficiency (Kianpour and Azizian, 2014; Yu et al., 2016). However, the high cost of ILs can be compensated by regeneration of ionic liquid. For the hydrophobic ILs, regeneration is usually performed by distillation followed by adsorption, while for hydrophilic ILs it is performed by firstly dilution with water and then followed by distillation process (Abro et al., 2014).

2.3.2 Extraction through Deep eutectic solvents

Deep eutectic solvents (DESs) have gained considerable attention in recent years as a low-cost alternative to ILs. DESs can be synthesized from low-cost, non-toxic, fully biodegradable and biocompatible substances (Gano et al., 2015). DESs are generally a mixture of at least two components (hydrogen bond donor and acceptor), and the melting point of the new eutectic mixture is lower than that of each individual component (Tomé et al., 2018). Application of DESs in extractive desulfurization showed high extraction ability in comparison with most of the ILs (Campos-Martin et al., 2010). The performance of EDS process was mainly influenced by the type of hydrogen bond donor associated with the salt in the structure of DESs (Li et al., 2013). $FeCl_3$ and $ZnCl_2$-based DESs have been utilized for EDS, and it was found that $FeCl_3$ based DESs showed higher solvation towards sulfur compounds as compared to $ZnCl_2$-based DESs (Gano et al., 2015). Ammonium and phosphonium-based DESs were used as an efficient extracting solvent for the nitrogen compounds and demonstrated that the values of estimated selectivity and capacity at infinite dilution depends on following factors such as structure of nitrogen compound, salt:HBD molar ratio, choice of hydrogen bond donor, cation and anion respectively (Hizaddin et al., 2014). Tetra-butyl ammonium bromide (TBAB) and polyethylene glycol based DES showed high extraction efficiencies for DBT (100%) and thiophene (95%) (Rahma et al., 2017). Extraction with DESs is a potential method, but the single extraction efficiency is low. Therefore, limited researchers have used the DESs in combination with the oxidant to obtain better desulfurization performance. Liu et al. (2016) synthesized various DESs (extractants), and employed them in combination with HPW (catalyst) and H_2O_2 (oxidant) for the extractive catalytic oxidative desulfurization of sulfur compounds.

Table 2.3 EDS and EDN of organosulfur and nitrogen compounds under optimum reaction conditions.

Model Oil	Contaminant	Extractant	Temperature (°C)	C_o (ppm)	% removal	Oil/Extractant	Reference
n-decane	DBT	[Omim][NO_3]	25	500	95	1:1	Safa et al. (2016)
n-dodecane	Th,BT,DBT	[Omim][CH_3COO]	25	498	98	1:1	Le Bui et al. (2017)
n-octane	DBT	[C1pyr]H_2PO_4	25	500	98	1:1	Gao et al. (2016)
n-heptane and xylol	Th	[BPy]BF_4	25	498	96	1:1	Jian-long et al. (2007)
n-dodecane Diesel Gasoline	DBT	[BMIM]Br	30	500 385 180	79 49 73	1:1 5:1 5:1	Dharaskar et al. (2015)
n-octane	BT,DBT,DMDBT	Polyether-based ionic liquids	30	500	85,91,81	3.5:1	Yu et al. (2016)
n-hexane	Quinoline	[MeIm][H_2PO_4]	25	138.37 (mg/L)	13	10:1	Wang et al.(2014a)
n-octane	BT,DBT, DMDBT	[Omim]Cl.2$FeCl_3$	25	200	99,99,96	20:1	Ban et al. (2013)
n-dodecane	Pyridine	[MeBuIm][BF_4]	30	779	45	5:1	Zhang et al. (2004)
hexadecane/toluene	Quinoline, Indole, Carbazole	[MeOcIm][Cl]	30	87, 64,160	8.5,92.4,92.7	20:1	Laredo et al. (2015)
n-heptane	DBT	Polyethylene glycol	25	500	98	1:1	Kianpour and Azizian (2014)
n-octane	Th, DBT, DMDBT	N,N-dimethylformamide	29	50,150,300	90,97,77	1:1	Mokhtar et al. (2014)

2.4 Adsorptive desulfurization (ADS) and Adsorptive denitrogenation (ADN)

ADS and ADN have been studied worldwide, and implemented for abatement of refractory sulfur and nitrogencompounds from fuels. Adsorption process has gained immense attraction of researchers as it can be conducted under mild operating conditions without any use of hydrogen gas, which makes the process economic. Various sorbents such as zeolites (Hernandez-Maldonado and Yang, 2004b; Tang et al., 2008), activated carbon (Wen et al., 2010; Saleh and Danmaliki, 2016), metal oxides (Rashidi et al., 2015), mesoporous silicas (Sentorun-Shalaby et al., 2011; Mohammadian et al., 2017) have been studied widely for the removal of aromatic sulfur and nitrogen compounds from hydrocarbon streams. In the following section, different sorbents employed for adsorptive desulfurization and denitrogenation have been discussed.

2.4.1 Activated carbon

Activated carbon has been widely used in adsorption process due to its excessive surface area, good porosity, and easily functionalization with different types of functional groups. Adsorption capacities of activated carbon are directly connected to the surface area and functional group. Adsorption of sulfur and nitrogen compounds strongly depends on the surface chemistry and porosity of activated carbon (Wen et al., 2010). Sano et al. (2004) demonstrated that high surface area and the presence of oxygen containing functional groups plays important role in the ADS and ADN of real gas oil. In addition, adsorption of sulfur and nitrogen compounds is influenced by the nature of oxygen containing functional groups. For example, acidic oxygen containing functional groups favors the adsorption of DBT and quinoline, whereas basic oxygen containing functional groups favors the adsorption of indole (Laredo et al., 2013).

In order to improve its capacity, various modifications of activated carbon have been done by researchers. It has been found from the literature data that the treatment of activated carbon with acid or base can improve the adsorption capacity of activated carbon, and the acid treated activated carbon shows more adsorption capacity as compared to base treated activated carbon and virgin activated carbon (Jung and Jhung, 2015). Activation of activated carbon with various acids such as sulfuric acid, phosphoric

acid improves the adsorption of sulfur and nitrogen compounds owing to the addition of specific oxygen functional groups (Laredo et al., 2013). Modifications of activated carbon with metal species and metal oxides have been also studied in order to enhance the adsorption capacity of activated carbon (Thaligari et al., 2016a; Xiong et al., 2010). Desulfurization and denitrogenation performance of modified activated carbon along with optimum condition is given in Table 2.4. It was found that incorporation of aluminum on activated carbon increased the adsorption capacity as compared to virgin activated carbon (Ganiyu et al., 2016). Few investigators have also made an attempt to derive activated carbon from waste sources (Saleh and Danmaliki, 2016; Nunthaprechachan et al., 2013). Nejad et al. (2013) synthesized ordered mesoporous carbons such as CMK 5 & CMK 3 for removal of DBT. In their outcome, CMK 5 acquire more sorption capacity as compared to CMK 3, and this higher sorption capacity of CMK 5 was ascribed to its exclusive structure constitute of ordered cluster of carbon nanopipes, which are isolated by ordered arrays of mesoporous channels in a system of the bimodal pore.

2.4.2 Metal-organic frameworks (MOFs)

MOFs are crystalline solids of three-dimensional framework which is formed by reaction between organic and inorganic species, and where an organic linker connects the metal ion or cluster of metal ions (Perry Iv et al., 2009). The unique feature of MOFs is its broad span of chemical and physical properties. MOFs have been attracting the attention of many researchers for the use as a support material for catalyst, and as a adsorbents because of its special features such as easy to tailored pore size, shape from microporous to mesoporous range, designable crystalline structure, high and regular porosity (Khan and Jung, 2012). MOFs have been used for desulfurization and denitrogenation of liquid fuels (Khan and Jung, 2012; Ahmed et al., 2013). Cychosz et al. (2008) used MOFs firstly for the desulfurization of liquid fuel, and a series of MOFs which included HKUST-1, UMCM-150, MOF-5, MOF-505, MOF-177 was utilized to remove BT, DBT, and DMDBT. It is well known that materials with high porosity and pore volume possess superior adsorption capacity. Nevertheless, in this research a different pattern was observed, which indicates that adsorption of organosulfur compounds on MOFs slightly depend on the porosity of MOFs. In addition, the adsorption capacity of MOFs for

organosulfur removal depends on the functionality of active sites rather than its porosity (Cychosz et al., 2008). MOFs showed more adsorption capacity for nitrogen containing compounds than sulfur compounds, and this can be ascribed to the exothermic and coordinative interaction of nitrogen compounds with coordinatively unsaturated sites of MOFs (Ahmed and Jhung, 2016). Functionalization of MOFs has gained immense attraction as it can induce desired characteristic to the MOFs to improve its adsorption capacity. Functionalization of MOFs can be achieved by grafting appropriate ingredients on the coordinatively unsaturated sites of metals available in MOFs (Sarker et al., 2018). The effect of acidity or basicity of MOFs on the adsorptive desulfurization and denitrogenation was also studied. It was found that adsorption of basic sulfur (BT) and nitrogen (quinoline) was improved remarkably by introducing acidic sites in MOFs (Ahmed et al., 2013), and the adsorption phenomena can be explained with aid of HSAB concept. Various adsorption mechanisms such as hydrogen bonding, van der Waals interaction, acid-base interactions, cation- π interaction and π-complexation have been used to describe the adsorption of sulfur and nitrogen compounds from liquid fuels (Ahmed and Jhung, 2016).

2.4.3 Mesoporous silica

Mesoporous materials are those materials having a pore diameter in the range of 2 nm-50 nm. Among mesoporous materials, mesoporous silicas MCM-41 and SBA-15 have gained remarkable recognition in the field of adsorption due to its high surface area, high thermal stability, and a larger pore size, which encourages the easier diffusion of larger molecules into pores (Wan and Zhao, 2007). The main drawback associated with these materials is the low adsorption capacity and selectivity, and this problem can be tackled by incorporation of metal into nanochannels. The size of incorporated metal also plays a crucial role in ADS process, the adsorption capacity of the adsorbent for the removal of organosulfur compounds with high steric hindrance can be enhanced by reducing the size of metal nanoparticles (Teymouri et al. 2013). Several d-block metals cations such as Cu^{+}, Ag^{+}, Pd^{2+}, and Pt^{2+} are capable of π complexation bonding (Khan and Jhung, 2012). Yang et al. (2003) developed sorbents which can form π complexation for ADS. Numerous researchers studied the π complexation mechanism for adsorption of sulfur

compounds onto the metal species incorporated mesoporus material. In this bonding organosulfur compounds are adsorbed in a flat, face down orientation, which helps in adsorbing the alkylated DBTs with steric hindrance (Ahmed and Jhung, 2016). Wang et al. (2008) conducted desulfurization of JP-5 light fraction (841 ppmw) by π - complexation adsorption mechanism with CuCl and $PdCl_2$ supported on the MCM-41 and SBA-15 mesoporous materials. It was found that Pd^{2+} gives better π complexation bonding as compared to Cu^{+} for the benzothiophene and its derivatives. Zhang and Song (2012) studied ADN of model oil and commercial diesel with the aid of various mesoporous materials (Ti-HMS, HMS, MCM-41), and it was found that the adsorption mechanism was governed by acid-base interactions. Xin and Ke (2016) employed MCM-41 and cobalt oxide loaded MCM-41 for the adsorption of quinoline. Cobalt oxide loaded MCM-41 showed better adsorption capacity than MCM-41 which was ascribed due to the strong acidity and chemisorption between cobalt species and quinoline. Koriakin et al. (2010) employed lithium incorporated mesoporous silica for the adsorption of nitrogen compounds from HDS diesel. They observed that synthesized mesoporous materials showed better adsorption capacity for nitrogen containing compounds than sulfur compounds.

2.4.4 Other adsorbents

Alumina has been widely employed as a catalyst, and an adsorbent both owing to its high specific surface area, regular pore size distribution, and it is also quite stable within a wide range of temperature. It has the capability to stabilize, disperse the active component very well, and also exhibits moderate acidity (Bazyari et al., 2016). IRVAD process uses alumina-based adsorbents. Alumina is modified with an inorganic promoter in this process to increase the adsorption capacity and selectivity (Irvine, 1998). This process was used commercially in the past to decrease the amount of sulfur in the fuel. It was reported in the literature that presences of carbon-oxygen functional groups on the surface of alumina were proved to be very effective in the adsorptive removal of DBT onto alumina (Srivastav and Srivastava, 2009). Almarri et al. (2009) studied adsorption of nitrogen compounds in batch adsorption system and a fixed-bed flow adsorption system with the aid of three activated alumina samples. It was found that adsorption of nitrogen

compounds is influenced by the acidity and basicity of alumina. The removal of quinoline was enhanced with an increase in acidic nature of alumina while removal of indole was increased on increasing the basicity of alumina. Alumina has been reportedly used in conjunction with other oxide supports in order to overcome the drawback of other oxides, and to give high adsorption efficiency. For example, titanium oxide contains a large number of acidic sites, and provides better dispersion of active phase than another surface. However, it is not commercially available in the high surface area which results into lower adsorption capacity (Nair and Tatarchuk, 2010). One way of tackling down this obstacle is to disperse the titanium oxide onto the surface of the higher surface area supports such as alumina. Metal species supported on various supports materials have been utilized for the adsorptive desulfurization and denitrogenation of liquid fuels. For example, Zn or Ni supported GAC was used for the simultaneous removal of DBT and quinoline from model oil (Thaligari et al., 2015; Thaligari et al., 2016b). Metal oxide and mixed metal oxide supports have also been employed for the adsorptive desulfurization. Graphene oxide as a support framework for nanoparticles has been used in various field due to its high specific area, light weight, good thermal and electrical conductivity (Menzel et al., 2016). A series of mixed metal oxides and mixed metal oxides supported on graphene oxide was studied for adsorption of DBT from dodecane (Menzel et al., 2016). It was shown that DBT uptake was increased up to 170 % by incorporating only 5 % of graphene oxide in mixed metal oxides. Zirconia based materials exhibit better adsorption characteristics, and has been utilized for the adsorption of sulfur compounds such as thiophene and DBT. Kumar et al. (2011) demonstrated the desulfurization ability of zirconia based catalyst (normal dried zirconia, zirconia calcined at 893 K, zirconia sulfated and calcined at 893 K) for removal of DBT from Iso-octane. It was reported that adsorption process of DBT was exothermic in nature. Further, copper supported on zirconia proved to be very effective for removal of DBT (Baeza et al., 2008). Si-Zr cogel was used for the removal of nitrogen compounds from the light gas oil, and it was reported that adsorbent exhibited high selectivity for nitrogen compounds owing to the presence of zirconia on the cogel. Zeolites were also employed for the desulfurization and denitrogenation of liquid fuels. Hernandez-Maldonado and Yang (2004b) demonstrated

the cu-zeolite could reduce the nitrogen content of commercial diesel from 83 ppm to below 0.1 ppm.

2.4.5 Regeneration of adsorbents

Regeneration of adsorbents is the prime concern of adsorptive desulfurization and denitrogenation process because it assess whether the developed adsorbent feasible for industrial scale or not. Regenerable adsorbents not only make the process economic but also environment-friendly. Different regeneration methods have been adopted by the researchers such as thermal regeneration, and chemical regeneration (Saleh et al., 2016; Xiong et al. 2012). In thermal regeneration process, spent adsorbent is treated at higher temperature. Employed temperature was higher than the boiling point of adsorbed compounds so that the all adsorbed compounds desorbed from the adsorbent. In chemical regeneration method, various types of solvents such as methanol, acetonitrile, chloroform, and toluene have been utilized for the regeneration of spent adsorbents (Shah et al., 2017). Palomino et al. (2015) employed solvent rinsing procedure to regenerate spent adsorbents. Diethyl ether was used as the solvent to regenerate adsorbent. It removed both sulfur compounds and some of the hydrocarbons which are adsorbed due to Van der Waals interactions. Regeneration of saturated sorbents with solvent is beneficial as compared to the thermal method because it overcomes the drawback of using a high temperature for regeneration and also avoids oxidation of metal species (Palomino et al., 2015).

Table 2.4 ADS and ADN of organosulfur and nitrogen compounds under optimum reaction condition.

Activated carbon								
Model Oil	Contaminant	Adsorbent	Reactor	Temperature (°C)	Pressure (atm)	C_o (ppm)	% removal	Reference
Iso-octane	DBT	Al/AC	BR	Room temperature	-	50-200	95	Ganiyu et al. (2016)
Hexane(85 %)+Toluene(15%)	Th, BT, DBT	AC from waste rubber tires	BR	25	-	50	100,30,20	Saleh et al. (2016)
Cyclohexane	DBT	Sn/AC	BR	60	-	1000	99.4	Shah et al. (2016)
Iso-octane	DBT	Zn/GAC	BR	30	-	574	96.8	Thaligari et al. (2016a)
Iso-octane	DBT, indole	Co/ATGAC	BR	30	1	500,500	92, 96	Present study
Iso-octane	DBT	Mo/ATGAC	BR	30	1	500,500	91, 94	Present study
Mesoporous silica								
Model Oil	Contaminant	Adsorbent	Reactor	Temperature (°C)	Pressure (atm)	C_o (ppm)	% removal	Reference
Octane	Th	MoO_3/MCM-41	BR	30	-	300	68	Shao et al. (2012)
JP-8	-	Ag/ DDA-15	BR	Room temperature	1	734	46	Palomino et al. (2015)
JP-5 light	-	$PdCl_2$/SBA-15	FBR	Room temperature	-	841	50	Wang et al. (2008)
Metal organic frameworks								
Model Oil	Contaminant	Adsorbent	Reactor	Temperature (°C)	Pressure (atm)	C_o (ppm)	Adsorption capacity (mg/g)	Reference
n-octane	BT	Cu^+/MIL-	BR	25	-	1000	154	Khan and Jhung

		100-Fe						(2012)
75 vol% n-octane + 25 vol% p-xylene	Quinoline, indole	$CuCl_2$/MIL-100(Cr)	BR	25	-	300–1200	457, 171	Ahmed and Jhung (2014)
75 vol% n-octane + 25 vol% p-xylene	Quinoline	$AlCl_3$/MIL-100(Fe),	BR	25		400	417	Xu et al.(2015)
Others								
Model Oil	Contaminant	Adsorbent	Reactor	Temperature (°C)	Pressure (atm)	C_o (ppm)	% removal	Reference
Kerosene, Cyclohexane	DBT	Zn/MMT Clay	BR	25	1	1000	76 ,81	Ahmad et al. (2017)
Iso-octane	Th	AgCl Nanoparticle	BR	Room temperature	-	550	95	Li et al. (2015)
Decane	Quinoline, Carbazole	MSU-S, CoO-MSU-S	BR	30	1	200- 800	-	Mohammadian et al.(2017)
Isooctane	Th	Ga/Y zeolite	BR	60	-	500	97	Tang et al. (2008)
Hexane	DBT	Activated alumina	BR	30	-	500	60	Srivastav and Srivastava (2009)
Hexane	Th, BT	Zeolites	BR	30	1	500	63	Ngamcharussrivichai et al. (2007)
n-hexadecane	Quinoline, Carbazole	Cr-MSU-S, Fe- MSU-S,	BR	30	1	200–1000	-	Ahmadi et al.(2017)

2.5 Oxidative desulfurization (ODS) and Oxidative denitrogenation (ODN)

Oxidation is considered as a promising alternative for removal of refractory sulfur and nitrogen compounds from liquid fuels. It is highly advantageous in comparison to conventional hydrotreating process as it can occur at the mild condition with no use of hydrogen (Dehkordi et al., 2009). ODN, a complementary technique to the HDN, involves the oxidation of nitrogen containing compounds to N-oxides compounds followed by the selective adsorption of the N-oxides. In the ODS process, sulfur compounds in liquid fuels are oxidized into their corresponding sulfoxides and sulfones with the help of a selective oxidant. The ODS process possesses reaction mechanism which enhances the polarity of sulfur compounds and enables easier separation from the fuel.These oxidized compounds possess enhanced relative polarity due to which they can be easily extracted from the fuel (Aitani et al., 2000). Oxidation of organosulfur compound (DBT) to the corresponding sulfone is shown in Figure 2.2.

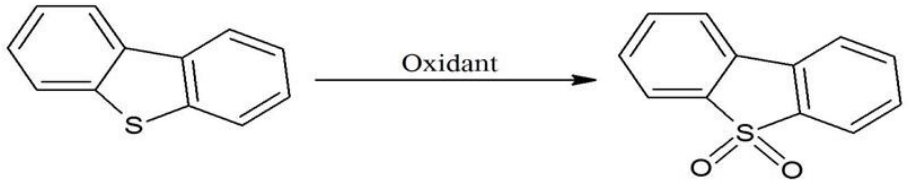

Figure 2.2 Oxidation of DBT into the corresponding sulfone (Xie et al., 2015).

2.5.1 Oxidants

A wide variety of oxidants were used for desulfurization and denitrogenation of liquid fuels i.e. hydrogen peroxide (Fraile et al., 2016), molecular oxygen (Sampanthar et al., 2006; Ma et al., 2007), organic hydroperoxides (Chang et al., 2010).

2.5.1.1 Hydrogen peroxide

Hydrogen peroxide is one of the fascinating oxidants because of its low cost, easy availability, and environmental friendliness. It is one of the most chosen oxidants for ODS and ODN studies as it only produces water as a by-product (Fraile et al., 2016). Various researchers have investigated oxidative desulfurization and denitrogenation process by employing H_2O_2 as an oxidant (Krivtsov and Golovko, 2014) Oxidation has been studied with H_2O_2 in presence of various catalyst such as various acidic catalyst

(Duarte et al., 2011; de-Souza et al., 2009), ionic liquids (Gao et al., 2010), supported and unsupported metal oxides (Sampanthar et al., 2006; Huang et al., 2008; Ogunlaja et al., 2017; Zhou et al., 2010) etc. Table 2.5 presents the ODS and ODN performance of different catalytic systems when H_2O_2 is used as an oxidant. The conversion process of DBT to its corresponding sulfoxides and sulfones can be catalyzed with the help of acidic catalyst (Ali et al., 2006). Acidic catalysts polarize the O-O bond present in hydrogen peroxide. When the oxidation system consists of hydrogen peroxide, and carboxylic acids (formic and acetic acid), it generates in situ peracids radical which are efficient for the fast oxidation of organosulfur compounds (Yan et al., 2009). Effect of stronger (hydrochloric acid) and weaker acids (acetic acid) than formic acid on ODS process is also investigated. Formic acid gave better oxidation results as compared to both HCl and acetic acid (Ali et al., 2006). de -Souza et al. (2009) studied catalytic oxidation of nitrogen and sulfur organic model compounds by using an equimolar mixture of H_2O_2 and HCOOH as an oxidant, and they monitored it with the help of electrospray ionization mass spectrometry. It was found that DBT, quinoline, and methylene blue were oxidized through a mechanism of successive hydroxylation. Experimental findings showed that the reaction of H_2O_2 on the surface of the catalyst produced highly reactive hydroxyl radicals, which are responsible for the oxidation process. Oxidation reactivity pattern for the sulfur-containing fuel in a formic acid catalyzed system with H_2O_2 was reported by Otsuki et al. (2000) at a temperature of 50 °C and atmospheric pressure. The limonite–glycerol composite was utilized for oxidation of quinoline and DBT containing model oil (Guimarães et al., 2013). In order to synthesize highly active catalyst for desulfurization and denitrogenation, limonite was impregnated with glycerol–acetone and the obtained composite was thermally treated at 400 °C under nitrogen atmosphere to reduce iron species. The synthesized catalyst oxidize quinoline and DBT by transferring hydroxyl groups to them, which in turn enhance their polarity to allow their removal from fuel by extraction with the aid of polar solvent. Transition metal-based catalysts along with H_2O_2 as an oxidizing agent are investigated widely by the researchers for ODS and ODN. Capel-Sanchez et al. (2010) studied removal of BT, DBT, DMDBT via oxidation using H_2O_2, amorphous silica-loaded titanium oxide as an oxidant and catalyst respectively. Shiraishi et al. (2003) used mesoporous vanadosilicate and titanosilicates as catalysts and

hydrogen peroxide as an oxidant for the oxidative removal of sulfur and nitrogen compounds. Leng et al. (2016) reported on ODS for removal of DBT with Ti-modified hierarchical mordenite as a catalyst and H_2O_2 as an oxidant, 98 % of removal of sulfur was achieved at 333 K in 120 min. One of the major issue associated with the use of H_2O_2 that it is an oil insoluble oxidant due to which it forms biphasic liquid system. Interface establishment between aqueous and oil phase causes low mass transfer rate which eventually results into the excessive requirement of oxidant. Phase transfer agents are also added in order to improve the mass transfer coefficient (diffusion), but the addition of these agents create hurdles in separating oil phase from aqueous phase owing to the formation of the emulsion, and hence reduces overall oil yield. Moreover, the aqueous phase (H_2O_2) create several other problems such as corrosion of equipment, the high volume ratio of aqueous phase to oil phase leads to low efficiency of the reactor (Fraile et al., 2016), and production of oil with high moisture content.

2.5.1.2 Organic hydroperoxides

Organic hydroperoxides, particularly tertbutyl hydroperoxides (TBHP) have been widely employed as oxidants for the elimination of sulfur and nitrogen containing molecules from liquid fuels. TBHP is an oil soluble oxidant, which minimizes mass transfer limitation, and enhances the overall oxidation rate of sulfur-containing molecules. Various catalysts such as TiO_2–SiO_2 (Bazyari et al. 2016), $Co/Mn/Al_2O_3$ (Mokhtar et al., 2015), MoO_3/Al_2O_3 (Ishihara et al., 2005) have been used in conjunction with TBHP as an oxidant. Operating conditions of few catalytic system employed with TBHP are reported in Table 2.5. Prasad et al. (2008) investigated the ODS of DMDBT for the catalytic system composed of TBHP and molybdenum oxide supported on following supports alumina, silica–alumina, and magnesia–alumina, and achieved highest catalytic activity with MoO_3/Al_2O_3. Ishihara et al. (2005) studied oxidative denitrogenation for nitrogen compounds containing model oil and light gas oil in presence of $MoO_{3/}Al_2O_3$ (catalyst) and TBHP (oxidant).

Some researchers also explored other organic hydroperoxides i.e. cumene hydroperoxide (CHP), cyclohexanone peroxide (CYHPO) for oxidation of refractory sulfur compounds in oil fractions. DBT oxidation was carried out in a fixed bed reactor with CHP as an

oxidizing agent and MoP_xO/SiO_2 as a catalyst. They found that sulfur content in the diesel was decreased from 298 to 5 ppmw (Han et al., 2013). Safa and Ma (2016) also reported the oxidation of DBT, 4-methyldibenzothiophene (MDBT), and dimethyl DMDBT in a model fuel with CHP as an oxidant over a $MoO_3/\gamma\text{-}Al_2O_3$ catalyst. Details of ODS system comprising of CHP and different catalysts is given in Table 2.5. CYHPO is also an oil-soluble oxidant, and possesses better oxidation capability, cheap in comparison with other oil soluble oxidant, and available in large scale. ODS was investigated using various alkyl peroxides, and it was found that activity decreases in the following order CYHPO >tert-amyl hydroperoxide> TBHP, reversing the order of the peroxy oxygen electronic density (Zhou et al., 2007).

2.5.1.3 Other oxidants

Few studies have also been conducted on the ODS with the following oxidants such as ozone (Otsuki et al., 1999), oxygen (Lü et al., 2007), potassium ferrate (Liu et al., 2008) Fenton's reagent (Dai et al., 2008), nitric acid (Tem et al., 1990a; Tem et al.1990b), nitrogen (Tem et al.,1990a) etc. Among these, nitrogen dioxide was used as the oxidant in the first study of ODS process. Ma et al. (2007) investigated ODS process for model and real jet fuel (JP-8) in a batch system with the aid of molecular oxygen as an oxidant followed by adsorption over activated carbon. Tang et al. (2014) also reported oxidation of DBT using molecular oxygen as an oxidant catalyzed by tetradecavandaphosphate. Few ODS studies have also employed Ferrate (Fe (VI)) as an oxidant. It exhibits strong oxidizing properties in comparison with other oxidants such as O_3, H_2O_2 and $KMnO_4$, and also possesses a reduction potential of +2.20 V in an acidic medium (Sharma, 2002). It is also an environmental friendly oxidant since Fe (VI) is converted to harmless Fe (III) (Liu et al., 2008). ODS of diesel oil was studied by employing Fe(VI)-acetic acid system with manganese acetate as the catalyst, and different phases transfer agents such as hexadecyl trimethyl ammonium bromide, benzyl trimethyl ammonium chloride and tetramethyl ammonium chloride (Liu et al., 2008).

2.5.2 Catalyst

In the oxidation process, catalyst plays a very important role as it is responsible for the activation of oxidant. Both homogeneous and heterogeneous catalysts have been used in oxidative process (Otuski et al., 2001; Huang et al., 2008; Green et al., 2007; Zhang et al., 2011). Particularly heterogeneous catalyst has attracted more attention as compared to the homogeneous catalyst, and it is composed of the active phase and support material. The active component present in the catalyst is able to alter both structural and morphologic characteristics of the supported catalyst, and thereby increase in activity and stability of the catalyst (Zhao et al., 2009). The surface of the support material should be covered with a thin layer of the active component. The active phase of catalysts is primarily constituted of transition metals viz, molybdenum, iridium, palladium, nickel, platinum, tungsten, and rhodium (Qiu et al., 2016). Oxides of d block contain lewis acidic sites when these oxides disperse over the support (high superficial area) it maximizes the contact area between active sites and reactants, and thereby promotes oxidation process (Bakar et al., 2012).

Transition metal oxides proved to be an efficient catalyst for catalytic oxidative process because they can easily alter their valence state and encourage the redox cycle (Franco et al., 2013). Among transition metal oxides, molybdenum oxide acts as a very effective catalyst for the oxidation process. Molybdenum-based catalyst has attracted the considerable attention of many researchers in oxidation of liquid fuels due to its unique physical-chemical characteristic, and it is also very reactive and highly potent for oxidation process (Gonzalez-Garcia and Cedeno-caero 2009). However, the usage of transitional metal oxides alone as a catalyst is limited because of its low pore diameter, volume, and specific surface area (Samadi-Maybodi et al., 2011). In addition, generation of organic sulfides during the ODS process on the surface would lead to blocking of active sites in the pores, and eventually decreases the capability to remove sulfur compounds (Guo et al., 2012). Furthermore, these active components can't be used directly due to the difficulty in separation from organic phase (Yang et al., 2016). Therefore, a support material with the high specific surface area is needed in order to remove the drawbacks associated with the catalytically active component (Transition

metal oxides). The support material is responsible for the number and nature of active sites present in the catalyst. As a result, support material affects the catalytic activity of the catalyst, and it also promotes the separation of catalyst from the fuel (Yang et al., 2016; Qiu et al., 2016). Selection of an appropriate support is a very significant step in oxidation process as it may affect both reaction selectivity and activity. Various supports have been used in oxidation studies such as alumina (Zhou et al., 2010; Jia et al., 2011), MCM-41 (Xie et al., 2015), molecular sieve (Hulea et al., 2001), TiO_2, SiO_2 (Han et al., 2013; Ogunlaja et al., 2017), SBA-15 (Chamack et al., 2014; Cho and Lee, 2014).

Ishihara et al. (2005) studied oxidative denitrogenation followed by adsorption for nitrogen compounds containing model oil and light gas oil. The employed oxidative (MoO_3/Al_2O_3) and adsorptive system was able to remove 94 % of nitrogen from light oil. Vanadium pentaoxide supported on silica in conjunction with TBHP was employed to oxidize quinoline in both batch and flow process (Ogunlaja and Alade, 2018). Wang et al. (2003) reported that Mo catalyst supported on alumina showed the best sulfur removal capacity as compared with Mo supported on titania and silica. Modification of molybdenum based catalyst was also carried out by many researchers to improve its catalytic activity. The Mo-based catalyst was modified with bismuth to increase the catalytic activity of desulfurization of light cycle oil (Prasad et al., 2008). Chang et al. (2010) introduced a series of alkaline earth metal dopant on Mo, and reported that $CaMo/Al_2O_3$ showed the high catalytic activity. In order to improve the catalyst stability and ODS activity, different synthesis methods for synthesis have been adopted by researchers. For example, the MoO_3-SiO_2 mixed oxide was synthesized by the sol-gel method. Due to the strong interaction between MoO_3 and SiO_2, the loss of the active metal was inhibited which eventually enhanced the stability of MoO_3-SiO_2. The ODS activity of MoO_3-SiO_2 was further promoted by the addition of a proper amount of CeO_2. The introduction of CeO_2 enhanced the dispersion of MoO_3, and small amounts of Mo^{5+} may have been formed owing to the electronic interactions between Mo and Ce species (Zhang et al,. 2009).

Transition metals oxides supported on mesoporous materials are promising choice for the preparation of catalysts to fulfill the demands imposed by industries. Mesoporous silica

materials such as MCM-41 and SBA-15 exhibits high surface area, good thermal stability, narrow and controllable pore size, and offers several other benefits such as it allows the processing of various sizes molecules, allowing good diffusion of several compounds, and as a result enhancing the effectiveness of reaction at internal surface (Kwong et al., 2008). The oxidative removal of nitrogen compounds was enhanced by using vanadium incorporated mesoporous molecular sieve than titanium incorporated mesoporous molecular sieve. The following trend was obtained for the oxidative removal of nitrogen by using V-HMS, DBT > aniline > indole > BT > carbazole. The obtained trend suggested that carbazole was most difficult to oxidize (Shiraishi et al., 2003). Abdalla and Li (2012) prepared MCM-41 $(Bu_4N)_4H_3(PW_{11}O_{39})$ supported MCM-41, and examined its capability for ODS Process. It was found that synthesized catalyst showed high catalytic activity, and can be reused for ODS of organosulfur compounds. Complete removal of DBT and Th was achieved under mild operating conditions, and 97 % of sulfur removal was obtained for ODS of FCC cycle. Li et al. (2011) synthesized mesoporous silicate with the incorporation of phosphotungstic acid, and achieved 98-99 % DBT conversion for model oil in ODS process. Molecular sieve as a support material has gained much attention in recent years owing to its inherent properties, and environmental friendliness (Subhan et al., 2014). Moreover, 4A molecular sieve occupies the high surface area (600–800 m^2/g) for dispersion of active component, and in addition it is economic and non-toxic also (Yang et al., 2016). The performance of catalytic ODS by using Mo supported 4A molecular sieve as a catalyst and cyclohexanone peroxide (CYHPO) as an oil-soluble oxidizing agent for removal of BT and DBT was investigated. Under the optimum condition, 99 % of DBT conversion was achieved (Yang et al., 2016).

Polyoxometalates (POMs) have been applied in various fields, among them, catalysis is the most significant application of it. The peroxocomplexes are formed when the transitional metal derivatives react with hydrogen peroxide, peroxocomplexes are more strong oxidizing agent than the original peroxide (Arcoria et al., 1983). POM catalysts have also been used for the ODS process, and high sulfur removal efficiency was observed due to their special unique properties (Nogueira et al., 2014; Ribeiro et al., 2013). POMs composed of transition metals like Ti, Mo, V, and W are potential catalysts

for the ODS when used with H_2O_2. Ribeiro et al. (2016) investigated desulfurization efficiency of various hybrid zinc-substituted polyoxometalates.

2.5.3 Oxidative reaction mechanism and reactivity trend

Typically, in the ODS process, the sulfur compound is oxidized to the corresponding sulfone by the electrophilic addition of oxygen atoms with the help of catalyst and oxidant (Bhutto et al., 2016; Song and Ma, 2003). Many oxidative reaction mechanisms have been reported in the literature. As an example, the reaction mechanism of DBT over MoO_3/Al_2O_3 was proposed in the presence of CHP (Safa et al., 2016). It was proposed that initial reaction might occur due to the pseudo-cyclic structure, which was generated owing to the coordination between peroxide and polar Mo-O band and formation of nascent oxygen. Further, this oxygen attack on the sulfur presents in DBTs to form sulfoxides, and finally oxidation leads to the corresponding sulfones. DBT reacted with CHP in presence of MoO_3/Al_2O_3 to produce DBT sulfoxide as an intermediate product. The obtained intermediate product further reacts with an oxidant in presence of the catalyst to form DBT sulfone and cumyl alcohol as the final product of oxidation. Xie et al. (2015) proposed the two-step mechanism of catalytic oxidation using H_2O_2 as an oxidant. In the first step, sulfur atom of DBT stages a nucleophilic attack on the oxygen atom in the catalyst due to which active oxygen is transferred to DBT and transformation of DBT to DBTO or $DBTO_2$. In the second and last step, H_2O_2 comes in contact with catalyst and peroxide bond regenerates. Catalytic ODS of DBT in the presence oxidant (TBHP) is depicted in Figure 2.3 (Mokhtar et al., 2015). Initially, the active metal species (Co/Mn) react with TBHP to form a complex structure. Due to the formation of complex species, electrophilic characteristics of the oxygen enhanced and become more active. Subsequently, the active oxygen attacks on the sulfur atom present in the DBT to form the DBT sulfoxide and tert-butanol as the byproduct. In the last step, DBT sulfoxide further oxidized to form DBT sulfone.

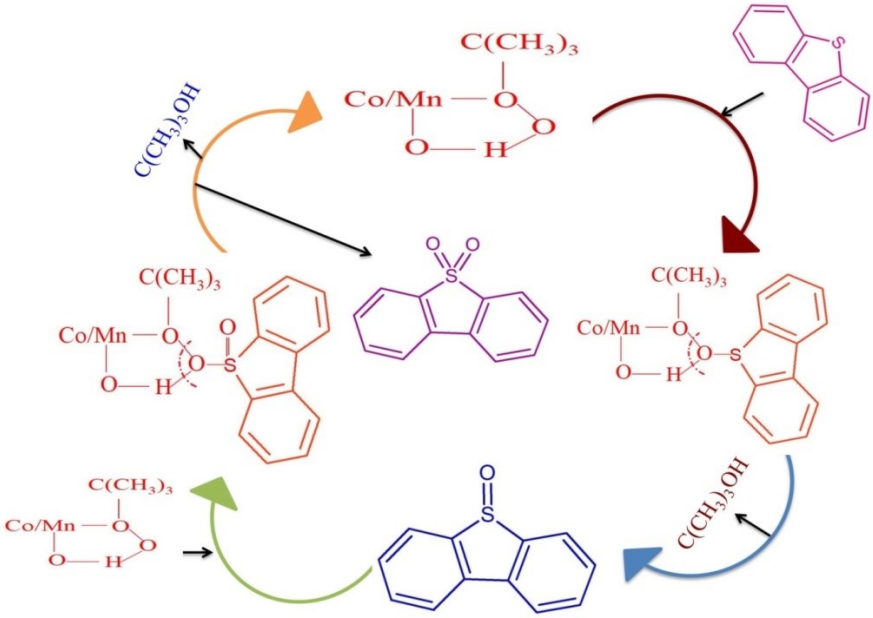

Figure 2.3 Cyclic reaction for ODS of DBT in presence of TBHP and $CoMn/Al_2O_3$ (Mokhtar et al., 2015).

Generally, two factors governed the reactivity trend of aromatic sulfur compounds namely, electron density, and steric hindrance. The higher electron density of sulfur atom present in sulfur containing compound promotes an electrophilic attack on the sulfur atom present in sulfur compound by the activated oxygen. Otsuki et al. (2000) obtained the following decreasing order of oxidation reactivity for the DBTs, DMDBT > MDBT > DBT. This reactivity pattern was obtained since sulfur atom of DMDBT has higher electron density than MDBT and DBT. On the other hand, Wang et al. (2003) observed following for oxidation reactivity of sulfur compounds, DBT > MDBT >DMDBT ≫ BT. They considered that the steric hindrance of methyl substitution has lowered down the oxidation activity of methyl-substituted DBT, and BT was very difficult to oxidize because of its lower electron density.

Oxidation products of nitrogen compounds depend upon the conditions and oxidative system employed for the oxidative denitrogenation. At mild operating conditions indole can be transformed into indoxyl, it can further convert into isatin, indigo or indirubin on spontaneous oxidation with air (Ishihara et al., 2005). Moreover, strong operating

conditions lead to the breaking of pyrrole ring of indole. Indole was catalytically converted into indigo in presence of H_2O_2 (Zhang et al., 2011). The oxidation products of aniline, carbazole, and indole were recognized as azoxybenzene, carbazole-1,4-dione, and polymerized material in presence of V-HMS (catalyst) and H_2O_2 (oxidant) (Shiraishi et al., 2003). Oxidation of carbazole in presence of TBHP and Mo(VI) complexes as catalyst showed the formation of compounds of similar polarity and boiling point (Zhou et al., 2010). It has been reported that mineralization of quinoline takes place in presence of iron as an active phase in catalyst. For example, Quinoline was mineralized completely in presence of H_2O_2 and Fe/C (Mambrini et al., 2017), and the active iron phase present in the catalyst was found to be responsible for the mineralization of quinoline. Similar results were reported by de Souza et al. (2010) for the oxidation of quinoline in presence of H_2O_2 and goethite. Ogunlaja and Alade (2018) conducted oxidation of quinoline in presence of TBHP using V_2O_5/SiO_2. In batch process, the oxidation of quinoline was initiated by formation of hydroxyl radical, the attack of radicals on different position of quinoline molecule led to the formation of several products (nicotinic acid , 3-nicotinaldehyde, 2-nicotinaldehyde (10%), 1-(pyridin-2-yl) ethanone, pyridine-2,3-dicarboxylic acid, quinolin-5-ol). However, when flow micro-reactor is used quinoline is selectively oxidized to quinoline-*N*-oxide at quinoline to TBHP ratio of 1:7. A hybrid material ($[Bmim]_3PMo_{12}O_{40}$) was employed for the oxidative removal of nitrogen compounds from model oil in presence of hydrogen peroxide (Zhang et al., 2011). It was shown that oxidative system was able to oxidize nitrogen compounds and following trend for ODN activity was obtained: indole > quinoline > carbazole. The higher oxidative removal of indole than quinoline was attributed to the higher electron density of nitrogen atom in indole whereas low ODN activity of carbazole was ascribed to the steric hindrance caused by the aromatic rings.

2.5.4 Effect of nitrogen compounds on ODS

In order to achieve deep desulfurization, several researchers studied effect of nitrogen compounds on ODS activity. Though concentration of nitrogen compounds is very less in liquid fuels but their presence severely inhibit the ODS process. Otuski et al. (2001) reported the influence of nitrogen compounds, olefins, and aromatic hydrocarbons on

ODS of DBT. It was found that ODS of DBT was not effected by presence of aliphatic and aromatic hydrocarbons. However, the presence of indole and olefin (diisobutylene) reduced the ODS activity, and the decrease in ODS activity was ascribed to the higher reactivity of these compounds than DBT. Ishihara et al. (2005) reported oxidative desulfurization and denitrogenation in presence MoO_3/Al_2O_3 catalyst and TBHP as an oxidant, and it was observed that ODN reduced ODS activity in the following trend: indole > quinoline > acridine > carbazole. Caero et al. (2006) reported that oxidation activity of sulfur compounds in presence of nitrogen compounds decrease in the following pattern: quinoline > indole > carbazole. To describe the inhibition effect, consecutive adsorption of quinoline and DBT catalyst was assed with the help of FTIR, and it was found that quinoline displaced the DBT from the active sites. Jia et al. (2009) studied the oxidation of sulfur compounds in presence of nitrogen compounds with the aid of TS-1 and hydrogen peroxide. It was observed that thiophene removal was severely inhibited by presence of pyridine and pyrrole. However, the presence of quinoline and indole didn't influence the final removal rate of thiophene. Presence of quinoline, indole and carbazole reduced the oxidative removal of BT and DMDBT. The decrease in ODS activity due to the presence of nitrogen compounds was attributed to the strong adsorption of nitrogen compounds and its oxidized products on active sites of catalyst. Ti incorporated SBA-15 was employed for ODS of refractory sulfur compounds in presence of TBHP, effect of nitrogen compounds, aromatics, and aprotic solvent on ODS was also studied (Cho and Lee 2014). They observed that presence of nitrogen compounds inhibit the ODS in the following order: indole > quinoline > carbazole. It was found that addition of aromatics and aprotic solvent significantly improved the ODS activity due to the high solubility of oxidized sulfur and nitrogen compounds in the aromatics and aprotic solvent, which eventually aids in maximizing the number of active sites.

Table 2.5 ODS and ODN of organosulfur and nitrogen compounds under the optimum reaction conditions.

Oil soluble oxidant									
Model oil	Contaminant	Oxidant	Catalyst	System	C_o (ppm)	Temperature (°C)	Pressure (atm)	% removal	Reference
Kerosene	DBT	TBHP	16wt.% Mo/Al_2O_3	FBFR	55	110	1	86	Wang et al. (2003)
Decalin, Light gas oil	Quinoline	TBHP	16wt.% MoO_3/Al_2O_3	FBFR	20,13.5	80	1	70,94	Ishihara et al. (2005)
Toluene	DBT	CHP	MoO_3-CeO_2-SiO_2	FBR	-	40	1	97	Zhang et al. (2009)
Decalin	Carbazole	TBHP	MoO_3 /D113	BR	300	90	-	74.3	Zhou et al. (2010)
Decalin	DBT	CHP	P-MoO_3/SiO_2	FBR	298	50	1	92	Han et al. (2013)
Decane	Indole,Quinoline ,Carbazole	TBHP	Ti-SBA-15	BR	50 each	80	-	100,~20,~ 10	Cho and Lee (2014)
Decalin	DBT	TBHP	MCM-41	BR	500	80	1	-	Wang et al. (2014b)
n-Octane	DBT	CHP	Mo/MMS	BR	500	103	1	98	Qiu et al. (2016)
Tetradecane+ Hexane+tolu ene	DBT,MDBT,D MDBT	CHP	MoO_3/Al_2O_3	BR	820,806, 879	75	-	< 95	Safa and Ma (2016)
Ethanol	Quinoline	TBHP	V_2O_5/SiO_2	BR	172	70	-	78	Ogunlaja et al. (2017)
Iso-Octane	DBT, Indole, quinoline	TBHP	MoO_3/MCM-41	BR	600, 50,50	90	1	94, 69, 36	Present study

Iso-Octane	DBT, Indole, quinoline	TBHP	ExtMCM-41	BR	1000, 50,50	90	1	93,78, 48	Present study
Oil insoluble oxidant									
Model oil	Contaminant	Oxidant	Catalyst	System	C_o (ppm)	Temperature (°C)	Pressure (atm)	% removal	Reference
Diesel	-	H_2O_2	Mo/γ Al_2O_3	BR	320	80	1	96	García-Gutiérrez et al. (2008)
Gasoline, diesel, Toluene+ Hexane	DBT	H_2O_2	H_2SO_4 +acetic acid	-	670,10 45,500	80	-	84,92 ,98	Ali et al. (2009)
Petroleum ether	DBT,DMDB,BT	H_2O_2	HPW/TiO_2	BR	500	60	1	100,97, 94	Yan et al. (2009)
Iso-octane	DBT	H_2O_2	Chromium promoted sulfated Zirconia	BR	800	60	-	79	Kumar et al. (2011)
Toluene	Indole,Quinoline ,Carbazole	H_2O_2	$[Bmim]_3PMo_{12}O_{40}/SiO_2$	BR	2000	60	-	80,50,2 0	Zhang et al. (2011)
n-Octane	DBT	H_2O_2	$C_{18}H_{37}N(CH_3)_3]_4[H2Se^{IV}_3W_6O_{34}]$/ MCM-41	BR	500	45	-	98	Xie et al. (2015)
n-Decane	DBT,BT,DMDBT	H_2O_2	$NaHCO_3$,resin	BR	500,25 0,250	25	1	>99	Bokare and Choi (2016)

n-Octane	DBT,DMDBT	H_2O_2	Ti-modified hierarchical mordenites	BR	1000, 300	60	-	98,61	Leng et al.(2016)
Cyclohexane	Quinoline	H_2O_2	Fe/C and FeMo/C	BR	50	25	1	100	Mambrini et al.(2017)

2.6 Research gaps

A comprehensive literature survey was carried out to better understand all the technologies available for the desulfurization and denitrogenation of liquid fuels. On the basis of literature reviews following research gaps have been identified.

- Limited work has been reported by using MCM-41 as a catalyst for the removal of sulfur and nitrogen compounds from liquid fuels using the oxidative technique.
- No research work has been carried out by employing MCM-41 derived from coal fly ash for desulfurization and denitrogenation of liquid fuels.
- No work has been reported for removal of sulfur and nitrogen compounds on modified activated carbon with organic acid and metal species (molybdenum and cobalt).
- Only few studies were carried out for simultaneous adsorptive removal of sulfur and nitrogen compounds. However, no studies have been reported on simultaneous adsorptive removal of sulfur and nitrogen compounds by employing response surface methodology.

CHAPTER 3 MATERIALS AND METHODS

This chapter contains information about chemicals, materials, and model oils employed for conducting the research work. It describes the synthesis procedure of catalysts and adsorbents used in the experimental studies, and the details of characterization techniques employed to explore the physico-chemical characteristics of synthesized catalysts and adsorbents. Characterization of adsorbents and catalysts were performed at Materials Research Center, MNIT, Jaipur and the BET surface area analysis was done at Indian Institute of Technology Madras, Chennai. The information about the experimental setup used in the oxidative process is also included and it also explains the typical experimental procedure for the oxidative and adsorptive process. The analytical procedure for determining the concentration of sulfur and nitrogen compounds in model gasoline is also described in this chapter. It also contained information about the models used for adsorption isotherm study, kinetic study, and thermodynamic study.

3.1 Materials and reagents

All the chemicals employed in the present study were of analytical reagent grade. CFA was collected from a nearby thermal power plant, Kota, Rajasthan, India. Isooctane (≥ 99 % purity) and sodium hydroxide were obtained from Fisher Scientific, India and DBT was procured from HiMedia, Bombay, India. Ammonium molybdate tetrahydrate (98 %), granular activated charcoal, and cetyl trimethyl ammonium bromide (CTAB) (99 %) were procured from Loba Chemie, Bombay, India. Ammonium hydroxide (aqueous solution, 25%) and tert-Butyl hydroperoxide (aqueous solution, 70%) were obtained from Vetec and Alfa Aesar, respectively. Cobalt nitrate hexahydrate (99 %) and glacial acetic acid were purchased from Fisher Scientific, Mumbai, India, and Merck, Mumbai, India, respectively. Indole and quinoline were obtained from HPLC lab reagents, India and Sigma-Aldrich, India respectively.

3.2 Model gasoline

For the desulfurization experiments, model oil was prepared by mixing an appropriate quantity of DBT in iso-octane. The model oil was prepared on weight by volume ratio

(W/V) by adding an appropriate quantity of DBT (50 mg/l to 2000 mg/l) in iso-octane solution. For the denitrogenation experiments, model oil was prepared by adding nitrogen contaminants (indole /quinoline) in iso-octane. Model fuel oil was prepared by adding indole (50 – 1000 mg/l) or quinoline (50 – 1000 mg/l) in iso-octane solution. For the simultaneous desulfurization and denitrogenation experiments, model oil was prepared by mixing the required amount of both DBT and indole compounds in iso-octane solution (w/v)".

3.3 Synthesis of catalysts for oxidative process

3.3.1 Synthesis of Mo/MCM-41

Two-step synthesis procedure was adopted for the preparation of the catalyst. Firstly, the support was synthesized, and in the next stage, active species were loaded onto the support to obtain the Mo/MCM-41 catalyst. Synthesis procedure of support is as follows. The amorphous silica present in CFA was used to synthesize mesoporous silica support (MCM-41). In order to obtain silica from CFA, the fusion method was adopted (Kumar et al., 2001). Accordingly, 1:1.2 weight ratios of CFA powder and NaOH pellets were mixed and kept in the furnace at 823 K for 2 h. The resultant product was cooled and grounded into fine powder, thereafter mixed with deionized (DI) water in the weight ratio of 1:4 under continuous stirring for one day. Subsequently, to get sodium silicate solution the solution was separated using the filtration process. The obtained sodium silicate solution was mixed with a surface directing agent (CTAB) and ammonium hydroxide. The resulting mixture was in suspension for 4 h with continuous stirring and the solution pH was maintained at ~10–11 using diluted H_2SO_4. After this, obtained gel was transferred into polypropylene bottle and kept in an oven for 2 days at 373 K. The resulting white solid was separated by filtration, washed repeatedly with DI water and dried in an oven at 333 K. The dried sample was calcined at 823 K for 5 h in an air atmosphere to remove the template; the resultant support is denoted as MCM-41.

Ammonium molybdate tetrahydrate was used as a precursor for molybdenum, and incipient wet-impregnation technique was adopted to load Mo on MCM-41. 1.0 g of MCM-41 was mixed with an aqueous solution containing the appropriate quantity of

ammonium molybdate tetrahydrate. Thereafter the obtained material was kept in an oven at 333 K, and then calcined at 823 K for 4 h in the furnace. The purpose of calcination is to convert Mo species loaded on the MCM-41 channels into their corresponding active metal oxides (MoO_3) species over the MCM-41 support. The synthesized catalyst was designated as Mo/MCM-41.

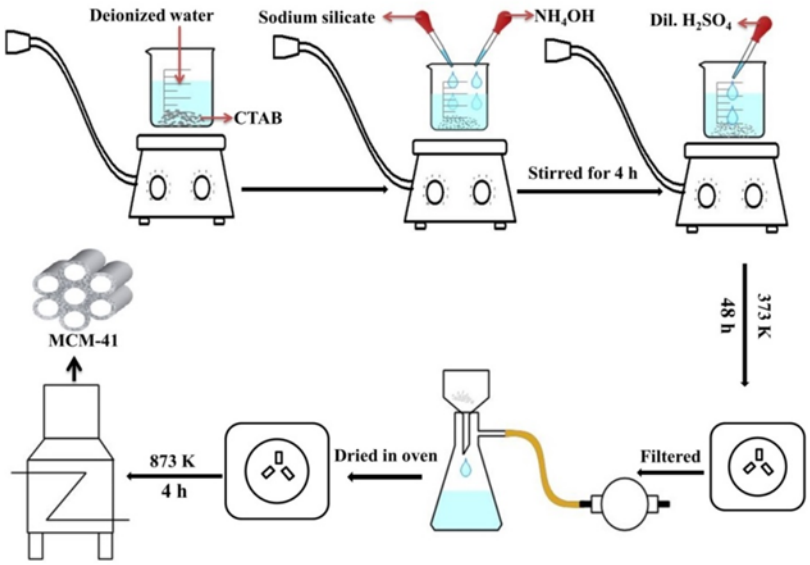

Figure 3.1 Synthesis procedure of MCM-41 from CFA

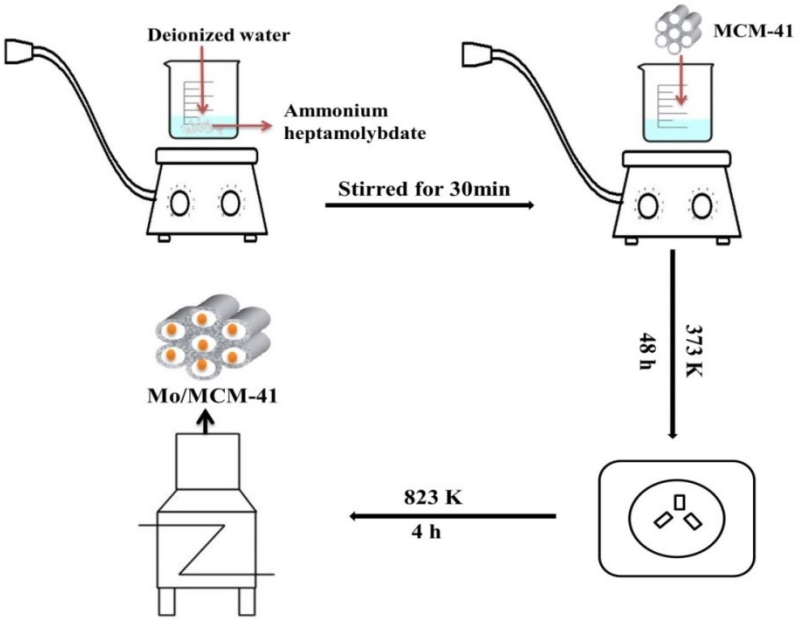

Figure 3.2 Synthesis procedure of Mo/MCM-41

3.3.2 Synthesis of ExtMCM-41

For the extraction of silica from CFA, fusion process was adopted (Kumar et al., 2001). NaOH pellets were mixed with CFA in a weight ratio of 1:1.2, the resultant mixture was kept in the furnace at 823 K for 2 h. Subsequently, the obtained alkali fused powder was grounded into fine powder and mixed with DI water in a weight ratio of 1:4 under continuous stirring for 24 h. The extracted supernatant solution was utilized as a silica precursor in the synthesis process of MCM-41. To synthesize MCM-41, surfactant (CTAB) was dissolved in DI water and the extracted silica precursor was added to it along with ammonium hydroxide. The resultant solution was kept under continuous stirring for 4 h, the pH of the solution was maintained at 10~11 with the aid of diluted sulfuric acid. The resultant gel was poured in a polypropylene bottle and kept in the oven at 373 K for 48 h. The solid product was recovered by filtration, washed with DI water, and kept for drying in an oven. To de-template, obtained sample (5 g) was mixed with a solution consisting of 8:1 volume ratio of ethanol and concentrated hydrochloric acid. The extraction process was carried out in a round bottom flask equipped with a reflux condenser; the resultant mixture was kept for stirring at 363 k for 8 h. Afterward, the mixture was filtered, washed with DI water and kept in a vacuum oven for drying. The obtained product was denoted as ExtMCM-41.

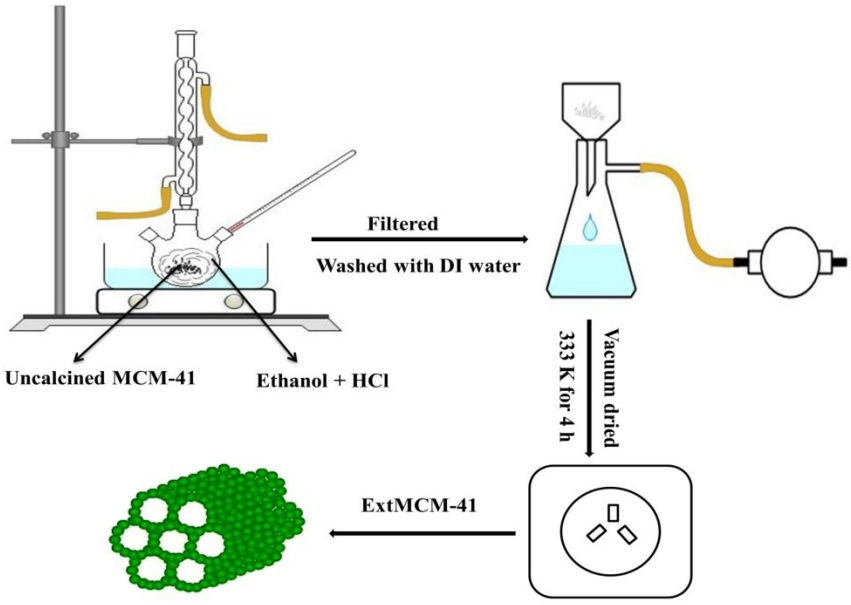

Figure 3.3 Synthesis procedure of ExtMCM-41

3.4 Synthesis of adsorbents for adsorptive process

3.4.1 Pretreatment of granular activated carbon (GAC) with acetic acid

GAC pores were activated by physical method, followed by a chemical method as mentioned below. Initially, GAC pores were activated by a physical method where GAC was soaked with hot DI water (383 K) for 1 h to remove the impurities present in the pores of GAC. The washed GAC was dried in an oven at 383 K to remove the moisture present inside the GAC. In the second step, GAC was activated through a chemical process, for this the dried GAC was pretreated at 323 K with acetic acid for 3 h. Chemically activated GAC was filtered and washed with plenty of DI water until the pH of the water became neutral. Washed GAC was kept in an oven for drying at 383 K for 10 h. The prepared sample was designated as ATGAC (acid-treated granular-activated carbon).

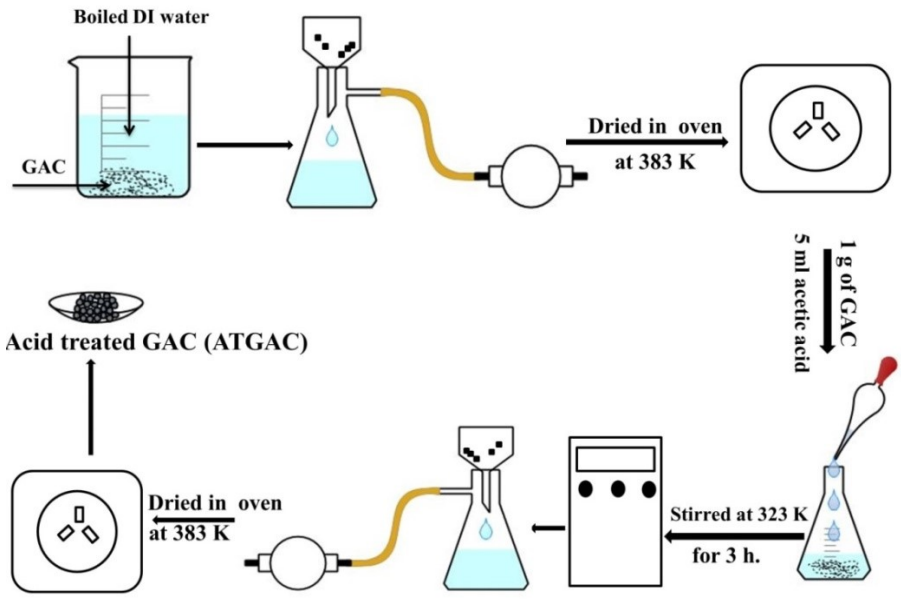

Figure 3.4 Pretreatement of GAC with acetic acid

3.4.2 Synthesis of cobalt impregnated ATGAC

Different weight ratios (1, 2, 3, and 4%) of cobalt active metal were loaded on ATGAC by using an incipient impregnation process where cobalt nitrate hexahydrate was used as

a precursor. After the impregnation of active metal on ATGAC, the samples were kept in an oven at 383 K for complete drying, followed by calcination at 573 K for 3 h. The resulting adsorbent was designated as 1 wt % Co/ATGAC, 2 wt % Co/ATGAC, 3 wt % Co/ATGAC and 4 wt % Co/ATGAC.

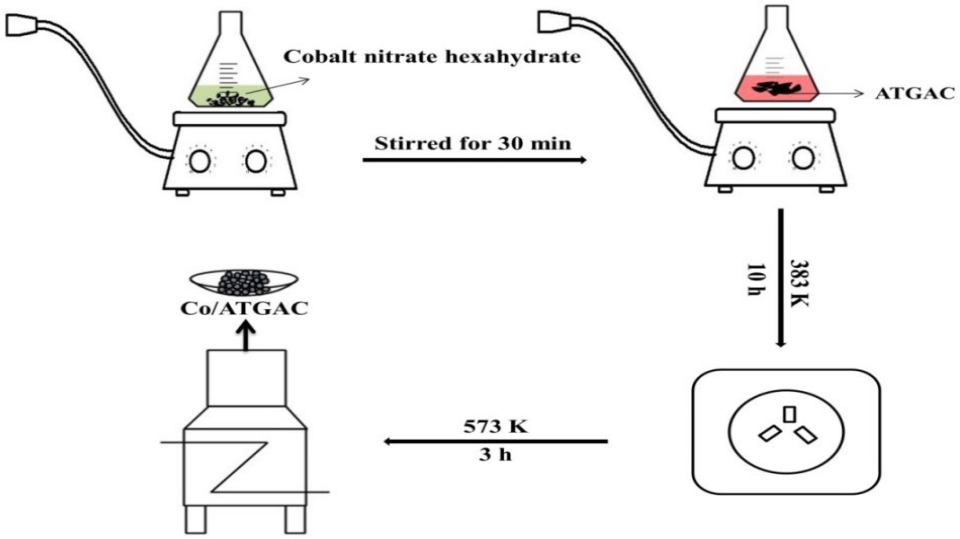

Figure 3.5 Synthesis procedure of Co/ATGAC

3.4.3 Synthesis of molybdenum impregnated ATGAC

ATGAC was impregnated with aqueous solution of molybdenum precursor (ammonium molybdate tetrahydrate). A stoichiometric amount of ATGAC was added to the corresponding metal salt solution and stirred at room temperature. Afterwards, the obtained samples were kept for drying in an oven followed by calcination at 573 K for 3 h. The synthesized adsorbent was designated as Mo/ATGAC for 1 wt % loading of active species. All adsorbents were stored in an airtight packet for further use.

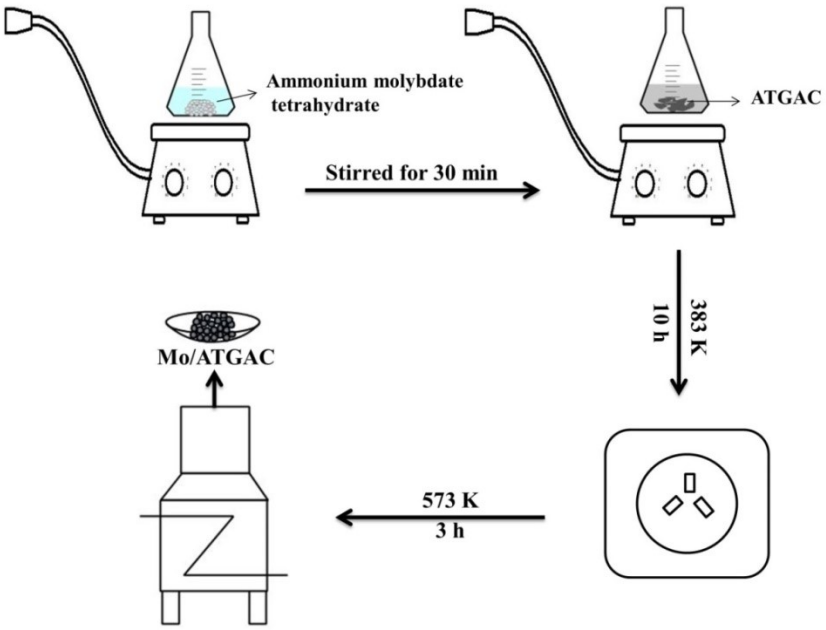

Figure 3.6 Synthesis procedure of Mo/ATGAC

3.5 Characterization techniques

The characterization study of synthesized samples is very important as it aids in determining its physical and chemical properties which are responsible for its performance in the process. The synthesized samples were characterized using various characterization techniques to explore the pore structure, surface area, surface morphology, structure and functional groups

3.5.1 SEM

SEM analysis was carried out using Nova Nano FE-SEM 450 (FEI) to understand the surface morphology of synthesized catalysts, adsorbents, and the dispersion of active species. Before the sample analysis, the sample was coated with gold to provide conductivity to the sample using spin coater (spin coating system, APEX).

3.5.2 TEM

TEM was performed to evaluate the internal structure of the synthesized sample using Tecnai G2 20 S-Twin, FEI Netherlands. Prior to the analysis, absolute ethanol was used to disperse the sample with the aid of ultrasonicator (Buehler Ultramet). Subsequently, a

droplet of the resultant solution was placed on a Cu grid covered with perforated carbon, and then the grid was mounted into the high-resolution microscope for analysis

3.5.3 XRD

XRD was carried out for the investigation of the bulk structure and to identify the chemical phase composition. XRD patterns of samples were collected on a Panalytical X Pert Pro apparatus. Small angle X-ray diffraction (XRD) patterns were recorded when the instrument was controlled at 40 mA, 40 kV, Cu-Kα radiation (k=1.54060 Å) as a target over a 2θ range of 1.5°–10° with a 0.02° step size and 4 s step time. For the wide angle XRD, the instrument was operated at 40 mA, 40 kV, Cu Kα radiation (k =1.54060 Å) as a target over a 2θ range of 10−90° with a 0.02° step size and 4 s step time. For the determination of phases present in samples, the obtained diffraction data was compared with the standards of Joint Committee on Powder Diffraction Standards card number inbuilt in PANalytical X'Pert HighScore software. Scherrer equation given below was employed to calculate the crystallite size.

$$D_P = \frac{0.94\lambda}{\beta_{1/2}\cos\theta} \tag{3.1}$$

Where D_p = Average crystallite size, β = Line broadening in radians. θ = Bragg angle, λ = X-ray wavelength

3.5.4 FTIR

FTIR is employed for the identification of the bonding patterns and functional groups present in the samples. FTIR spectra of samples were recorded with aid of FTIR spectrophotometer (FT-IR Spectrum 2, PerkinElmer) in the frequency range of 400−4000 cm^{-1}. Prior to the analysis, the sample was mixed with KBr to eliminate the scattering effects owing to the large crystals. Subsequently, translucent pellets of samples were obtained with the help of a KBr press (Model M-15, Technosearch Instruments). The pellets were then placed into the spectrophotometer to obtain the spectra with the aid of software inbuilt in the instrument.

3.5.5 XPS

The XPS analysis was used to explore the surface chemistry of samples by using an XPS spectrometer (Scienta Omicron) with a monochromatic Al Kα source. For the analysis, approximately 100 mg of sample was compressed into a wafer. For the deconvolution of spectra, Shirley baseline was subtracted in the fitting, and the Gaussian−Lorentzian peak shape was assumed to perform the curve fitting.

3.5.6 BET

The physical characteristics of the samples were studied by using ASAP 2020 (Micromeritics, USA). The BET method was used for the calculation of surface area, whereas the Barrett-Joyner-Halenda (BJH) was used to calculate pore volume and pore diameter using desorption branch of isotherms. For the GAC based adsorbents, samples were degassed at 473 K for 12 h to eliminate impurities whereas the mesoporous catalysts were degased at 623 K for 4 h.

3.6 Adsorption studies

3.6.1 Adsorption experiments

To understand the adsorption capacity of the modified GAC, batch ADS, ADN, and simultaneous ADS & ADN were performed with model oils containing DBT, Indole, and both, respectively. To perform adsorption process, a known amount of model oil was taken in a 100 ml conical flask (Borosil) and required amount of adsorbent was added into the flask under continuous stirring (140 rpm) in a constant temperature chamber (293−323 K). In the batch adsorption process, effect of varying parameters such as metal loading, initial concentration of sulfur & nitrogen compounds, contact time, adsorbent dosage, and temperature were observed. Influence of each operating variable was analyzed by keeping remaining variables constant. After the adsorptive process, model oil was filtered with the help of a polytetrafluoroethylene syringe (PTFE) filter (hydrophobic, 0.5 μm) and residual concentration of DBT and indole was analyzed using gas chromatography (GC) and UV-vis spectroscopy. Gas chromatograph (GC) (Trace 1310, Thermo Scientific, USA) equipped capillary column (TG-1MS: 60 m X 0.32 mm X 1 μm) with flame ionization detector, and UV−vis double-beam spectrophotometer (UV-

1800, Shimadzu, Japan) were employed for the analysis of residual concentration of DBT and Indole in model oil. For the analysis of residual concentration in GC, the injection was performed in splitless mode, the injector and detector temperature were maintained at 573 K and 593 K, respectively. Initially, the oven temperature was set to 343 K with a hold time of 1 min and it was increased with a ramp rate of 303 K/min until it reached 573 K with a hold time of 2.5 min. The concentration of DBT and indole were analyzed with a UV spectrophotometer by measuring absorbance at 320 nm and 266 nm, respectively. The percentage removals of DBT and indole were obtained using the following relationships Equation (3.2) & (3.3).

$$\text{DBT removal}\,\% = \frac{C_{OD} - C_{tD}}{C_{OD}} * 100 \tag{3.2}$$

$$\text{Indole removal}\,\% = \frac{C_{OD} - C_{tD}}{C_{OD}} * 100 \tag{3.3}$$

The equilibrium adsorption capacity of the adsorbent for DBT and indole is given by following Equations (3.4) & (3.5)

$$q_D = \frac{C_{OD} - C_{eD}}{m} * V \tag{3.4}$$

$$q_I = \frac{C_{OI} - C_{eI}}{m} * V \tag{3.5}$$

here, C_{oD} (mg/L) and C_{eD} (mg/L) represent the initial and equilibrium concentration of DBT in the model oil, C_{oI} (mg/L) and C_{eI} (mg/L) represent the initial and equilibrium concentration of indole in the model oil, m (g) is the amount of adsorbent and V (ml) is the volume of model oil.

3.6.2 Adsorption isotherms

Adsorption isotherms were analyzed to understand the relationship between the DBT/indole adsorbed on the surface of GAC based adsorbents and the equilibrium concentration of DBT/indole in the model oil. The adsorption isotherms were employed

to visualize the effectiveness of the adsorbents in reducing the sulfur/nitrogen content of model gasoline and they also aids in evaluating the mechanism of adsorption. Experimental equilibrium data of all GAC based adsorbents were studied with the help of various isotherms namely, Langmuir, Freundlich, Temkin, and Redlich-Peterson (R-P) adsorption isotherms.

3.6.2.1 Langmuir adsorption isotherm

This adsorption isotherm was proposed by Irving Langmuir in 1916. It is assumed that maximum adsorption is equivalent to the monolayer surface assimilation without any lateral interaction between the adsorbed molecules (Hameed et al., 2009). It is also based on the assumption that surface of the adsorbent is homogeneous, all molecules adsorbed through the same mechanism, and the heat of adsorption is not dependent on the surface coverage.

Langmuir isotherm model can be expressed in Equation (3.6)

$$q_e = \frac{q_m C_e K_L}{(1 + K_L C_e)} \tag{3.6}$$

Where C_e (mg/L) and q_e (mg/L) represent the equilibrium concentration and adsorption capacity, respectively. q_m (mg/g) and K_L are Langmuir equilibrium constant indicating the theoretical maximum adsorption capacity, and the affinity of the adsorbate molecules to bind with adsorbent respectively.

3.6.2.2 Freundlich adsorption isotherm

This isotherm model was developed by Freundlich in 1909. The model assumes multilayer adsorption on heterogeneous surface. It is based on the assumption that adsorption takes place on heterogeneous surfaces with different adsorption energies.

The mathematical expression of Freundlich model is shown in Equation (3.7)

$$q_e = \left(K_F C_e^{1/n}\right) \tag{3.7}$$

here, K_F and 1/n are the Freundlich constants indicating adsorption capacity and intensity, respectively. The value of adsorption intensity lies between 0 and 1. The magnitude of the adsorption intensity gives an indication of the favorability of adsorption. Values of n > 1 indicate favorable adsorption condition.

3.6.2.3 Temkin adsorption isotherm

The Temkin adsorption isotherm assumes that reduction in the heat of sorption is linear and the heat of sorption would reduce linearly with the coverage owing to the adsorbent/adsorbate interactions (Vijayaraghavan et al., 2006).

The mathematical expression of Temkin model is shown below equation (3.8):

$$q_e = B_T \ln(K_T) + B_T \ln(C_e) \tag{3.8}$$

here, B_T (J/mol), and K_T (L/g), are heat of sorption and Temkin isotherm constant, respectively.

3.6.2.4 Redlich-Peterson (R-P) adsorption isotherm

The R-P isotherm combined the features of the both Langmuir and Freundlich isotherms, and therefore finds applicability in both homogeneous and heterogeneous systems. (Brouers et al., 2015).

The following expression (3.9) represents R-P isotherm:

$$q_e = \frac{K_R C_e}{(1 + \alpha_R C_e^{\beta})} \tag{3.9}$$

where K_R(L/g), α_R(L/mg) and β are the Redlich-Peterson adsorption isotherm constants. When the value of β becomes 1, the Redlich-Peterson model transforms in to Langmuir adsorption isotherm, and if the value of the term $\alpha_R C_e^{\beta}$ reaches infinity model converts in to the Freundlich adsorption isotherm (Tong et al., 2018).

3.6.3 Adsorption kinetics

For designing and modeling of the adsorption process requires adsorption kinetic data. The kinetic data helps in explaining the rate of solute uptake which eventually controls the residence of adsorbate uptake at the interface of adsorbent and model oil (Ho and McKay, 1999). Two kinetic models were studied in order to gain a better understanding

about the reaction pathway and adsorption mechanism of DBT/indole molecules onto GAC based adsorbents. Pseudo-first-order and pseudo-second-order kinetic models are employed to analyze the experimental data in the studied adsorption systems.

3.6.3.1 Pseudo first order model

Pseudo-first-order model was given by Lagergren in 1898 to explain the adsorption of oxalic acid and malonic acid onto charcoal. It is assumed the adsorption process follows first-order equation. Maximum adsorption capacity corresponds to the monolayer of adsorbed molecules on the surface of adsorbent and the adsorption occurs on limited active sites without any interaction among the adsorbed molecules. Adsorption system follows pseudo-first-order kinetics when the adsorption is governed by diffusion through a boundary.

Pseudo-first-order model is expressed as

$$q_t = q_e(1 - e^{-k_1 t}) \tag{3.10}$$

here, q_e (mg/g) and q_t (mg/g) represents the adsorption capacity at equilibrium and at any time 't' during the adsorption process, and $k_1(min^{-1})$ indicates the rate constant of pseudo first order model.

3.6.3.2 Pseudo second order model

This model was first presented by Ho and McKay to explain the adsorption of metal species onto peat. It is based on the assumption that adsorbate uptake on the adsorbent is governed by a second-order rate reaction, and the adsorption process follows Langmuir equation. The rate determining step might be chemical adsorption which involves sharing or transfer of electrons between the adsorbent and adsorbate.

The mathematical form of pseudo second order model is expressed as:

$$q_t = \frac{k_2 t q_e^2}{(1 + k_2 q_e t)} \tag{3.11}$$

where, q_e (mg/g) and q_t (mg/g) represents the adsorption capacity at equilibrium and at any time 't' during the adsorption process, and k_2 ($g.mg^{-1}.min^{-1}$) elucidated the rate constant of pseudo second order model.

3.6.4 Adsorption thermodynamic study

Study of thermodynamic parameters includes assessment of Gibbs free energy change (ΔG°), enthalpy change (ΔH°), and entropy change (ΔS°).

Change in Gibbs free energy (ΔG°) in an ADS process is determined with the aid of equation (3.12).

$$\Delta G^o = -RT \ln K_D \tag{3.12}$$

Where R is universal gas constant, T represents the adsorption temperature in Kelvin, K_D indicates thermodynamic equilibrium constant, and can be expressed as q_e/C_e.

To determine ΔH° and ΔS°, a graph was drawn between ΔG° vs temperature using van't Hoff equation (3.13), and ΔH° and ΔS° were estimated from the values of intercept and slope, respectively.

$$\Delta G° = \Delta H° - T\Delta S° \tag{3.13}$$

3.6.5 Mathematical modeling

The classical optimization is a time-consuming process it requires a huge number of experimental data. In addition, it also fails to provide valuable information about the interaction between operating parameters. The drawbacks of the conventional optimization method can be overcome by statistical experimental design such as response surface methodology (RSM). RSM is an effective tool used for the development appropriate predictive model which can be implemented to various processing parameters even in existence of complex interactions between variables to explain the response variables and to obtain an optimum set of operating conditions in a very less time (Asfaram et al., 2015).

3.6.5.1 Central composite design

Response surface methodology (RSM) is an effective method for modeling and optimization of the process in an economical and competent manner. In the present study, a subset of RSM known as central composite design (CCD) was implemented to better understand the factor affecting the simultaneous adsorption of sulfur (DBT) and nitrogen (indole) compounds, and to obtain the optimum set of factors in order to get the maximum removal of DBT and indole from model oil. The benefits of CCD are listed below:

(a) The quantity of knowledge it delivers is similar to the three-level factorial method.
(b) Less experiments are requires as compared with full factorial design.
(c) It is a potent technique for narrating the most of the steady-state process responses.

CCD was applied by using Minitab software (version 17, Minitab Inc., USA), four adsorption parameters (temperature, adsorbent dose, the concentration of DBT and indole) with five levels affecting the removal of DBT and indole were studied. Generally, CCD is characterized by following experimental runs namely, 2^k factorial runs (k is the number of variables), 2k axial runs and number of central runs (Dashamiri et al., 2017). Replicates of the experiments at the center values of factors are significant as they give an idea about the experimental error. The axial points which are located at the equal distance from the design center provide rotatability to the model, which in turn guarantees that variance of the model, will be the same for all points. In the present study the total number of experiments (31) includes, 16 factorial points, 8 axial points, and 7 replicates at the center.

The mathematical association between the four independent factors and its response was modeled by a second-order polynomial equation consisting of linear, quadratic, and cross product terms as shown below:

$$y = \beta_0 + \sum_{i=1}^{k} \beta_i X_i + \sum_{i=1}^{k} \beta_{ii} X_i^2 + \sum_{i=1}^{k} \sum_{j=1}^{k} \beta_{ij} X_i X_j + \varepsilon \tag{3.14}$$

here, y is the predicted response, k is number of parameters, X_i and X_j are the coded parameters, β_o, β_i, β_{ii}, β_{ij} indicates regression coefficient for intercept, linear, and interaction terms, respectively, and ε represents a residual error.

For statistical calculations, following relationship was used to code the independent parameters.

$$X_i = \frac{x_i - x_o}{\Delta x_i} \tag{3.15}$$

Where, x_i is the actual value of independent variable, x_o is the actual value at the center point, X_i is the coded value and Δx_i is the step change value (Sarkar and Majumdar, 2011).

The analysis of variance (ANOVA) was employed to justify the adequacy of the developed regression model and the importance of parameters. Validation of the model was carried out by using F value and P value. When the F value is high and the P value is less than 0.05, it shows that the model and independent parameters are significant (Vafaei et al., 2018). The fit of the obtained models was expressed by the coefficient of determination (R^2). To evaluate the reliability of obtained CCD models, the analysis of residual plots (the difference between the predicted and experimental values) were carried out. Residual plots are used to describe the variation of the obtained model according to the normal distribution. A model is considered reliable if residuals are normally and randomly distributed. Response optimizer function available in Minitab software was used to optimize the response variables. For both DBT and indole, target values were set at 100 %, lower bounds were based on the lowest values of removal obtained for both compounds in CCD design, and upper values were set at 110 % as it has to be more than the target value. The weights for both compounds were set at 1. The three-dimensional (3D) plots were used to show the interaction between the variables by holding two parameters at their central levels and changing the remaining factors. The slope of these plots indicates the sensitivity of the response to a particular factor. A relatively flat line represents that the response is unaffected by variation of that particular factor while a

steep slope shows that response is sensitive to that certain parameter (Bimakr et al., 2013).

3.7 Oxidation studies

3.7.1 Experimentation and analytical method

The experimental studies were performed in a 100 ml capacity of a three-necked round bottom reactor equipped with a total reflux condenser in order to prevent the loss of iso-octane vapor. The reactor setup was placed in a silicone oil bath, and bath temperature was maintained with help of hot plate with a magnetic stirrer (5 MLH REMI, India). In a typical oxidation process, at first, the model oil was heated to the desired temperature, once it reaches the desired temperature, the required quantity of oxidant and catalyst were added into the reactor to initiate the reaction. After the oxidative process, model oil was filtered with the help of a PTFE syringe filter (hydrophobic, 0.5 μm) to remove the catalyst from the reaction mixture and filtered reaction mixture was analyzed using gas chromatography and the method is described in section 3.6.1.

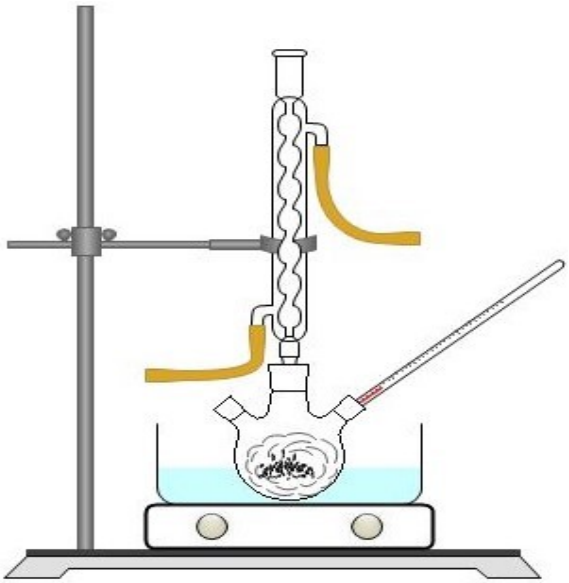

Figure 3.7 Schematic diagram of experimental setup

3.7.1.1 Reusability of catalyst

In order to make the ODS process economic and environmentally feasible, it is mandatory to study the regeneration potential of used adsorbent. The reusability study was conducted under optimized operating conditions. After the desulfurization reaction, the catalyst was separated from the oxidized model oil by employing filtration technique. The spent catalysts were regenerated under naptha atmosphere at room temperature for 30 min with continuous stirring of catalyst in methanol to desorb sulfur compounds. Subsequently, the resultant mixture was filtered and dried at a temperature of 363 K for 4 h, and then the regenerated catalyst was reused for the next cycle.

3.7.1.2 ODN of model oil

ODN of the model oil containing nitrogen compounds (indole, quinoline) were conducted under the optimum operating conditions obtained in ODS process of DBT containing model oil.

3.7.1.3 Effect of nitrogen compounds on ODS

To investigate the effects of various nitrogen compounds on the desulfurization process, the oxidation runs were conducted for various model feed mixtures containing quinoline/indole, typical nitrogen compounds. The influence of nitrogen compounds on model gasoline was studied under optimum conditions obtained for ODS of DBT.

3.8 Oxidation process was carried out using mesoporous catalysts derived from CFA. Experiments conducted for oxidation process are summarized below:

3.8 Summary of experimental runs

Oxidation of DBT containing model oil was conducted using Mo/MCM-41 and conventional optimization technique is adopted to get optimum set of operating conditions for maximum removal of DBT. ODN of model was carried out at the optimum conditions obtained for the ODS of DBT using Mo/MCM-41 as a catalyst. ODS of model oil was conducted using ExtMCM-41 as a catalyst and the process is optimized using conventional optimization approach. ODN of model oil containing indole and quinoline was conducted using the optimized conditions obtained for DBT removal.

Adsorption process was carried out using metal species loaded GAC based adsorbents. ADS of DBT containing model oil were performed using Co/ATGAC and Mo/ATGAC adsorbents. Experiments were conducted using different loads of metal species to find out the optimum load on GAC and to obtain optimum adsorbent dose. Experiments at different temperatures with various concentrations of DBT were conducted to study the adsorption equilibrium and thermodynamics. Kinetic study was carried out using different concentrations of DBT at one temperature w.r.t time.

Similarly, ADN was performed by employing Co/ATGAC and Mo/ATGAC adsorbents. Experiment was conducted using different loads of metal species to find out the optimum load on GAC. Experiments were conducted to obtain optimum adsorbent dose. Experiments at different temperatures with various concentrations of indole were conducted to study the adsorption equilibrium and thermodynamics. Kinetic study was carried out using different concentrations of DBT at one temperature w.r.t time.

Simultaneous ADS and ADN was performed using the optimum adsorbent obtained for removal of DBT. Simultaneous adsorption was carried out with the help central composite design and 31 experiments were performed to obtain the optimum set of operating conditions.

CHAPTER 4 RESULTS AND DISCUSSION

This chapter enlightens about the desulfurization and denitrogenation potential of various adsorbents and catalysts synthesized in the present work through batch experiments. This chapter included the results of the physiochemical characterization of all catalysts and adsorbents used in the present study. Catalyst and adsorbents synthesized in the present research work have been employed for the oxidative and adsorptive removal of sulfur/nitrogen compounds from model oil, respectively. The effect of operating variables on the performance of ODS process (e.g., the effect of catalyst dose, temperature, oxidant to sulfur molar (O/S) ratio, an initial concentration of DBT) has been discussed in detail. In addition, kinetics and reusability studies were conducted, and plausible mechanism of oxidation of sulfur compounds is proposed. Effect of nitrogen compounds on ODS process is also investigated along with the ODN of model oil by using optimized ODS conditions. Adsorbents synthesized in the present study employed for the batch adsorptive desulfurization and adsorptive denitrogenation of model oil, and the results of these batch processes are described in this chapter. Various adsorption isotherms and kinetic models were investigated to understand the adsorption mechanism. Moreover, this chapter also included the plausible adsorption mechanisms which were proposed to better understand the interaction between adsorbent and adsorbate. Optimization studies by employing response surface methodology were conducted for simultaneous removal of sulfur and nitrogen compounds from model oil by using optimized adsorbents, and the developed CCD models which represent DBT and indole removal were discussed in this chapter.

4.1 Oxidative studies using mesoporous silica catalysts

For the oxidation process, mesoporous silica catalysts have been synthesized and investigated the catalytic oxidation of sulfur/nitrogen compounds from model oil. Generally, mesoporous silica catalysts are synthesized by using high-cost synthetic silica precursors such as n-alkyl amines, aerosol, n-alkoxysilanes, TEOS, and water glass. In order to make the process economic, low-cost silica source derived from coal fly ash was used to synthesize mesoporous silica. Synthesis of mesoporous silica by using CFA not

only makes the process economic but also addresses the issue of waste management of CFA. Two different synthesis methods were adopted for the synthesis of mesoporous catalysts derived from CFA. The catalytic performance of synthesized catalyst were investigated for the removal of sulfur and nitrogen compounds in model oil, they are discussed in detail in section 4.1.1 and 4.1.2.

4.1.1 Oxidative study using Mo/MCM-41

In this study, mesopourous silica MCM-41 derived from coal fly was used as a support material, and molybdenum was dispersed on its framework as an active metal species. The synthesis procedure of MCM-41 and molybdenum loaded MCM-41 (Mo/MCM-41) is described in section 3.3.1. As synthesized catalyst was characterized by using various characterization techniques and the results of the characterization techniques are discussed in below section (4.1.1.1).

4.1.1.1 Characterization of MCM-41and Mo/MCM-41catalyst

Characterization of support and catalyst was carried out in order to explore the physical and chemical characteristics of the synthesized catalyst. To understand the internal structure of synthesized support TEM analysis was performed. Figure 4.1 shows the TEM images of calcined MCM-41 taken along in two different directions with same magnification. It can be clearly depicted from Figure 4.1 the that MCM-41exhibited well-ordered hexagonal arrays of pore structure results obtained from the TEM images match well with the previously reported results for mesoporous MCM-41 (Kumar et al., 2001; Misran et al., 2007).

Nitrogen adsorption-desorption isotherm of MCM-41 and Mo/MCM-41 along with their pore size distribution are presented in Figure 4.2. The obtained isotherm of MCM-41 and Mo/MCM-41 is of type IV confirming the mesoporous nature of the catalyst. The Nitrogen adsorption–desorption isotherm conatained well defined hysteresis loop indicating the capillary condensation of nitrogen in mesopores (Bhagiyalakshmi et al., 2010). The pore size distribution of MCM-41 and Mo/MCM-41 indicates that the pores lies in the mesoporous range. The BET surface area of MCM-41 was found to be 605 m^2/g; monolayer volume and pore diameter were found to be 0.428 cm^3/g and 2.860 nm,

respectively. The BET surface area of MCM-41 was found to be 314 m^2/g; monolayer volume and pore diameter were found to be 0.323 cm^3/g and 3.16 nm, respectively.The surface area of MCM-41 was redcued significantly on incorporating the molybdenum species in MCM-41 framework. This could be due to the formation of non-framework MoO_3 species in framework of MCM-41.

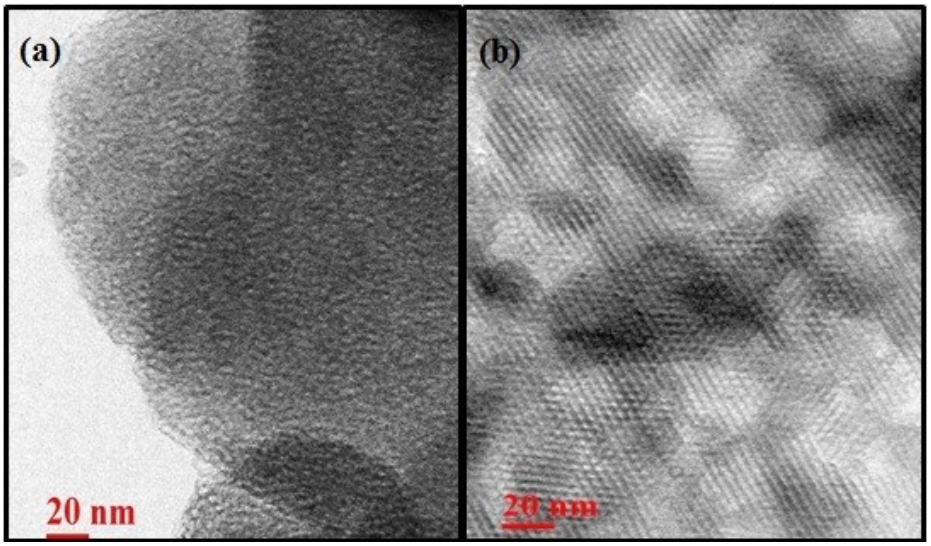

Figure 4.1 TEM images of MCM-41viewed (a) through the pore axis; (b) along the channel

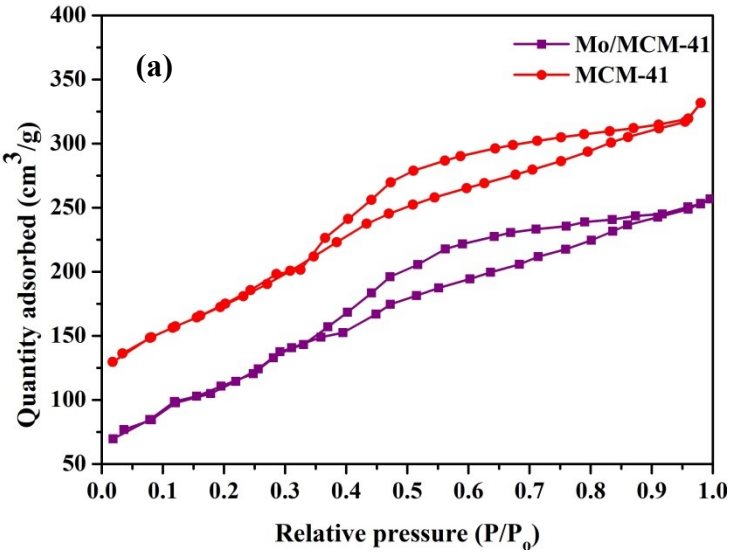

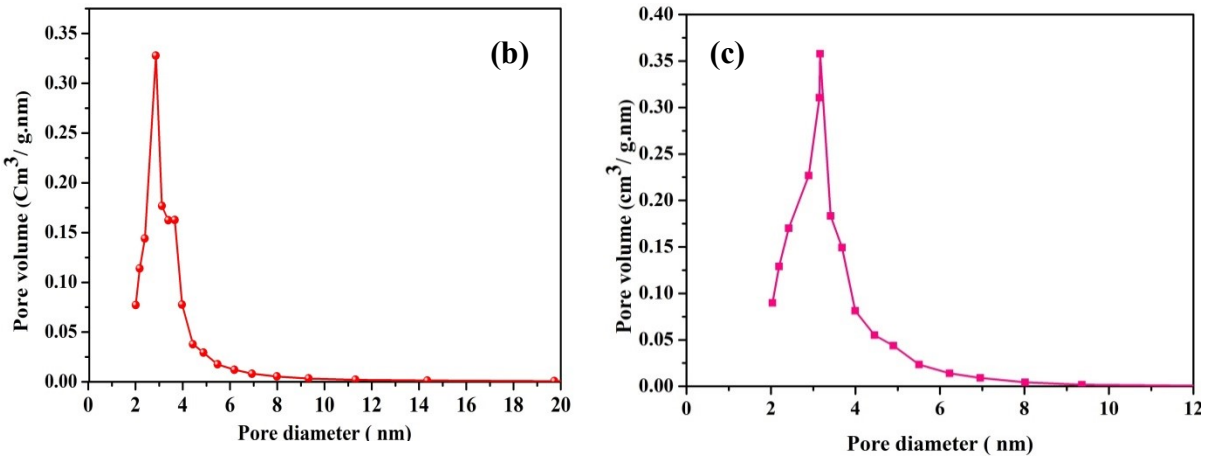

Figure 4.2 (a) Nitrogen adsorption desorption isotherm of MCM-41 and Mo/MCM-41, pore size distribution of (b) MCM-41 and (c) Mo/MCM-41.

The structure of the MCM-41and molybdenum impregnated MCM-41was studied with the aid of small angle XRD. The obtained low angle XRD pattern in the 2θ range of 1.5°–10° for uncalcined and calcined MCM-41 is depicted in Figure 4.3. The X-ray diffraction patterns of uncalcined and calcined MCM-41 exhibited well-ordered reflections at 2.1855° and 2.5592° respectively, ascribed to the reflection from (100) plane. These reflections are the prime feature of the hexagonal pore structure of typical MCM-41 materials (Dhokte et al., 2011). XRD results confirmed that synthesized MCM-41 possesses ordered hexagonal mesoporous structures, and this well-ordered hexagonal pore structure was retained after calcination also. The reflection from (100) plane moved to a higher 2θ angle in the surfactant-free MCM-41 owing to the reduction in interplanar d-spacing from 4.04 nm to 3.54 nm. It can be seen from the XRD pattern of Mo/MCM-41 that intensity of peak arised from (100) plane was decreased, and a broad peak was obtained as compared to calcined MCM-41. This might be due to the formation of non-framework MoO_3 species within the mesopores during calcination (Tang et al., 2016).

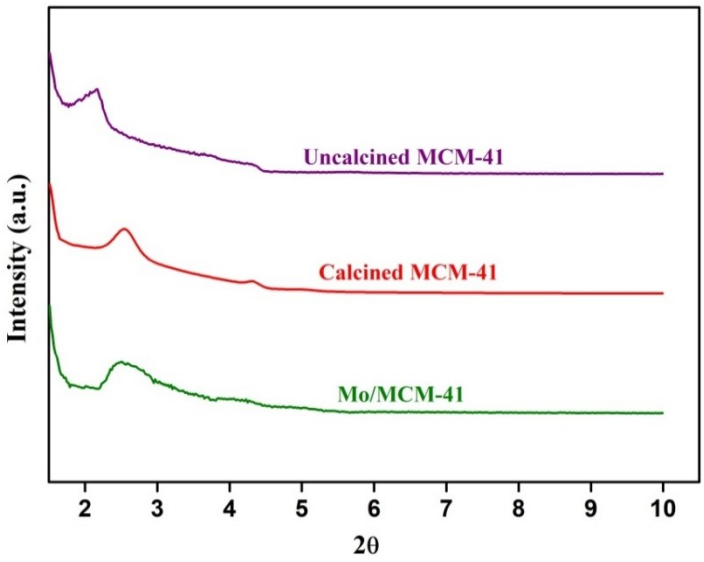

Figure 4.3 X-ray diffraction patterns of uncalcined, calcined MCM-41, and Mo/MCM-41.

SEM images of MCM-41and Mo/MCM-41are shown in Figure 4.4. It can be clearly seen from the images that MCM-41exhibits spherical top and tortuous as well as a ribbon-shaped particle. Morphology of synthesized MCM-41 is in good agreement with the literature (Asghari et al., 2016). The morphology of MCM-41is retained after loading of molybdenum, which depicts that molybdenum was successfully incorporated into the MCM-41 framework. Particle size of MCM-41 and MoMCM-41 were found to be 142 and 145 nm, respectively.

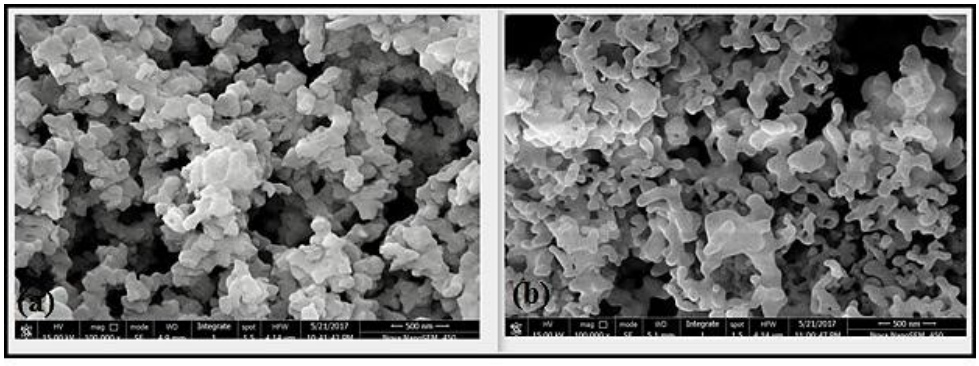

Figure 4.4 SEM images of a) MCM-41and b) Mo/MCM-41.

Figure 4.5 presents the FT-IR spectra of MCM-41 and Mo/MCM-41. Peaks at 1084 cm^{-1} and 800 cm^{-1} represented the asymmetric and symmetric Si–O–Si stretching vibrations (Shu et al., 2015). A peak at 462 cm^{-1} was due to the bending vibrations of $Si{-}O^{-}$ groups

on the catalyst surface, which represents the existence of the hexagonal mesoporous structure (Zhou et al., 2015). The adsorption band located at a wave number of about 1631 cm^{-1} can be attributed to the physically adsorbed water and a broadband around at 3400 cm^{-1} maybe due to the surface silanols and adsorbed water (Asghari et al., 2016). Compared with MCM-41 and Mo/MCM-41, a new peak appeared at approximately 905 cm^{-1} over Mo/MCM-41, it can be attributed to the formation of Si-O-Mo bonds (Shao et al., 2012). Obtained results confirmed that Mo species dispersed uniformly on MCM-41 framework.

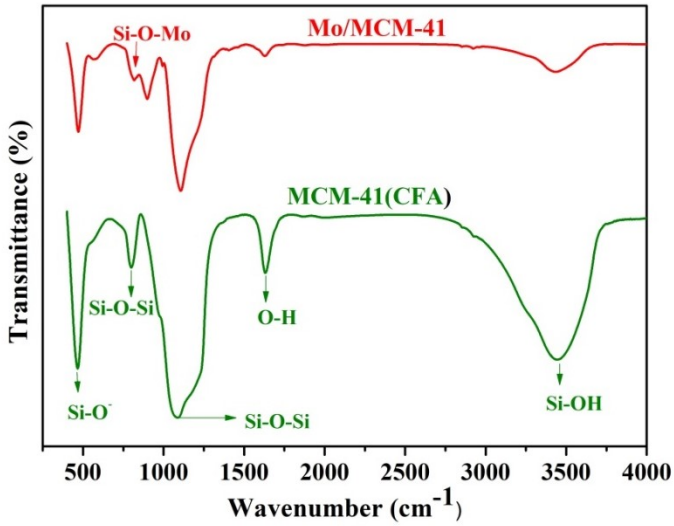

Figure 4.5 FTIR spectra of MCM-41and Mo/MCM-41.

4.1.1.2 Effect of metal loading

The effect of active metal (wt% of Mo on MCM-41) on ODS was investigated with different weight percentages of molybdenum (2.5 wt %, 5 wt %, 10 wt %, and 15 wt %) on MCM-41 framework. It was found that with an increase in active metal weight percentage the removal efficiency was increased i.e. 33%, 45%, 86% and 72% of DBT removal was obtained at 363 K, O/S- 2:1, catalyst dose-5 g/L, with an initial DBT concentration of 600 mg/L. The increase in removal efficiency due to increase in the active sites by increasing active metal weight percentage. Beyond the certain critical weight percentage (above 10 wt%) of active metal the removal efficiency of DBT was decreased from 86% to 72%, it may be due to pore blocking of active metal at higher weight percentage (15 wt%). However, at higher loading (15 wt%) multilayer dispersion

takes place on MCM-41 pore which leads to pore blocking and agglomeration there by decrease in available surface area for the oxidation of DBT (Yang et al., 2016). On the basis of above results an optimum load of 10 wt % was chosen for the further experimental study.

4.1.1.3 Effect of catalyst dosage

The effect of catalyst dose is a significant parameter in ODS process, and it also has an important impact on the operating cost of the ODS process. The effect of catalyst dose on the ODS of DBT was studied with the dose range of 5-15 g/L, whereas other operating parameters remained constant i.e. initial concentration of DBT 200 mg/L, temperature 363 K, reaction time of 3 h and oxidant/sulfur molar (O/S) ratio of 2:1. As seen in Figure 4.6, DBT removal rate rose significantly as catalyst dose enhanced from 5 g/L to 6 g/L, for further increase in catalyst dose up to 15 g/L, removal percentage was increased only slightly.

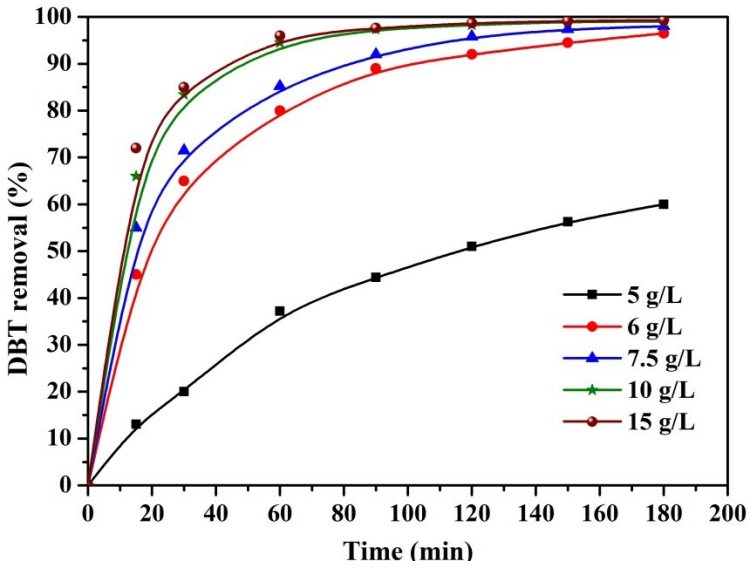

Figure 4.6 Effect of catalyst amount on removal of DBT (200 mg/L DBT solution, T = 363 K, O/S = 2.1, t = 3 h).

From the obtained results, only 60% of DBT removal was obtained at a catalyst dose of 5 g/L because lack of active/vacant sites availability for the oxidation of DBT and the available active sites were saturated with DBT molecules leading to a low removal. On increasing the catalyst dose from 5 g/L to 6 g/L, DBT removal rate was enhanced from

58% to 96% since higher dose provides more active sites, which in turn provides more chances for DBT molecules to come into contact with a catalyst to get oxidized. Nevertheless, the further increment in catalyst amount from 6 g/L to 15 g/L, the sulfur removal enhanced gradually since DBT containing model oil and active sites present on catalyst reaches equilibrium. Similar results were observed for the removal of DBT by chromium promoted sulfated zirconia (Kumar et al., 2012). From this study author conclude that catalyst dose of 6 g/L chosen to be the best dose and was used for further work.

4.1.1.4 Effect of initial concentration of DBT

DBT oxidation was conducted at different initial concentrations ranging from 200 mg/L to 800 mg/L, while other experimental conditions, i.e. catalyst dose 6 g/L, O/S ratio molar ratio of 2:1, 363 K, and 3 h were kept as a constant. As seen in Figure 4.7, when the initial concentration of DBT enhanced from 200 mg/L to 800 mg/L, the percentage removal of DBT decreased substantially from 96% to 81%. For a fixed dose, the active sites are the limited quantity for the oxidation of DBT. With an increase in the initial concentration of DBT beyond optimal concentration, the percentage removal of DBT was observed to declined due to insufficient sites for DBT oxidation (because catalyst dose was in fixed quantity). For further optimization study, DBT concentration of 600 mg/L was chosen as the optimum dose for 6 g/L of catalyst dose.

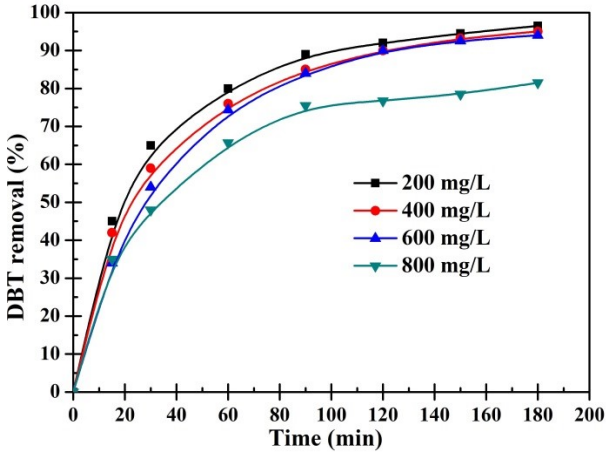

Figure 4.7 Effect of initial concentration of DBT (200 – 800 mg/L DBT solution, catalyst dose = 6 g/L, T = 363 K, O/S = 2.1, t = 3 h).

4.1.1.5 Effect of oxidant/sulfur molar ratio (O/S)

In order to gain more understanding, the effect of oxidant i.e O/S ratios on ODS with the presence of Mo/MCM-41 catalyst was studied. Experiments were performed at different O/S ratios in the range of 1:1 to 5:1 using TBHP at 363 K, 3 h reaction time. According to the stoichiometry of oxidative desulfurization of DBT reaction i.e. 1 mole of DBT would require 2 moles of TBHP to oxidize into DBT sulfone. Figure 4.8 depicted that the removal of DBT rose significantly with an increment in the O/S molar ratio, DBT removal was raised from 55% to 94%, when O/S ratio enhanced from 1:1 to 2:1 (Figure 4.8). Upon further increase in O/S up to 5:1, the final removal percentage was observed almost constant without appreciable change in final removal percentage but an increase in O/S molar ratio resulted in reaction equilibrium very quickly from 3 h to 15 min (Prasad et al., 2008). It was found from the present study that beyond certain value of O/S, the removal was insignificant for 3 h of reaction time. Similar observations were made by Wang et al. (2014b) for ODS of DBT using ordered mesoporous silica as a catalyst and TBHP as an oxidant. In subsequent studies O/S ratio of 2:1was chosen as an optimum ratio for an initial concentration of DBT 600 mg/L with 6 g/L of catalyst dose.

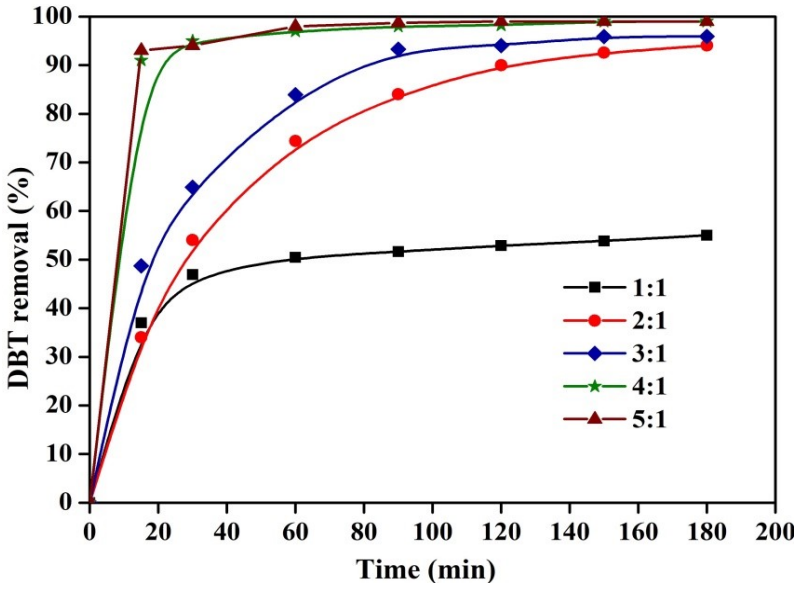

Figure 4.8 Effect of O/S ratio on DBT removal (600 mg/L DBT solution, catalyst dose = 6 g/L, T = 363 K, t = 3 h).

4.1.1.6 Effect of temperature

In ODS process operating temperature play a pivotal role in desulfurization of organic sulfur from fuel oil. ODS process was conducted at various operating temperatures and times to understand the significance of reaction temperature. As seen in Figure 4.9, the removal of DBT was enhanced by an increase in the temperature from 323 K to 363 K, and decreased on further increase in the temperature. However, the operating temperature has a significant influence on DBT oxidation during the different time range. As reaction temperature enhanced from 323 K to 363 K, the percentage removal of DBT rose to 94%. The reason for this remarkable improvement in removal might be attributed to the movement of molecular speeding up at high temperature, which may provide more reaction probability between DBT and oxidant (Abdullah et al., 2016; Qiu et al., 2016)..

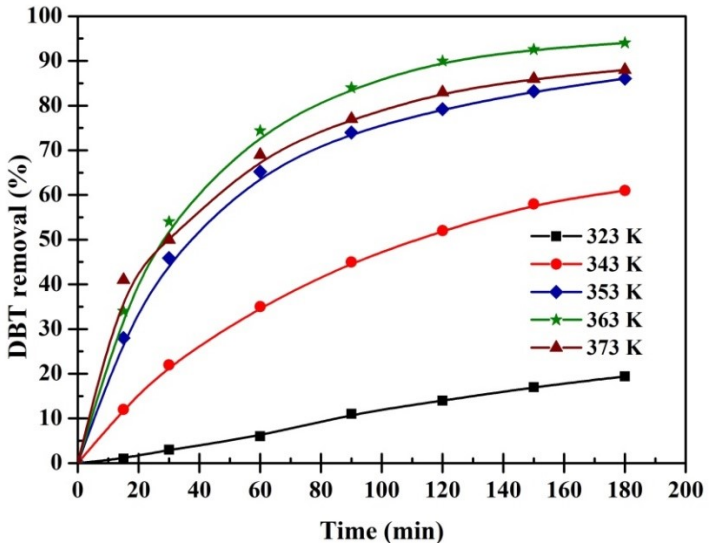

Figure 4.9 Effect of temperature on removal of DBT (600 mg/L DBT solution, catalyst dose = 6 g/L, T = 363 K, O/S = 2.1, t =3 h).

Higher temperature not only aids in accelerating the reaction but also promotes desorption of $DBTO_2$ which is formed during the ODS process and creates the vacant position of the active site for new molecule oxidation. Only 20% removal was observed at 323 K this may be due to the fact that the final product ($DBTO_2$) was more polar than DBT so as to easily adsorb on catalyst active sites at a lower temperature (Wang et al., 2014b). Furthermore, when ODS study was carried out at 373 K, oxidation of DBT decreased remarkably because of low thermal stability of TBHP at a higher temperature (Wang et

al., 2003). In this study an optimal temperature, 363 K was chosen as optimum temperature for further study

4.1.1.7 Kinetic study of ODS

In order to analyze the kinetics of DBT, ODS of model fuel was carried out at various temperatures while remaining operating parameters kept constant i.e. O/S ratio of 2:1, DBT concentration 600 mg/L, catalyst dose 6 g/L. Several authors suggested that oxidation of DBT through ODS method follows the pseudo-first-order kinetics (Kumar et al., 2012). Obtained experimental data was analyzed with pseudo-first-order and pseudo-second-order kinetics. The values of k_f and k_s are summarized in Table 4.1 from pseudo-first-order kinetics and pseudo-second-order kinetics. Further, pseudo first-order kinetics was found to be good with the correlation coefficients (R^2>0.99) with the experimental data when compared with second-order kinetics. In addition, the apparent rate constant k_f enhanced as the temperature increased which indicates that the oxidative process follows pseudo-first-order kinetics (Li et al., 2017). Therefore, the DBT oxidation by Mo/MCM-41 catalyst is well described by pseudo-first-order reaction kinetics. Arrhenius equation (ln k versus 1/T plot) was used to calculate the apparent activation energy (E) from the slope of Arrhenius plots. The activation energy for the DBT oxidation by Mo/MCM-41 was found to be 84 kJ/mol for the first order and 108 kJ/mol for the second order kinetics. The activation energy of ODS reaction was much lower than that of conventional HDS process, which may be due to the fact that ODS process was carried out at a much lower operating temperature (<363 K) when compared with HDS process (523-573 K) (Wang et al., 2004). Furthermore, the high apparent activation energy for DBT oxidation in the presence of Mo/MCM-41 using TBHP oxidant implies that the tested (present) system is highly sensitive to the temperature. The kinetic study is in good agreement with the present experimental results. More than 70 % of DBT was oxidized within 60 min of reaction time at a temperature of 363 K whereas insignificant removal was observed in a reaction time of 60 min at 323 K. The obtained results were in good agreement with Safa and Ma (2016) for the oxidation of DBT over Mo/Al_2O_3 catalyst using cumene hydro-peroxide as an oxidant.

Table 4.1 Kinetic and thermodynamic properties of DBT oxidation by ODS process using TBHP oxidant.

Temperature (K)	Pseudo-first order			Pseudo-second order		
	K_f (1/min)	R^2	E_a (kJ/mol)	k_s (l/mg.min)	R^2	E_a (kJ/mol)
323	9×10^{-4}	0.9938	84	5.43×10^{-6}	0.9936	108
343	1.10×10^{-2}	0.9994		1.51×10^{-5}	0.9994	
353	2.34×10^{-2}	0.9987		1.71×10^{-4}	0.9839	
363	2.42×10^{-2}	0.9991		4.06×10^{-4}	0.9725	

4.1.1.8 Reusability of Mo/MCM-41

Reusability of the catalyst was carried out at optimum operating conditions. After first cycle the catalyst was regenerated under methanol atmosphere at room temperature for 30 min with continuous stirring of catalyst in methanol to desorb sulfur compounds. Subsequently, resultant mixture was filtered, and dried at a temperature of 363 K for 4 h, and the regenerated was reused for the next cycle. Figure 4.10 depicted the reusability of catalyst, it conclude that almost stable performance of catalyst with marginal decrease in efficiency from 94% to 92% in 3 cycles, and the decrease in performance might be due to the leaching of Mo species in reaction media. However, the obtained results showed that catalyst can be successfully reused without significant loss in its catalytic activity.

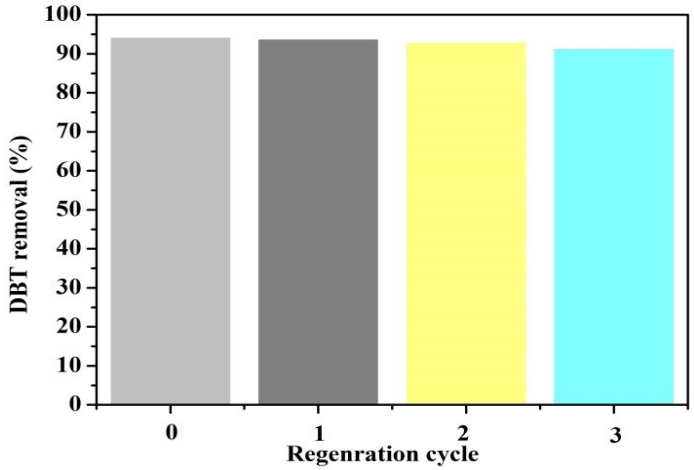

Figure 4.10 Regeneration ability of the Mo/MCM-41 catalyst at optimum operation conditions (600 mg/L DBT solution, catalyst dose = 6 g/L, T = 363 K, t = 3 h, O/S = 2:1)

4.1.1.9 Proposed desulfurization mechanism

Oxidation of DBT in the presence of Mo/MCM-41 using TBHP as an oxidant can be explained as follows: ODS reaction may start initially through the generation of pseudo-cyclic structure with the aid of Mo species and TBHP as shown in Scheme 4.1. Generation of nascent oxygen takes place owing to the coordination of polarized Mo-O bond with the peroxide. Sulfur atom present in DBT is electrophilically attacked by nascent oxygen to produce DBT sulfoxide, which acts as an intermediate radical during the ODS process, tert-butanol produced as a byproduct and molybdenum species regenerated. Regenerated molybdenum species again form complex species with TBHP, and further oxidation of formed intermediate radical (DBT sulfoxides) into DBT sulfones by reacting again with nascent oxygen in a similar manner. The above studies were confirmed by measuring DBT concentration using gas chromatography with the retention time compared with those of pure compound and the corresponding peaks. Oxidized DBT compounds were identified using high-resolution mass spectrometry. In the MS study, samples before and after oxidation were tested. DBT was identified in the un-oxidized sample, and DBT sulfones was detected in the oxidized model oil (after reaction), whereas DBT peak was almost disappeared in the oxidized sample, GC chromatograms and HR-MS results are depicted in Figure 4.11. Generally, oxidation of DBT is known to be a series reaction where $DBT \rightarrow DBT-sulfoxides \rightarrow DBT-sulfones$. In the present study, no DBT sulfoxide was analysed in both GC and HR-MS analysis. Therefore, the rate determination step is $DBT \rightarrow DBT-sulfones$. On the basis of the obtained results, hereby the authors proposed DBT oxidation mechanism on Mo/MCM-41 catalyst in the presence of TBHP as shown in Scheme 4.2. The obtained results match well with previously reported findings by Wang et al., (2003) for the oxidation of sulfur compounds through ODS in the presence of MoO_3/Al_2O_3 catalyst using TBHP as an oxidant.

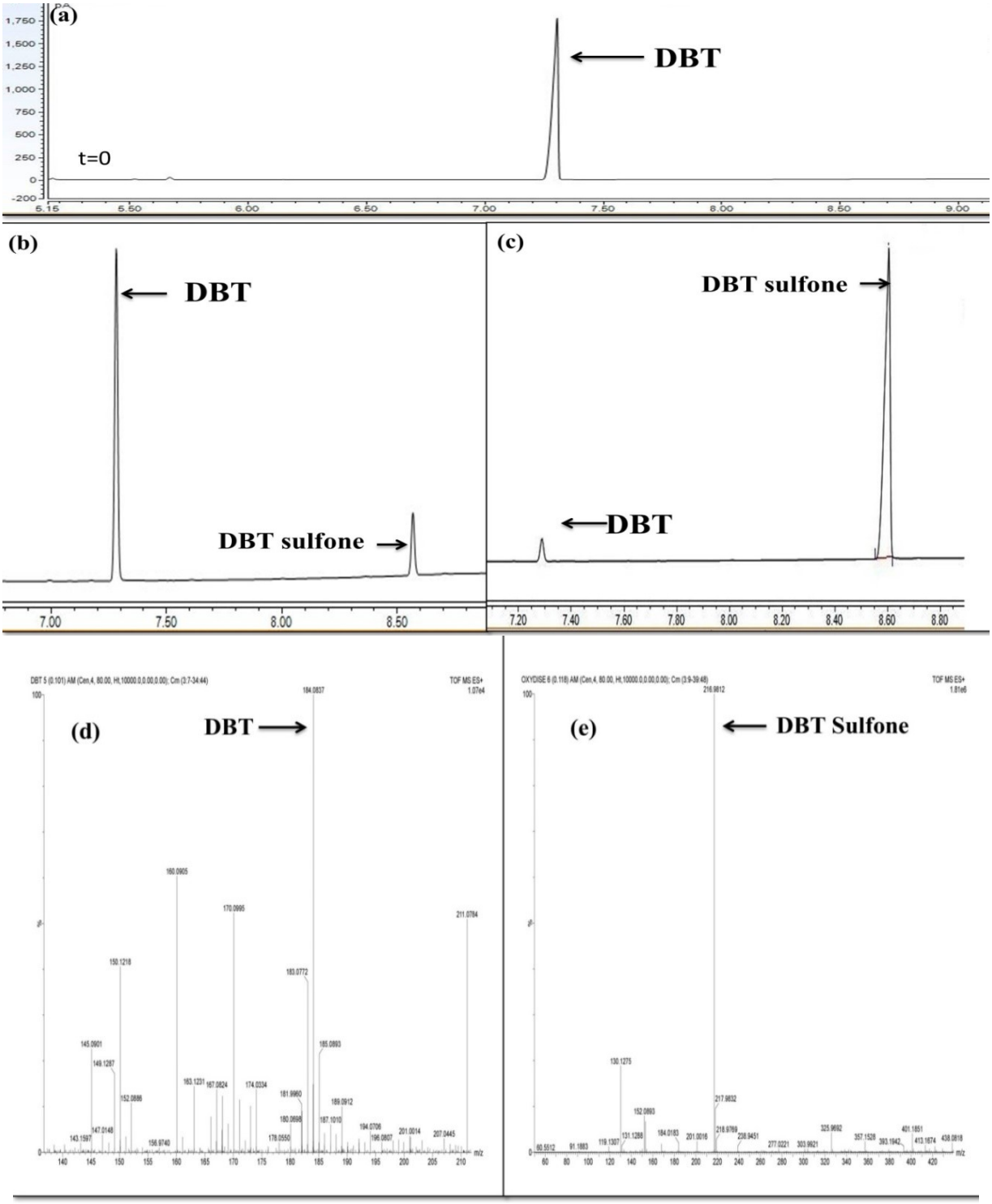

Figure 4.11 GC - chromatogram of a) model oil, b) treated model oil after t = 1 h, c) treated model oil after t = 3 h, and HR-MS results of d) model oil, e) oxidized model oil.

Scheme 4.1 Formation of pseudocyclic structure.

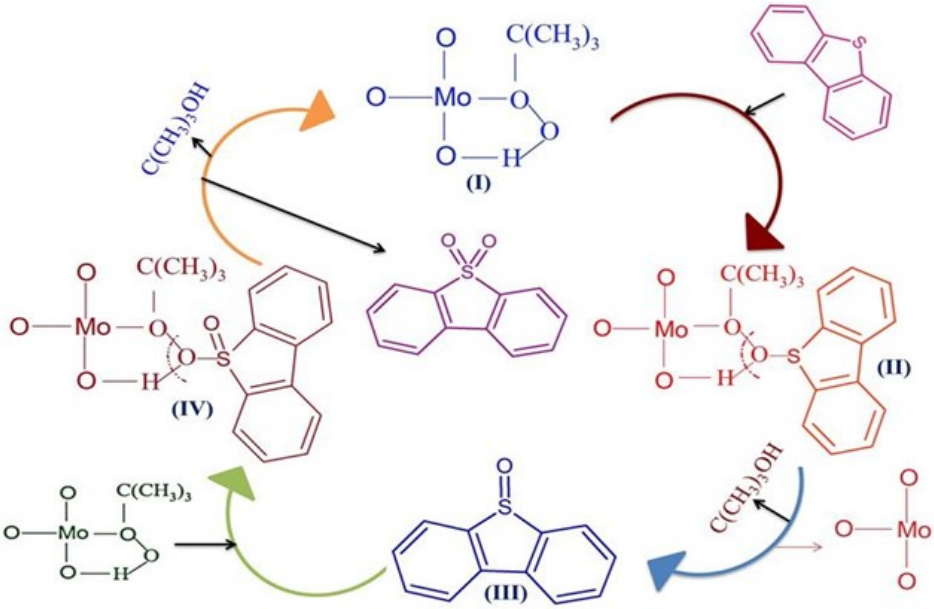

Scheme 4.2 Proposed reaction mechanism for ODS of DBT in presence of Mo/MCM-41.

4.1.1.10 ODN of model oil & effect of nitrogen compounds on ODS

ODN of model oil was carried out under the optimum conditions obtained for ODS of DBT. Composition of model oil used for the batch experiments of oxidative denitrogenation and simultaneous desulfurization and denitrogenation is shown in Table 4.2

Table 4.2 Composition of model feed oils.

Notation	Sulfur/nitrogen contaminant	Model Oil
MD	DBT (600 mg/L)	Iso-octane
MI	Indole (50 mg/L)	Iso-octane
MQ	Quinoline (50 mg/L)	Iso-octane
MDI	DBT(600 mg/L) + Indole (50 mg/L)	Iso-octane
MDQ	DBT(600 mg/L) + Quinoline (50 mg/L)	Iso-octane

ODN of model oil was carried out under the optimum conditions obtained for ODS of DBT. It can be seen from Figure 4.12 that indole (69%) was oxidized more as compared to the quinoline (36%). The better removal of indole was ascribed to the more electron density of nitrogen in indole (Zhang et al., 2011). Similar results were reported by Ishihara et al. (2005); it was shown that nitrogen compounds could be oxidized in the ODS system and oxidation activity decreased in the order: indole > quinoline. To investigate the effects of various nitrogen compounds on the desulfurization process, the oxidation runs were conducted for various model feed mixtures containing quinoline (MDQ) and indole (MDI), typical nitrogen compounds. ODS activity was declined severely in presence of nitrogen compounds as indicated in Figure 4.12. However, the presence of indole inhibited the ODS activity more as compared to the quinoline. Obtained results matches well with the previously conducted studies. For example, Cho and Lee (2014) studied the effect of nitrogen compounds on ODS activity over over Ti-SBA-15, and they demonstrated that nitrogen compounds inhibit the ODS process in the following order: indole > quinoline > carbazole. Ishihara et al. (2005) also reported that presence of nitrogen compounds inhibited the ODS process in the following trend: indole > quinoline > acridine > carbazole. The obtained results indicated that nitrogen compounds inhibited the ODS activity, which can be ascribed to the competition between sulfur and nitrogen compounds for the active sites. In addition, this reduction in ODS activity can also be attributed to the strong adsorption of nitrogen compounds and oxidation products of indole/quinoline on vacant sites of catalyst.

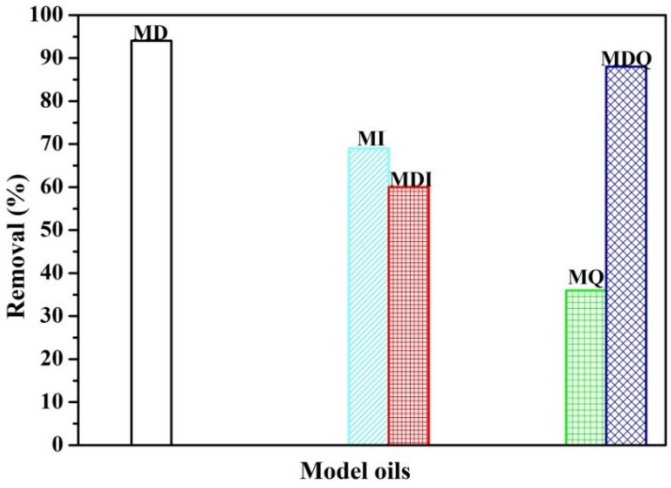

Figure 4.12 ODN of model oils (dose = 6 g/L, T= 363 K, O/N = 2:1, t = 3 h, Model oils = MQ, MI) & Effect of nitrogen compounds on ODS(dose = 6 g/L, T= 363 K, O/(S+N) = 2:1 , t = 3 h, Model oils = MDQ, MDI)

4.1.2 Oxidative study using ExtMCM-41

Mesoporous silica was synthesized from CFA via solvent extraction route. In the synthesis procedure, removal of the template was carried out by using solvent extraction rather than the conventional calcination method. Silanol groups available on the surface of mesoporous silica might act as catalytic active sites for the desulfurization process. Therefore, the amount of surface silanol groups present on the surface of catalysts is directly proportional to the ODS activity. In conventional synthesis process, calcination takes place at a higher temperature which results into the destruction of mesopores and also leads to the loss of active sites i.e surface silanol groups, whereas solvent extraction method occurs at very low temperatures (below 100 °C), which aids in preserving the mesoporous structure as well as the surface silanol groups. In addition, calcination requires a huge amount of energy which eventually makes the process costly. The synthesis procedure of mesoporous silica via solvent extraction route is described in section 3.3.2.

4.1.2.1 Characterization of ExtMCM-41 catalyst

A small-angle powder XRD pattern of the synthesized ExtMCM-41 is shown in Figure 4.13. ExtMCM-41 exhibited an intense diffraction peak at 2.1° arising from (100) plane, together with an additional peak at 3.6° arising from (100), and a very weak peak at 4.2°

(Sikarwar et al., 2018b). These reflections are the characteristic of the well-ordered hexagonal pore structure of typical MCM-41.

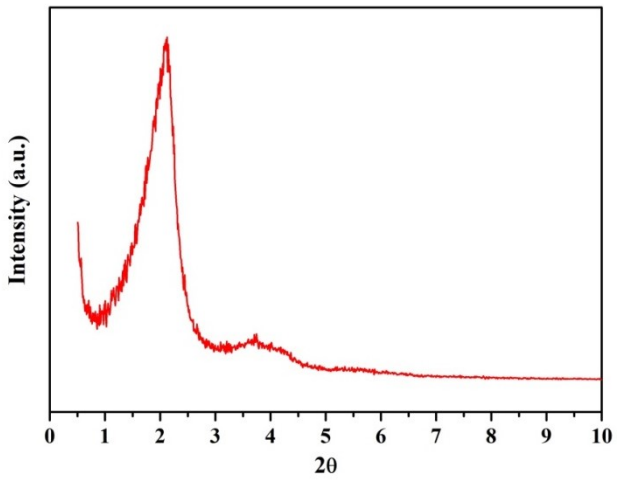

Figure 4.13 XRD pattern of ExtMCM-41.

Nitrogen adsorption-desorption isotherms are presented in Figure 4.14. The ExtMCM-41 exhibited type IV isotherms confirming the mesoporous nature of the catalyst. Figure 4.14 possess hysteris loop which indicates the capillary condensation of nitrogen in mesopores (Bhagiyalakshmi et al., 2010). The pore size distribution of ExtMCM-41 is presented in Figure 4.14 (b), and it shows that pores of ExtMCM-41 lies in the mesoporous range. The peak with maximum intensity was observed at 3.66 nm which indicates the average pore diameter of ExtMCM-41. The BET surface area and monolayer pore volume of ExtMCM-41 was found to be 691.107 m^2/g and 0.528 cm^3/g, respectively.

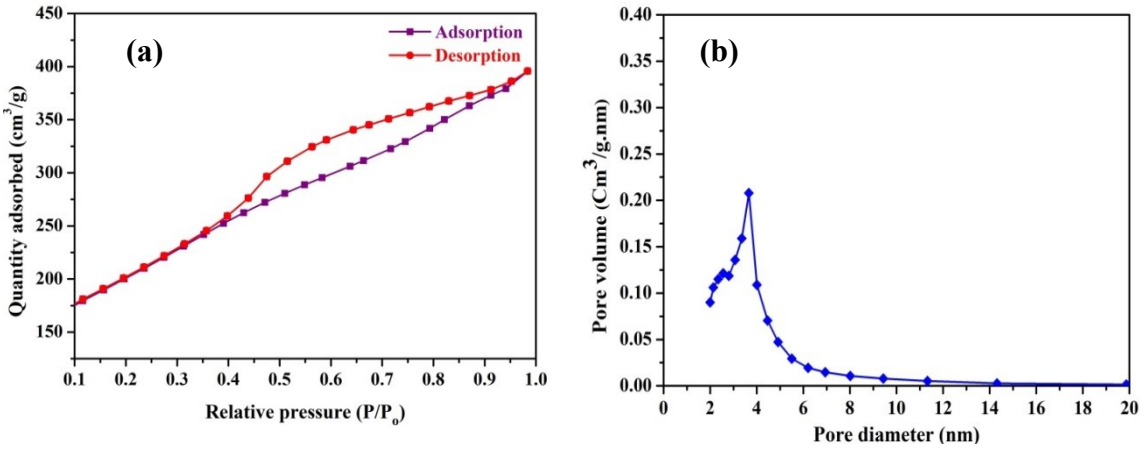

Figure 4.14 (a) Nitrogen adsorption-desorption isotherm of ExtMCM-41, (b) pore size distribution of ExtMCM-41.

FTIR analysis was performed to explore the characteristic functional groups available on surface of catalyst (Figure 4.15). The peaks observed at 799 cm^{-1} and 1085cm^{-1} are related to symmetric stretching vibration of Si-O-Si bond (Dhokte et al., 2011). The adsorption band appeared at 462 cm^{-1} can be ascribed to the bending vibrations of $Si-O^-$ group (Sikarwar et al., 2018b). The adsorption band located at a wave number of about 1631 cm^{-1} can be attributed to the physically adsorbed water and a broadband around 3400 cm^{-1} maybe due to the surface silanols and adsorbed water respectively (Asghari et al., 2016).

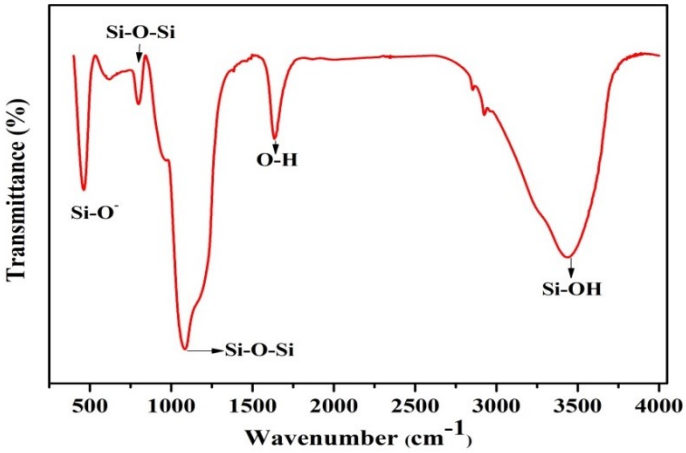

Figure 4.15 FTIR spectra of ExtMCM41.

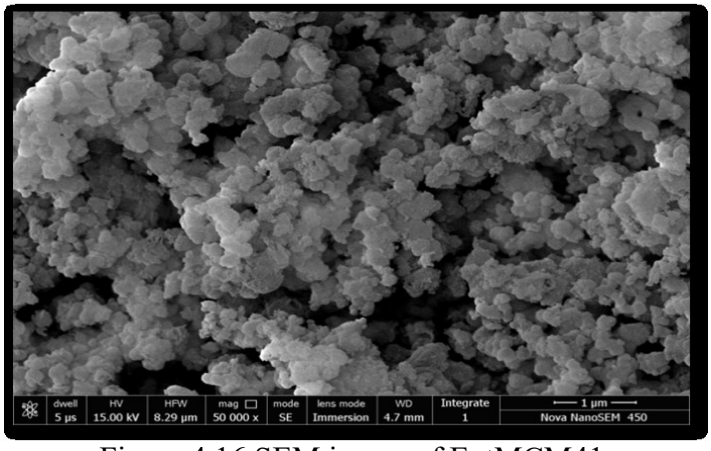

Figure 4.16 SEM image of ExtMCM41.

Figure 4.16 shows SEM images of mesoporous ExtMCM-41, the SEM images reveal that as synthesized catalyst exhibits spherical morphology. The obtained morphology of

catalyst matches well with previously reported literature (Dhokte et al., 2011). The average particle size of ExtMCM-41 was found to be 150 nm.

4.1.2.2 Effect of catalyst dosage

The amount of catalyst dose significantly contributes to the available active sites for the catalytic reaction. To evaluate the role of catalyst dosage, the ODS process was carried out at different dosages, ranging from 0.25 g/L to 2 g/L, while other operating parameters remained constant. It was observed that increasing the amount of catalyst oxidation of DBT enhanced significantly (74 % to 99 %). It can be seen from Figure 4.17, on increasing the catalyst dosage from 0.25 g/L to 0.75 g/L, the removal of DBT increased remarkably from 74 % to 94 %. This could be attributed to the availability of the vacant sites which in turn provide more opportunity for DBT to get oxidized. However, on further increasing the catalyst dose form 0.75 g/L to 2 g/L, DBT removal was increased from 94% to 100% removal. At higher loading, vacant sites were plenty which leads the complete sulfur removal was achieved (Qiu et al., 2016).

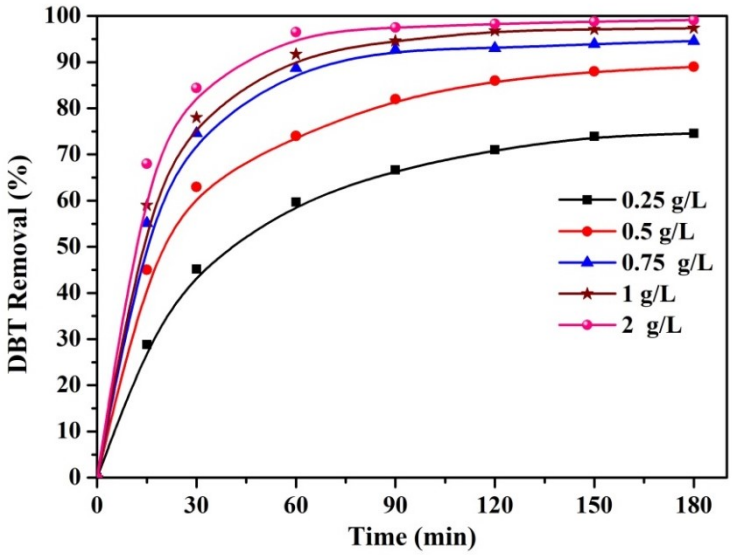

Figure 4.17 Effect of catalyst amount on removal of DBT (500 mg/L DBT solution, catalyst dose = 0.25 g/L to 2 g/L, T = 353 K, O/S = 2:1, t = 3 h).

4.1.2.3 Effect of initial concentration of DBT

To investigate the influence of initial concentration of DBT in model oil on ODS process, a series of experiments were conducted with varying initial concentrations (500 mg/L to 2000 mg/L) while keeping other reaction conditions as a constant (catalyst dose 0.75 g/L,

oxidant = 0.0522 ml (It is equalant to O/S ratio 2:1 for DBT concentration of 500 mg/l), 353 K). As seen in Figure 4.18, the oxidative removal of DBT decreased significantly with an increase in the initial concentration of DBT. On increasing the initial concentration from 500 mg/L to 2000 mg/L, DBT removal declined drastically from 94% to 52 %. This might be due to the non-availability of sufficient quantity of oxidant and vacant sites on catalyst surface because experiments were conducted at a fixed catalyst dose and oxidant concentration. For a fixed dose and oxidant, the active sites are the limited quantity for the oxidation of DBT, due to this reason low removal was observed. For further study, an initial concentration of 1000 mg/L opted.

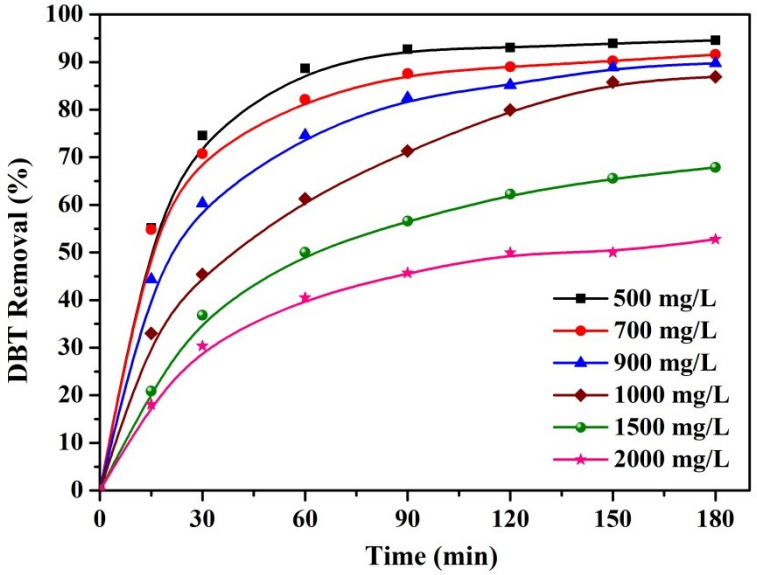

Figure 4.18 Effect of initial concentration of DBT (500 – 2000 mg/L DBT solution, catalyst dose = 0.75 g/L, T = 353 K, oxidant = 0.052 ml, t = 3 h).

4.1.2.4 Effect of oxidant/sulfur molar ratio (O/S)

In ODS process, the effect of O/S ratios plays a key role in the removal of DBT from fuel oil. To explore the effect of oxidation dosage on oxidative removal of DBT by ExtMCM-41 catalyst, a series of experiments conducted with varying oxidant O/S ratio (1:1 to 4:1) while keeping other parameters as a constant. As depicted in Figure 4.19, removal of DBT raised quickly from 46 % to 86 % with an increasing the O/S ratio from 1:1 to 2:1. At a low O/S ratio (1:1), DBT removal was insignificant due to unavailability of oxidant (TBHP) in sufficient quantity, because as per the stoichiometry of the reaction 1 mole of

DBT would consume 2 moles of TBHP to produce one mole of DBT sulfone (Zheng et al., 2015). However, on the increasing the O/S from 2:1 to 4:1 DBT conversion was increased but not appreciable quantity. In order to make the process economic, O/S of 2:1 was a suitable choice for further experiments.

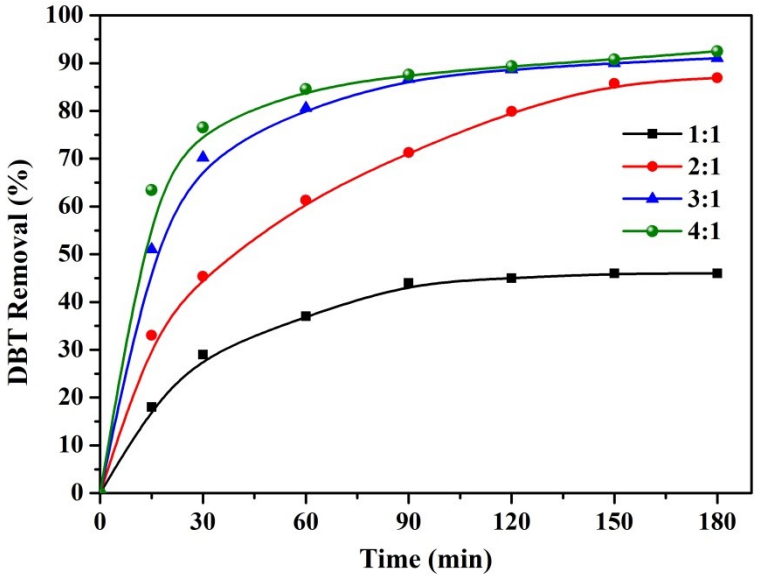

Figure 4.19 Effect of oxidant to sulfur molar Ratio (1000 mg/L DBT solution, catalyst dose = 0.75 g/L, T = 353 K, O/S = 1:1 to 4:1, t = 3 h).

4.1.2.5 Effect of temperature

In the ODS, one of the main processing parameters impacting the removal of DBT is temperature. The effect of temperature was studied by carrying out the ODS process at different temperatures ranging from 323 K to 363 K. As can be seen in Figure 4.20, conversion of DBT improved significantly from 53 % to 93 % with an increase of temperature from 323 K to 363 K. This remarkable improvement in oxidative removal of DBT can be ascribed to the movement of molecular speeding up which in turn provides more opportunity of interaction between sulfur compound and oxidant (Abdullah et al., 2016). In addition, higher temperature favors desorption of DBTsulfones from the active sites, and this leads to the availability of more vacant sites for the oxidation of DBT (Wang et al., 2014b). The temperature study was not investigated beyond 363 K owing to the low thermal stability of TBHP (Sikarwar et al., 2018b). Further, the temperature higher than 363 K results into the loss of model oil because of the volatilization and gasification at higher temperatures.

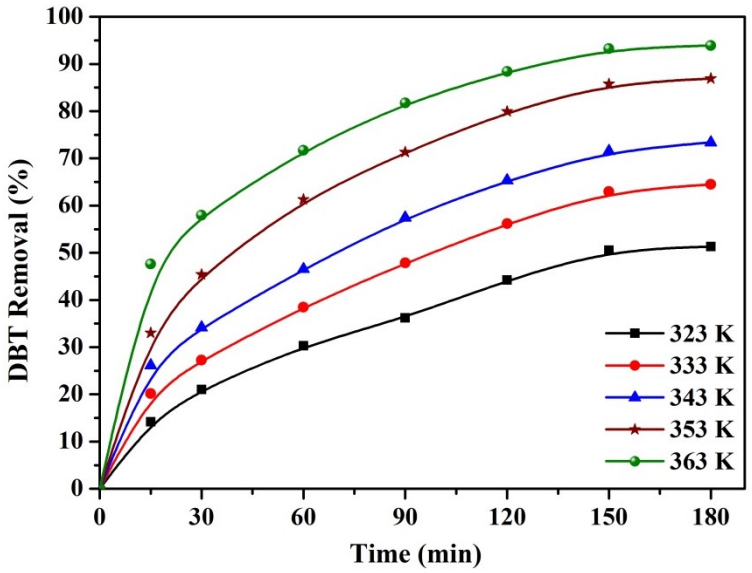

Figure 4.20 Effect of temperature (1000 mg/L DBT solution, catalyst dose = 0.75 g/L, T = 323 K to 363 K, O/S = 2:1, t = 3 h).

4.1.2.6 Kinetic study of ODS

To gain a better understanding of the catalytic oxidation of DBT reaction kinetic study was explored. To examine the kinetics of the oxidation of DBT, ODS of model oil was investigated at different temperatures while keeping other operating parameters remained constant. Both pseudo-first-order and pseudo-second-order models were employed to analyze the experimental data. The parameters obtained from fitting are shown in 4.3. As can be seen from Table 4.3, the highest value of the regression coefficient (R^2) was obtained for the pseudo-first-order model as compared with the pseudo-second-order model. The obtained results suggest that catalytic oxidation of DBT follows the pseudo-first-order model, which is in good agreement with the previously reported results (Zhu et al., 2013; Yang et al., 2016). The apparent activation energy (E) was evaluated by employing the Arrhenius equation and it was found to be 32.81 kJ/mol and 66.35 kJ/mol for pseudo-first-order and pseudo-second-order model. The activation energy of ODS process is much lower than that of the conventional hydro-desulphurization process, this could be due to the fact that oxidative reaction occurs very easily at a mild temperature as compared to HDS process (Wang et al., 2001).

Table 4.3 Kinetic and thermodynamic parameters for pseudo first order and pseudo second order reaction.

	Pseudo-first order			Pseudo-second order		
Temperature (K)	**K_f (1/min)**	**R^2**	**E_a (kJ/mol)**	**k_s (L/mg.min)**	**R^2**	**E_a (kJ/mol)**
323	0.0036	0.9792	32.82	0.000005	0.9848	66.66
333	0.0052	0.9861		0.000008	0.9891	
343	0.0065	0.9865		0.00001	0.9906	
353	0.0103	0.9863		0.00003	0.9723	
363	0.0138	0.9884		0.00008	0.9361	

4.1.2.7 Plausible oxidative desulfurization mechanism

Desulfurization mechanism of DBT on ExtMCM-41 in presence of TBHP is depicted in scheme 4.3. According to literature (Kropp et al., 2000) and our results, a hypothesized oxidative reaction mechanism was put forward. Surface silanol groups available on the surface of ExtMCM-41 act as an active site for the oxidation of DBT. Initially, the reaction mechanism involves the formation of a five-membered ring with the help of TBHP and silanol groups as shown in scheme 4.4. Both TBHP and silanol group act as hydrogen bond donor and acceptor in the formation of complex species. Due to the formation of this complex species, electrons are withdrawn from the peroxy oxygen and due to which its electrophilicity may be enhanced. Desulfurization reaction was preceded by a nucleophilic attack of sulfur atom present in DBT on the five-membered ring structures to form DBT sulfoxide and tert-butanol. Afterward, DBT sulfoxide undergoes further oxidation by the five-membered ring to produce DBT sulfone.

Scheme 4.3 Formation of 5 membered ring via coordination of TBHP and silanol group present on ExtMCM-41

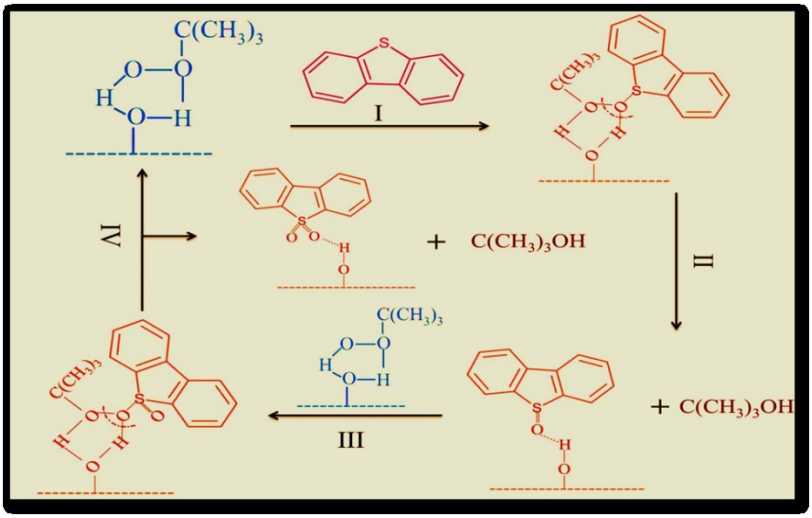

Scheme 4.4 Proposed cyclic oxidative desulfurization mechanism of DBT on ExtMCM-41.

4.1.2.8 Reusability of the catalyst

The reusability study was conducted under optimized operating conditions for the oxidative removal of DBT in model fuel oil. After the desulfurization reaction, the catalyst was separated from the oxidized model oil by employing filtration technique. Subsequently, the catalyst was washed with methanol and kept in the oven for drying at a temperature of 363 K for 4 h. The recovered catalyst was processed for the subsequent catalytic ODS, and the obtained results are depicted in Figure 4.21. The catalyst was recycled 5 times with a slight reduction (about 5%) in desulfurization efficiency as compared to the fresh catalyst. This reduction in catalytic activity can be ascribed to the adsorption of oxidation products of DBT on the active sites of ExtMCM-41.

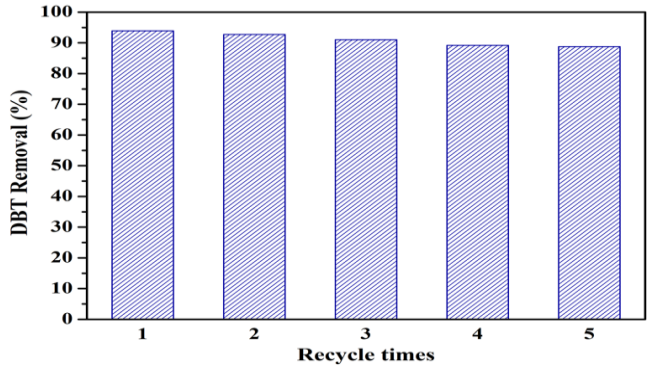

Figure 4.21 Recycling performance of ExtMCM-41 catalyst for ODS of DBT containing model oil (1000 mg/L DBT solution, catalyst dose = 0.75 g/L, T = 363 K, t = 3 h, O/S = 2:1).

4.1.2.9 ODN of model oil & effect of nitrogen compounds on the ODS

Denitrogenation of model oil containing indole/quinoline was conducted under the optimum conditions obtained for ODS of DBT. Composition of model oil used for the batch experiments of oxidative denitrogenation and simultaneous desulfurization and denitrogenation is shown in Table 4.4.

Table 4.4 Composition of model feed oils.

Notation	Sulfur/nitrogen contaminant	Model Oil
MD	DBT(1000 mg/L)	Iso-octane
MI	Indole (50 mg/L)	Iso-octane
MQ	Quinoline (50 mg/L)	Iso-octane
MDI	DBT(1000 mg/L) + Indole (50 mg/L)	Iso-octane
MDQ	DBT(1000 mg/L) + Quinoline (50 mg/L)	Iso-octane

Denitrogenation of model oil containing indole/quinoline was conducted under the optimum conditions obtained for ODS of DBT. The present oxidation system was more effective for removal of indole as compared to the quinoline (Figure 4.22). The higher activity of indole can be attributed to the more electron density of nitrogen in indole (Zhang et al., 2011). To investigate the effects of various nitrogen compounds on the desulfurization process, the ODS of DBT was conducted in presence of typical nitrogen compounds (quinoline/indole). As can be seen from Figure 4.22, ODS activity was declined severely in presence of nitrogen compounds. However, the presence of indole inhibited the ODS activity more as compared to the quinoline. DBT removal was achieved to 52% in presence of indole, whereas 80% removal of DBT was achieved in presence of quinoline. Obtained results match well with the previously conducted studies. The decrease in ODS activity due to the presence of nitrogen compounds can be ascribed to the competition between sulfur and nitrogen compounds for the active sites. In addition, this reduction in DBT removal can also be attributed to the strong adsorption of nitrogen compounds and oxidation products of indole/quinoline on vacant sites of the catalyst.

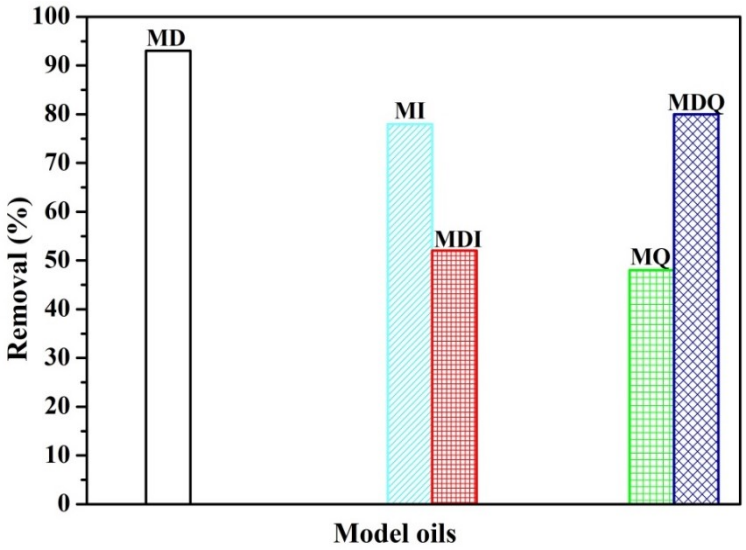

Figure 4.22 Effect of nitrogen compounds on ODS (MD, MDI, and MDQ indicates the removal of DBT) and ODN of model oils (catalyst dose = 0.75 g/L, T = 363 K, O/(S + N) = 2:1, O/N = 2:1, t = 3 h).

4.2 Adsorption studies using granular activated carbon based adsorbents

Granular activated carbon was treated with acetic acid and then impregnated with various amounts of molybdenum and cobalt salts, respectively. The procedure of treatment of GAC with acetic acid is described in section 3.4.1; the synthesis procedure of cobalt loaded ATGAC and molybdenum loaded ATGAC are given in sections 3.4.2 and 3.4.3, respectively. The synthesized adsorbents were utilized for the adsorptive desulfurization, adsorptive denitrogenation, and simultaneous adsorptive desulfurization and denitrogenation of model oil.

4.2.1 Adsorption studies using cobalt loaded ATGAC (Co/ATGAC)

Cobalt loaded acid treated GAC was characterized with the aid of various characterization techniques, and the results of these techniques are shown in section 4.2.1.1. This section describes the results of batch adsorptive desulfurization (section 4.2.1.2) and adsorptive denitrogenation (section 4.2.1.3) of model oil by using cobalt impregnated ATGAC. Further, this section also contained an optimization study of simultaneous adsorptive desulfurization and denitrogenation with the help of CCD design by using optimized adsorbent (section 4.2.1.4).

4.2.1.1 Characterization of cobalt loaded ATGAC

The SEM image of blank GAC, 1 wt % Co/ATGAC, and 2 wt % Co/ATGAC are presented in Figure 4.23 (a, b, & c) respectively. As depicted in Figure 4.23 (a) GAC shows porous nature and possess a rough surface. It can be seen from Figure 4.23 (b,c) that cobalt loaded GAC exhibits lesser porosity and more smooth surface as compared to blank GAC. Further agglomeration is not appeared on the surface of GAC indicating that metal dispersed uniformly on the carbon matrix (Ania and Bandosz, 2006).

XRD patterns of mere GAC, 1 wt % Co/ATGAC, and 2 wt % Co/ATGAC are depicted in Figure 4.24. A broad hump was observed at 24^{o} and 44^{o} in all samples and can be attributed to the amorphous carbon, originating from the reflection of (002) and (010) planes respectively (Prahas et al. 2008). The diffraction peak at 36.75° was obtained in cobalt loaded samples, originating from (311) plane corresponds to Co_3O_4 (Jongsomjit et al., 2001). The obtained results indicated that cobalt species loaded successfully into the framework of GAC. Scherrer equation was used to calculate the average Co_3O_4 particle size of the adsorbent with the help of peak obtained in XRD spectrum at 36.75°. The average Co_3O_4 crystallite size on GAC was found to be 13.8 nm for 1 wt % loading and for 2 wt % it was 14.5 nm.

FTIR spectra of mere GAC, acetic acid treated GAC, 1 wt % Co/ATGAC, and 2 wt % Co/ATGAC were performed to confirm the surface functionalities of the sample. Figure 4.25 depicted the FTIR spectrum of samples, a broad absorption band centered at 3435 cm^{-1} is assigned to O–H stretching vibrations of hydroxyl groups due to the presence of water molecules in the pores of GAC framework (Saleh and Danmalik, 2016). The bands at 2921 cm^{-1} and 2845 cm^{-1} might be due to the stretching vibrations of C-H. The peaks at 1737 cm^{-1} and 1628 cm^{-1} were associated with the carboxyl group and carbonyl group (Saleh et al., 2017). The absorption band at 1035 cm^{-1} was ascribed to the C-O stretching vibration (Danmaliki and Saleh, 2017). Although these bands were observed in mere GAC, acid treated GAC, 1 wt % Co/ATGAC, and 2 wt % Co/ATGAC. In acid treated GAC the intensity of oxygen containing bands (1722 cm^{-1}, 1630 cm^{-1}, 1088 cm^{-1}) get increased, which may be due to the increase of oxygen containing sites when treated with acetic acid. Similar trend was observed by Pradhan and Sandle (1999) for the oxidation of

GAC with nitric acid. FTIR spectra of 1 wt % Co/ATGAC, and 2 wt % Co/ATGAC exhibited two additional peaks around 568 cm^{-1} and 665 cm^{-1} as compared to GAC and acid treated GAC. These bands represents the Co-O bond in spinel phase Co_3O_4, former peak aroused owing to the Co^{+3} -O stretching vibration, and the latter peak contributed to the Co^{+2} -O vibrations (Tang and Hong, 2016; Zheng et al., 2010).

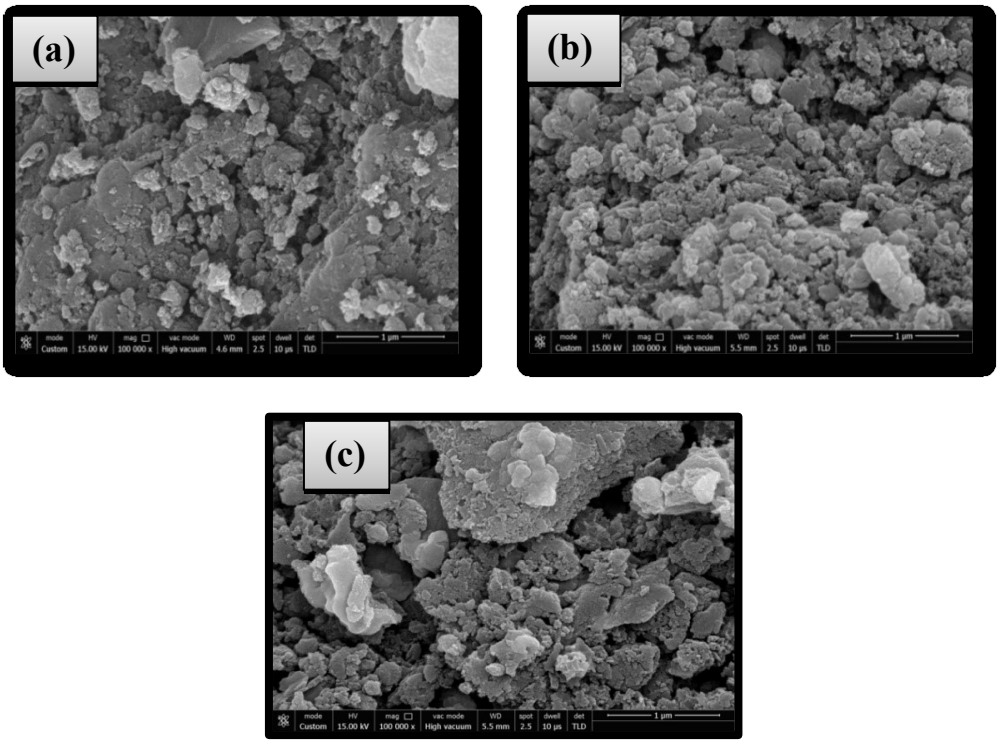

Figure 4.23 SEM micrograph of (a) blank GAC (b) 1 wt % Co/ATGAC (d) 2 wt % Co/ATGAC.

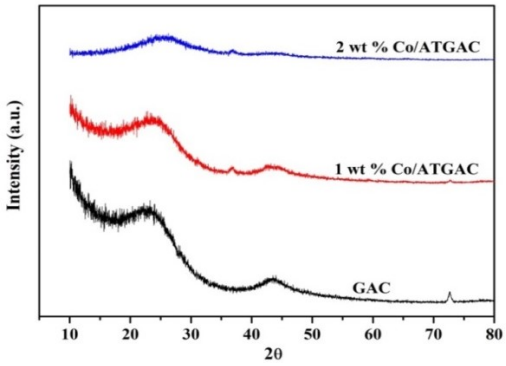

Figure 4.24 X-ray diffractograms of blank GAC, 1 wt % Co/ATGAC, and 2 wt % Co/ATGAC.

Nitrogen adsorption - desorption isotherms of GAC and 1 wt % Co/ATGAC, and 2 wt % Co/ATGAC are depicted in Figure 4.26. All samples are microporous in nature as nitrogen uptake for all samples was more at relative pressure less than 0.25 (Xiong et al., 2012). It can be clearly seen from Figure 4.26, that GAC is highly microporous in nature as compared to the cobalt loaded acid treated GAC samples. Presence of hysteresis loop can be seen in both 1 wt % Co/ATGAC, and 2 wt % Co/ATGAC indicating the presence of mesopores. The surface areas of 1 wt % Co/ATGAC (393 m^2/g) and 2 wt % Co/ATGAC (383 m^2/g) were more as compared with mere GAC (257 m^2/g). This increase in surface area can be attributed to the acidic treatment of GAC. Because of acid treatment, the inert materials present in the pores of GAC were removed, which increased the pore volume. 1 wt % Co/ATGAC exhibited higher surface area than 2 wt % Co/ATGAC owing to the destruction of GAC framework due to the higher loading amount. Pore size distribution of 1 wt % Co/ATGAC, and 2 wt % Co/ATGAC are depicted in Figure 4.26. The pore size distribution of 1 wt % Co/ATGAC is unimodal in nature whereas pore size distribution of 2 wt % Co/ATGAC is bimodal in nature. The average pore diameter of 1 wt % Co/ATGAC and 2 wt % Co/ATGAC are 7.248 Å and 18.764 Å, respectively.

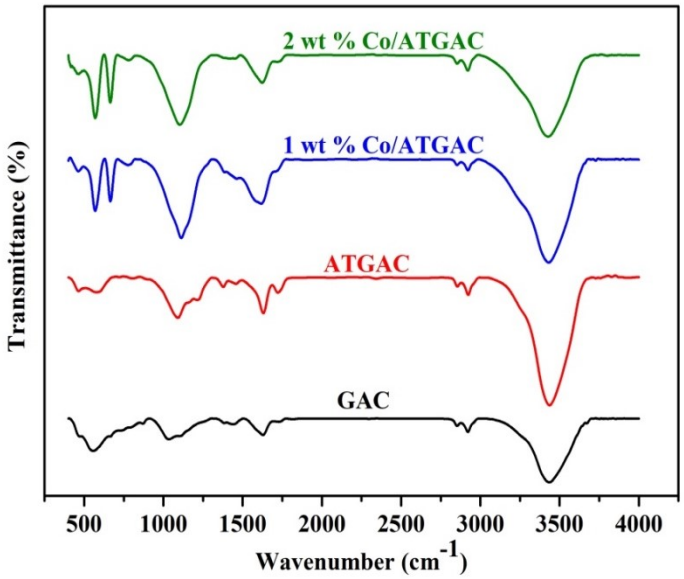

Figure 4.25 FTIR Spectra of GAC, ATGAC, 1 wt % Co/ATGAC, and 2 wt % Co/ATGAC.

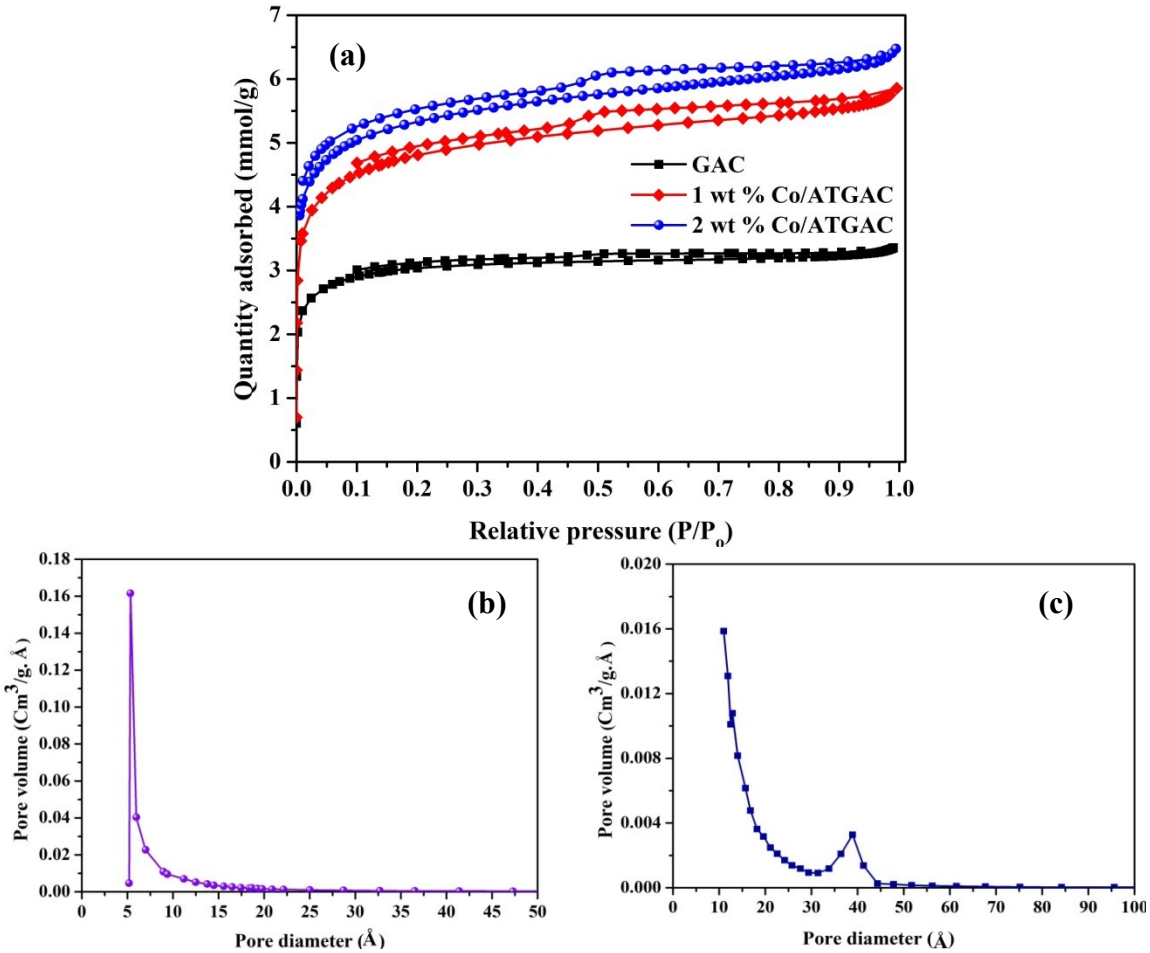

Figure 4.26 (a) Nitrogen adsorption−desorption isotherms for GAC, ATGAC, 1 wt % Co/ATGAC, and 2 wt % Co/ATGAC, (b) Pore volume distribution of 1 wt % Co/ATGAC, and (c) 2 wt % Co/ATGAC.

XPS spectra of 1 wt % Co/ATGAC and 2 wt % Co/ATGAC are shown in Figure 4.27 & Figure 4.28. Presence of carbon, oxygen, and cobalt in the adsorbent samples can be seen in the survey spectra of 1 wt % Co/ATGAC, and 2 wt % Co/ATGAC. Carbon present in the adsorbent samples was deconvoluted in to four peaks shown in Figure 4.27(b) and Figure 4.28(b). The deconvoluted C 1s spectra consist of following peaks, graphitic carbon (C-C, 284.6 eV), carbon present in phenolic, alcohol, and ether aromatic (C-O, 286 eV), carbonyl, quinone groups (C=O, 287.6 eV), ester or carboxyl groups (O-C=O, 288.6 eV) (Li et al., 2016). The decomposed O 1s spectra of 1 wt % Co/ATGAC, and 2 wt % Co/ATGAC are depicted in Figure 4.27(c) & Figure 4.28(c), respectively. Further, O 1s spectrum of adsorbent samples were deconvoluted in to five characteristics peaks

namely, 530.31(Co_3O_4), 531.37(C=O), 532.45(C-O), 533.36(O-H) (Abdedayem et al., 2014). The deconvoluted spectra of Co 2p for 2 wt % Co/ATGAC is presented in Figure 4.28(d). Binding energies of Co 2p3/2 and Co 2p1/2 peak for Co^{3+} and Co^{2+} ions were found to be 779.69, 781.5 and 795.19, 797.53 eV. It is reported in the literature that binding energies of Co 2p3/2 for Co^{3+} and Co^{2+} ions are 780.2 ± 0.6 and 781.8 ± 0.6 eV, respectively, and the energy difference between the Co 2p3/2 peak and the Co 2p1/2 peak is around 15 eV(Li et al., 2014).

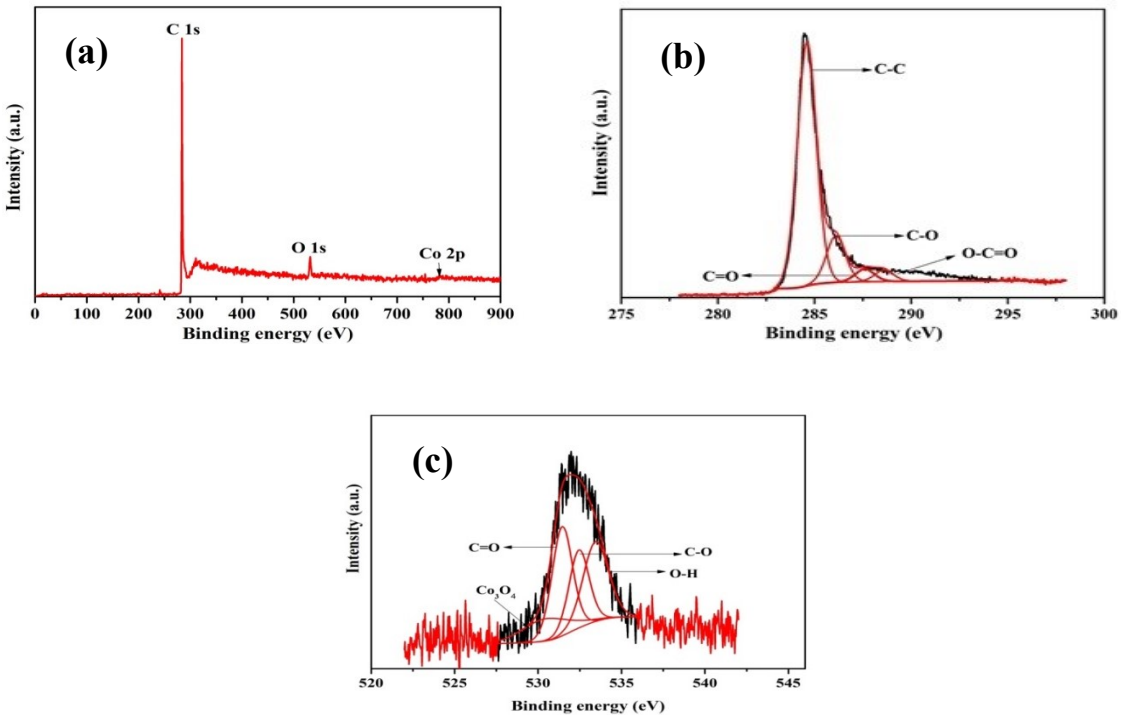

Figure 4.27 XPS spectra (a) full survey scan of Co/ATGAC, (b) XPS deconvoluted spectra of C 1s (c) XPS deconvoluted spectra of O1s

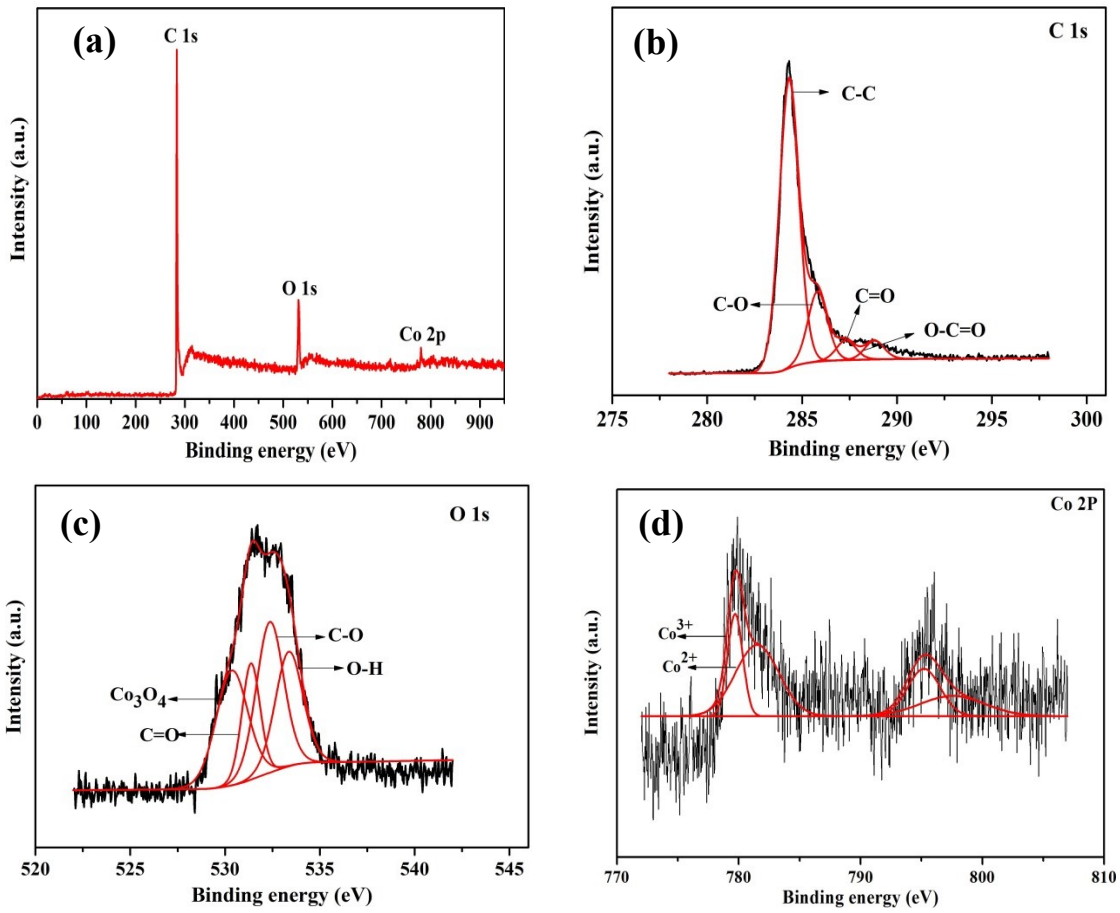

Figure 4.28 XPS Spectra (a) full survey scan, (b) deconvoluted C 1s spectra of 2 wt % Co/ATGAC, (c) deconvoluted O 1s spectra of 2 wt % Co/ATGAC, (d) deconvoluted Co 2p spectra of 2 wt % Co/ATGAC.

4.2.1.2 ADS using cobalt loaded ATGAC

4.2.1.2.1 Effect of various adsorbents

In order to investigate the performance of modified activated carbon for the ADS of DBT, few preliminary experiments were conducted. As can be seen from Figure 4.29, ATGAC shows more adsorption capacity (51% DBT removal) as compared to the mere GAC (40% DBT Removal). The observed improvement on ATGAC was due to the activation of pores, and the incorporation of oxygen-containing functional groups which lead to the high sorption capacity (Shi et al., 2015). Previous literature confirmed that the oxygen-containing functional groups present on the activated carbon surface can remarkably increase the adsorption capacity (Jiang et al., 2003; Subhan and Liu, 2011). Figure 4.29 depicted adsorption performance of different weight percentage of active metal on

ATGAC (1 wt % Co/ATGAC, 2 wt % Co/ATGAC, 3 wt % Co/ATGAC, and 4 wt % Co/ATGAC). The improvement of DBT adsorption onto Co/ATGAC as compared to mere GAC and ATGAC may be due to the formation of π complex between DBT and cobalt species. Maximum adsorption of DBT was observed for 1 wt % Co/ATGAC, as an increase in cobalt loadings, the DBT removal was decreased. The observed results suggested that higher cobalt loading resulted in the decline of surface adsorption sites due to the multilayer deposition of active metal species and agglomeration of cobalt particles on the GAC channel. Subhan and Liu (2011) observed a similar trend for ADS of DBT using nickel supported MCM-41. The obtained results indicate that the introduction of cobalt and acid treatment of GAC are the key factors for removal of DBT due to increase in acidic sites and the interaction of cobalt the sulfur compounds. Therefore, 1 wt % Co/ATGAC was taken as the potential adsorbent for further evaluation of the ADS process.

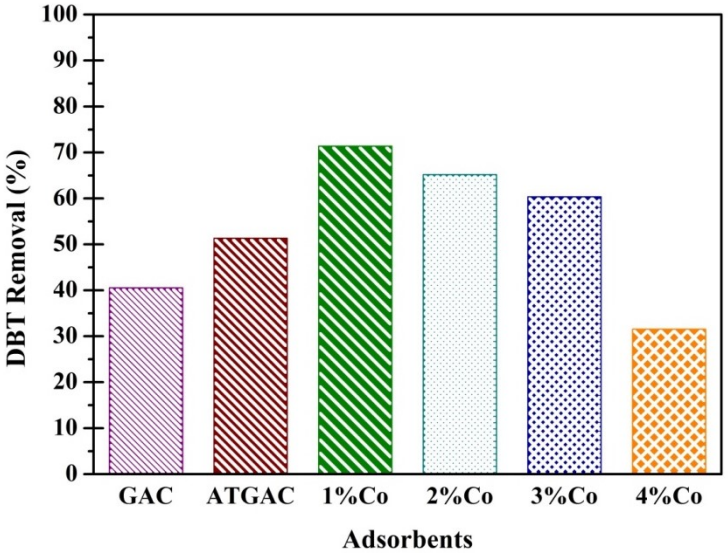

Figure 4.29 Effect of various adsorbents on DBT removal (DBT initial concentration = 500 mg/L, adsorbent dose = 10 g/L, reaction time = 3 h, temperature = 303 K).

4.2.1.2.2 Effect of adsorbent dose

To understand the effect of adsorbent dose various quantities of 1 wt % Co/ATGAC were utilized i.e. 5, 10, 15, 20, 25 and 30 g/L at 500 mg/L of DBT concentration. Effect of adsorbent quantity on desulfurization of DBT is shown in Figure 4.30. With an increase in 1 wt % Co/ATGAC dose the percentage removal of DBT increased from 45% to 96%.

This increment in adsorption may be attributed to the availability of large vacant sites, and hence more π complexation sites for the sulfur species adsorption (Ahmad et al., 2017). At a lower dose (5 g/L) of 1 wt % Co/ATGAC, the active/vacant sites were saturated with the DBT molecules, and no further enhancement in removal was observed, the DBT removal enhanced significantly on enhancing the dose from 5 g/L to 20 g/L. However, at a higher dose (above 20 g/L) only marginal increase in percentage removal (~4% increases from 20 g/L to 30 g/L) was observed. It may be ascribed to the insufficient number of DBT molecules at a higher dose as it was conducted at a fixed concentration of DBT molecules (500 mg/L). Finally, 20 g/L of 1 wt % Co/ATGAC adsorbent dose was selected as an optimum dose to perform further experiments.

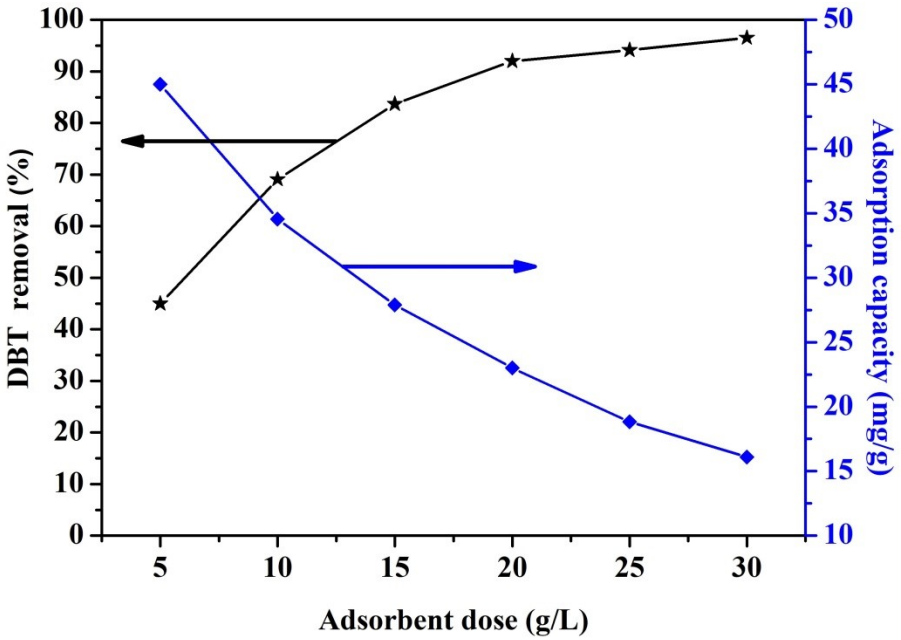

Figure 4.30 Effect of adsorbent dose on DBT removal (DBT initial concentration = 500 mg/L, time = 4 h, T = 303 K, adsorbent = 1 wt % Co/ATGAC).

4.2.1.2.3 Adsorption equilibrium study

The equilibrium adsorption of DBT with various concentrations ranging from 250 mg/L to 1000 mg/L at different temperature (283, 293, 303 and 313 K) was investigated using 1 wt % Co/ATGAC. The adsorption capacity of 1 wt % Co/ATGAC increased abruptly with an increase in operating temperature and adsorbate concentration as shown in Figure 4.31. The rise in adsorption capacity with an increase in temperature may be due to the faster diffusion of DBT species into the pores of the catalyst. In addition, at higher

temperature less retarding forces are imposing on the molecules which lead to the high adsorption (Kumar and Srivastava, 2012). In order to better understand the interactive behavior between adsorbate and adsorbent four different type of adsorption isotherms were studied namely Langmuir, Freundlich, Temkin, and Redlich and Peterson (R - P). Values obtained for all parameters at various temperatures are depicted in Table 4.5. q_m value rose with an increase in temperature which confirms the endothermic nature of the overall sorption process (Thaligari et al., 2016a). Moreover, the increase in maximum adsorption capacity may also be attributed to the chemisorption (Wen et al., 2010). As shown in Table 4.5, values of K_F increases with increase in temperature similar to the trend obtained for values of $q_{m.}$. Furthermore, the values of 1/n <1 for different temperatures, indicates that adsorption capacity is diminished marginally for lower $C_{e.}$. The Langmuir, Freundlich, Temkin, and R-P isotherm parameters along with correlation coefficient (R^2) and the sum of a square of error (SSE) are utilized to estimate the goodness of fit for the selection of optimum isotherms on to 1 wt % Co/ATGAC at various temperatures as shown in Table 4.5. It can be clearly seen from the table, R-P isotherm obtained the highest value of R^2 and least value for SSE. Hence, R-P model is the best fit for the equilibrium data obtained at different temperature. The Redlich Peterson isotherm model finds its applicability in homogenous as well as heterogeneous systems. Since this isotherm contains elements from Langmuir as well as Freundlich isotherm, therefore the adsorption of DBT on to 1 wt % Co/ATGAC is a mixture of both and doesn't follow monolayer adsorption. The adsorption of DBT molecules seems promising because value of β lies between 0 and 1. Figure 4.31 indicated the fit of R–P isotherm model for the obtained experimental results.

Table 4.5 Equilibrium parameters for the adsorption of DBT on 1 wt % Co/ATGAC (t = 4 h, initial concentration of DBT = 250 – 1000 mgl/L, dose = 20 g/L).

Langmuir				
Temperature (K)	q_m (mg/g)	K_L (L/mg)	R^2	SSE
283	37.560	0.0114	0.971	17.56
293	38.935	0.0192	0.970	22.21
303	40.554	0.0302	0.986	11.58
313	45.832	0.0347	0.980	20.58
Freundlich				

Temperature (K)	K_F [(mg/g)/(mg/L)$^{1/n}$]	1/n		R^2	SSE
283	2.878	0.406		0.969	18.69
293	4.086	0.377		0.978	16.58
303	5.847	0.338		0.986	11.46
313	5.950	0.377		0.985	15.39
Temkin					
Temperature (K)	K_T (L/g)	B_1 (J/mol)		R^2	SSE
283	0.195	7.051		0.959	24.84
293	0.192	8.367		0.958	16.24
303	0.335	8.329		0.993	05.59
313	0.355	9.759		0.988	11.84
Redlich–Peterson					
Temperature (K)	K_R (L/g)	α(L/mg)	B	R^2	SSE
283	1.982	0.316	0.722	0.993	03.62
293	2.010	0.268	0.721	0.999	15.64
303	2.683	0.156	0.834	0.999	09.65
313	3.268	0.256	0.759	0.988	12.08

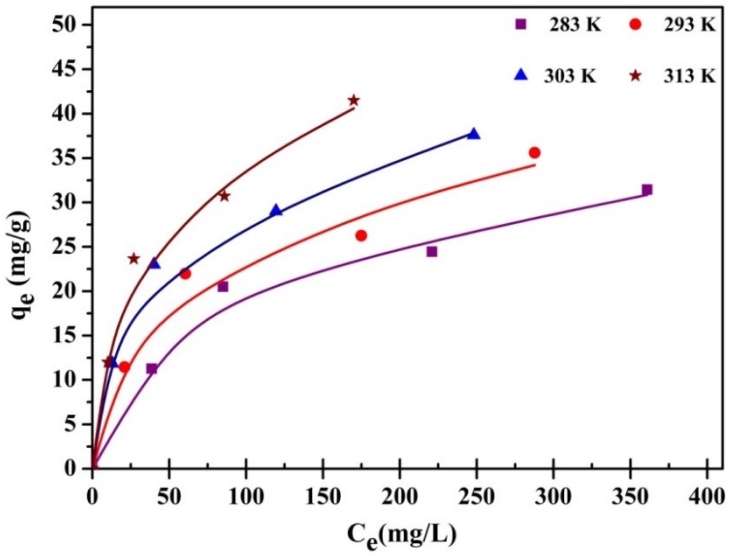

Figure 4.31 Equilibrium isothermal adsorption of DBT on to 1 wt % Co/ATGAC at different temperature (Symbols indicate the equilibrium data points, and the lines projected by the R - P model).

4.2.1.2.4 Adsorption kinetic study

In order to gain better understanding about the reaction pathway and adsorption mechanism of DBT molecules onto 1 wt % Co/ATGAC adsorption, pseudo first-order and pseudo second-order kinetic models were employed to analyze the experimental data

in the studied adsorption systems. Effect of contact time on the removal of the DBT from model fuel oil by 1 wt % Co/ATGAC is depicted in Figure 4.32. In the first 60 minutes rapid adsorption was observed afterwards adsorption rate slowly increased. After three hours, the adsorption approaches equilibrium. Pseudo first-order and pseudo second-order model have been utilized to fit the kinetics of adsorption of DBT onto 1 wt % Co/ATGAC by employing non-linear regression. The results obtained from fitted curves are displayed in Figure 4.32, and the calculated parameters are presented in Table 4.6. As can be seen from Table 4.6, the highest value of regression coefficient (R^2) and the least value of SSE were obtained for pseudo-second-order model as compared to pseudo-first-order. Therefore, the kinetics of DBT adsorption is best expressed by pseudo-second-order model indicating that the chemical reaction is rate-controlling step (Ho and McKay, 1999).

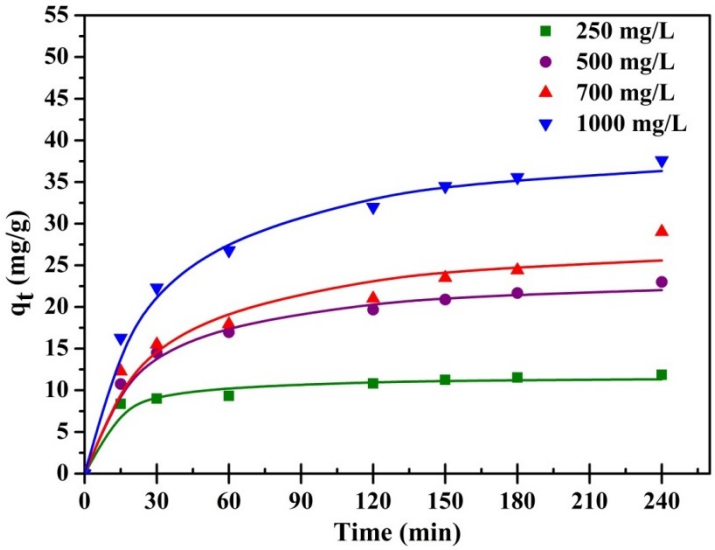

Figure 4.32 Kinetic data for the removal of DBT (Symbols indicate experimental data, solid lines predicted by pseudo second order model).

Table 4.6 Kinetic parameters for the adsorption of DBT on 1 wt % Co/ATGAC (t = 4 h, initial concentration of DBT = 250 – 1000 mg/L, dose = 20 g/L, Temperature = 303 K).

Pseudo first order					
C_o(mg/L)	$q_{e,exp}$ (mg/g)	$q_{e,cal}$ (mg/g)	k_1(min^{-1})	R^2	SSE
250	11.85	10.97	0.0932	0.967	03.795
500	23.00	21.11	0.0382	0.973	11.884
700	29.02	24.47	0.0316	0.923	47.488
1000	37.60	34.85	0.0326	0.974	30.815

Pseudo second order					
C_o(mg/L)	$q_{e,exp}$ (mg/g)	$q_{e,cal}$ (mg/g)	k_2(g. $mg^{-1}.min^{-1}$)	R^2	SSE
250	11.85	11.66	0.0113	0.980	02.005
500	23.00	23.87	0.0020	0.993	02.796
700	29.02	28.37	0.0013	0.956	24.718
1000	37.60	40.06	0.0010	0.993	07.171

4.2.1.2.5 Adsorption thermodynamic parameter

Study of thermodynamic parameters includes assessment of Gibbs free energy change, enthalpy change, and entropy change to gain the comprehensive knowledge about adsorption of DBT onto 1 wt % Co/ATGAC process such as spontaneity of the process, structural characteristics of adsorbent after adsorption of DBT.

Change in Gibbs free energy (ΔG°) is determined with the aid of Equation 3.12. The values of ΔG° calculated at different temperatures are listed in Table 4.7. The negative value of ΔG° indicates the spontaneous adsorption at the studied temperatures on 1 wt % Co/ATGAC surface, and the strong affinity of 1 wt % Co/ATGAC towards the DBT species. Values of ΔG° are decreasing with an increase in temperature which clearly shows that the adsorption of DBT is more spontaneous at a higher temperature. To determine ΔH° and ΔS°, a graph was drawn between ΔG° and temperature using Equation 3.13 (as shown in Figure 4.33). The calculated thermodynamic parameters are summarized in Table 4.7. The positive value of enthalpy change indicates that the adsorption of DBT is endothermic in nature. The change of enthalpy due to physisorption is usually lower than 40 kJ/mol (Seki and Yurdakoç, 2006), the adsorption of DBT is mainly dominated by physisorption. The positive ΔS° value illustrates a good affinity of DBT molecules onto the 1 wt % Co/ATGAC surface, and an enhancement in the degree of freedom for the adsorbed species (Han et al., 2015). The low entropy change for DBT adsorption implies enhanced randomness at the interface of adsorbent and model oil.

Table 4.7 Thermodynamics parameters for the adsorption of DBT onto 1 wt % Co/ATGAC (t = 4 h, Co = 250 – 1000 mg/L, m = 20 g/L).

Temperature (K)	ΔG° (kJ/mol K)	ΔH° (kJ/mol)	ΔS° (kJ/mol K)
283	-14.416		
293	-16.340	35.67	0.177
303	-18.652		

313	-19.517	

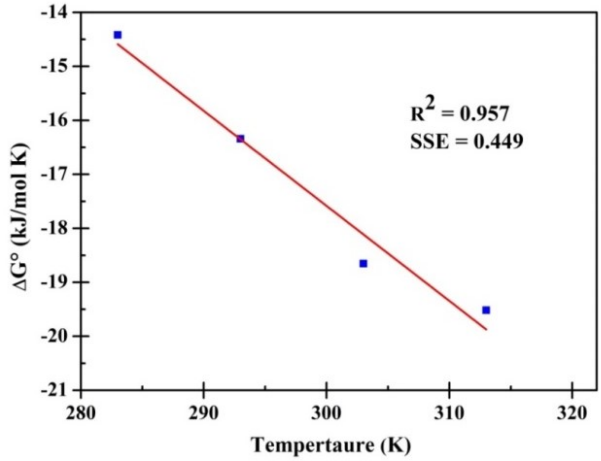

Figure 4.33 ΔG° versus temperature plot for adsorption of DBT on to 1 wt % Co/ATGAC.

4.2.1.2.6 Characterization of spent adsorbent

Characterization study of spent adsorbent was carried out in order to better understand the adsorption process of DBT onto 1 wt % Co/ATGAC. The FTIR spectra of fresh and spent adsorbent are presented in Figure 4.34. FTIR of DBT loaded 1 wt % Co/ATGAC exhibits either shifting in the peaks or change in the peak heights as compared to the fresh adsorbent, indicating that the functional groups which present in these wavelengths contribute in the adsorption of DBT (Rameshraja et al., 2012).

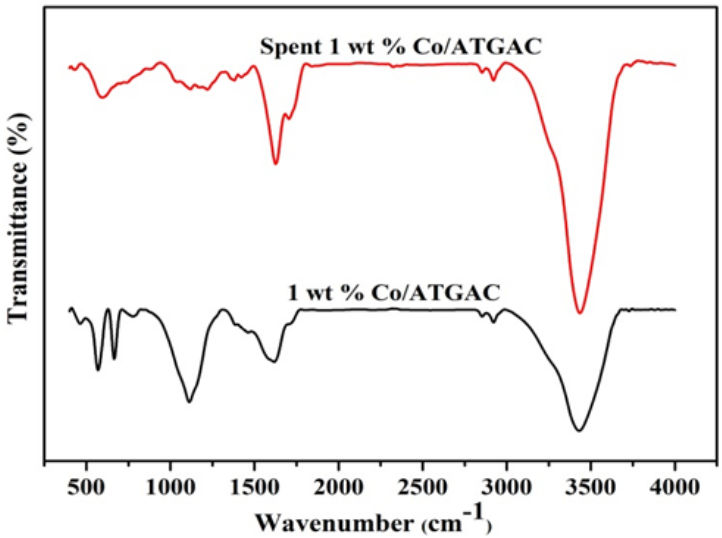

Figure 4.34 FTIR spectra of fresh and spent 1 wt % Co/ATGAC.

The XRD patterns of fresh and spent adsorbent are shown in Figure 4.35. Amorphous nature of adsorbent remains unchanged after adsorption of DBT (Thaligari et al., 2016b). No additional peak observed in XRD of spent adsorbent which indicates that the adsorption phenomenon involves electrostatic interaction between adsorbent and adsorbate (Parashar et al., 2016). SEM images of fresh and spent adsorbents are depicted in Figure 4.36 (a & b). It can be clearly indicated from the images that DBT loaded on to the fissures and channels presents on the surface of raw adsorbent signifies the successful adsorption of DBT onto 1 wt % Co/ATGAC.

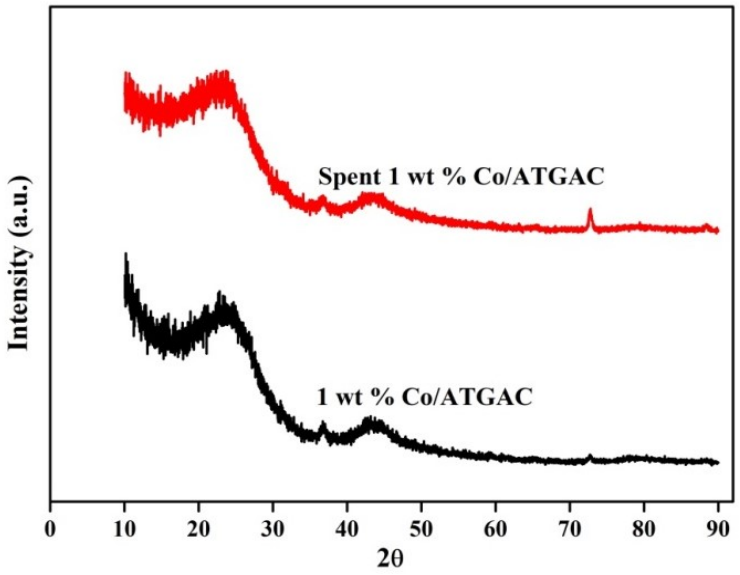

Figure 4.35 X-ray diffraction of fresh and spent 1 wt % Co/ATGAC.

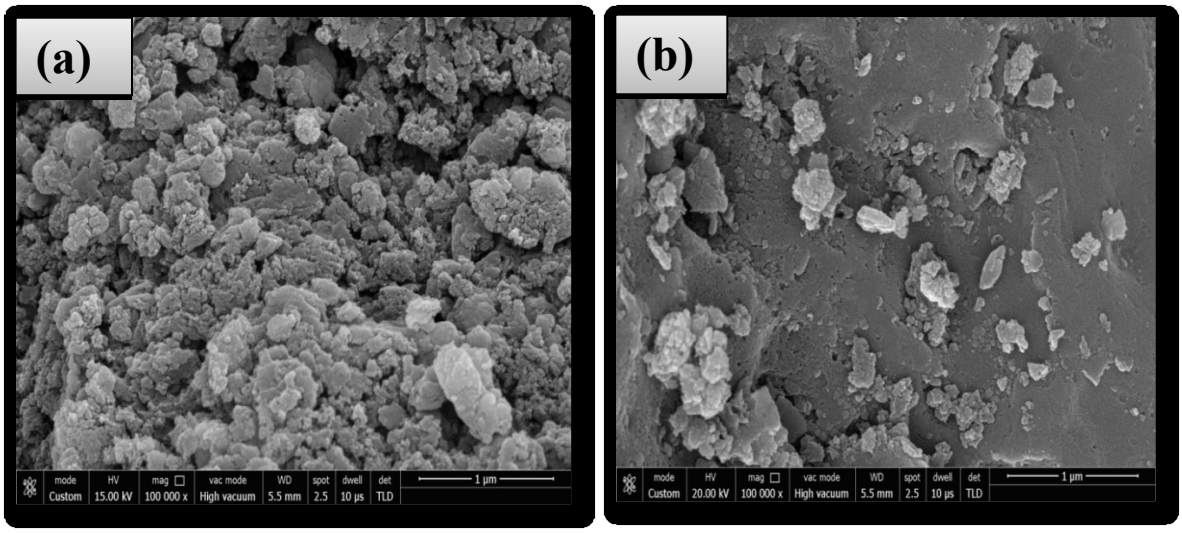

Figure 4.36 SEM images of 1 wt % Co/ATGAC a) before and b) after adsorption.

4.2.1.2.7 Effect of aromatics on ADS and reusability study

Selectivity of adsorbent is an important issue in ADS process. All liquid fuels such as gasoline, diesel contains various aromatics, and these compounds compete with sulfur species to get adsorbed on the adsorbent. Therefore, in order to investigate the selectivity of the adsorbent, competitive adsorption was conducted by mixing model fuel with aromatic compounds (benzene or toluene) under optimized reaction conditions. It was found that the addition of benzene (10 vol.%, 20 vol.%) or toluene (10 vol.%, 20 vol.%) decreases the adsorption of DBT onto adsorbent as shown in Figure 4.37. This decrease in adsorption capacity could be due to the competition between aromatic molecules and DBT molecules to get adsorbed on active sites. With the addition of toluene (10 vol.%, 20 vol.%) in the model oil, the adsorption performances were decreased with the DBT removal of 80% and 75% respectively. Similarly, by adding benzene (10 vol.%, 20 vol.%) to the model oil, DBT removal reduced to 77 and 72% respectively. Obtained results match well with the previously reported literature (Zhang et al., 2008). 1 wt% Co/ATGAC showed approximately same affinity for the adsorption of both aromatics as they both might get adsorbed through π complexation mechanism. Same preference may be given for the adsorption of both toluene and benzene as they both contained same number of π electrons. Moreover, DBT contained more number of π electrons as compared to toluene and benzene; therefore more DBT molecules were adsorbed as a result higher DBT removal was observed as compared to benzene and toluene. Weaker bonding of aromatics with the adsorbent as compared to DBT molecules confirms the selectivity of Co/ATGAC.

Regeneration of spent adsorbent was performed using a solvent extraction technique. In order to regenerate, 1 g of spent adsorbent was mixed with 10 ml of toluene and stirred at room temperature for 15 minutes. Subsequently, adsorbents were filtered and dried overnight at 90 °C. Then the regenerated adsorbent was reutilized for ADS process. After the first cycle, adsorption capacity was decreased from 23 (mg/g) to 21.67(mg/g), and in the next cycle, it reduced to 21.14 (mg/g).

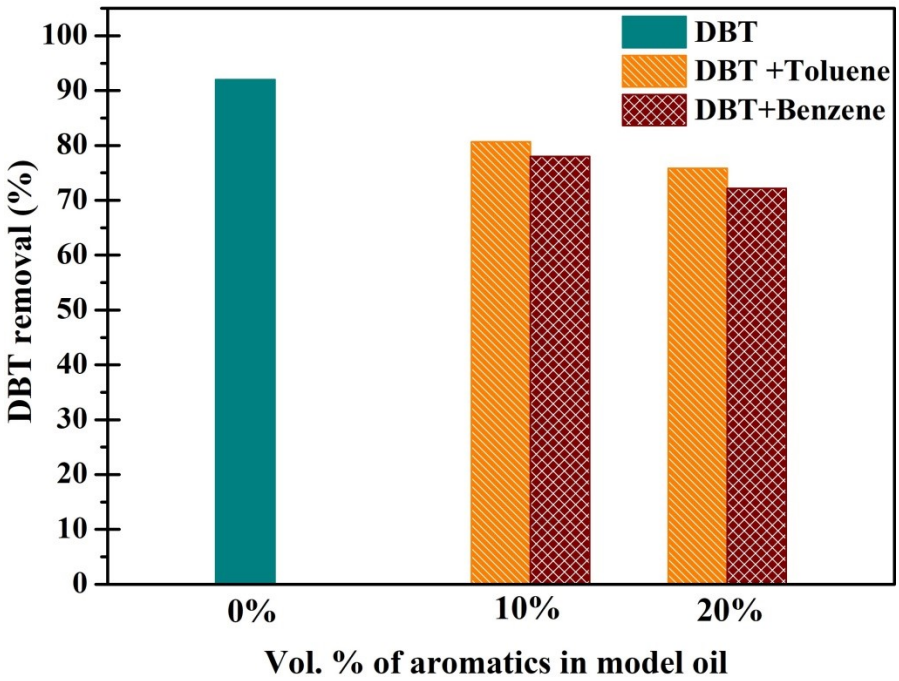

Figure 4.37 Effect of aromatic compounds on DBT adsorption (volume of model oil-10 ml, T = 303 K, adsorbent dose = 20 g/L, adsorption t = 4 h, benzene =10, 20 vol. %, toluene = 10, 20 vol. %).

4.2.1.2.8 Adsorption mechanism

The adsorption of DBT onto 1 wt % Co/ATGAC can be governed by following mechanisms such as π complexation, acid-base interaction, and other weak interactions such as van der Waals interactions. The generation of π complex takes place through dual bonding of Co^{2+} atoms with π electrons of DBT. In the π complexation, both Co^{2+} species and DBT acts as electron acceptor and donor. Molecular orbitals of DBT overlap with vacant s orbital of Co to form σ component of the bond. Simultaneously, the d orbitals of Co^{2+} back donate electrons form it to the antibonding orbitals of DBT in order to form π component of the bond (Khan et al., 2017). According to the HSAB principle, which is proposed by Pearson stated that soft areas of any system prefer to interact with soft region and vice versa. According to Pearson classification, DBT is considered as a soft base as its electronegativity is >2.8, and Co^{2+} belongs to borderline acids (Shah et al., 2016). Therefore, the loading of Co^{+2} ions on activated carbon could weaken the local hard acids present on the surface, and led to the increase in adsorption of DBT on to 1 wt % Co/ATGAC to a certain extent (Yu et al., 2007). Overall, the π complexation seemed

to be the main mechanism which governed the adsorption of DBT onto 1 wt % Co/ATGAC.

4.2.1.3 ADN using cobalt loaded ATGAC

4.2.1.3.1 Effect of various adsorbents

Virgin GAC, acid treated GAC, cobalt impregnated acid treated GAC (1 wt %, 2 wt %, 3 wt %, 4 wt %) were utilized for the ADN of model oil and obtained results are illustrated in Figure 4.38. Acetic acid treated GAC (53 % indole removal) has shown more adsorption affinity towards indole as compared to raw GAC (42% indole removal). This might be due to the presence of more number of oxygen-containing functional groups in ATGAC as compared to raw GAC (Shah et al., 2017). Further, immobilization of cobalt species on ATGAC remarkably improved the adsorption of indole. A significant enhancement in the removal of indole from 65 % to 83 % when increasing the loading of cobalt species from 1 wt % to 3 wt %. This remarkable progress in the adsorption of indole can be ascribed to the formation of π complexation between indole and Co^{+2}. However, on further increasing the loading of cobalt species (3 wt % to 4 wt %) on support material removal of indole decreased, and this might be owing to the agglomeration of cobalt species on a support material. On the basis of the results obtained, 2 wt % Co/ATGAC was taken as the potential adsorbent for the denitrogenation of indole-containing model oil.

4.2.1.3.2 Effect of adsorbent dose

To explore the effect of adsorbent dose, adsorbent doses ranging from 1 g/l to 30 g/l was employed for a 10 ml indole solution of 500 mg/L under constant operating conditions. As shown in Figure 4.39, on increasing the adsorbent dose from 1 g/L to 30 g/l an increase in the removal percentage from 44% to 99.18% was observed. High surface area and more active sites for adsorption of indole might be responsible for the enhancement in the removal of indole. On increasing the adsorbent dose from 1 g/L to 10 g/ L, a substantial increase in the percentage removal from 44% to 96% was obtained. Nevertheless, on further increasing the dose from 10 g/L to 30 g/L, only an increment of approximately 3 % in the removal of indole was achieved. This can be attributed to the

inadequate number of indole molecules for the adsorption at higher dose owing to the fixed concentration of model oil. Therefore, 10 g/L of 2 wt % Co/ATGAC adsorbent dose was chosen as an optimum dose to carry out further experiments.

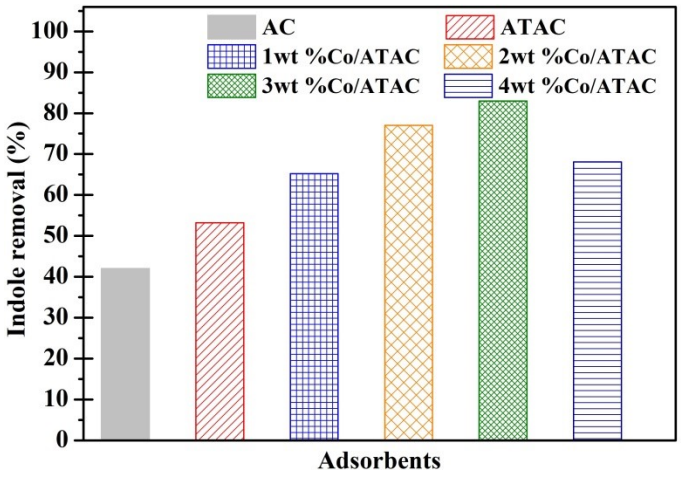

Figure 4.38 Effect of various adsorbents on indole removal (indole concentration = 500 mg/L, t = 4 h, adsorbent dose = 5g/L, temperature = 30 °C).

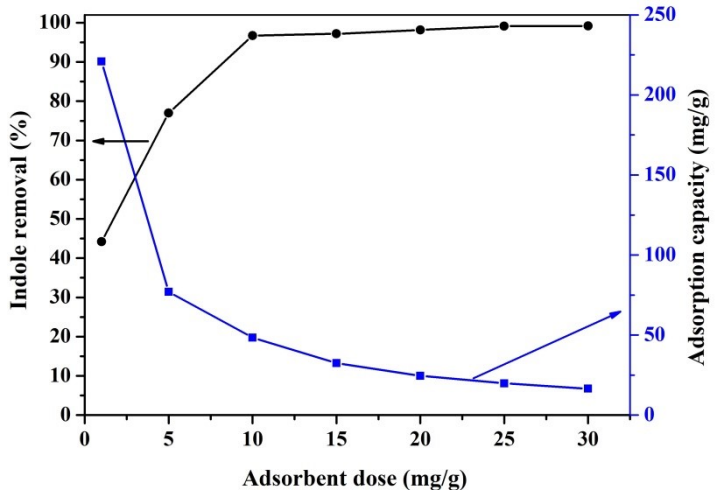

Figure 4.39 Effect of adsorbent dose on indole removal (indole concentration = 500 mg/L, time = 4 h, adsorbent dose = 1 g/L to 30 g/L, temperature = 30 °C, adsorbent = 2 wt % Co/ATGAC).

4.2.1.3.3 Adsorption equilibrium study

Adsorption models were analyzed to explore the adsorption nature of 2 wt % Co/ATGAC and to estimate the maximum adsorption capacities. Figure 4.40 presents the equilibrium data of adsorptive removal of indole over 2 wt % Co/ATGAC by using Langmuir,

Freundlich, Temkin, Redlich-Peterson isotherm models. Table 4.8 indicates the isotherm parameters for all studied adsorption isotherms along with correlation coefficient (R^2) and SSE values for the fit of the adsorption of indole onto 2 wt % Co/ATGAC at various temperatures. Data fitting for adsorption of indole is attained well by the Redlich-Peterson isotherm model with a higher value of R^2 and least value for SSE. It can be seen from Table 4.8 that β values were closer to unity, i.e., obtained experimentally can preferably be fitted with Langmuir adsorption isotherm. Figure 4.40 indicated the fit of R–P isotherm model for the obtained experimental results at different temperatures varying from 283 K to 313 K.

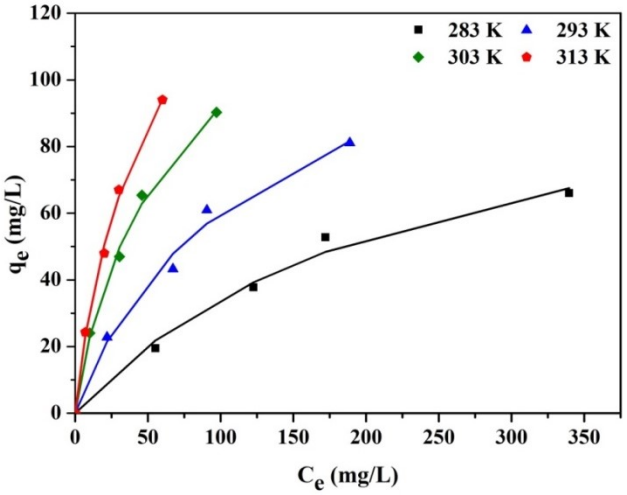

Figure 4.40 Equilibrium isothermal adsorption of indole onto 2 wt % Co/ATGAC at different temperature (Symbols indicate the equilibrium data points, and the lines projected by the R–P model).

Table 4.8 Equilibrium parameters for the adsorption of indole onto 2 wt % Co/ATGAC (t = 4 h, C_o = 250-1000 mgl/L, m = 10 g/L).

Langmuir				
Temperature (K)	q_m (mg/g)	K_L (L/mg)	R^2	SSE
283	113.60	0.0043	0.989	35.21
293	132.26	0.0084	0.990	39.55
303	142.43	0.0177	0.996	18.32
313	164.42	0.0222	0.998	12.92
Freundlich				
Temperature (K)	K_F $[(mg/g)/(mg/L)^{1/n}]$	1/n	R^2	SSE
283	2.335	0.580	0.974	69.10
293	4.352	0.562	0.986	53.96
303	7.342	0.552	0.993	31.93

313	8.126	0.601	0.995	24.18
Temkin				
Temperature (K)	K_T (L/g)	B_1 (J/mol)	R^2	SSE
283	0.037	26.27	0.995	20.49
293	0.095	27.24	0.982	72.26
303	0.204	29.19	0.987	61.10
313	0.270	32.38	0.996	72.36

Redlich–Peterson					
Temperature (K)	K_R (L/g)	α(L/mg)	β	R^2	SSE
283	0.490	0.004	1	0.993	29.46
293	1.271	0.019	0.874	0.999	38.89
303	3.271	0.067	0.790	0.999	15.51
313	4.421	0.068	0.799	0.988	11.06

4.2.1.3.4 Adsorption kinetic study

The adsorption capacity of 2 wt % Co/ATGAC was examined at a temperature of 303 K with respect to time (0- 240 min) to evaluate the adsorption equilibrium. The effect of contact time on the adsorption of indole is shown in Figure 4.41. It was found that the adsorption capacity of indole was increased significantly from 0 to 90 min, and then enhanced slowly after 90 min. The fast adsorption rate may be owing to the high concentration gradient between 2 wt % Co/ATGAC and indole molecules in model oil, and abundant availability of vacant sites in the beginning of the adsorption process (Arshadi et al., 2016). The adsorption equilibrium for removal of indole over 2 wt % Co/ATGAC was obtained at 240 min.

In the present study, two well-known kinetic models were employed to examine the experimental data namely, Pseudo-first-order model and Pseudo-second-order model. The model parameters and the statistical fits of the adsorption results for the two models are depicted in Table 4.9. The R^2 and SSE values obtained for removal of indole showed a better fit to the pseudo-second-order model as compared to the pseudo-first-order model. The obtained results suggested that the chemical reaction, which involves sharing and transfer of an electron, appeared to be significant in the rate determining step (Wang et al., 2016).

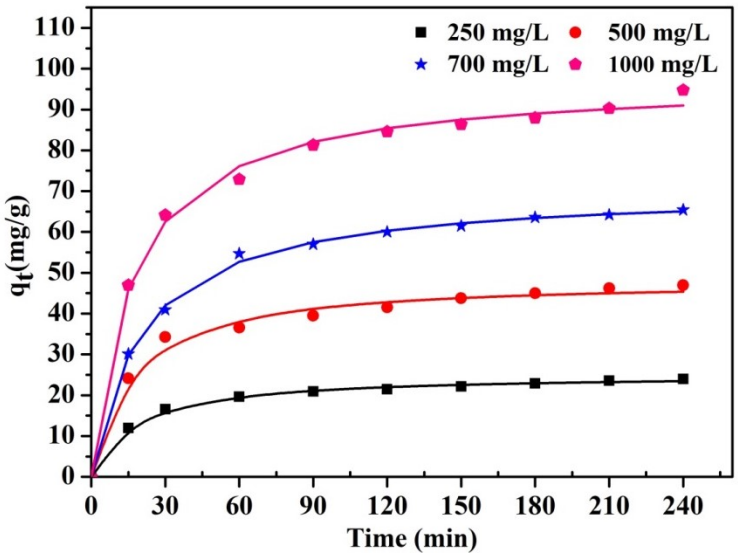

Figure 4.41 Effect of contact time on removal of indole (C_o = 250 – 1000 mg/l, m = 10 g/l, T = 303K, symbols indicate experimental data, solid lines predicted by pseudo second order model).

Table 4.9 Kinetic parameters for the adsorption of indole onto 2 wt % Co/ATGAC (t = 4 h, C_o = 250 – 1000 mg/l, m = 10 g/l, T = 303 K).

C_o(mg/L)	$q_{e,cal}$ (mg/g)	k_1(min^{-1})	R^2	SSE
250	22.51	0.044	0.982	8.652
500	43.51	0.048	0.967	60.866
700	62.50	0.037	0.989	41.471
1000	87.33	0.0434	0.975	179.35
C_o(mg/L)	$q_{e,cal}$ (mg/g)	k_2(min^{-1})	R^2	SSE
250	25.04	0.0024	0.997	1.118
500	48.24	0.0013	0.990	17.74
700	70.58	0.00069	0.998	6.258
1000	97.27	0.00061	0.994	39.69

4.2.1.3.5 Thermodynamic study

In order to evaluate the thermodynamics of the process, three significant parameters were studied namely, the Gibbs free energy of adsorption, entropy change, and the enthalpy change. Batch experiments at four different temperatures were conducted in order to determine the thermodynamic parameters.

Change in Gibbs free energy (ΔG°) is determined with the aid of Equation (3.12). To determine ΔH° and ΔS°, a graph was drawn between ΔG° vs temperature using van't Hoff Equation (Equation 3.13). A straight line was fit to this graph as shown in Figure

4.42; ΔH° and ΔS° were estimated from the values of intercept and slope, respectively. The calculated thermodynamic parameters were shown in Table 4.10. The negative values of ΔG° at all studied temperatures indicate the feasibility and spontaneity of the adsorption process (Manirethan et al., 2018). Values of ΔG° are reducing with an increase in temperature which reveals that adsorption of indole is more spontaneous and favorable at a higher temperature (Nashine and Tembhurkar, 2016). The positive value of entropy shows the good attraction of indole molecules towards adsorbent. It also signifies the enhanced disorder at the solid- solution interface during the adsorption of indole onto the adsorbent (Dursun and Kalayci, 2005). The positive value of enthalpy suggested that adsorption of indole is endothermic in nature (Wu et al., 2009; Ramesh et al., 2007). Value of enthalpy changes also indicates the type of adsorption mechanism, if ΔH° < 40 kJ/mol then the binding mechanism is mainly physisorption and if it is ΔH° > 40 kJ/mol then chemisorption (Li et al., 2014). In the present study value of ΔH° is more than 40 kJ/mol which suggests the binding mechanism is chemisorption.

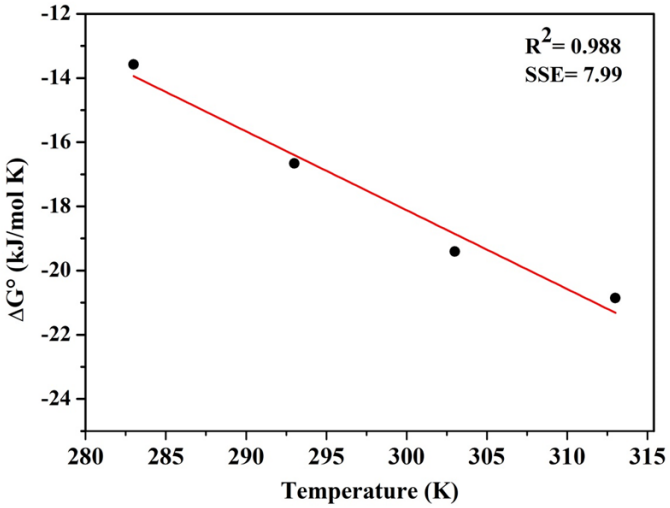

Figure 4.42 ΔG° versus temperature plot for adsorption of indole on to 2 wt % Co/ATGAC.

Table 4.10 Thermodynamics parameters for the adsorption of indole onto 2 wt % Co/ATGAC (t = 4 h, C_o = 250 – 1000 mg/L, m = 10 g/L).

Temperature (K)	ΔG° (kJ/mol K)	ΔH° (kJ/mol)	ΔS° (kJ/mol K)
283	-13.581		
293	-16.663	55.58	0.246
303	-19.410		
313	-20.854		

4.2.1.3.6 Characterization of spent adsorbent

SEM images of 2 wt % Co/ATAC (before and after indole adsorption) are displayed in the Figure 4.43 (a & b). It can be seen from the micrographs that indole loaded on to the fissures and channels available on the surface of 2 wt % Co/ATAC adsorbent. It can be clearly seen from the micrographs that porosity of spent adsorbent decreased fairly as compared with fresh adsorbent. This reduction in porosity might be contributed to the adsorption of indole onto the fissures and channels present on the surface of the fresh adsorbent.

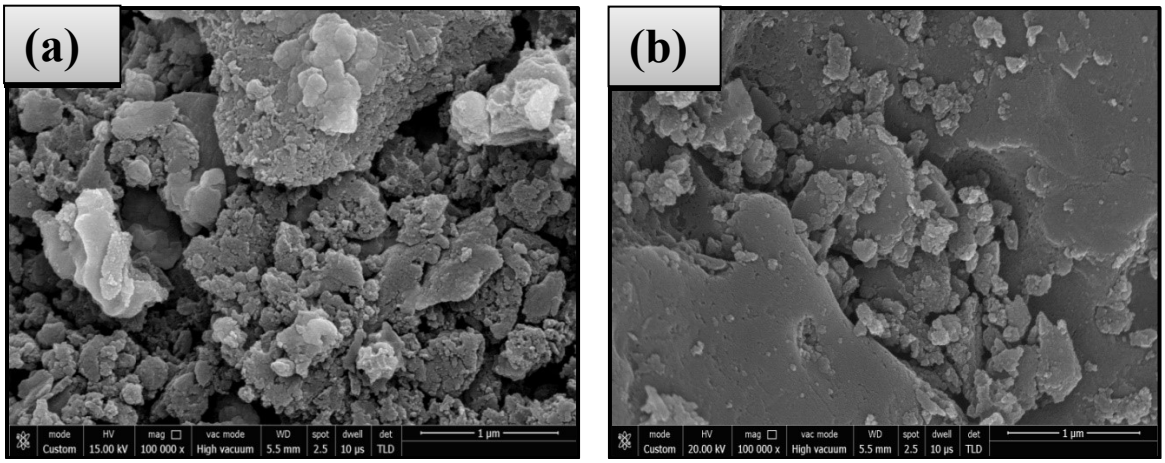

Figure 4.43 SEM images of 2 wt % Co/ATGAC before and after adsorption.

Figure 4.44 shows the XRD patterns of virgin 2 wt % Co/ATGAC and after adsorption of indole from model oil. The XRD patterns indicated that even after adsorption of indole amorphous nature of adsorbent remained intact. In addition, no extra peak was obtained in the diffraction pattern of spent adsorbent indicating that the adsorption of indole was governed by electrostatic interaction (Parashar et al., 2016). FTIR spectra of fresh and spent adsorbent are depicted in Figure 4.45. FTIR spectra revealed that the peaks at 568 cm^{-1} (Co^{3+} -O) and 665 cm^{-1} (Co^{2+} -O) were specifically involved in the adsorption of indole owing to their disappearance in the spent adsorbent (Ganiyu et al., 2016).

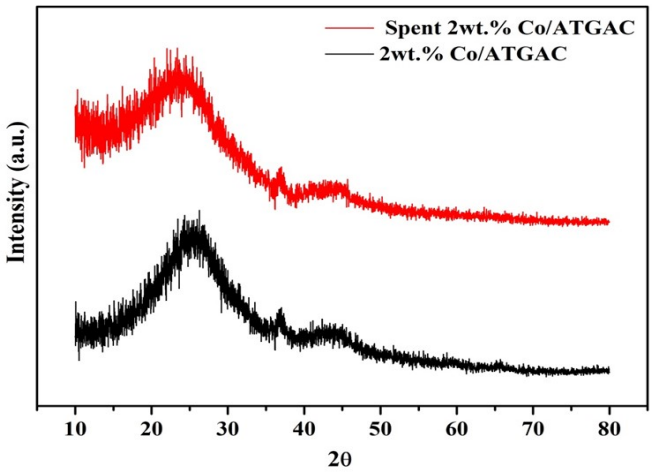

Figure 4.44 X-ray diffraction of fresh 2 wt % Co/ATGAC and spent 2 wt % Co/ATGAC.

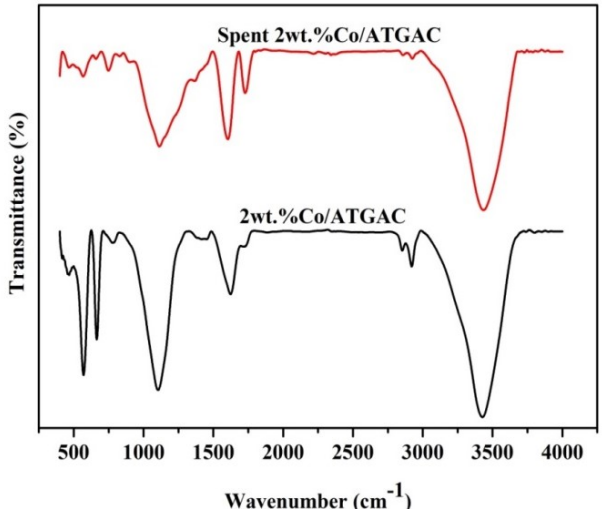

Figure 4.45 FTIR Spectra of fresh 2 wt % Co/ATGAC and spent 2 wt % Co/ATGAC

4.2.1.3.7 Adsorption mechanism and competitive adsorption

It is important to explore the possible adsorption mechanisms to recognize interactions taking place between an adsorbent and an adsorbate as well as for the industrial utilization of an adsorbent. The following adsorption mechanisms van der Waals forces, acid-base interactions, π-complexation, and H-bonding are reported in the literature for the adsorption of nitrogen compounds from liquid fuels. However, in the present study acid-base interactions are not applicable for adsorption of indole as it is a neutral nitrogen compound. The two important factors which govern the adsorption via van der Waals interactions are surface area and porosity. The increased adsorption of indole can be

attributed to the van der Waals forces as the surface area of 2 wt % Co/ATGAC was more than virgin GAC. Upon acidic treatment, the nitrogen removal was enhanced significantly, and this increment in adsorption capacity can be attributed to the H-bond interaction between N–H in indole and the oxygen-containing functional groups present on the surface of adsorbent (Qu et al., 2016). The removal of nitrogen was further enhanced on immobilizing the cobalt species on ATGAC. This might be due to the formation of π complexation between cobalt species and indole. The lone pair of electrons available in nitrogen atom is delocalized and contributes in π electrons (Ahmadi et al., 2017). Since Co^{2+} species exhibit vacant s orbital, and this vacant orbital interact with π electrons of indole to form π complexation. Adsorption of indole over 2 wt % Co/ATGAC might be governed by van der Waals interactions, H-bond interactions, and π complexation.

Competitive adsorption was carried out to explore the selectivity of adsorbent. For the competitive adsorption, toluene and naphthalene were chosen to investigate the ADS selectivity of 2 wt % Co/ATGAC. Competitive adsorption experiment results are shown in Figure 4.46, and it can be seen that the addition of both toluene and naphthalene inhibited the adsorption of indole. On incorporating toluene and naphthalene in the model fuel the removal of indole was reduced from~96 % to~87 % and~55%, respectively. The adsorption of indole was severely inhibited by naphthalene as compared to toluene. Based on the obtained results it seems that the degree of inhibition is dependent on π electron density of components. Naphthalene exhibits more π electron density than toluene and therefore poses more severe effect on adsorption of indole. Plausible adsorption mechanism was most likely to be π complexation as π electron density played an important role on removal of indole over 2 wt % Co/ATGAC.

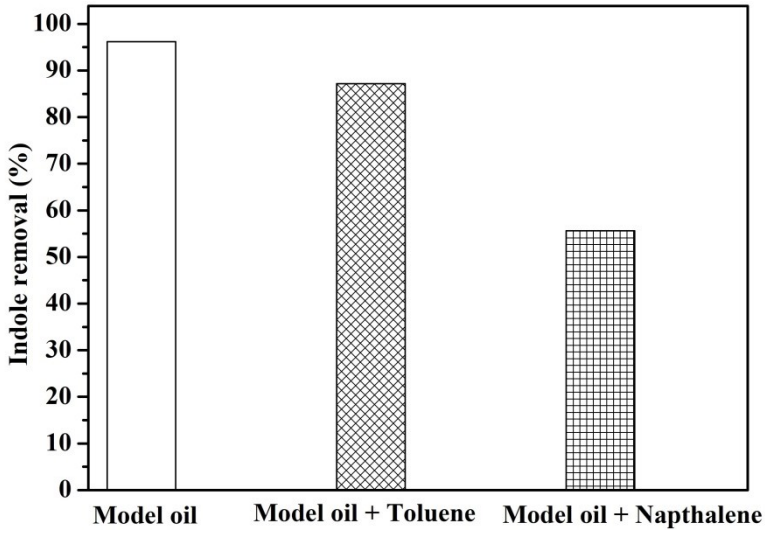

Figure 4.46 Effect of competitive adsorption on indole removal (toluene concentration = 10 vol. %, naphthalene concentration = 10 vol. %, indole concentration = 500 mg/L, t = 4 h, adsorbent dose = 10 g/L, temperature = 30 °C, adsorbent = 2 wt % Co/ATGAC).

4.2.1.3.8 Adsorbent reusability study

The regeneration of adsorbent was studied after the saturation of the 2 wt % Co/ATGAC with indole. The solvent regeneration technique was employed to regenerate spent adsorbent. Spent adsorbent was mixed with an appropriate amount of ethanol and stirred at room temperature for 15 min. Subsequently, the mixture was filtered and dried in an oven at 60 °C. The dried regenerated adsorbent was reused further for adsorption of indole from model oil. In the first regeneration cycle, the percentage removal of indole was decreased from 96.17% to 94.23%. Subsequently, in the second and third regeneration cycle removal was reduced to 92.17%, 89.89%, respectively. Obtained results showed that the regenerated adsorbent is efficient enough to remove the indole from model oil.

4.2.1.4 Simultaneous ADS and ADN using cobalt loaded ATGAC

The simultaneous adsorption of sulfur and nitrogen compounds from model oil was studied by using CCD design. CCD opted for statistical design of experiments as it helps not only in the optimization of main parameters with a minimum number of experimental runs but also aids in determining the interaction among the variables. In the present study, four adsorption parameters (concentration of DBT, the concentration of indole, temperature, and dose) with five levels affecting the removal of DBT and indole were

studied. The parameters were chosen on the basis of experiments conducted for ADS and ADN of model oil, the range and levels of factors are shown in Table 4.11. For the adsorption experiments, 1 wt % Co/ATGAC were used as an adsorbent and experiments were conducted for 4 h.

Table 4.11 Range and level of factors

Factors	**-α**	**-1**	**0**	**+1**	**+ α**
Concentration of DBT (A)	50	200	350	500	650
Concentration of indole (B)	50	200	350	500	650
Temperature	12.5	20	27.5	35	42.5
Dose	10	15	20	25	30

The influence of four major variables varied at five levels on DBT and indole removal from model oil was studied by conducting 31 experiments given by CCD design shown in Table 4.12. Results obtained from the experiments were analyzed with the aid of ANOVA and statistics to obtain empirical equations which can predict actual behavior of adsorption system.

4.2.1.4.1 Statistical analysis

The empirical model's equations in terms of coded parameters for percentage removal of both DBT and indole are given as Equations (4.1) and (4.2), respectively.

DBT removal (%) = 73.41 - .517A + 6.194B + 3.260C + 7.375D + 0.551A*A + 0.573B*B + 1.536C*C + 0.171D*D + 1.866A*B + 0.524A*C + 0943A*D - 0.705B*C + 1.383B*D - 0.155C*D (4.1)

Indole removal (%) = 72.29 - 6.204A - 6.918 B + 4.8 C + 8.158 D + 0.286 A*A + 0.275B*B + 0.821C*C - 0.080 D*D + 3.746A*B - 1.459A*C + 0.386A*D + 1.393B*C + 2.416 B*D - 1.348C*D (4.2)

For the DBT removal, significant model terms were A, B, C, D, A*B, C*C, and insignificant terms were B*B, D*D, A*C, A*D, B*C, B*D, and C*D. For the indole removal, significant model terms were A, B, C, D, A*B, B*D, and insignificant terms were C*C, D*D, A*C, A*D, B*C, B*D, and C*D. The positive coefficient in the model equations depicts the positive effect of that term on response variable whereas negative coefficient indicates the negative effect. Temperature and adsorbent dose have a

synergistic effect on the removal of both DBT and indole, whereas concentrations of DBT and indole have an antagonistic effect.

ANOVA was used to verify the statistical adequacy of the developed regression model and the importance of parameters. Table 4.13 and Table 4.14 show the ANOVA for the response surface quadratic model of DBT and indole. Validation of the model was carried out by using F value and P value. When the F value is high and the P value is less than 0.05, it shows that the model and independent parameters are significant (Vafaei et al., 2018). The model F values of 26.36 and 21.40, and the P value of 0.000 and 0.000 for DBT removal and indole, respectively. It indicated that the obtained model was significant. The fitness of the developed adsorption models was depicted by their insignificant lack of fit, p= 0.123, 0.101 for DBT and indole removal, respectively. The high values of the coefficient of determination (R^2) values for both DBT (0.958) and indole (0.949) adsorption models also indicated that obtained models were suitable to represent the experimental data. The standard error of regression (s) indicates that how well our experimental observations fit into the developed regression model (Danmaliki et al., 2017). It also measures the average distance between the obtained experimental values and the regression line. The low value of S indicates that the model is appropriate for representing experimental data, here a value of 3.162 and 3.944 were obtained for DBT and indole adsorption models, respectively. The results obtained from the statistical analysis indicated that CCD models were appropriate in predicting the removal of both indole and DBT within the range of studied parameters.

Table 4.12 Design matrix for the central composite design.

Run	A (mg/L)	B (mg/L)	C (°C)	D (g/L)	A(% removal)	A (predicted % removal)	B (% removal)	B (predicted % removal)
1	350	350	27.5	20	77.1100	73.4074	76.0000	72.2914
2	500	500	35.0	15	61.0573	58.9267	58.3989	59.3391
3	500	500	35.0	25	77.8517	78.0174	76.7657	78.5627
4	350	350	27.5	20	75.1510	73.4074	74.9500	72.2914
5	50	350	27.5	20	88.2450	88.6461	86.2962	85.8418
6	200	200	35.0	15	91.4096	89.3621	90.8357	91.3196
7	200	200	35.0	25	96.1606	99.1525	95.0723	99.3348
8	350	350	27.5	20	73.1510	73.4074	72.9500	72.2914
9	500	200	35.0	25	85.0432	85.3180	82.7657	77.2887
10	350	350	27.5	20	72.1100	73.4074	70.1400	72.2914
11	350	350	27.5	30	87.1429	88.8401	86.4286	88.2862
12	200	500	35.0	25	87.4630	84.3871	85.6629	85.6252
13	350	350	27.5	20	71.1100	73.4074	69.0000	72.2914
14	350	350	42.5	20	88.1265	86.0728	87.5779	85.1755
15	200	500	20.0	25	81.3511	80.6329	77.9798	73.0159

16	350	650	27.5	20	60.0000	63.3103	58.0000	59.5549
17	500	200	35.0	15	70.5898	71.7574	64.6139	67.7301
18	350	350	27.5	10	58.0597	59.3397	55.9415	55.6554
19	350	350	12.5	20	68.0000	73.0310	62.0000	65.9740
20	500	500	20.0	15	55.0000	52.4576	53.2841	47.1739
21	200	500	35.0	15	65.2823	69.0665	69.7969	67.9450
22	200	200	20.0	15	81.8864	82.1702	82.5360	78.8913
23	200	200	20.0	25	93.8759	92.5798	92.9625	92.2985
24	350	50	27.5	20	88.4211	88.0880	87.2119	87.2286
25	500	200	20.0	25	79.9844	76.6496	76.0843	76.0885
26	650	350	27.5	20	60.0000	62.5761	59.0000	61.0259
27	500	500	20.0	25	73.5467	72.1675	71.9972	71.7894
28	200	500	20.0	15	68.3946	64.6931	44.1907	49.9437
29	350	350	27.5	20	74.1100	73.4074	73.0000	72.2914
30	350	350	27.5	20	71.1100	73.4074	70.0000	72.2914
31	500	200	20.0	15	62.8206	62.4698	60.8240	61.1379

Table 4.13 ANOVA for removal of DBT

Source	Sum of squares	Degree of freedom	F value	P value
Model	3690.12	14	26.36	0.000
DBT (A)	1019.47	1	101.96	0.000
INDOLE (B)	920.90	1	92.10	0.000
Temperature (C)	255.13	1	25.52	0.000
Dose (D)	1305.41	1	130.56	0.000
DBT*DBT(A*A)	8.68	1	0.87	0.365
INDOLE*INDOLE (B*B)	9.39	1	0.94	0.347
Temperature*Temperature (C*C)	67.48	1	6.75	0.019
Dose*Dose (D*D)	0.83	1	0.08	0.777
DBT*INDOLE (A*B)	55.72	1	5.57	0.031
DBT*Temperature (A*C)	4.39	1	0.44	0.517
DBT*Dose (A*D)	14.21	1	1.42	0.251
INDOLE*Temperature (B*C)	7.94	1	0.79	0.386
INDOLE*Dose (B*D)	30.58	1	3.06	0.099
Temperature*Dose (C*D)	0.38	1	0.04	0.84
Lack of fit	130.43	10	2.65	0.123
Pure Error	29.55	6		
Total	3850.10	30		

Table 4.14 ANOVA for removal of indole.

Source	Sum of squares	Degree of freedom	F value	P value
Model	4659.60	14	21.40	0.000
DBT (A)	923.74	1	59.38	0.028
INDOLE (B)	1148.75	1	73.85	0.000
Temperature (C)	553.05	1	35.55	0.000
Dose (D)	1597.15	1	102.67	0.000
DBT*DBT (A*A)	2.33	1	0.15	0.704
INDOLE*INDOLE (B*B)	2.16	1	0.17	0.714
Temperature*Temperature (C*C)	19.27	1	1.24	0.282
Dose*Dose (D*D)	0.18	1	0.01	0.915
DBT*INDOLE (A*B)	224.51	1	14.43	0.002
DBT*Temperature (A*C)	34.06	1	2.19	0.158
DBT*Dose (A*D)	2.38	1	0.15	0.701
INDOLE*Temperature (B*C)	31.06	1	2	0.177
INDOLE*Dose (B*D)	93.41	1	5	0.026
Temperature*Dose (C*D)	29.07	1	1.87	0.190
Lack of fit	206.42	10	2.92	0.101
Pure Error	42.47	6		
Total	4908.50	30		

Figure 4.47 compares the experimental and predicted model values for DBT and indole removal, respectively. To obtain a good correlation between experimental and predicted values, obtained R^2 values should be no less than 0.80 (Ghanbari et al., 2017). In the present work, R^2 value was found to be 0.958 for DBT removal, and 0.949 for the indole removal, indicating good fit.

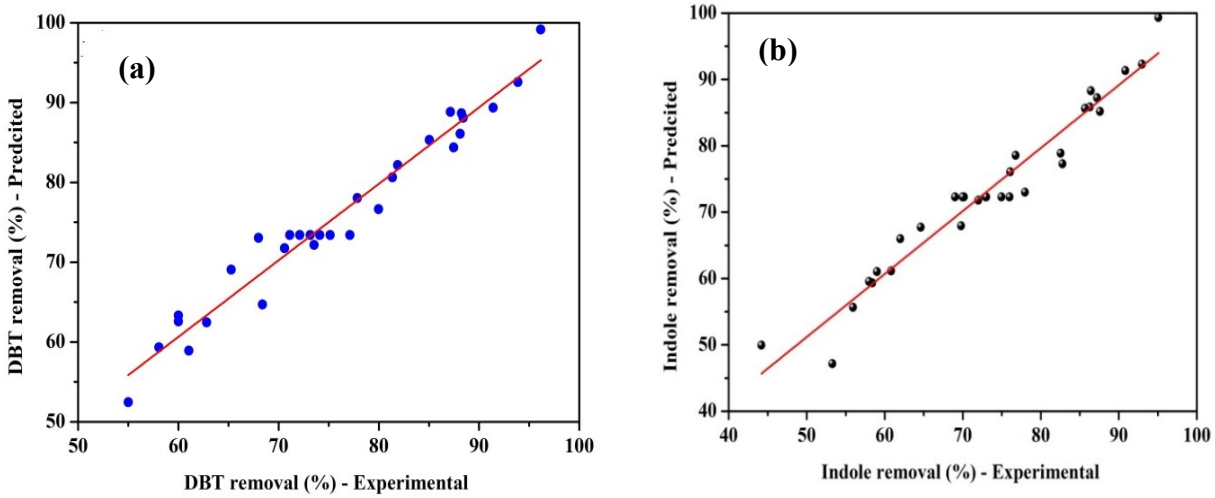

Figure 4.47 Comparison of experimental (actual) and predicted values of the responses for percentage removal of (a) DBT, (b) Indole.

4.2.1.4.2 Effect of single factor on the response variables

The single effect of processing variables on DBT and indole removal is represented in factorial plots as shown in Figure 4.48. These plots give information on the mean effect of each variable and the response variable. As can be seen from Figure 4.48(a,b), on increasing the concentration of DBT and indole, removal of DBT decreased significantly. This significant decrease in removal of DBT could be attributed to the decrease in number of adsorption sites due to the increase in the number of species of DBT and indole (Olgun et al., 2011). In addition, the decrease in removal of DBT due to the presence of indole could be ascribed to the competition between DBT and indole to get adsorbed on active sites of adsorbent. Similarly, removal of indole was reduced significantly on increasing the concentration of DBT and indole in model oil. However, temperature and adsorbent dose had synergistic effect on both DBT and indole removal. Higher amount of dose provide more number of vacant active sites for the adsorption of DBT and indole, while

higher temperature gives better removal as adsorption of DBT and indole on 1 wt % Co/ATGAC is endothermic in nature.

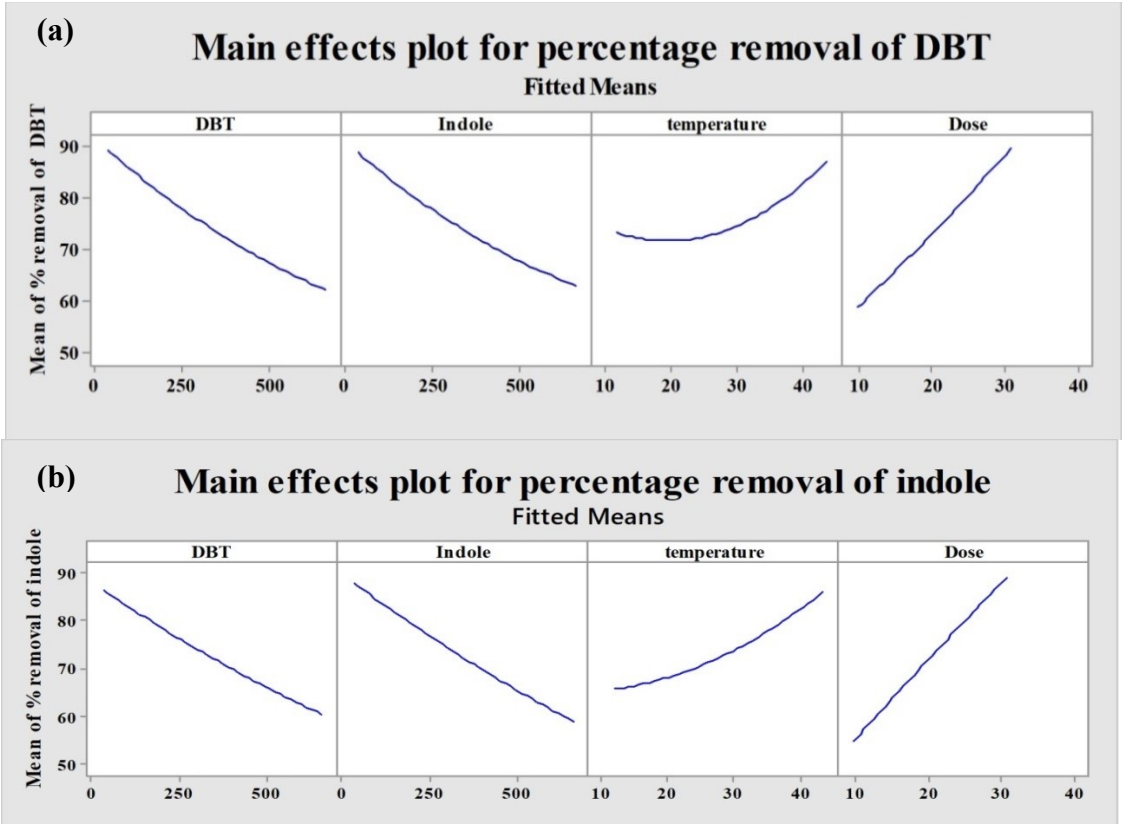

Figure 4.48 Main effects plot for the removal of (a) DBT and (b) indole from model oil.

4.2.1.4.3 Effect of interactions between factors

To explore the interaction between the processing parameters and response variables, 3D surface and contour plots were constructed. These plots provide benefit of giving summarized information in one single figure. The plots were constructed by holding two processing variables at central levels and varying other two variables. For the DBT removal, only one interaction i.e. interaction between concentration of DBT and indole was found to be significant. Figure 4.49(a,b) represents the interaction effect of concentration of DBT and indole on DBT removal. It can be seen from the Figure 4.49 (b) that DBT removal reduced significantly on increasing the concentration of both DBT and indole. The highest removal of DBT was achieved when the concentration of DBT and indole was lowest in the model oil. For indole removal, two interactions (A*B and B*D) were found to be important. The interaction between concentration of DBT and

indole on indole removal was depicted in Figure 4.50(a,b). Both concentration of DBT and indole had negative impact on removal of indole. It can be seen from Figure 4.50(a) that the effect of concentration of DBT was more pronounced at lower concentration of indole as compared to the higher concentration of indole. Figure 4.51(a,b) depicted the interaction effect of concentration of indole and adsorbent dose. It can be seen from the Figure 4.51 (a) that concentration of indole had negative impact on removal of indole whereas adsorbent dose had positive effect on indole removal. Adsorbent dose had more significant effect on indole removal at higher concentration of indole as compared to the lower concentration of indole. A relatively flat line on Figure 4.51(a) at highest adsorbent dose indicated that there was no as such impact of of increasing the concentration of indole at highest adsorbent dose.

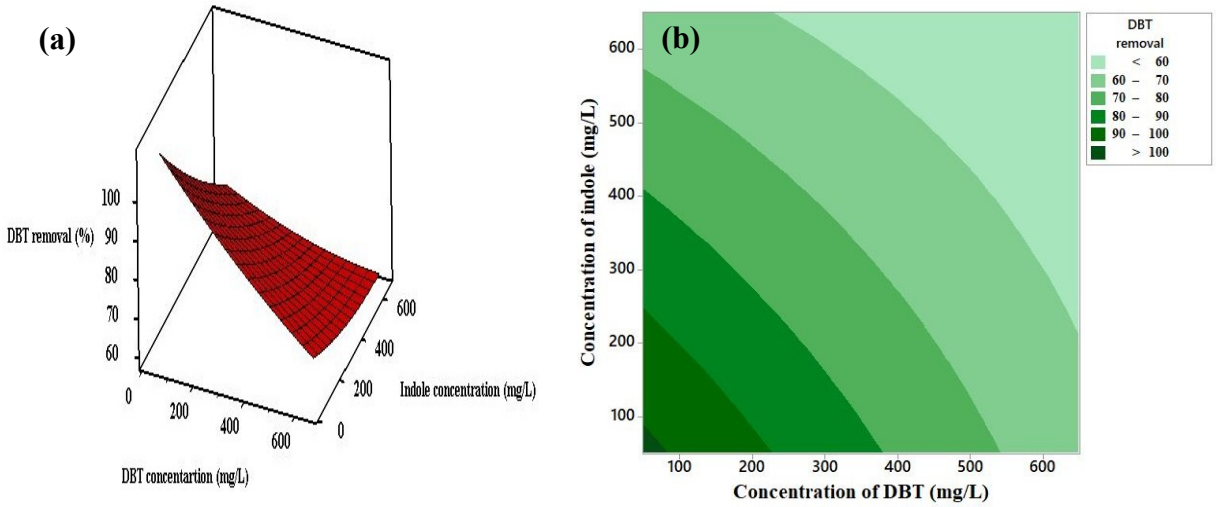

Figure 4.49 Surface(a) and contour(b) plots of DBT removal for interaction between concentration of DBT and concentration of indole.

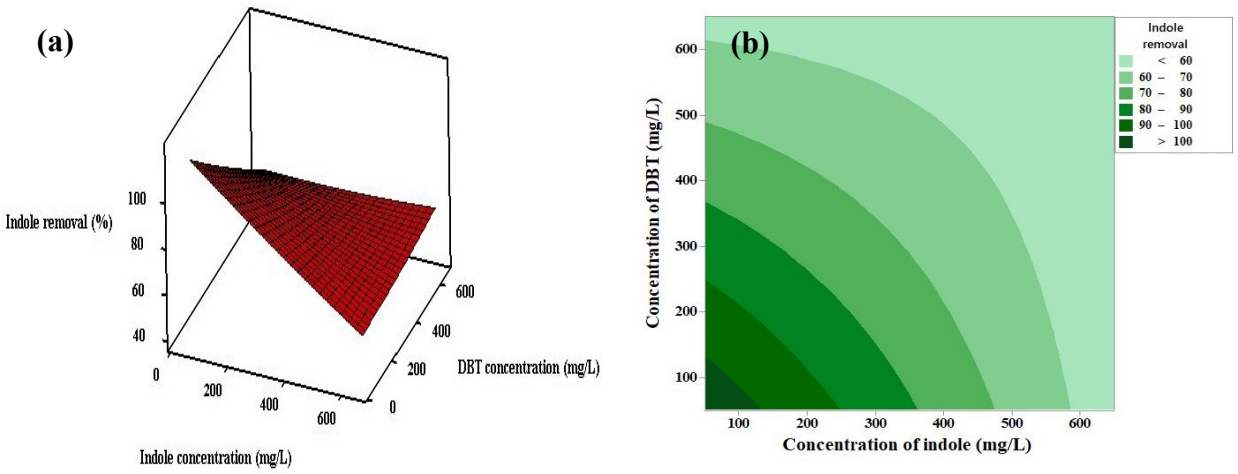

Figure 4.50 Surface(a) and contour(b) plots of indole removal for interaction between concentration of indole and concentration of DBT.

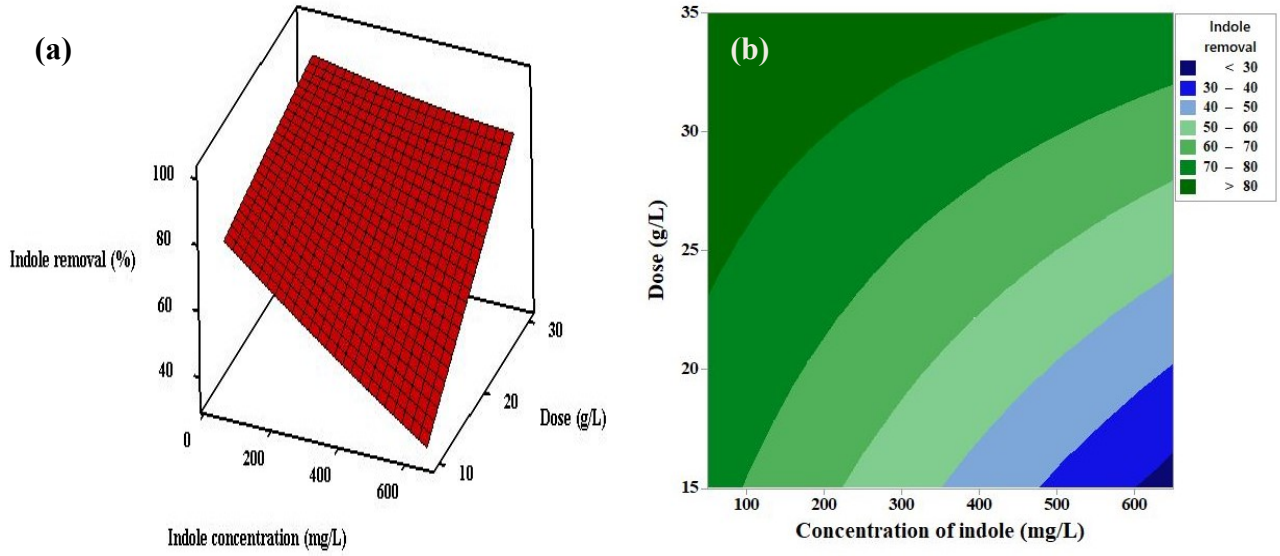

Figure 4.51 Surface(a) and contour(b) plots of indole removal for interaction between concentration of indole and dose.

4.2.1.4.4 Analysis of residual graphs

To evaluate the reliability of obtained CCD models, the analysis of residual plots (the difference between the predicted and experimental values) were carried out. Residual plots are used to describe the variation of the obtained model according to the normal distribution. A model is considered reliable if residuals are normally and randomly distributed. One technique of testing for a normal distribution is to check how closely the normal probability plot of residuals follows a straight line. The normal probability plot for

both DBT and indole removal are depicted in Figure 4.52(a,b). It can be clearly seen from the figure that maximum number of data points follows a straight line which conforms the normal distribution of data. The residuals versus fitted values are shown in Figure 4.52(a,b). It can be observed from the figures that residuals are randomly distributed about zero and the distribution can be approximated as normal. The plot of residual values against frequency is provided in the histograms. It can be seen from the histograms that residuals fluctuate in a random manner and roughly symmetrical around the mean with most of the residual values. The plot of residuals versus observation order shows that residuals are scattered randomly and close to the center value. Residual graph analysis showed that developed CCD model for DBT and indole removal is acceptable.

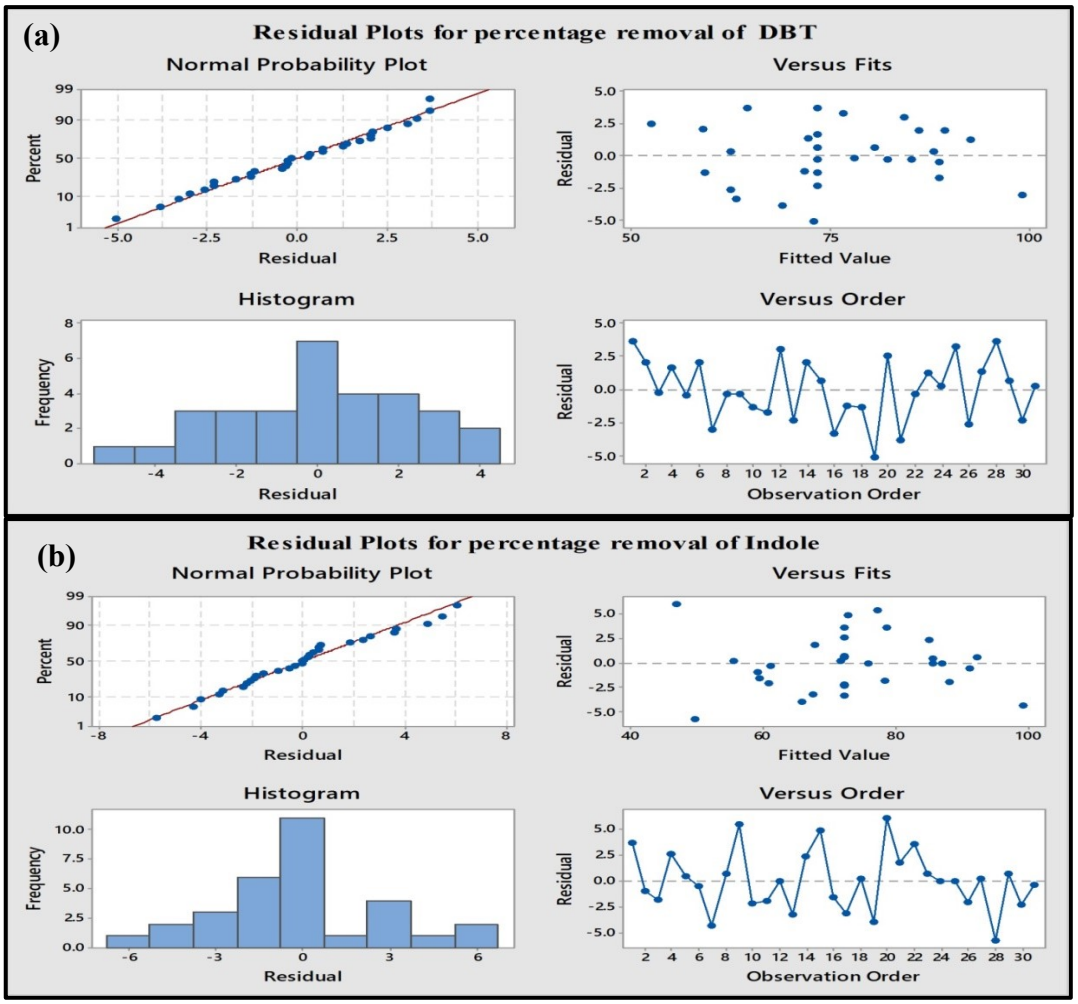

Figure 4.52 Residual plots for a) DBT removal and b) indole removal.

4.2.1.4.5 Optimization analysis

One of the objectives of the present work was to identify the optimum process conditions to obtain the maximum removal of DBT and indole from model oil. Here, the four operating variables were assessed in order to get the optimum response. The response optimizer function available in Minitab software was used to optimize the response variables. For both DBT and indole, target values were set at 100 %, lower bounds were based on the lowest values of removal obtained for both compounds in CCD design, and upper values were set at 110 % as it has to be more than target value. At the optimum operating conditions, the predicted DBT and indole removal values were found to be 97.86 % and 99.58 %, respectively with a composite desirability score of 0.9724. To achieve such a remarkable removal for both sulfur and nitrogen compounds, a temperature of 30 °C, a dosage of 19 g/L, 223 mg/L of DBT concentration and 50 mg/L of indole concentration in model oil is required. These optimum values were checked experimentally which resulted in to 95.4% removal of DBT and 98.1 % removal of indole. The obtained values were sufficiently close enough to the predicted values which indicated the reliability of the CCD model for the appraisal of the real conditions.

4.2.2 ADS using molybdenum loaded ATGAC

Molybdenum loaded ATGAC was characterized with the aid of various characterization techniques, and the results of these techniques are described in the section 4.2.2.1. This section describes the batch adsorptive desulfurization (section 4.2.2.2) and adsorptive denitrogenation (section 4.2.2.3) of model oil by using molybdenum impregnated ATGAC. Further, this section also contained optimization study of simultaneous adsorptive desulfurization and denitrogenation with the help of CCD design by using optimized adsorbent (section 4.2.2.4).

4.2.2.1 Characterization of molybdenum loaded ATGAC

The SEM images of virgin GAC and molybdenum loaded ATGAC is shown in Figure 4.53 (a,b). As shown in Figure 4.53(a), the surface of GAC possesses porous nature when compared to the surface of Mo/ATGAC (Figure 4.53(b)). Further, rod shape particles aggregation can be clearly seen on the surface of Mo/ATGAC which indicates the

successful impregnation of molybdenum species on GAC. Obtained results match well with the previously reported literature (Qiu et al., 2016; Yang et al., 2016).

Powder X-ray diffraction pattern for the Mo/ATGAC is depicted in Figure 4.54 A broad hump was observed around 24^{o} and 44^{o} in the Mo/ATGAC indicates the presence of amorphous carbon in the sample (Prahas et al. 2008). Peaks appearing at 12.90°, 23.62°, 25.86°, 27.54°, 33.9°, and 39.13° represented the presence of MoO_3 with orthorhombic phase (Bakar et al., 2015; Shetty et al.,2015; Mokhtar et al., 2015). The average crystallite size of MoO_3 was found to be 23.2 nm.

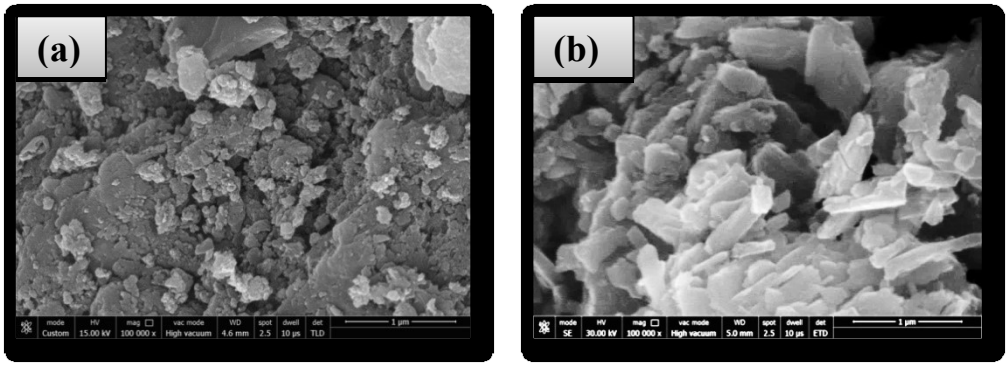

Figure 4.53 SEM images of a) GAC and b) Mo/ATGAC.

FTIR spectra of Mo/ATGAC is presented in Figure 4.55, and the Mo/ATGAC maintained the characteristic peaks of GAC. The peaks at 1737 cm^{-1} and 1628 cm^{-1} were ascribed to carboxyl group and carbonyl group, respectively (Saleh et al., 2017). The absorption band at 1035 cm^{-1} was associated with C-O stretching vibration (Danmaliki and Saleh, 2017). The broad absorption band centered at 3441 cm^{-1} is assigned to O–H stretching vibrations of hydroxyl groups due to the presence of water molecules in the pores of GAC framework (Saleh and Danmalik, 2015). The bands at 2919 cm^{-1} and 2850 cm^{-1} indicated the stretching vibrations of C-H. These all peaks are presented in the framework of GAC (Figure 4.25). However, the two additional peaks were obtained in the spectra of Mo/ATGAC. The peak at 900 cm^{-1} represented the asymmetric stretching of Mo-O-Mo whereas the band at 776 cm^{-1} showed the stretching of Mo=O (Qiu et al., 2016).

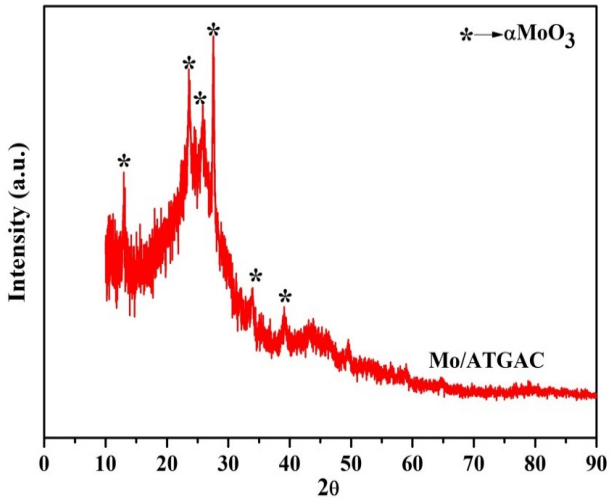

Figure 4.54 X-ray diffraction pattern of Mo/ATGAC.

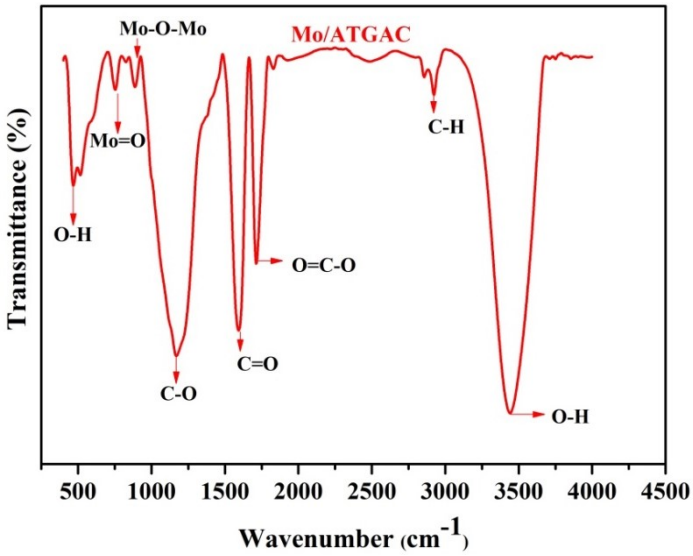

Figure 4.55 FTIR spectra of Mo/ATGAC

Nitrogen adsorption-desorption isotherm of GAC and Mo/ATGAC is shown in Figure 4.56 (a). Pore size distribution of Mo/ATGAC is given in Figure 4.56 (b). It can be clearly seen from the Figure 4.56 (a), that GAC is highly microporous in nature due to the high uptake of nitrogen at relative pressure less than 0.25 (Xiong et al., 2012). Pore size didtribution also indicate high microporous volume. Hysteresis loop can be seen in Mo/ATGAC which indicates that incorporation of molybdenum species in GAC framework induces mesoporosity in the sample. Further, the surface area of GAC enhanced from 257 m^2/g to 316 m^2/g upon modification with acid treatment and

molybdenum species. This increase in surface area can be attributed to the acidic treatment of GAC. Because of acid treatment, the inert materials present in the pores of GAC were removed and increased the pore volume.

XPS spectra of Mo/ATGAC is depicted in Figure 4.57, and survey spectra of Mo/ATGAC (Figure 4.57(a)) indicated that the adsorbent sample mainly consist of carbon, oxygen, and molybdenum. The deconvoluted C 1s XPS spectra is presented in Figure 4.57 (b), and spectra is decomposed into four peaks namely, C-C (284.2 eV), C-O (285.3 eV), C=O (287.4 eV), and O-C=O (289.4 ev). O 1s XPS spectra as shown in Figure 4.57 (c) is deconvoluted into five characteristics peaks namely, MoO_3 (530.2 eV), C=O (531.1 eV), C-O (532 eV), O-H (533.1 eV). Figure 4.57(d) displays the Mo 3d XPS spectra of Mo/ATGAC. Binding energies of Mo $3d_{5/2}$ and Mo $3d_{3/2}$ peak for Mo^{6+} were found to be 232.6 and 235.9 eV (Abdullah et al., 2014).

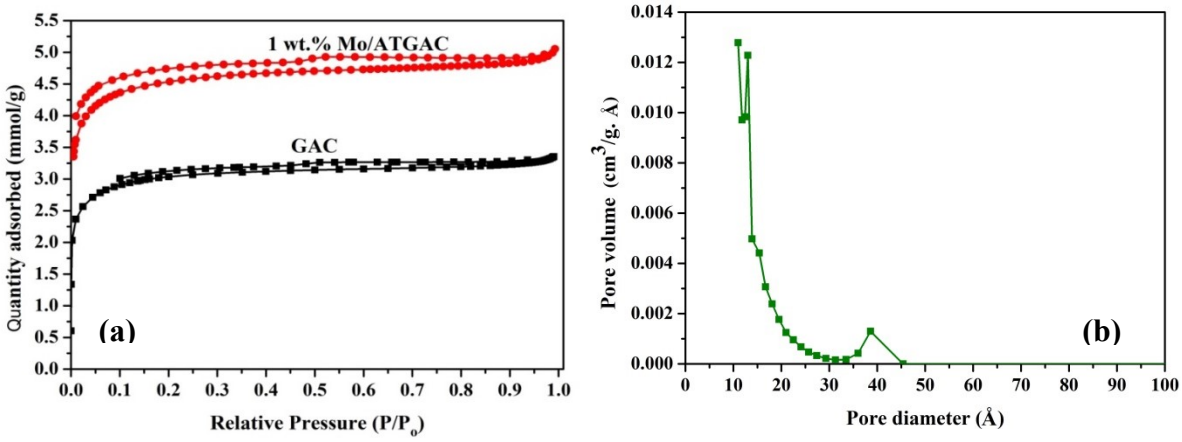

Figure 4.56 (a) Nitrogen adsorption desorption isotherm for GAC and 1 wt % Mo/ATGAC (b) Pore size distribution of 1 wt % Mo/ATGAC.

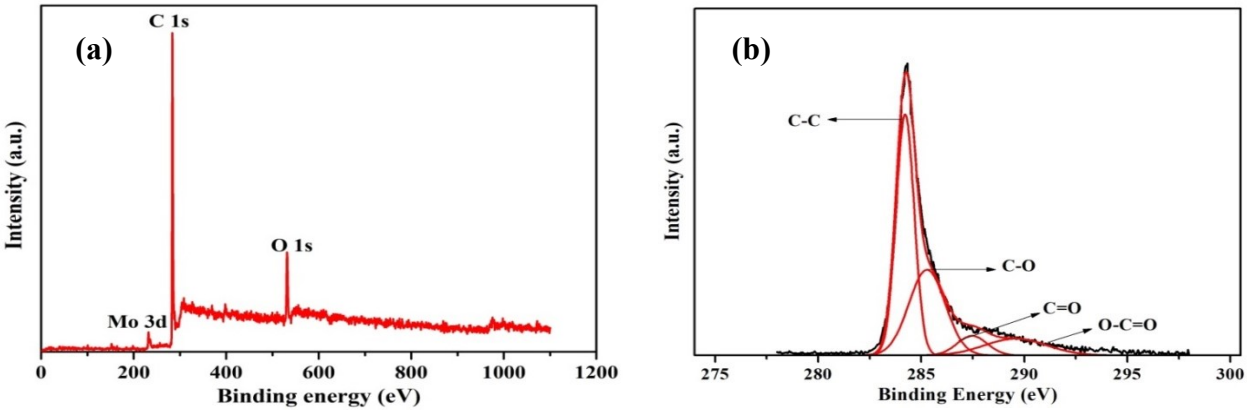

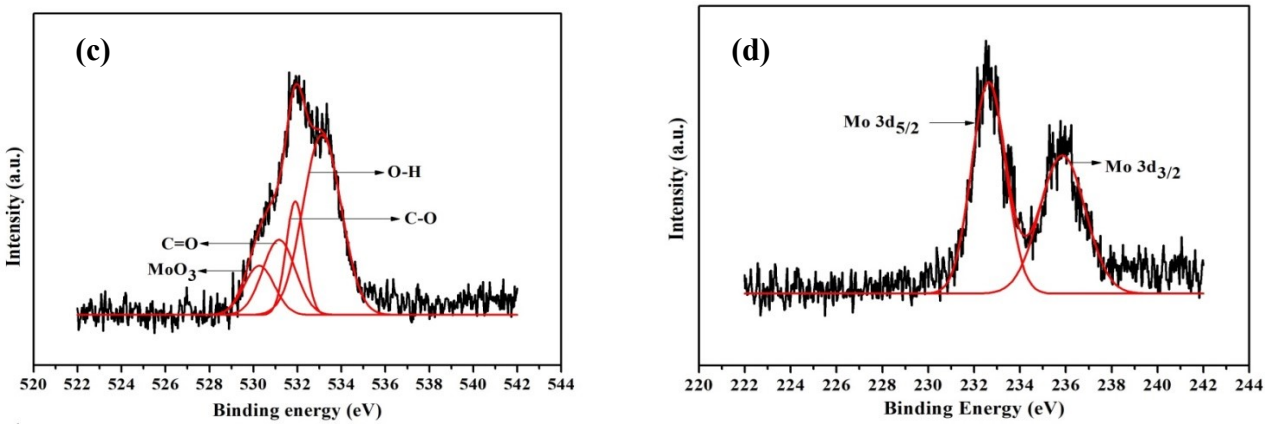

Figure 4.57 XPS spectra (a) full survey scan, (b) deconvoluted C 1s spectra of Mo/ATGAC, (c) deconvoluted O 1s spectra of Mo/ATGAC, (d) deconvoluted Mo 3d spectra of Mo/ATGAC.

4.2.2.2 ADS using molybdenum loaded ATGAC

4.2.2.2.1 Effect of various adsorbents

The deduction of DBT from the model oil with the aid of various adsorbents under identical operating conditions is presented in Figure 4.58. It can be seen from the Figure 4.58 that ATGAC (49 % DBT removal) is more efficient in removing DBT as compared to GAC (38 % DBT removal). This remarkable enhancement in DBT removal can be attributed to the additional oxygen functional group on the surface of ATGAC because of acetic acid treatment (Jiang et al., 2003). ATGAC was modified with molybdenum loading were also tested. As can be seen from Figure 4.58, Mo loaded ATGAC showed better adsorption capacity as compared with virgin GAC and ATGAC. Modification of ATGAC with molybdenum species increases both Brönsted and Lewis acidic site which eventually increases its adsorption capacity (Solar et al., 1991; Shao et al., 2012). The maximum removal of DBT was achieved by 1 wt% Mo/ATGAC; DBT removal was declined with the increase in molybdenum species loading. This could be due to the excessive loading which can cause blockage of pores and channel of adsorbent which resulted into low adsorption capacity. Among all the molybdenum loaded adsorbents, 1 wt. % of Mo/ATGAC showed better DBT removal.

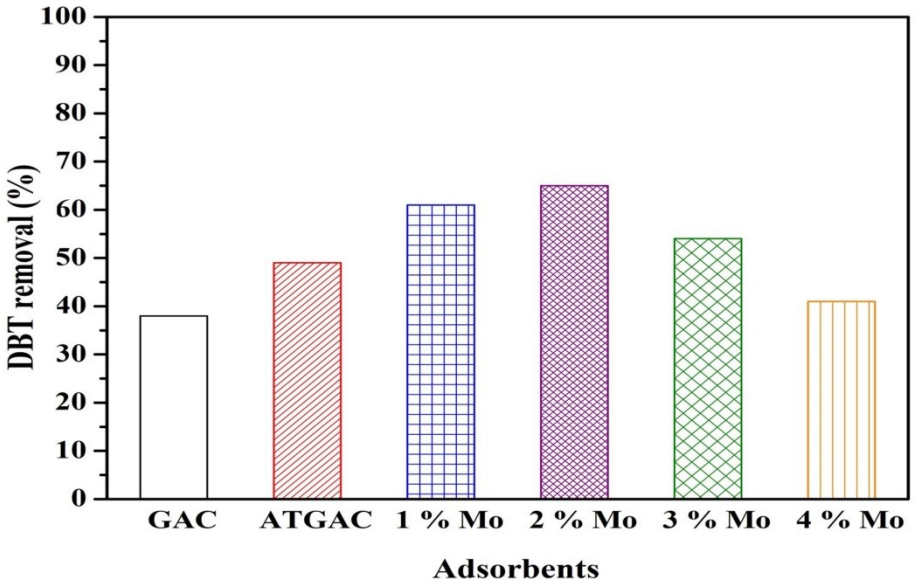

Figure 4.58 Effect of various adsorbents on DBT removal (DBT initial concentration = 500 mg/L, adsorbent dose = 10 g/L, reaction time = 4 h, T = 303 K).

4.2.2.2.2 Effect of adsorbent dose

The effect of the adsorbent dose on the reduction of DBT content in model oil was analyzed by varying dosage in the range of 5 g/L to 40 g/L. It was observed that on increasing the adsorbent amount from 5 g/L to 25 g/L, a remarkable improvement in DBT removal from 34 % to 91 % was obtained (Figure 4.59). This enhanced removal of DBT can be attributed to the presence of more surface area and a large number of adsorption sites (Kumar et al., 2011). However, on further increasing the adsorbent dose from 25 g/L to 40 g/L DBT removal increased gradually from 91 % to 96 %. This could be ascribed to the fact that active sites and DBT reaches to equilibrium as other operating conditions are remained constant (Bandyopadhyay and Biswas, 1998).

4.2.2.2.3 Adsorption equilibrium study

In order to understand the interactive behavior between adsorbent and adsorbate, the adsorption isotherm study was done (Langmuir, Freundlich, Temkin, Redlich–Peterson isotherm). Table 4.15 shows the model parameters and the statistical fits for the adsorption of DBT onto Mo/ATGAC at different temperatures. The obtained results showed that the adsorption of DBT was best represented by R-P isotherm at all temperatures due to the highest value of R^2 and the least value of SSE. Adsorption data at

a temperature of 303 K and 313 K, R-P isotherm is converted into Langmuir isotherm as the value of β becomes 1. The obtained results showed that at a temperature above 293 K, the adsorption data were best represented by Langmuir adsorption isotherm. It can be seen from Table 4.15 that temperature has a positive effect on the adsorption of DBT. A rise in temperature from 283 k to 313 K leads to an increase in q_m from 16.78 mg/g to 30.01 mg/g. The fit of R−P adsorption isotherm for the obtained adsorption data was shown in Figure 4.60. As can be seen from Figure 4.60, the adsorption capacity of adsorbent enhanced significantly with increasing temperature. This rise in adsorption capacity could be ascribed to the faster rate of diffusion of DBT molecules into the pores of Mo/ATGAC.

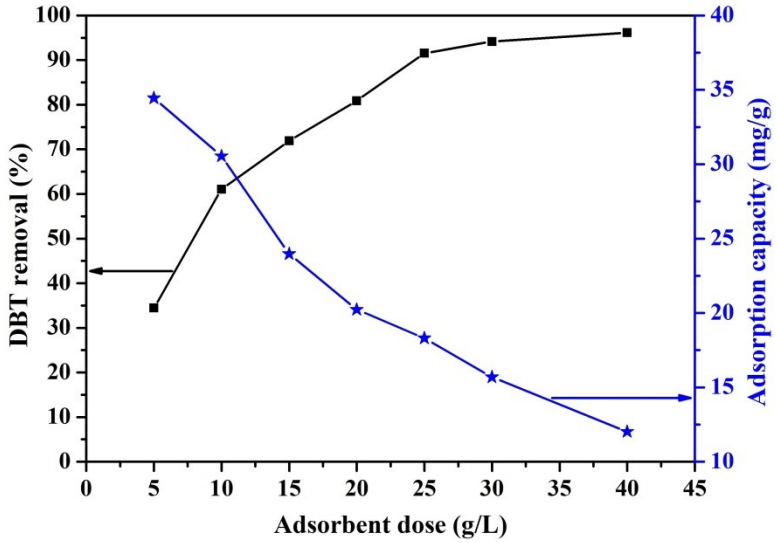

Figure 4.59 Effect of adsorbent dose on DBT removal (DBT solution = 500 mg/L, t = 4 h, T = 303 K, adsorbent dose (1 wt % Mo/ATGAC) = 5 to 40 g/L).

Table 4.15 Equilibrium parameters for adsorption of DBT onto Mo/ATGAC (t = 4 h, C_o = 200 – 800 mgl/L, m = 25 g/L).

Langmuir				
Temperature (K)	q_m	K_L	R^2	SSE
283	16.779	0.0050	0.983	1.516
293	19.847	0.0068	0.987	1.841
303	27.590	0.0136	0.998	0.435
313	30.008	0.0195	0.999	0.800
Freundlich				
Temperature (K)	K_F	1/n	R^2	SSE
283	0.707	0.458	0.982	1.700

293	1.083	0.434	0.981	2.643
303	2.215	0.412	0.980	5.998
313	2.885	0.402	0.993	5.303
Temkin				
Temperature (K)	K_T	B_T	R^2	SSE
283	3.802	0.046	0.983	1.631
293	4.471	0.063	0.985	2.019
303	6.256	0.122	0.996	1.062
313	6.844	0.170	0.998	1.405
Redlich–Peterson				
Temperature (K)	K_R	α	β	R^2	SSE
283	0.1101	0.0198	0.835	0.985	1.454
293	0.1518	0.0125	0.925	0.987	1.814
303	0.3758	0.0136	1	0.998	0.434
313	0.5849	0.0194	1	0.999	0.800

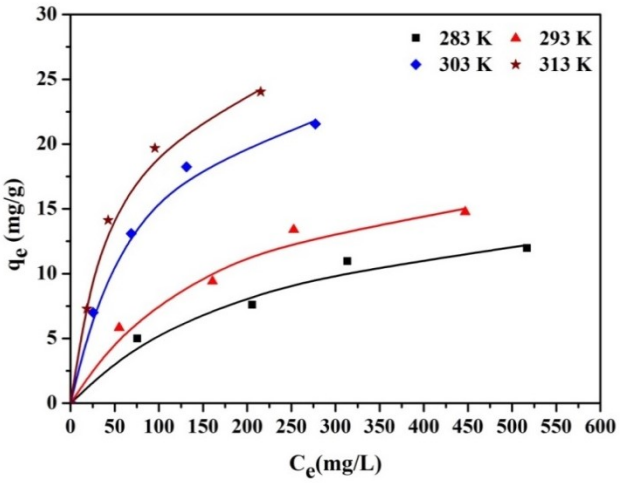

Figure 4.60 Equilibrium isothermal adsorption of DBT onto Mo/ATGAC at different temperature (symbols indicate the equilibrium data points, and the lines are projected by the R−P model).

4.2.2.2.4 Adsorption kinetic study

In order to study the kinetic parameters and to find out the equilibrium contact time, and DBT adsorption experiments were conducted by using 1 wt % Mo/ATGAC as an adsorbent at various time intervals ranging from 15 to 240 min with different initial concentrations (200 - 800 mg/L). This study was carried out at a temperature of 303 K with an optimum adsorbent dose of 25 g/L. Rapid adsorption of DBT molecules was observed initial 60 min of the adsorption process, and the adsorption reaches equilibrium around 240 min (Figure 4.61). It can be seen from Figure 4.61 that the rate of adsorption

of DBT is limited by its initial concentration. The rate of adsorption of DBT rises with the rise in initial concentration owing to the increase in the driving force (Rameshraja et al., 2012). The values of kinetic parameters along with R^2 and SSE values for pseudo-first-order and pseudo-second-order models are displayed in Table 4.16. As can be seen from Table 4.16, the adsorption data is best represented by the pseudo-second-order model.

Table 4.16 Kinetic parameters for the adsorption of DBT onto Mo/ATGAC (t = 4 h, C_o = 200 – 800 mg/l, m = 25 g/l, T = 303 K).

Pseudo first order					
C_o(mg/L)	$q_{e,exp}$ (mg/g)	$q_{e,cal}$ (mg/g)	k_1(min^{-1})	R^2	SSE
200	6.421	6.128	0.0529	0.902	3.641
400	13.09	11.87	0.0449	0.942	8.400
600	18.24	17.43	0.0838	0.959	11.49
800	21.63	20.10	0.0885	0.974	9.663
Pseudo second order					
C_o(mg/L)	$q_{e,exp}$ (mg/g)	$q_{e,cal}$ (mg/g)	k_2(g. mg^{-1}.min^{-1})	R^2	SSE
200	6.42	6.79	0.0104	0.954	1.717
400	13.09	13.24	0.0046	0.986	2.684
600	18.24	18.05	0.0091	0.992	2.208
800	21.63	21.22	0.0076	0.992	5.178

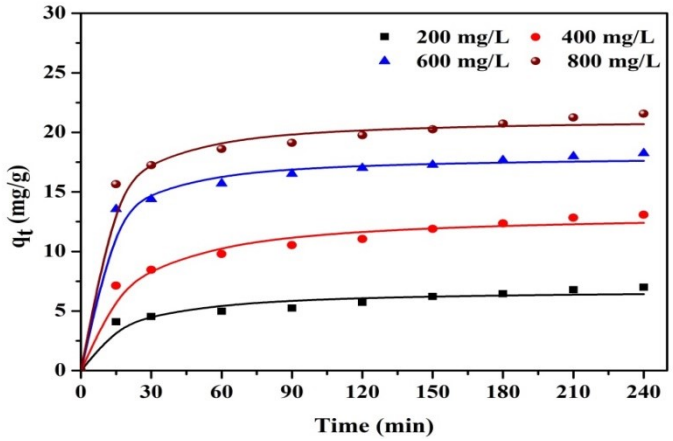

Figure 4.61 Kinetic data for the removal of DBT at different concentrations (symbols indicate experimental data, solid lines are predicted by pseudo-second-order model).

4.2.2.2.5 Adsorption thermodynamic parameter

Change in Gibbs free energy (ΔG°) is determined with the aid of Equation (3.12). To determine ΔH° and ΔS°, a graph was drawn between ΔG° vs temperature using Vant's

Hoff equation (Equation 3.13). A straight line was fit to this graph as shown in Figure 4.62; ΔH° and ΔS° were estimated from the values of intercept and slope, respectively. The calculated values of ΔG°, ΔH°, and ΔS° were shown in Table 4.17. It can be observed from Table 4.17 that ΔG° values were decreasing with increasing temperature. The obtained trend shows that adsorption of DBT onto Mo/ATGAC is more favorable and spontaneous at higher temperatures. The positive value of entropy (ΔS°) demonstrates the affinity of DBT molecules towards Mo/ATGAC surface, and the enhanced disorder at the solid-liquid interface (Dursun and Kalayci, 2005). The positive values of enthalpy (ΔH°) indicate that the adsorption process is endothermic which matches well with our experimental results as the adsorption capacity of adsorbent was found to be increased on increasing the temperature.

Table 4.17 Thermodynamics parameters for the adsorption of DBT onto Mo/ATGAC (t = 4 h, C_o = 200 – 800 mg/L, m = 25 g/L).

Temperature (K)	ΔG°(kJ/mol)	ΔH° (kJ/mol)	ΔS° (kJ/mol K)
283	-10.273		
293	-11.904	49.64	0.211
303	-14.812		
313	-16.345		

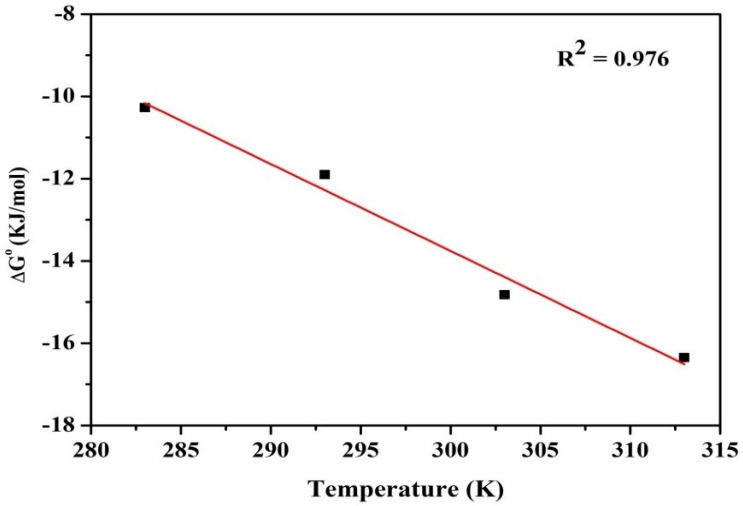

Figure 4.62 Plot of ΔG° vs. Temperature.

4.2.2.2.6 Characterization of spent adsorbent

SEM technique was employed to analyze the effect of DBT adsorption on the morphology of Mo/ATGAC. SEM micrographs of fresh Mo/ATGAC and after adsorption

of DBT is shown in Figure 4.63. It can be seen from Figure 4.63(b) that after adsorption of DBT species the pores available on the surface of Mo/ATGAC disappeared completely. This reduction in porosity after adsorption could be attributed to the entanglement of the DBT species into the pores of Mo/ATGAC (Shah et al., 2017). FTIR technique was implemented to elucidate the interaction between Mo/ATGAC and DBT molecules. Figure 4.64 depicts the FTIR spectra of fresh and spent adsorbent. As can be seen from Figure 4.64, adsorption band at 900 cm^{-1} (Mo-O-Mo) and 776 cm^{-1} (Mo=O) disappeared in the spectra of spent adsorbent which indicates these bands were specifically involved in the adsorption of DBT molecules (Ganiyu et al., 2016). In addition, a new peak appeared at 868 cm^{-1} which might appear due to the interaction between molybdenum species and DBT molecules (Al-Ghouti and Al-Degs, 2014).

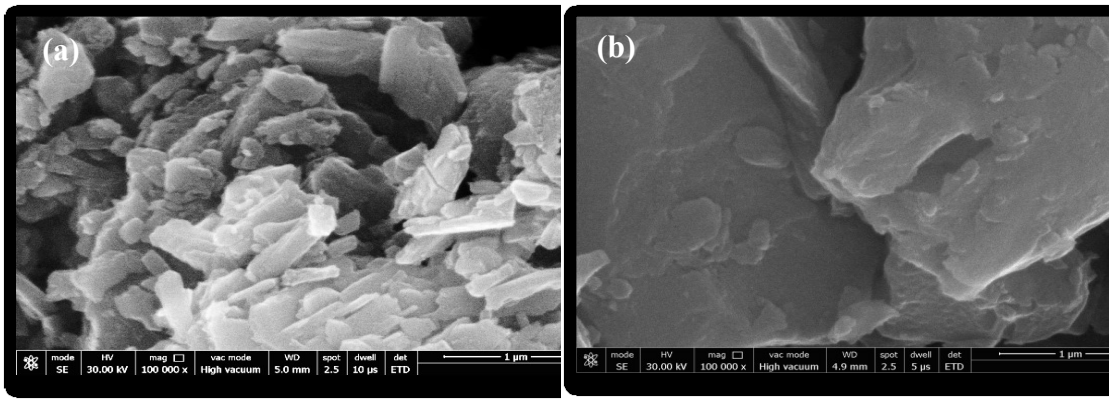

Figure 4.63 SEM images of a) fresh Mo/ATGAC and b) spent Mo/ATGAC.

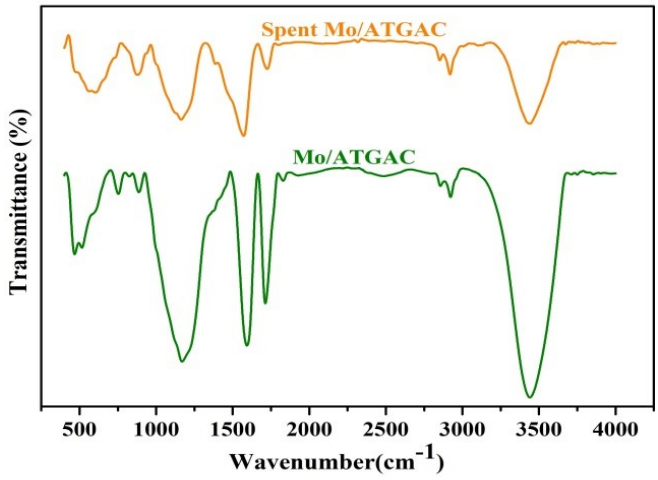

Figure 4.64 FTIR spectra of fresh Mo/ATGAC and spent Mo/ATGAC.

The XRD pattern of fresh and spent Mo/ATGAC is displayed in Figure 4.65. It is clear from Figure 4.65 that amorphous nature of Mo/ATGAC remained unchanged after adsorption of DBT. Further, no additional peak appeared in the spent sample which indicates that adsorption is mainly governed by electrostatic interaction.

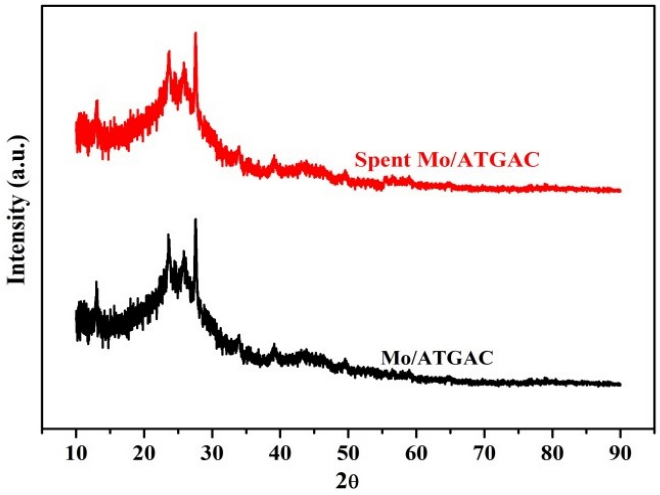

Figure 4.65 X-ray diffraction pattern of fresh Mo/ATGAC and spent Mo/ATGAC

4.2.2.2.7 Adsorption mechansim and reusability study

The better performance of Mo/ATGAC for the adsorption of DBT as compared with GAC and ATGAC is probably an outcome of specific interactions between the acidic centers generated by molybdenum species and the basic structure of DBT molecules (Santos et al., 2012). The enhancement in adsorption capacity due to the molybdenum species loading can also be attributed to the formation of π-complex between molybdenum species and DBT molecule.

Regeneration of spent adsorbent was performed using the solvent extraction technique. To regenerate, 1 g of spent adsorbent was mixed with 10 mL of toluene and stirred at room temperature for 15 min. Subsequently, adsorbents were filtered and dried overnight at 90 °C. After the first cycle, the adsorption capacity was decreased from 18.30 (mg/g) to 17.65 (mg/g), and in the next cycle, it reduced to 16.32 (mg/g). The reusability studies showed that the spent adsorbent can be regenerated and could be used effectively for the removal of DBT without appreciable decrease in its adsorption capacity.

4.2.2.3 ADN using molybdenum loaded ATGAC

4.2.2.3.1 Effect of various adsorbents

Virgin GAC, acid treated GAC, molybdenum supported ATGAC (1wt %, 2 wt %, 3 wt %, 4 wt %) were employed for the adsorption of indole-containing model oil. As can be seen from Figure 4.66, ATGAC showed better removal of indole as compared to the virgin GAC. This might be due to the presence of more number of oxygen-containing functional groups in ATGAC as compared to raw GAC (Shah et al., 2017). Further, impregnation of molybdenum species on ATGAC remarkably enhanced its adsorption capacity towards indole. This remarkable progress in the adsorption of indole can be ascribed to the formation of π complexation between indole and molybdenum species. However, increasing molybdenum species loading from 1 wt % to 2 wt % only a slight increase from 74 % to 79 % in the removal of indole was observed. In addition, on further increasing the molybdenum loading from 2 wt % to 3 wt %, the removal of indole was reduced to from 79% to 75 %. This reduction in indole removal might be owing to the agglomeration of molybdenum species on a support material. On the basis of the obtained results, 1 wt % Mo/ATGAC was taken as the potential adsorbent for the further study.

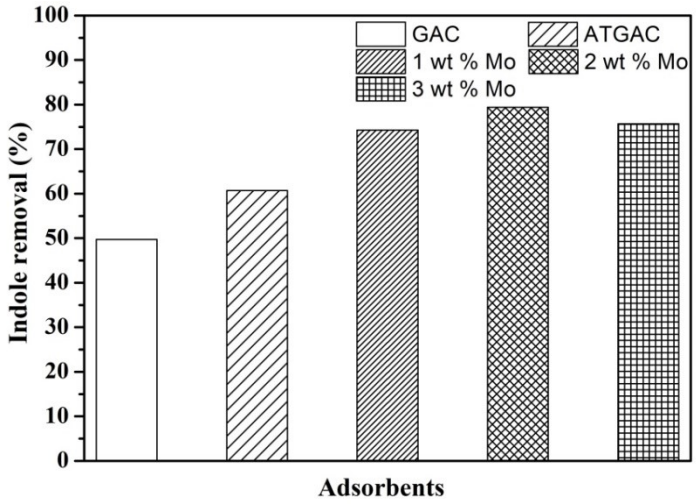

Figure 4.66 Effect of various adsorbents on indole removal (indole solution = 500 mg/L, adsorbent dose = 10 g/L, t = 4.5 h, T = 303 K).

4.2.2.3.2 Effect of adsorbent dose

To study the effect of adsorbent dose on indole, the adsorbent dose was varied from 5 g/L to 40 g/L while other operating variables remained constant. It was found that removal of

indole enhanced significantly from 47 % to 98 % with the increase in adsorbent dose from 5 g/L to 40 g/L (Figure 4.67). The removal of indole improved remarkably upto 20 g/L (47 % to 94 %), beyond that the removal enhanced very slowly (94 % to 98 %). Therefore, 20 g/L was taken as the optimum adsorbent dose for further studies for removal of indole.

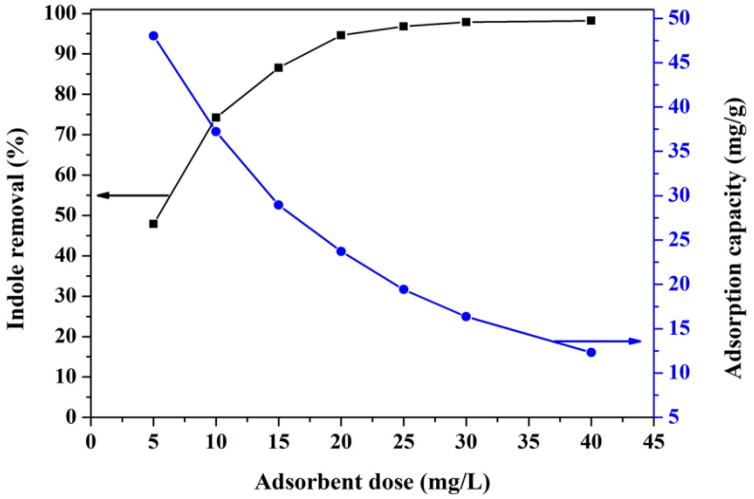

Figure 4.67 Effect of adsorbent dose on DBT removal (DBT solution 500 mg/L, t = 4.5 h, temperature = 303 K, adsorbent dose = 5 to 40 g/L).

4.2.2.3.3 Adsorption equilibrium study

Adsorption isotherm models (Langmuir, Freundlich, Temkin, R-P isotherm) were employed to fit the equilibrium adsorption data of indole adsorption onto Mo/ATGAC using non-linear regression fit. Isotherm parameters of studied isotherms along with their R^2 and SSE values are shown in

Table 4.18 that the equilibrium adsorption data is best represented by R-P isotherm. The adsorption capacity of Mo/ATGAC increased from 30.56 mg/g to 45.83 mg/g on increasing the temperature from 283 K to 313 K. The rise in adsorption capacity with the increase in temperature indicates the endothermic nature of adsorption process. This may be owing to the fact that the diffusion of indole into the pores of Mo/ATGAC is one of the rate limiting step, and as diffusion is an endothermic process which eventually makes the adsorption of indole endothermic in nature (Hiwarkar et al., 2015). The fit of R−P adsorption isotherm for the obtained adsorption data was shown in Figure 4.68.

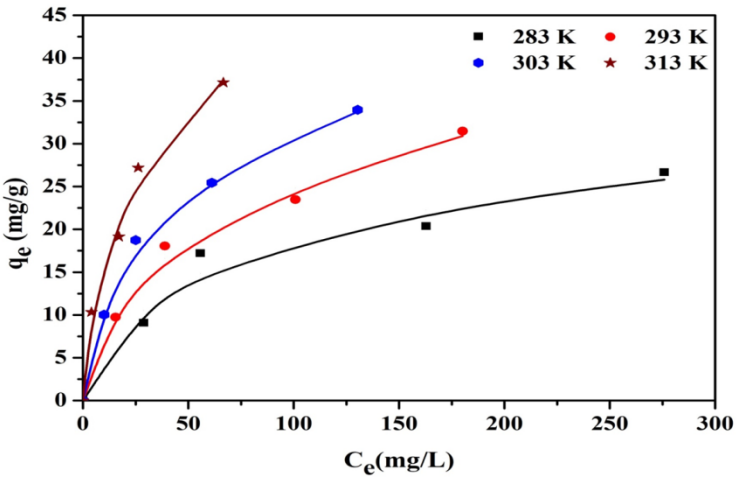

Figure 4.68 Equilibrium isothermal adsorption of indole onto Mo/ ATGAC at different temperature (symbols indicate the equilibrium data points, and the lines are projected by the R - P model).

Table 4.18 Equilibrium parameters for the adsorption of indole onto Mo/ATGAC (t = 4.5 h, C_o = 200 – 800 mgl/L, m = 20 g/L).

Langmuir				
Temperature (K)	q_m (mg/g)	K_L (L/mg)	R^2	SSE
283	30.652	0.0174	0.970	12.73
293	37.835	0.0213	0.985	8.570
303	41.391	0.0308	0.994	3.817
313	45.832	0.0347	0.984	13.30
Freundlich				
Temperature (K)	K_F [(mg/g)/(mg/L)$^{1/n}$]	1/n	R^2	SSE
283	3.101	0.380	0.967	14.01
293	3.385	0.428	0.991	5.665
303	4.456	0.419	0.992	5.561
313	5.802	0.377	0.990	7.854
Temkin				
Temperature (K)	K_T (L/g)	B_1 (J/mol)	R^2	SSE
283	0.154	6.905	0.974	11.16
293	0.204	8.367	0.991	5.589
303	0.274	9.219	0.995	2.830
313	0.627	9.550	0.979	17.079
Redlich–Peterson				
Temperature (K)	K_R (L/g)	α(L/mg)	β	R^2	SSE
283	0.728	0.056	0.853	0.972	12.05
293	1.834	0.251	0.703	0.992	4.788
303	1.882	0.121	0.810	0.997	1.772
313	6.997	0.731	0.655	0.991	6.770

4.2.2.3.4 Adsorption kinetic study

Figure 4.69 shows the effect of time for the adsorption of indole onto Mo/ATGAC. The effect of contact time was studied at a temperature of 303 K with different initial concentrations (200- 800 mg/L) and an optimum adsorbent dose of 20 g/L. Uptake of indole was found to be dependent on the concentration of indole in model oil. It can be observed from Figure 4.69 that adsorption of indole was very fast at the beginning and then it tends to slow down with the decrease in the remaining amount of indole. Further, equilibrium time was also found to be dependent on the initial concentration of indole in model oil. For a lower concentration of indole (200 mg/L) equilibrium was achieved in 90 minutes while for a higher concentration of indole (800 mg/L) equilibrium was achieved in 210 minutes. Pseudo-first-order and second-order models were investigated to determine the best fit for the adsorption data. Kinetic parameters of these models were determined with the aid of non-linear regression; obtained results were illustrated in Table 4.19. The adsorption data is best represented by the pseudo-second-order model due to the higher value of R^2 and the least value of SSE.

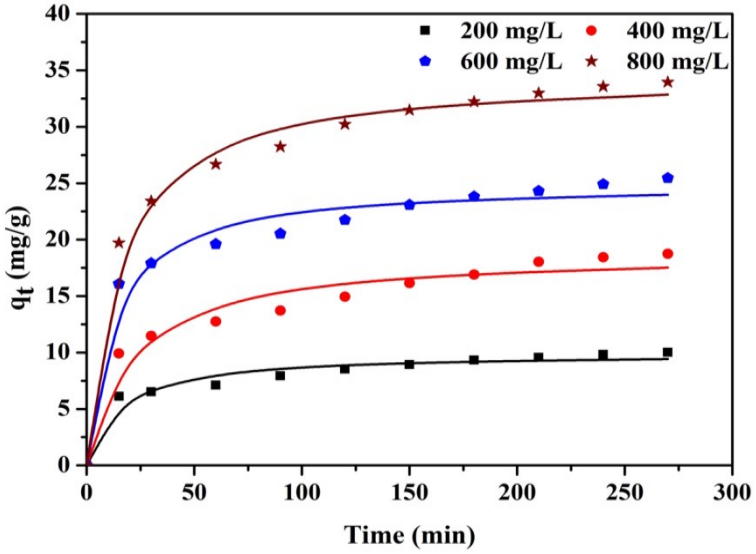

Figure 4.69 Kinetic data for the removal of indole (symbols indicate experimental data, solid lines are predicted by pseudo-second-order model).

Table 4.19 Kinetic parameters for the adsorption of DBT onto Mo/ATGAC (t = 4.5 h, C_o = 200 – 800 mg/l, m = 20 g/l, T = 303 K).

Pseudo first order					
C_o(mg/L)	$q_{e,exp}$ (mg/g)	$q_{e,cal}$ (mg/g)	k_1(min^{-1})	R^2	SSE
200	10.02	9.010	0.0517	0.908	7.4990
400	18.74	16.71	0.0381	0.897	29.918
600	25.45	23.01	0.0626	0.934	34.192
800	33.95	31.50	0.0507	0.954	44.235
Pseudo second order					
C_o(mg/L)	$q_{e,exp}$ (mg/g)	$q_{e,cal}$ (mg/g)	k_2(g. mg^{-1}.min^{-1})	R^2	SSE
200	10.02	9.886	0.0073	0.962	3.1182
400	18.74	18.75	0.0027	0.955	13.050
600	25.45	24.90	0.0037	0.975	12.933
800	33.95	34.42	0.0021	0.989	10.775

4.2.2.3.5 Thermodynamic study

Thermodynamic parameters were studied to evaluate the feasibility and nature of adsorption process. Equation (3.12) is employed to determine the value of ΔG°, and obtained values of ΔG° at different temperatures are shown in Table 4.20. Values of ΔG° are found to be decreasing with the increase in temperature indicating the adsorption is more spontaneous and favorable at a higher temperature. A graph was plotted between ΔG° and temperature with the aid of Equation (3.13) to obtain the value of ΔH° and ΔS° (Figure 4.70). Calculated values of ΔH° and ΔS° are presented in Table 4.20. The positive value of ΔH° suggests the endothermic nature of the adsorption process. Positive value of ΔS° indicates enhanced randomness at the solid/solution interface along with few structural variations attained in the adsorbate and adsorbent system (Onal et al., 2006).

Table 4.20 Thermodynamics parameters for the adsorption of indole onto Mo/ATGAC (t = 4.5 h, C_o = 200 – 800 mg/L, m = 20 g/L)

Temperature (K)	**ΔG°(kJ/mol)**	**ΔH° (kJ/mol)**	**ΔS° (kJ/mol K)**
283	-14.567		
293	-16.392	41.32	0.197
303	-18.141		
313	-20.582		

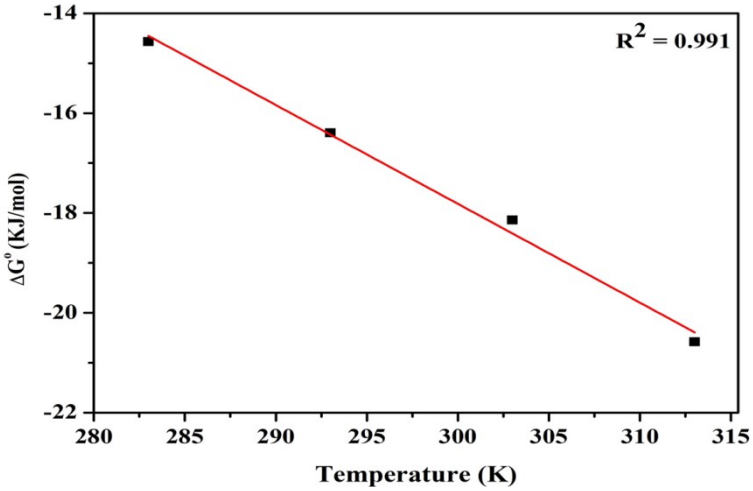

Figure 4.70 Plot of ΔG° vs. T for thermodynamic parameter's estimation.

4.2.2.3.6 Characterization of spent adsorbent

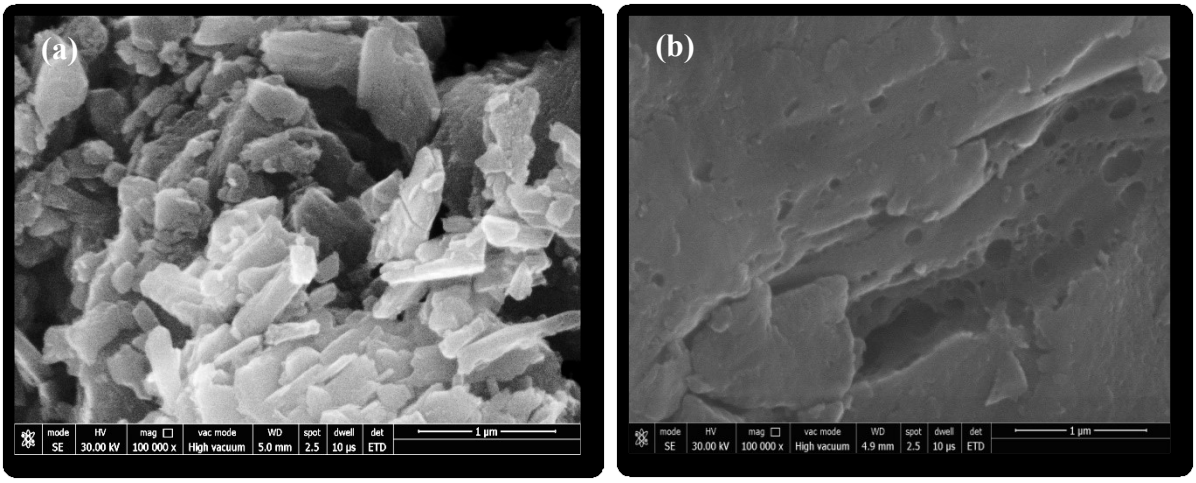

Figure 4.71 SEM images of a) fresh Mo/ATGAC and b) indole loaded Mo/ATGAC.

Figure 4.71 presents the SEM images of Mo/ATGAC of before and after adsorption of indole. The SEM image of Mo/ATGAC before adsorption revealed the porous morphology with small rod like structures. Nevertheless, after adsorption of indole porosity of Mo/ATGAC reduced due to the filling of pores with indole species. In addition, spherical rods available on Mo/ATGAC disappeared after adsorption of indole indicating specific interactions (π complexation) between indole species and adsorbent surface. FTIR spectra of fresh and spent adsorbent are shown in Figure 4.72. As can be seen from Figure 4.72, FTIR spectra of spent adsorbent shows shifting and change in the peaks present at 900 cm^{-1} (Mo-O-Mo), 776 cm^{-1} (Mo=O) and 467 cm^{-1} (O-H) and disappearance of peak at 1700 cm^{-1} (O=C-O) as compared to the FTIR spectra of fresh

adsorbent, which indicates these peaks are specifically involved in adsorption of indole onto Mo/ATGAC (Rameshraja et al., 2012). XRD spectra of fresh and spent Mo/ATGAC are displayed in Figure 4.73. As can be seen from Figure 4.73, the XRD spectra of Mo/ATGAC remained unchanged after the adsorption of indole revealing that indole adsorption doesn't influence the amorphous nature of adsorbent. Further, absence of any additional peak in the XRD spectra of spent adsorbent indicates that adsorption is mainly governed by electrostatic interaction.

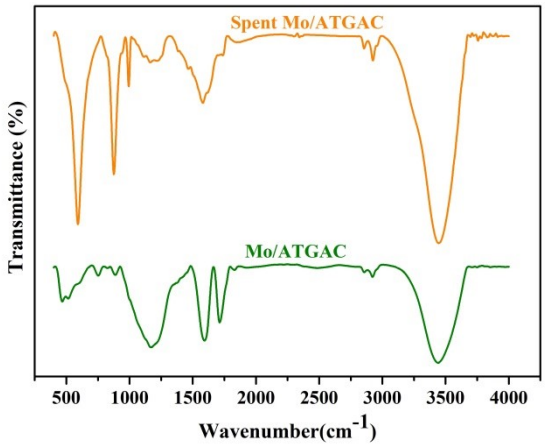

Figure 4.72 FTIR spectra of fresh Mo/ATGAC and spent Mo/ATGAC.

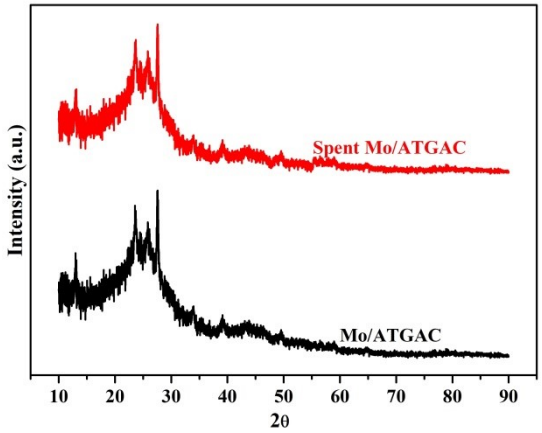

Figure 4.73 X-ray diffraction pattern of fresh Mo/ATGAC and spent Mo/ATGAC.

4.2.2.3.7 Adsorption mechanism and reusability study

The adsorption of indole onto Mo/ATGAC can be governed by following mechanisms such as π complexation, hydrogen bonding and other weak interactions such as van der Waals interactions. Surface area and porosity are plays a significant role in the adsorption

of indole via van der Waals interactions (Van de Voorde et al., 2013). Enhanced adsorption of indole by Mo/ATGAC can also be attributed to its higher surface area. Acid-base interaction is not applicable here as indole is a neutral compound. The indole could also interact with oxygen-containing compounds available on the surface of adsorbent through hydrogen bonding as indole could behave as a hydrogen bond donor through the hydrogen atom attached with the nitrogen atom (Sarker et al., 2018). Further, the better adsorption capacity of Mo/ATGAC can be ascribed to the formation of π complex between molybdenum species and indole.

The solvent regeneration technique was employed to regenerate spent adsorbent. Spent adsorbent was mixed with an appropriate amount of ethanol and stirred at room temperature for 15 min. Subsequently, the mixture was filtered and dried in an oven at 60 °C. In the first regeneration cycle, the percentage removal of indole was decreased from 94.58% to 93.10%. Subsequently, in the second and third regeneration cycle removal was reduced to 91.80%, 88.58%, respectively. The obtained results showed that the removal efficiency of the regenerated Mo/ATGAC doesn't reduce severely after three cycle of regeneration, indicating that Mo/ATGAC can be reused efficiently. However, the reduction in adsorption capacity of Mo/ATGAC after recycling can be ascribed to the entanglement of indole species into the pores of adsorbents and leaching of molybdenum species.

4.2.2.4 Simultaneous ADS and ADN using molybdenum loaded ATGAC

The simultaneous removal of sulfur and nitrogen compounds from model oil is explored with the aid of CCD, a subset of RSM. The aim of the study is to optimize the adsorption process with minimum experimental runs and to determine the significant interaction among processing parameters. In the present study, four adsorption parameters (concentration of DBT, the concentration of indole, temperature, and dose) with five levels influencing the removal of sulfur and nitrogen compounds were studied. The parameters were chosen on the basis of experiments conducted for ADS and ADN of model oil using Mo/ATGAC as an adsorbent, the range and levels of factors are shown in Table 4.21. For the adsorption experiments, 1 wt % Mo/ATGAC was used as an adsorbent and experiments were conducted for 4.5 h.

Table 4.21 Range and levels of factors.

Factors	**-α**	**-1**	**0**	**+1**	**+ α**
Concentration of DBT (A)	50	200	350	500	650
Concentration of indole (B)	50	200	350	500	650
Temperature	12.5	20	27.5	35	42.5
Dose	15	20	25	30	35

The influence of four major variables varied at five levels on DBT and indole removal from model oil was studied by conducting 31 experiments given by CCD design. Results obtained from the experiments (Table 4.22) were analyzed with the aid of ANOVA and statistics to obtain empirical equations which can predict actual behavior of adsorption system.

4.2.2.4.1 Statistical analysis

The empirical model's equations in terms of coded parameters for percentage removal of both DBT and indole are given as Equations (4.3) and (4.4), respectively.

$$\text{DBT removal (\%)} = 69.20 - 6.684A - 6.361B + 3.094C + 7.792D + 0.207A^2 - 0.104B^2 + 1.442C^2 - 0.173D^2 + 1.741A*B + 0.524A*C + 0.318A*D - 0.580B*C + 1.633B*D - 0.280C*D \quad (4.3)$$

$$\text{Indole removal (\%)} = 67.43 - 6.617A - 6.998B + 4.554C + 7.911D + 0.148A^2 - 0.112B^2 + 0.558C^2 - 0.343D^2 + 2.876A*B - 1.954A*C - 0.109A*D + 0.899B*C + 1.922B*D - 1.468C*D \quad (4.4)$$

For the DBT removal, significant model terms were A, B, C, D, A*B, C*C, and insignificant terms were B*B, D*D, A*C, A*D, B*C, B*D, and C*D. For the indole removal, significant model terms were A, B, C, D, C*C A*B, A*C, B*D, and insignificant terms were A*A, B*B, D*D, A*D, B*C, and C*D. The results obtained from the statistical analysis indicated that models were appropriate in predicting the removal of both indole and DBT with in the range of studied parameters. The positive coefficient in the model equations depicts the positive effect of that term on response variable whereas negative coefficient indicates the negative effect. Temperature and adsorbent dose have a synergistic effect on the removal of both DBT and indole, whereas concentrations of DBT and indole have an antagonistic effect. ANOVA was used to

verify the statistical adequacy of the developed regression model and the importance of parameters. Table 4.23 and Table 4.24 shows the ANOVA for the response surface quadratic model of DBT and indole, respectively. Validation of the model was carried out by using F value and P value. When the F value is high and P value is less than 0.05, it shows that the model and independent parameters are significant (Vafaei et al., 2018). The model F values of 36.13 and 26.78, and P value of 0.000 and 0.000 for DBT and indole removal, respectively indicated that obtained models were significant. The fitness of the developed adsorption models was depicted by their insignificant lack of fit, p= 0.184, 0.195 for DBT and indole removal, respectively.

The high values of the coefficient of determination (R^2) values for both DBT (0.969) and indole (0.959) adsorption models also indicated that obtained models were suitable to represent the experimental data. The standard error of regression (s) indicates that how well our experimental observations fit into the developed regression model (Danmaliki et al., 2017). It also measures the average distance between the obtained experimental values and the regression line. The low value of S indicates that the model is appropriate for representing experimental data, here a value of 2.775 and 3.480 were obtained for DBT and indole adsorption models, respectively.

Table 4.22 Design matrix for the central composite design.

Run	A (mg/L)	B (mg/L)	C(°C)	D (g/L)	A (% removal)	A (predicted % removal)	B(% removal)	B (predicted % removal)
1	350	350	27.5	25	69.6000	69.2000	69.0000	67.4286
2	200	500	20.0	20	60.3946	57.9848	42.1907	45.6068
3	500	200	20.0	30	73.9844	71.2746	71.0843	70.8313
4	350	350	27.5	25	68.8000	69.2000	65.0000	67.4286
5	350	350	27.5	25	71.0000	69.2000	69.0000	67.4286
6	350	50	27.5	25	81.4211	82.3380	80.2119	80.9750
7	350	350	27.5	25	67.0000	69.2000	64.0000	67.4286
8	350	350	27.5	35	82.1429	84.0901	80.4286	81.8802
9	200	200	35.0	30	91.1606	94.2775	90.0723	94.4110
10	500	500	35.0	20	54.0573	53.0517	51.3989	52.1832
11	200	500	20.0	30	76.3511	76.7579	70.9798	68.4254
12	500	200	35.0	20	66.5898	66.7158	60.6139	62.4730
13	200	500	35.0	20	59.2823	62.5249	63.7969	63.3545
14	350	350	27.5	25	72.0000	69.2000	71.0000	67.4286
15	350	350	42.5	25	82.1265	81.1561	81.5779	78.7696

16	350	650	27.5	25	55.0000	56.8937	52.0000	52.9823
17	500	500	35.0	30	71.8517	71.9758	65.8517	68.6962
18	50	350	27.5	25	83.2450	83.3961	81.2962	81.2549
19	350	350	27.5	25	66.0000	69.2000	65.0000	67.4286
20	200	200	20.0	20	75.8864	76.2952	74.5360	70.9962
21	500	200	35.0	30	80.0432	79.1097	75.7657	71.2995
22	350	350	27.5	25	70.0000	69.2000	69.0000	67.4286
23	350	350	27.5	15	52.0597	52.9231	49.9415	50.2352
24	200	500	35.0	30	83.4630	80.1787	81.6629	80.3026
25	500	500	20.0	20	49.0000	46.4159	47.2841	42.2501
26	200	200	35.0	20	85.4096	83.1537	84.8357	85.1494
27	500	500	20.0	30	67.5467	66.4592	65.9972	64.6335
28	500	200	20.0	20	57.8206	57.7615	55.8240	56.1343
29	350	350	12.5	25	65.0000	68.7810	56.0000	60.5537
30	650	350	27.5	25	54.0000	56.6595	53.0000	54.7867
31	200	200	20	30	90.8759	88.5381	87.9625	86.1282

Table 4.23 ANOVA for removal of DBT.

Source	Sum of squares	Degree of freedom	F value	P value
Model	3896.76	14	36.13	0.000
DBT (A)	1072.27	1	139.20	0.000
INDOLE (B)	971.12	1	126.07	0.000
Temperature (C)	229.72	1	29.82	0.000
Dose (D)	1457.07	1	189.16	0.000
DBT*DBT(A*A)	1.22	1	0.16	0.695
INDOLE*INDOLE (B*B)	0.31	1	0.04	0.844
Temperature*Temperature (C*C)	59.47	1	7.72	0.013
Dose*Dose (D*D)	0.86	1	0.11	0.743
DBT*INDOLE (A*B)	48.51	1	6.3	0.023
DBT*Temperature (A*C)	4.39	1	0.57	0.461
DBT*Dose (A*D)	1.61	1	0.21	0.653
INDOLE*Temperature (B*C)	5.38	1	0.7	0.413
INDOLE*Dose (B*D)	42.64	1	5.54	0.032
Temperature*Dose (C*D)	1.25	1	0.16	0.692
Lack of fit	96.13	10	2.13	0.184
Pure Error	27.12	6		
Total	4020.00	30		

Table 4.24 ANOVA for removal of indole

Source	Sum of squares	Degree of freedom	F value	P value
Model	4540.84	14	26.78	0.000
DBT (A)	1050.85	1	86.76	0.000
INDOLE (B)	1175.38	1	97.04	0.000
Temperature (C)	497.73	1	41.03	0.000
Dose (D)	1502.11	1	124.01	0.000
DBT*DBT(A*A)	0.63	1	0.05	0.823
INDOLE*INDOLE (B*B)	0.36	1	0.03	0.865
Temperature*Temperature (C*C)	8.91	1	0.74	0.404
Dose*Dose (D*D)	3.36	1	0.28	0.606
DBT*INDOLE (A*B)	132.37	1	5.57	0.004
DBT*Temperature (A*C)	61.07	1	10.93	0.039
DBT*Dose (A*D)	0.19	1	5.04	0.902
INDOLE*Temperature (B*C)	12.92	1	0.02	0.317
INDOLE*Dose (B*D)	59.08	1	1.07	0.042
Temperature*Dose (C*D)	34.46	1	4.88	0.111
Lack of fit	150.09	10	2.06	0.195
Pure Error	43.71	6		
Total	4734.64	30		

Figure 4.74(a) and Figure 4.74(b) compare the experimental and adsorption model predicted values for DBT and indole removal, respectively. To obtain good correlation between experimental and predicted values, obtained R^2 values should be no less than 0.80 (Ghanbari et al., 2017). In the present work, R^2 value was found to be 0.968 for DBT removal, and 0.958 for the indole removal, indicating good fit.

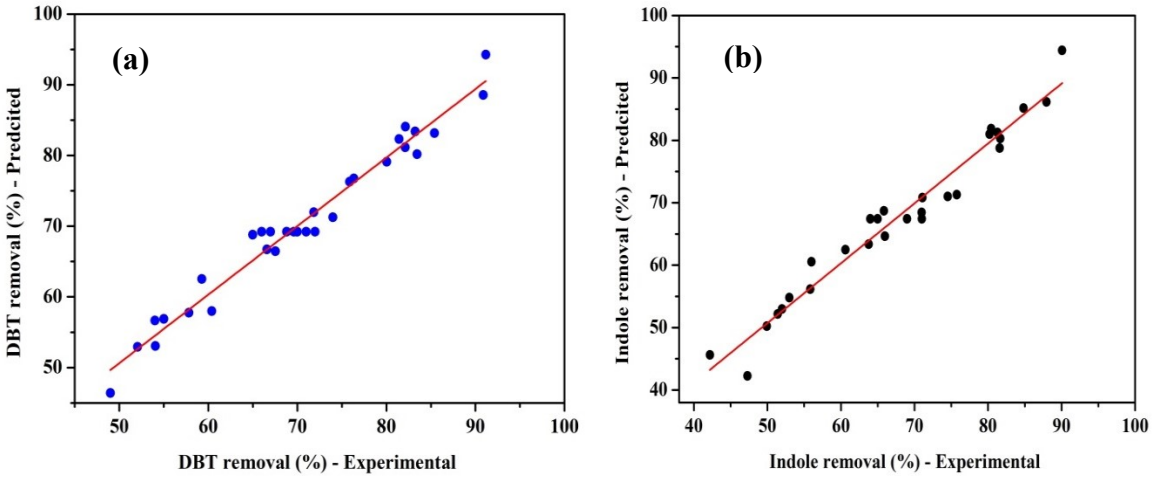

Figure 4.74 Comparison of experimental (actual) and predicted values of the responses for percentage removal of (a) DBT, (b) Indole.

4.2.2.4.2 Effect of main parameters on the response variables

The effect of main factors on DBT and indole removal is depicted in the form of factorial plots as shown in Figure 4.75(a&b), respectively. These plots give information on the mean effect of each variable and the response variable. The effect of concentration of DBT and indole on DBT removal is depicted in Figure 4.75(a). On increasing the concentration of DBT and indole, removal of DBT decreased significantly. This significant decrease in removal of DBT could be attributed to the decrease in number of adsorption sites due to the increase in the number of species of DBT and indole (Olgun et al., 2011). In addition, the decrease in removal of DBT due to the presence of indole could be ascribed to the competition between DBT and indole to get adsorbed on active sites of adsorbent. Similarly, removal of indole was reduced significantly on increasing the concentration of DBT and indole in model oil. However, temperature and adsorbent dose had synergistic effect on both DBT and indole removal. Higher amount of dose provide more number of vacant active sites for the adsorption of DBT and indole, while

higher temperature gives better removal as adsorption of DBT and indole on Mo/ATGAC is endothermic in nature.

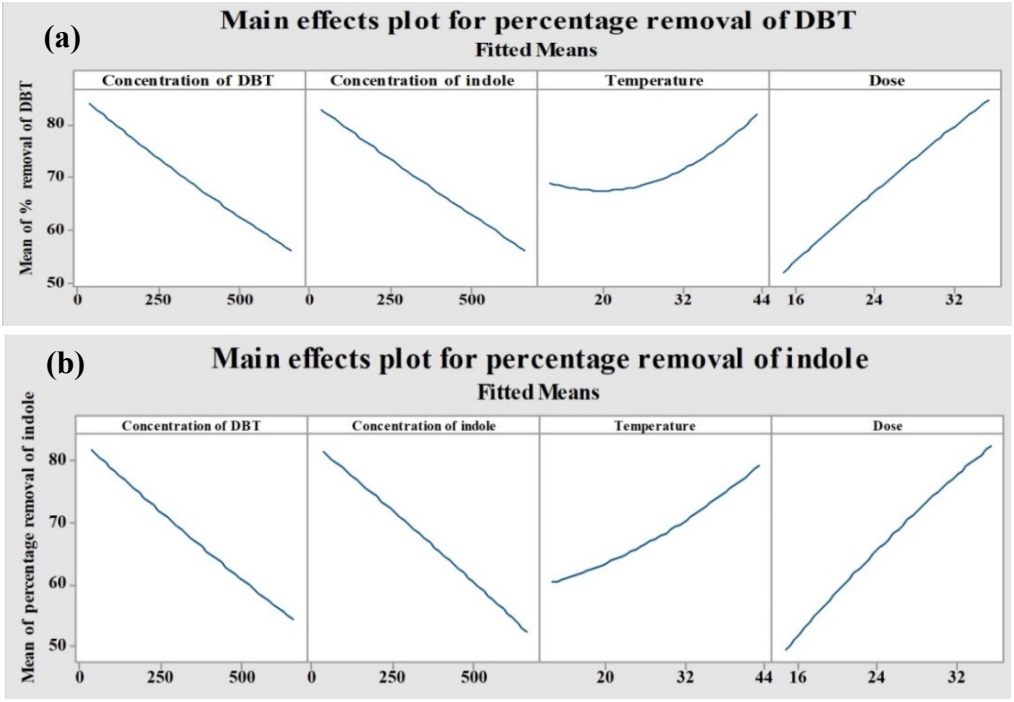

Figure 4.75 Main effects plot for the removal of (a) DBT and (b) indole from model oil.

4.2.2.4.3 Effect of interactions between factors

To explore the interaction between the processing parameters and response variables, 3D surface and contour plots were constructed. These plots provide the benefit of giving summarized information in one single figure. The plots were constructed by holding two processing variables at central levels and varying other two variables. For the DBT removal, only one interaction i.e. interaction between the concentration of DBT and indole was found to be significant. Figure 4.76(a,b) represents the interaction effect of concentration of DBT and indole on DBT removal. It can be seen from Figure 4.76 that DBT removal reduced significantly on increasing the concentration of both DBT and indole. The highest removal of DBT was achieved when the concentration of DBT and indole was lowest in the model oil. For indole removal, three interactions (A*B, A*C, and B*D) were found to be important. The interaction between the concentration of DBT and indole on indole removal was depicted in Figure 4.77(a,b). Both concentrations of DBT and indole had a negative impact on removal of indole. At lower concentration of indole,

removal of indole reduced drastically on increasing the concentration of DBT whereas at higher concentration of indole removal of indole was unaffected by the amount of DBT in model oil (Figure 4.77(a)). Effect of interaction between the concentration of DBT and temperature on indole removal is provided in Figure 4.78(a,b). As can be seen from Figure 4.78(a) that highest removal of DBT was obtained at higher temperature and lower concentration of DBT in model oil. Figure 4.79(a,b) depicted the interaction effect of concentration of indole and adsorbent dose. It can be seen from the Figure 4.79(a) that at higher amount of adsorbent dose there is only slight effect of increasing the concentration of indole. However, at lower amount of adsorbent dose removal of indole reduced significantly on increasing the concentration of indole.

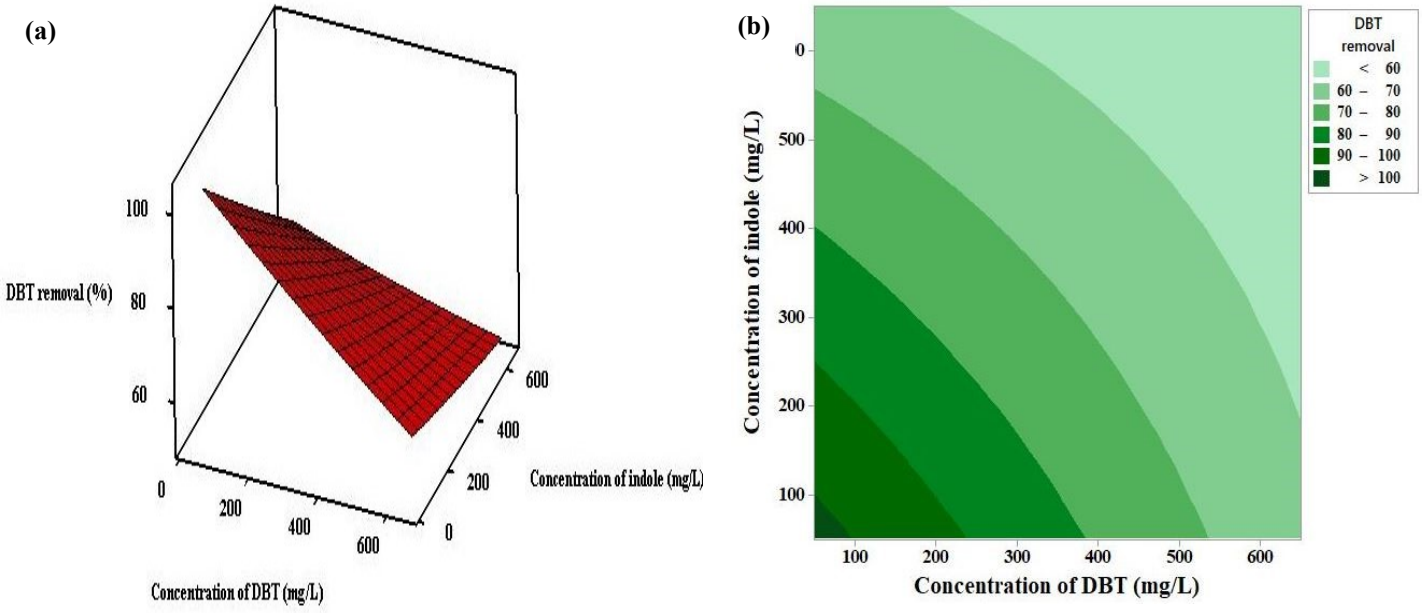

Figure 4.76 Surface(a) and contour(b) plots of DBT removal for interaction between concentration of DBT and concentration of indole.

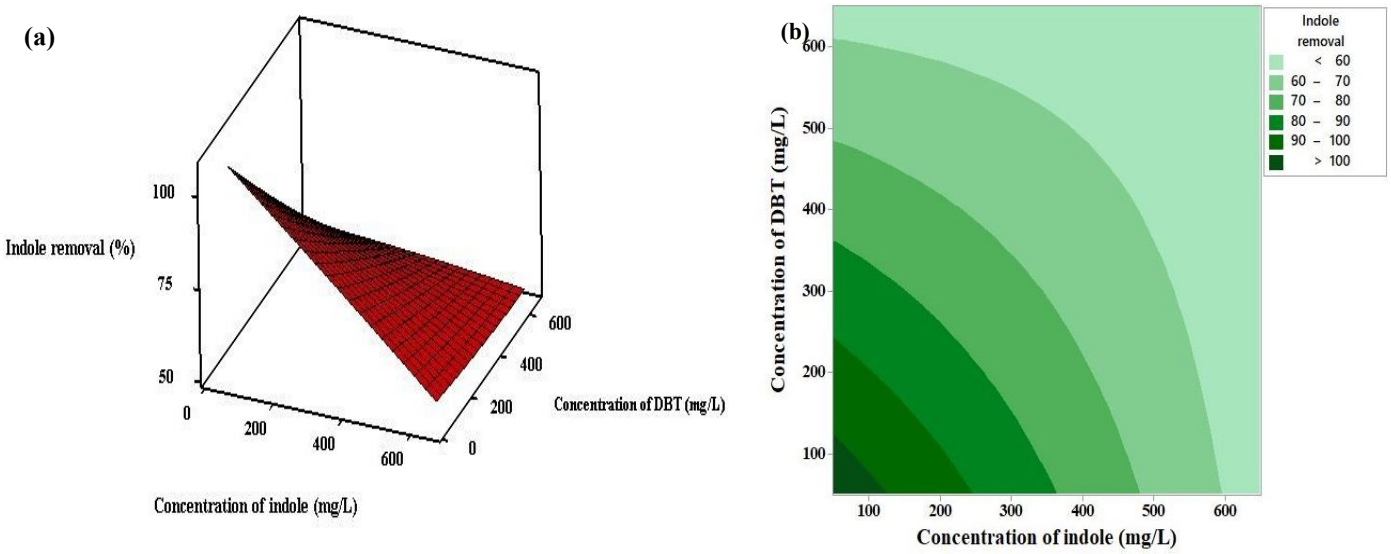

Figure 4.77 Surface(a) and contour(b) plots of indole removal for interaction between concentration of DBT and concentration of indole.

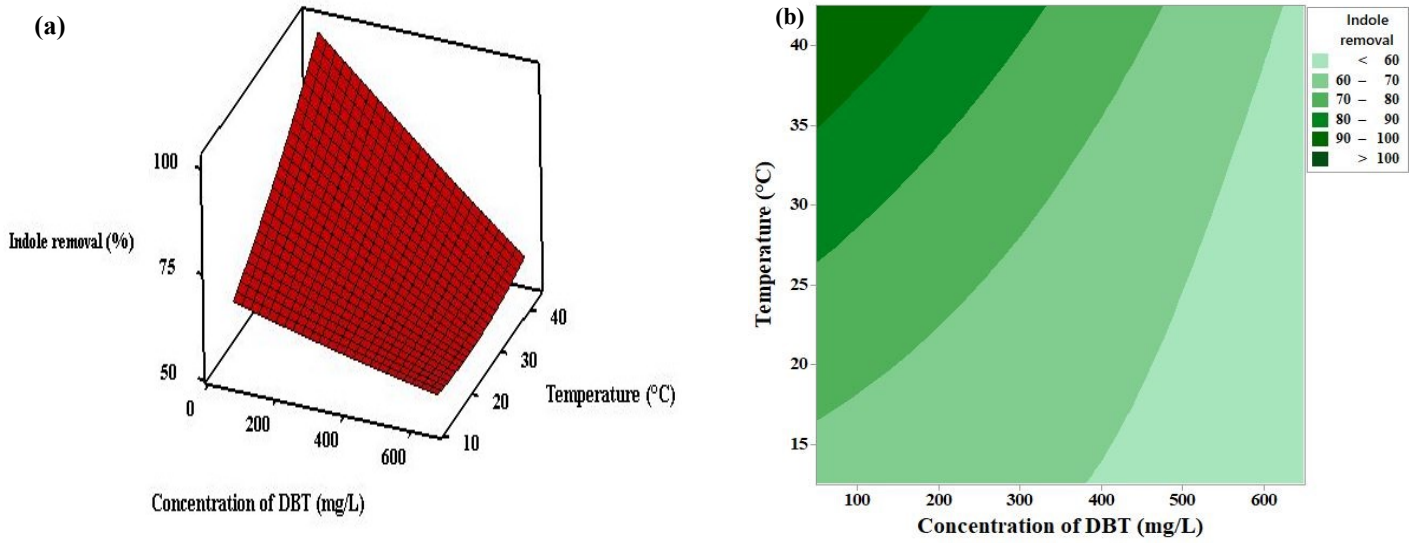

Figure 4.78 Surface(a) and contour(b) plots of indole removal for interaction between concentration of DBT and temperature.

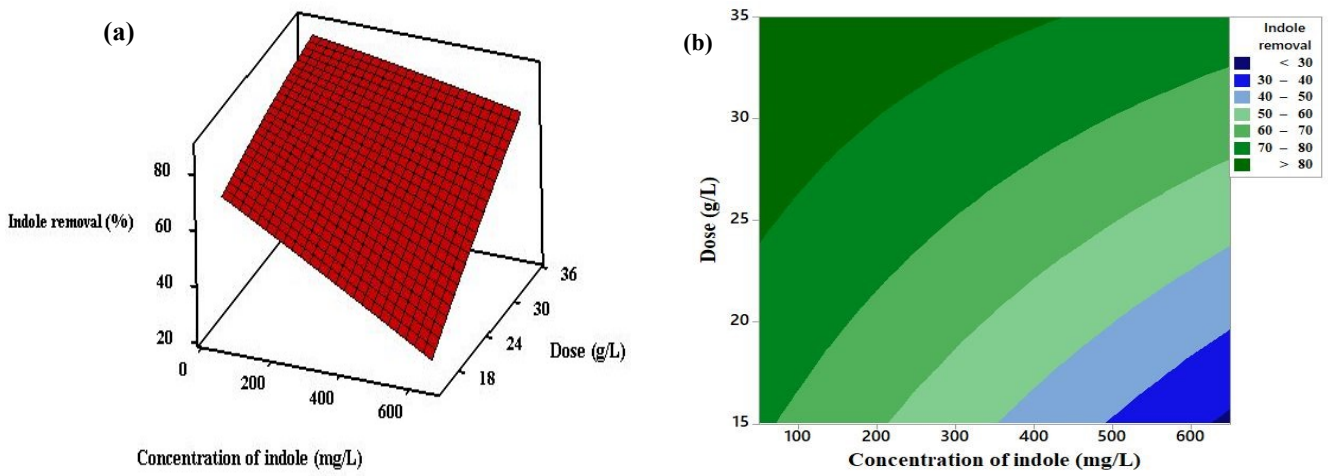

Figure 4.79 Surface(a) and contour(b) plots of indole removal for interaction between concentration of indole and dose.

4.2.2.4.4 Analysis of residual

Assessment of residual plots was carried out to study the reliability of obtained CCD models. Residuals graphs are used to describe the variation within the obtained model with the help of normal distribution. Residual plots for DBT and indole removal are depicted in Figure 4.80(a&b), respectively. As can be seen from the normal probability plot of both DBT and indole removal, most of the data points lie on the normality line indicating that data is normally distributed. It is clear from the residual versus fitted values of both responses, residuals are arbitrarily scattered around zero showing that distribution can be considered as normal. The histograms of residual vs frequency for both DBT and indole removal shows that residuals fluctuate in a random manner and roughly symmetrical around the mean with most of the residual values. The graph of residuals versus observation order shows that residuals are scattered randomly and close to the center value. The obtained results indicated that developed CCD models are reliable to represent the experimental data.

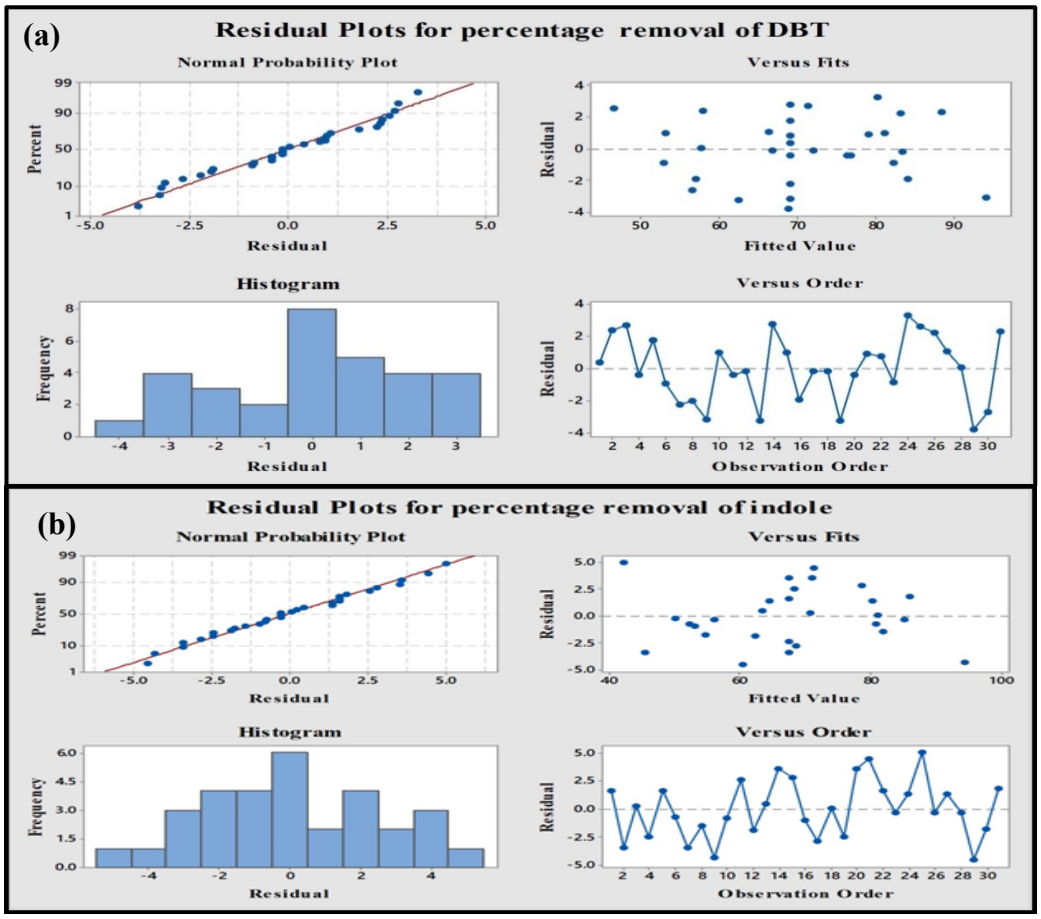

Figure 4.80 Residual plots for a) DBT removal and b) indole removal.

4.2.2.4.5 Optimization analysis

The optimization of DBT and indole adsorption onto Mo/ATGAC was conducted by using response optimizer function available in Minitab software. In the optimization analysis, target values were set at 100 %, lower bounds were based on the lowest values of removal obtained for both compounds in CCD design, and upper values were set at 110 % as it has to be more than the target value. The optimum adsorption conditions obtained were the adsorbent dosage of 32 g/L, the temperature of 25.5 °C, DBT concentration of 186 mg/L and indole concentration of 50 mg/L in model oil, respectively. The predicted and experimental values found at optimum conditions were 98.36% and 97.16% for DBT as well as 99.08% and 98.41% for indole.

4.3 Discussion and implications

The present study explores the alternative technologies for the reduction of sulfur and nitrogen content in liquid fuels. For the oxidative process, mesoporous silica catalysts were developed owing to its high surface area, high porosity, and good thermal stability. Generally, high cost silica reagents (TEOS) is required for the synthesis of MCM-41. This study made an attempt to extract silica precursor from industrial waste (CFA) and utilize it in the synthesis of mesoporous silica.

Approximately 500 million tons of CFA is produced every year in electric power plants, and only 15 % of generated CFA is utilized. Consequently, disposal of CFA has become a serious concern. The present study helps in waste management of CFA by utilizing it in to value added product. In a nutshell, production of MCM-41 with low cost silica source can reduce the operating cost of oxidative process along with productive usage of industrial waste. Mesoporous catalysts developed in this study were successfully employed for ODS process. During the ODS process, sulfur compound is converted to their corresponding sulfones which are highly polar in nature and can be easily removed from the oil with the help of solvent such as acetonitrile, methanol etc. Pervious reported literature also indicated that sulfones generated ODS process can be easily removed with the help of solvents.

Mesoporous materials synthesized in the present study can also find their applicability in other fields as catalyst, catalytic support or adsorbent due to their high surface area, large pore volume and high thermal stability. They can be employed as catalyst for organic transformations and also used as catalytic support for the advanced oxidation processes of wastewater treatment. They can also be used for the adsorption of CO2 by incorporating basic functional groups to enhance its capacity and selectivity (Tari et al., 2016). They can be used for the treatment of wastewater for the removal of organic pollutants and pharmaceuticals.

For the adsorption process, GAC was chosen because of its unique surface characteristics (high density of oxygen containing surface functional groups) along with high volume of pores. Further, the features of the GAC can be altered by adopting different techniques to make it effective according to the application. In the present work, chemical modification

of GAC was carried out with the aid of cobalt and molybdenum oxides to improve its selectivity for sulfur and nitrogen compounds. Developed adsorbents (Co/ATGAC and Mo/ATGAC) were found to be very effective in removing sulfur and nitrogen compounds from model oil. Developed adsorbents in the present study can also find its applicability as adsorbents for the removal of dyes from industrial effluents and can also be utilized as catalyst in advanced oxidation process for removal of organic pollutants from wastewater.

CHAPTER 5 CONCLUSION

This chapter presents the summary of the entire work of this thesis. It also included main findings and substantial contribution to the existing knowledge.

Stringent environmental rules & regulations, as well as the application of cleaner fuels in refinery operations and fuel cells, are putting immense pressure on refineries to produce fuels of lower sulfur and nitrogen content. Currently, hydrotreating is industrially used for the desulfurization and denitrogenation of transportation fuel. This process encounters difficulty in removing aromatic sulfur and nitrogen compounds from transportation fuels. Moreover, a huge amount of hydrogen and severe operating conditions are required in order to meet the increasing demand. Therefore, in the present work, two alternative techniques (oxidation and adsorption) have been explored for the removal of refractory sulfur and nitrogen compounds from liquid fuels.

5.1 Mesoporus material derived from coal fly ash (Mo/MCM-41 & ExtMCM-41) for oxidation process:

- Characterization study revealed that mesoporous silica (MCM-41) was successfully synthesized from coal fly ash: The SEM images of MCM-41 revealed that it exhibits spherical top and tortuous as well as a ribbon-shaped particle. HRTEM revealed that the MCM-41 exhibits hexagonally ordered porous structure.
- Mesoporous silica material (ExtMCM-41) derived from coal fly ash was successfully synthesized by using solvent extraction de-template technique.
- The small-angle powder XRD pattern of the synthesized ExtMCM-41 catalyst exhibited the well-ordered hexagonal pore structure of typical MCM-41.
- ExtMCM-41 possesses high BET surface area, pore volume when compared with conventional synthesised MCM-41 (derived from coal fly ash). For ExtMCM-41 surface area and pore volume was found to be 691 m^2/g and 0.528 cm^3/g, and for surface area and pore volume was found to be MCM-41 605 m^2/g and 0.428 cm^3/g, respectively.

- Desulfurization of DBT containing model fuel was investigated using synthesized catalyst (Mo/MCM-41), approximately 94 % of DBT removal was achieved by optimizing the influencing parameters of ODS (DBT concentration = 600 mg/L, T = 363 K, t = 3 h, O/S = 2:1,catalyst dose = 6 g/L).
- The oxidative reaction of DBT with the presence of Mo/MCM-41 catalyst follows the pseudo-first-order reaction kinetics, and plausible DBT oxidation mechanism was proposed.
- At the optimum operating conditions (T = 363 K, t = 3 h, catalyst dose = 0.75 g/L, DBT concentration = 1000 mg/L) approximately 93 % of DBT removal was achieved by ExtMCM-41. The oxidative reaction of DBT follows the pseudo-first-order reaction kinetics, and plausible DBT oxidation mechanism was also proposed.
- Nitrogen compounds inhibited the oxidation of DBT. The inhibition effect can be ascribed to the competition between sulfur and nitrogen compounds for the active sites, and strong adsorption of nitrogen compounds and oxidation products of indole/quinoline on vacant sites of the catalyst.

From the oxidation studies, it was found that both mesoporous catalysts are highly effective for oxidative desulfurization of liquid fuels. However, ExtMCM-41 showed better catalytic performance than Mo/MCM-41. The catalytic systems used in the present study is not very effective for removing nitrogen compounds from liquid fuels and can be used successfully only when presence of nitrogen compounds in fuel is very less.

5.2 Cobalt or molybdenum impregnated acetic acid treated GAC (Co/ATGAC or Mo/ATGAC) for adsorptive desulfurization and adsorptive denitrogenation:

- FTIR analysis demonstrated that acid treated GAC exhibited more oxygen-containing functional groups as compared to raw GAC.
- The surface area of Co/ATGAC or Mo/ATGAC increased significantly as compared with mere GAC. The increase in surface area can be attributed to the

acidic treatment of GAC. Because of acid treatment, the inert materials present in the pores of GAC have removed thereby an increase in the pore volume.

- Modification of granular activated carbon with acetic acid and incorporation of cobalt or molybdenum species significantly improved its adsorption capacity when compared with virgin GAC.
- Approximately 92 % adsorptive removal of DBT was achieved using 1 wt % Co/ATGAC under the optimized operating conditions (T = 30 °C, time = 4 h, adsorbent dosage = 20 g/L, DBT concentration = 500 mg/L). For indole adsorption, approximately 96 % of indole removal was achieved by 2 wt % Co/ATGAC under optimized operating conditions (T = 30 °C, t = 4 h, adsorbent dosage = 10 g/L, indole concentration = 500 mg/L).
- Thermodynamic properties of DBT adsorption on 1 wt % Co/ATGAC were estimated including the change in entropy and heat of adsorption to be 0.177 kJ/mol K and 35.67 kJ/mol respectively. Similarly, for indole adsorption on 2 wt% Co/ATGAC the change in entropy and heat of adsorption were assessed to be 0.246 kJ/mol K and 55.58 kJ/mol respectively.
- The effect of active metal (Mo) loading on GAC was studied for both ADS and ADN process, and it was found that 1 wt % Mo/ATGAC gave the maximum removal of DBT and indole, respectively.
- At the optimum operating conditions (T = 30 °C, t = 4 h, adsorbent dosage = 25 g/L, DBT concentration = 500 mg/L) approximately 91 % of DBT removal was achieved. For indole adsorption study, approximately 94 % removal of indole was achieved (T = 30 °C, t = 4.5 h, adsorbent dosage = 20 g/L, indole concentration = 500 mg/L).
- The heat of adsorption for DBT and indole adsorption onto 1 wt % Mo/ATGAC was found to be 49.64 and 41.31 kJ/mol, respectively. The change in entropy for DBT and indole adsorption onto Mo/ATGAC was found to be 0.211 and 0.197 kJ/mol K, respectively.
- Adsorption of DBT and indole on Mo/ATGAC & Co/ATGAC was best represented by R - P isotherm and pseudo-second-order model found to be the best fit for the kinetic data of adsorption of both DBT and indole.

- The adsorption of DBT onto the adsorbent (Co/ATGAC & Mo/ATGAC) is governed by π complexation, acid-base interaction, and other weak interactions such as van der Waals interactions, while adsorption of indole on Co/ATGAC & Mo/ATGAC is governed by π complexation, hydrogen bonding, and van der Waals interactions.
- Solvent regeneration technique was carried out on the synthesized adsorbents (Co/ATGAC & Mo/ATGAC) which show stable efficiency in the adsorptive desulfurization and denitrogenation upto three regeneration cycles.
- Simultaneous ADS of DBT and ADN of indole in the presence of 1 wt % Co/ATGAC was examined with help of CCD design. ~ 95.4% removal of DBT and 98.1 % removal of indole was achieved at the best-optimized conditions such as a temperature of 30 °C, a dosage of 19 g/L, 223 mg/L DBT concentration and 50 mg/L indole concentration.
- The high values of coefficient of determination (R^2) for both DBT (0.958) and indole (0.949) adsorption models indicate that obtained models were suitable to represent the experimental data
- Simultaneous ADS of DBT and ADN of indole in the presence of 1 wt% Mo/ATGAC was examined with help of CCD design. ~ 97.16 % removal of DBT and ~98.41 % removal of indole was achieved at the best-optimized conditions such as a temperature of 25.5 °C, a dosage of 32 g/L, DBT concentration of 186 mg/L and indole concentration of 50 mg/L. The fitness of the developed adsorption models was depicted by their insignificant lack of fit, p= 0.184, 0.195 for DBT and indole removal, respectively.

5.3 Recommendations for Future Work

- In the present work, waste coal fly ash was used as a silica precursor for the synthesis of mesoporous silica. Other alternative green source of silica such as rice husk ash can be explored for the synthesis of mesoporous catalyst.
- Other forms of mesoporous silica such as MCM-48, SBA- 15 can be synthesized with the help of CFA and tested for the oxidation process.
- Incorporation of bimetallic species in the synthesized adsorbents to enhance their adsorption capacity.
- Solvent regeneration technique was employed to test the recyclability of samples; other regeneration method might be investigated such as thermal regeneration to increase the reusability of the catalyst/adsorbent.
- Application of synthesized catalysts and adsorbents for reducing the sulfur content of HDS treated fuel oil should be studied.

REFERENCES

Abdalla ZEA, Li B. Preparation of MCM-41 supported $(Bu_4N)_4H_3(PW_{11}O_{39})$ catalyst and its performance in oxidative desulfurization. Chem Eng J 2012; 200: 113–121.

Abdedayem A, Guiza M, Toledo FJ, Ouederni A. Nitrobenzene degradation in aqueous solution using ozone/cobalt supported activated carbon coupling process: A kinetic approach. Sep Purif Technol 2017; 184: 308−318.

Abdullah WN, Bakar WA, Ali R, Embong Z. Oxidative desulfurization of commercial diesel catalyzed by tert-butyl hydroperoxide polymolybdate on alumina: optimization by Box-Behnken design. Clean Technol Envir 2015; 17: 433-441.

Abdullah WNW, Ali R, Bakar WAWA. In depth investigation of $Fe/MoO_3–PO_4/Al_2O_3$ catalyst in oxidative desulfurization of Malaysian diesel with TBHP-DMF system. J Taiwan Inst Chem Eng 2016; 58: 344-350.

Abin-Fuentes A, Mohamed ME, Wang DI, Prather KL. Exploring the mechanism of biocatalyst inhibition in microbial desulfurization. Appl Environ Microbiol 2013; 79: 7807-7817.

Abro R, Abdeltawab AA, Al-Deyab SS, Yu G, Qazi AB, Gao S, et al. A review of extractive desulfurization of fuel oils using ionic liquids. RSC Adv 2014; 67: 35302- 35317.

Ahmad W, Ahmad I, Ishaq M, Ihsan K. Adsorptive desulfurization of kerosene and diesel oil by Zn impregnated montmorollonite clay. Arab J Chem 2017; 10: S3263–S3269.

Ahmadi M, Anvaripour B, Khosravi-Nikou MR, Mohammadian M. Selective denitrogenation of model fuel through iron and chromium modified microporous materials (MSU-S). J Environ Chem Eng 2017; 5: 849-860.

Ahmadi M, Anvaripour B, Khosravi-Nikou MR, Mohammadian M. Selective denitrogenation of model fuel through iron and chromium modified microporous materials (MSU-S). J Environ Chem Eng 2017; 5 :849-860.

Ahmed I, Hasan Z, Khan NA, Jhung SH. Adsorptive denitrogenation of model fuels with porous metal-organic frameworks (MOFs): Effect of acidity and basicity of MOFs. Appl Catal B Environ 2001; 129: 123-129.

Ahmed I, Jhung SH. Adsorptive denitrogenation of model fuel with CuCl-loaded metal–organic frameworks (MOFs). Chem Eng J 2014; 251: 35-42.

Ahmed I, Jhung SH. Adsorptive desulfurization and denitrogenation using metal-organic frameworks. J Hazard mater 2016; 301: 259-276..

Ahmed I, Jun JW, Jung BK, Jhung SH. Adsorptive denitrogenation of model fossil fuels with Lewis acid-loaded metal–organic frameworks (MOFs). Chem Eng J 2014; 255: 623-629.

Ahmed OU, Mjalli FS, Al-Wahaibi T, Al-Wahaibi Y, AlNashef IM. Optimum performance of extractive desulfurization of liquid fuels using phosphonium and pyrrolidinium-based ionic liquids. Ind Eng Chem Res 2015; 54: 6540-6550.

Aicher T, Lenz B, Gschnell F, Groos U, Federici F, Caprile L, Parodi L. Fuel processors for fuel cell APU applications. J Power Sources 2006; 154: 503-508.

Aitani AM, Ali MF, Al-Ali HH. A review of non-conventional methods for the desulfurization of residual fuel oil. Pet Sci Technol 2000; 18: 537–553.

Alcon A, Santos VE, Martin AB, Yustos P, Garcia-Ochoa F. Biodesulfurization of DBT with *Pseudomonas putida* CECT5279 by resting cells: Influence of cell growth time on reducing equivalent concentration and HpaC activity. Biochem Eng J 2005; 26: 168-175.

Al-Ghouti MA, Al-Degs YS. Manganese-loaded activated carbon for the removal of organosulfur compounds from high-sulfur diesel fuels. Energy Technol 2014; 9-10: 802-810.

Ali MF, Al-Malki A, Ahmed S. Chemical desulfurization of petroleum fractions for ultra-low sulfur fuels. Fuel Process Technol 2009; 90: 536–544.

Almarri M, Ma X, Song C. Selective adsorption for removal of nitrogen compounds from liquid hydrocarbon streams over carbon-and alumina-based adsorbents. Ind Eng Chem Res 2009; 48: 951-960.

Ania CO, Bandosz TJ. Metal-loaded polystyrene-based activated carbons as dibenzothiophene removal media via reactive adsorption. Carbon 2006; 44: 2404-2412.

Ansari F, Grigoriev P, Libor S, Tothill IE, Ramsden JJ. DBT degradation enhancement by decorating *Rhodococcus erythropolis* IGST8 with magnetic Fe_3O_4 nanoparticles. Biotechnol Bioeng 2009; 102: 1505-1512.

Arcoria A, Ballisterri FP, Tomaselli GA, Di Furia F, Modena G. Kinetics and mechanism of the tungsten-catalyzed oxidation of organic sulphides and alkenes by hydrogen peroxide. J Mol Catal 1983; 18: 177–188.

Arshadi M, Shakeri H, Salvacion JW. A green adsorbent for the removal of BTEX from aqueous media. RSC Adv 2016; 17: 14290-14305.

Asfaram A, Ghaedi M, Hajati S, Rezaeinejad M, Goudarzi A, Purkait MK. Rapid removal of Auramine-O and Methylene blue by ZnS: Cu nanoparticles loaded on activated carbon: a response surface methodology approach. J Taiwan Inst Chem Eng 2015; 53: 80-91.

Asghari E, Haghighi M, Rahmani F. CO_2 Oxidative Dehydrogenation of Ethane to Ethylene over Cr/MCM-41 Nanocatalyst Synthesized via Hydrothermal/Impregnation Methods: Influence of Chromium Content on Catalytic Properties and Performance. J Mol Catal A Chem 2016; 418: 115-124.

Babich IV, Moulijn JA. Science and technology of novel processes for deep desulfurization of oil refinery streams: a review. Fuel 2003; 82: 607-631.

Baeza P, Aguila G, Gracia F, Araya P. Desulfurization by adsorption with copper supported on zirconia. Catal Commun 2008; 5: 751–755.

Bahuguna A, Lily MK, Munjal A, Singh RN, Dangwal K. Desulfurization of dibenzothiophene (DBT) by a novel strain *Lysinibacillus sphaericus* DMT-7 isolated from diesel contaminated soil. J Environ Sci 2011; 23: 975-982.

Bailes PJ. Solvent extraction in an electrostatic field. Ind Eng Chem 1981; 20: 564-570.

Bakar WA, Ali R, Kadir AA, Mokhtar WN. Effect of transition metal oxides catalysts on oxidative desulfurization of model diesel. Fuel Process Technol 2012; 101: 78–84.

Bakar WA, Ali R, Kadir AA, Mokhtar WN. The role of molybdenum oxide based catalysts on oxidative desulfurization of diesel fuel. Mod Chem appl 2015; 3: 150 (doi:10.4172/2329-6798.1000150)

Ban LL, Liu P, Ma CH, Dai B. Deep extractive desulfurization of diesel fuels by $FeCl_3$/ionic liquids. Chin Chem Lett 2013; 24: 755-758.

Bandyopadhyay A, Biswas MN. Removal of hexavalent chromium by synergism modified adsorption. Indian J Environ Port 1998; 18: 662–671.

Bauserman JW, Mushrush GW, Hardy DR. Organic nitrogen compounds and fuel instability in middle distillate fuels. Ind Eng Chem Res 2008; 47: 2867-2875.

Bazyari A, Mortazavi Y, Khodadadi AA, Thompson LT, Tafreshi R, Zaker A, Ajenifujah OT. Effects of alumina phases as nickel supports on deep reactive adsorption of (4,6-dimethyl) dibenzothiophene: comparison between γ, δ, and θ-alumina. Appl Catal B 2016; 180: 312–323.

Bhagiyalakshmi M, Yun LJ, Anuradha R, Jang HT. Utilization of rice husk ash as silica source for the synthesis of mesoporous silicas and their application to CO_2 adsorption through TREN/TEPA grafting. J Hazard Mater 2010; 175: 928-938.

Bhatia S, Sharma DK .Thermophilic desulfurization of dibenzothiophene and different petroleum oils by *Klebsiella* sp. 13T. Environ Sci Pollut Res 2012; 19: 3491-3497.

Bhutto AW, Abro R, Gao S, Abbas T, Chen X, Yu G. Oxidative desulfurization of fuel oils using ionic liquids: A review. J Taiwan Inst Chem Eng 2016; 62: 84-97.

Bimakr M, Rahman RA, Taip FS, Adzahan NM, Sarker MZ, Ganjloo A. Supercritical carbon dioxide extraction of seed oil from winter melon (Benincasa hispida) and its antioxidant activity and fatty acid composition. Molecules 2013; 18: 997-1014.

Bokare AD, Choi W. Bicarbonate-induced activation of H_2O_2 for metal-free oxidative desulfurization. J Hazard Mater 2016; 304: 313–319.

Boniek D, Figueiredo D, dos Santos AF, de Resende Stoianoff MA. Biodesulfurization: a mini review about the immediate search for the future technology. Clean Technol Envir 2014; 17: 29-37.

Bordoloi NK, Rai SK, Chaudhuri MK, Mukherjee AK. Deep-desulfurization of dibenzothiophene and its derivatives present in diesel oil by a newly isolated bacterium *Achromobacter* sp. to reduce the environmental pollution from fossil fuel combustion. Fuel Process Technol 2014; 119: 236-244.

Bösmann A, Datsevich L, Jess A, Lauter A, Schmitz C, Wasserscheid P. Deep desulfurization of diesel fuel by extraction with ionic liquids. Chem Commun 2001; 23: 2494-2495.

Bowker RH, Ilic B, Carrillo BA, Reynolds MA, Murray BD, Bussell ME. Carbazole hydrodenitrogenation over nickel phosphide and Ni-rich bimetallic phosphide catalysts. Appl Catal A Gen 2014; 482: 221-230.

Brouers F, Al-Musawi TJ. On the optimal use of isotherm models for the characterization of biosorption of lead onto algae. J Mol Liq 2015; 212: 46–51.

Caero LC, Jorge F, Navarro A, Gutiérrez-Alejandre A. Oxidative desulfurization of synthetic diesel using supported catalysts: Part II. Effect of oxidant and nitrogen-compounds on extraction–oxidation process. Catal today 2006; 1160: 562-568.

Campos-Martin JM, Capel-Sanchez MC, Perez-Presas P, Fierro JLG. Oxidative processes of desulfurization of liquid fuels. J Chem Technol Biotechnol 2010; 85: 879-890.

Capel-Sanchez MC, Perez-Presas P, Campos-Martin JM, Fierro JL. Highly efficient deep desulfurization of fuels by chemical oxidation. Catal Today 2010; 157: 390–396.

Chamack M, Mahjoub AR, Aghayan H. Cesium salts of tungstensubstituted molybdophosphoric acid immobilized onto platelet mesoporous silica: efficient catalysts for oxidative desulfurization of dibenzothiophene. Chem Eng J 2014; 255: 686–694.

Chang J, Wang A, Liu J, Li X, Hu Y. Oxidation of dibenzothiophene with cumene hydroperoxide on MoO_3/SiO_2 modified with alkaline earth metals. Catal Today 2010; 149: 122–126.

Chen W, Maugé F, van Gestel J, Nie H, Li D, Long X. Effect of modification of the alumina acidity on the properties of supported Mo and CoMo sulfide catalysts. J Catal 2013; 304: 47-62.

Cho KS, Lee YK. Effects of nitrogen compounds, aromatics, and aprotic solvents on the oxidative desulfurization (ODS) of light cycle oil over Ti-SBA-15 catalyst. Appl Catal B Environ 2014; 147: 35-42.

Cychosz KA, Wong-Foy AG, Matzger AJ. Liquid phase adsorption by microporous coordination polymers: removal of organosulfur compounds. J Am Chem Soc 2008; 130: 6938–6939.

Dai Y, Qi Y, Zhao D, Zhang H. An oxidative desulfurization method using ultrasound/Fenton's reagent for obtaining low and/or ultra-low sulfur diesel fuel. Fuel Process Technol 2008; 89: 927–932.

Danmaliki GI, Saleh TA, Shamsuddeen AA. Response surface methodology optimization of adsorptive desulfurization on nickel/activated carbon. Chem Eng J 2017; 313: 993-1003.

Danmaliki GI, Saleh TA. Effects of bimetallic Ce/Fe nanoparticles on the desulfurization of thiophenes using activated carbon. Chem Eng J 2017; 307: 914-927.

Dasgupta S, Gupta P, Nanoti A, Goswami AN, Garg MO, Tangstad E, Vistad ØB, Karlsson A, Stöcker M. Adsorptive desulfurization of diesel by regenerable nickel based adsorbents. Fuel 2013; 108: 184-189.

Dashamiri S, Ghaedi M, Asfaram A, Zare F, Wang S. Multi-response optimization of ultrasound assisted competitive adsorption of dyes onto $Cu(OH)_2$ nanoparticle loaded activated carbon: central composite design. Ultrason Sonochem 2017; 34: 343-353.

de Souza WF, Guimarães IR, Oliveira LC, Giroto AS, Guerreiro MC, Silva CL. Effect of Ni incorporation into goethite in the catalytic activity for the oxidation of nitrogen compounds in petroleum. Appl Catal A Gen 2010; 381: 36-41.

Deepa G, Sankaranarayanan TM, Shanthi K, Viswanathan B. Hydrodenitrogenation of model N-compounds over NiO-MoO_3 supported on mesoporous materials. Catal today 2012; 198: 252-262.

Dehkordi AM, Sobati MA, Nazem MA. Oxidative desulfurization of non-hydrotreated kerosene using hydrogen peroxide and acetic acid. Chin J Chem Eng 2009; 17: 869–874.

de-Souza WF, Guimaraes IR, Guerreiro MC, Oliveira LC. Catalytic oxidation of sulfur and nitrogen compounds from diesel fuel. Appl Catal A Gen 2009; 360: 205–209.

Dharaskar SA, Wasewar KL, Varma MN, Shende DZ. Imidazolium ionic liquid as energy efficient solvent for desulfurization of liquid fuel. Sep Purif Technol 2015; 155: 101-109.

Dhokte AO, Khillare SL, Lande MK, Arbad BR. Synthesis, characterization of mesoporous silica materials from waste coal fly ash for the classical Mannich reaction. Ind Eng Chem 2011; 17: 742-746.

Ding L, Zheng Y, Zhang Z, Ring Z, Chen J. HDS, HDN, HDA, and hydrocracking of model compounds over Mo-Ni catalysts with various acidities. Appl Catal A Gen 2007; 319: 325-337.

Duan X, Li X, Wang A, Teng Y, Wang Y, Hu Y. Effect of TiO_2 on hydrodenitrogenation performances of MCM-41 supported molybdenum phosphides. Catal Today 2010; 149: 11-18.

Duarte FA, Mello PD, Bizzi CA, Nunes MA, Moreira EM, Alencar MS, Motta HN, Dressler VL, Flores ÉM. Sulfur removal from hydrotreated petroleum fractions using ultrasound-assisted oxidative desulfurization process. Fuel 2011; 90: 2158–2164.

Dursun AY, Kalayci CS. Equilibrium, kinetic and thermodynamic studies on the adsorption of phenol onto chitin. J Hazard Mater 2005; 123: 151-157.

Escobar J, Toledo JA, Cortés MA, Mosqueira ML, Pérez V, Ferrat G, López-Salinas E, Torres-García E. Highly active sulfided CoMo catalyst on nano-structured TiO_2. Catal today 2005; 106: 222-226.

Farag H, Kishida M, Al-Megren H. Competitive hydrodesulfurization of dibenzothiophene and hydrodenitrogenation of quinoline over unsupported MoS_2 catalyst. Appl Catal A 2014; 469: 173-182.

Feng J, Zeng Y, Ma C, Cai X, Zhang Q, Tong M. The surfactant tween 80 enhances biodesulfurization. Appl Environ Microbiol 2006; 72: 7390-7393.

Forsyth SA, Prigle JM, MacFarlane DR. Ionic liquids- an overview, Aust J Chem 2004; 57: 113-119.

Forte P, inventor. Process for the removal of sulfur from petroleum fractions. 1996; 5582714.

Fraile JM, Gil C, Mayoral JA, Muel B, Roldán L, Vispe E, Calderón S, Puente F. Heterogeneous titanium catalysts for oxidation of dibenzothiophene in hydrocarbon solutions with hydrogen peroxide: on the road to oxidative desulfurization. Appl Catal B 2016; 180: 680–686.

Franco RLM, Oliveira TG, Pedrosa AMG, Naviciene S, Souza MJB. Textural properties of nickel, palladium and titanium oxides supported on MCM-41 materials and their application on oxidative desulfurization of dibenzothiophene. Mater Res 2013; 16: 1448–1456.

Freemantle M. Designer liquids in polymer systems. Chem Eng News 2004; 18: 26-29.

Funakoshi I, Aida T, inventors. Process for recovering organic sulfur compounds from fuel oil. 1998; 5,753,1020.

Furimsky E, Massoth FE. Hydrodenitrogenation of petroleum. Catal Rev 2005; 47: 297-489.

Ganiyu SA, Alhooshani K, Sulaiman KO, Qamaruddin M, Bakare IA, Tanimu A, Saleh TA. Influence of aluminium impregnation on activated carbon for enhanced desulfurization of DBT at ambient temperature: role of surface acidity and textural properties. Chem Eng J 2016; 303: 489–500.

Gano ZS, Mjalli FS, Al-Wahaibi T, Al-Wahaibi Y, AlNashef IM. Extractive desulfurization of liquid fuel with $FeCl_3$-based deep eutectic solvents:

experimental design and optimization by central-composite design. Chem Eng Process Process Intensif 2015; 93: 10-20.

Gao H, Guo C, Xing J, Zhao J, Liu H. Extraction and oxidative desulfurization of diesel fuel catalyzed by a Bronsted acidic ionic liquid at room temperature. Green Chem 2010; 12: 1220–1224.

Gao S, Yu G, Abro R, Abdeltawab AA, Al-Deyab SS, Chen X. Desulfurization of fuel oils: mutual solubility of ionic liquids and fuel oil. Fuel 2016; 173: 164–171.

García-Gutiérrez JL, Fuentes GA, Hernández-Terán ME, Garcia P, Murrieta-Guevara F, Jiménez-Cruz F. Ultra-deep oxidative desulfurization of diesel fuel by the Mo/Al_2O_3-H_2O_2 system: the effect of system parameters on catalytic activity. Appl Catal A 2008; 334: 366–373.

García-Gutiérrez JL, Laredo GC, Fuentes GA, García-Gutiérrez P, Jiménez-Cruz F. Effect of nitrogen compounds in the hydrodesulfurization of straight-run gas oil using a $CoMoP/g\text{-}Al_2O_3$ catalyst. Fuel 2014; 138: 98-103.

Gary JH, Handwerk GE, editors. Petroleum refining: technology and economics, 4th ed., New York, USA: Marcel Dekker, 2001.

Geng W, Zhang H, Zhao X, Zan W, Gao X, Yao X. Theoretical studies of the nitrogen containing compounds adsorption behavior on Na(I)Y and rare earth exchanged RE(III) Y zeolites. J Mol Model 2015; 21: 10.

Ghanbari M, Hadian AM, Nourbakhsh AA, MacKenzie KJ. Modeling and optimization of compressive strength and bulk density of metakaolin-based geopolymer using central composite design: a numerical and experimental study. Ceram Internat 2017; 43: 324-335.

Gochi Y, Ornelas C, Paraguay F, Fuentes S, Alvarez L, Rico JL, Alonso-Núñez G. Effect of sulfidation on Mo-W-Ni trimetallic catalysts in the HDS of DBT. Catal today 2005; 107: 531-536.

Gonzalez-Garcia O, Cedeno-Caero L. V-Mo based catalysts for oxidative desulfurization of diesel fuel. Catal Today 2009; 148: 42–48.

Gray KA, Mrachko GT, Squires CH. Biodesulfurization of fossil fuels. Curr Opin Microbiol 2003; 6: 229-235.

Green MLH, Al-Shahrani F, Xiao T, Llewellyn SA, Barri S, Jiang Z, Shi H, Martinie G. Desulfurization of diesel via the H_2O_2 oxidation of aromatic sulfides to sulfones using a tungstate catalyst. Appl Catal B 2007; 73: 311–316.

Guimarães IR, Giroto AS, de Souza WF, Guerreiro MC. Highly reactive magnetite covered with islands of carbon: Oxidation of N and S-containing compounds in a biphasic system. Appl Catal A Gen 2013; 450: 106-113.

Guo K, Ding Y, Yu Z. One-step synthesis of ultrafine MoNiS and MoCoS monolayers as high-performance catalysts for hydrodesulfurization and hydrodenitrogenation. Appl Catal B Envion 2018; 239: 433-440.

Gupta N, Roychoudhury PK, Deb JK. Biotechnology of desulfurization of diesel: prospects and challenges. Appl Microbiol Biotechnol 2005; 66: 356-366.

Guzmán MA, Huirache-Acuña R, Loricera CV, Hernández JR, de León JD, de los Reyes JA, Pawelec B. Removal of refractory S-containing compounds from liquid fuels over P-loaded NiMoW/SBA-16 sulfide catalysts. Fuel. 2013; 103: 321-333.

Hameed BH, Salman JM, Ahmad AL. Adsorption isotherm and kinetic modeling of 2, 4-D pesticide on activated carbon derived from date stones. J hazard mater 2009; 163: 121-126.

Han X, Lin H, Zheng Y. Adsorptive denitrogenation and desulfurization of diesel using activated carbons oxidized by $(NH_4)_2S_2O_8$ under mild conditions. Can J Chem Eng 2015; 93: 538-548.

Han X, Wang A, Wang X, Li X, Wang Y, Hu Y. Catalytic performance of P-modified MoO_3/SiO_2 in oxidative desulfurization by cumene hydroperoxide. Catal Commun 2013; 42: 6–9.

Hayes R, Warr GG, Atkin R. Structure and nanostructure in ionic liquids. Chem Rev 2015; 115: 6357-6426.

Hernández-Maldonado AJ, Yang RT. Desulfurization of transportation fuels by adsorption. Cat Rev-Sci Eng 2004a; 46: 111-150.

Hernandez-Maldonado AJ, Yang RT. Denitrogenation of transportation fuels by zeolites at ambient temperature and pressure. Angew Chem Int Ed. 2004b; 116: 1022–1024.

Hicks RW, Castagnola NB, Zhang Z, Pinnavaia TJ, Marshall CL. Lathlike mesostructured γ-alumina as a hydro-desulfurization catalyst support. Appl Catal A 2003; 254: 311-317.

Hiwarkar AD, Srivastava VC, Mall ID. Comparative studies on adsorptive removal of indole by granular activated carbon and bagasse fly ash. Environ Prog Sustain Energy 2015; 4: 492-503.

Hizaddin HF, Ramalingam A, Hashim MA, Hadj-Kali MK. Evaluating the performance of deep eutectic solvents for use in extractive denitrification of liquid fuels by the conductor-like screening model for real solvents. J Chem Eng Data 2014; 59: 3470-3487.

Ho YS, McKay G. Pseudo-second order model for sorption processes. Process Biochem 1999; 34: 451-465.

Ho YS, McKay G. The sorption of lead (II) ions on peat. Water res 1999; 33: 578-584.

Honda H, Sugiyama H, Saito I, Kobayashi T. High cell density culture of *Rhodococcus rhodochrous* by pH-state feeding and dibenzothiophene degradation. J Fermen Bioeng 1998; 85: 334-338.

Hou Y, Kong K, Yang J, Zhang J, Shi D, Xin W. Biodesulfurization of dibenzothiophene by immobilized cells of *Pseudomonas stutzeri* UP-1. Fuel 2005; 84: 1975-1979.

Huang B, Wang YJ, Cui YC. Direct synthesis of mesoporous TiO_2 and its catalytic performance in DBT oxidative desulfurization. Microporous Mesoporous Mater 2008; 116: 378–385.

Hulea V, Fajula F, Bousquet J. Mild oxidation with H_2O_2 over Ti-containing molecular sieves – a very efficient method for removing aromatic sulphur compounds from fuels. J Catal 2001; 198: 179–186.

Hwang IC, Kim KL, Park SJ, Han KJ. Liquid− Liquid Equilibria for Binary System of Ethanol+ Hexadecane at Elevated Temperature and the Ternary Systems of Ethanol+ Heterocyclic Nitrogen Compounds+ Hexadecane at 298.15 K. J Chem Eng Data 2007; 52: 1919-1924.

Hwang IC, Park SJ, Seo DW, Han KJ. Binary Liquid− Liquid Equilibrium (LLE) for N-Methylformamide (NMF)+ Hexadecane between (288.15 and 318.15) K and Ternary LLE for Systems of NMF+ Heterocyclic Nitrogen Compounds+ Hexadecane at 298.15 K. J Chem Eng Data. 2008; 54: 78-82.

Ishihara A, Wang D, Dumeignil F, Amano H, Qian EW, Kabe T. Oxidative desulfurization and denitrogenation of a light gas oil using an oxidation/adsorption continuous flow process. Appl Catal A Gen 2005; 279: 279-287.

Ishii Y, Konishi J, Okada H, Hirasawa K, Onaka T, Suzuki M. Operon structure and functional analysis of the genes encoding thermophilic desulfurizing enzymes of *Paenibacillus* sp. A11-2. Biochem Biophys Res Commun 2000; 270: 81-88.

Jia Y, Li G, Ning G, Jin C. The effect of N-containing compounds on oxidative desulphurization of liquid fuel. Catal Today 2009; 140: 192-196.

Jia Y, Li G, Ning G. Efficient oxidative desulfurization (ODS) of model fuel with H2O2 catalyzed by MoO_3/γ-Al_2O_3 under mild and solvent free conditions. Fuel Process Technol 2011; 92: 106–111.

Jiang Z, Liu Y, Sun X, Tian F, Sun F, Liang C, You W, Han C, Li C. Activated carbons chemically modified by concentrated H_2SO_4 for the adsorption of the pollutants from wastewater and the dibenzothiophene from fuel oils. Langmuir 2003; 19: 731-736.

Jianlong W, Xiangchun Q, Liping H, Yi Q, Hegemann W. Microbial degradation of quinoline by immobilized cells of Burkholderia pickettii. Wat. Res 2002; 36: 2288–2296.

Jian-long WA, Zhao DS, Zhou EP, Dong Z. Desulfurization of gasoline by extraction with N-alkyl-pyridinium-based ionic liquids. J Fuel Chem Technol 2007; 35: 293–296.

Jongsomjit B, Panpranot J Goodwin JG. Co-Support Compound Formation in Alumina-Supported Cobalt Catalysts. J Catal 2001; 204: 98-109.

Jung BK, Jhung SH. Adsorptive removal of benzothiophene from model fuel, using modified activated carbons, in presence of diethylether. Fuel 2015; 145: 249–255.

Kaiser JP, Feng Y, Bollag JM. Microbial metabolism of pyridine, quinoline, acridine, and their derivatives under aerobic and anaerobic conditions. Microbiol Rev 1996; 60: 483–498.

Kareem SA, Aribike DS, Nwachukwu SC, Latinwo GK. Microbial desulfurization of diesel by *Desulfobacterium indolicum*. J Environ Sci Eng 2012; 54: 98-103.

Karimi E, Jeffryes C, Yazdian F, Akhavan Sepahi A, Rasekh B, Rashedi H, Omidi M, Ebrahim-Habibi MB, Ashrafi SJ, Hatamian A., Ashrafi SJ, Hatamian A. DBT desulfurization by decorating *Rhodococcus erythropolis* IGTS8 using magnetic Fe_3O_4 nanoparticles in a bioreactor. Eng Life Sci 2017; 17: 528-535.

Khan NA, Jhung SH. Adsorptive Removal and Separation of Chemicals with Metal-Organic Frameworks: Contribution of Π-Complexation. J Hazard Mater 2017; 325: 198-213.

Khan NA, Jhung SH. Low-temperature loading of Cu^+ species over porous metal-organic frameworks (MOFs) and adsorptive desulfurization with Cu^+-loaded MOFs. J Hazard Mater 2012; 237: 180–185.

Kianpour E, Azizian S. Polyethylene glycol as a green solvent for effective extractive desulfurization of liquid fuel at ambient conditions. Fuel 2014; 137: 36-40.

Kilbane JJ. Desulfurization of coal: the microbial solution. Trends Biotechnol 1989; 7: 97-101.

Klimova T, Reyes J, Gutiérrez O, Lizama L. Novel bifunctional NiMo/Al-SBA-15 catalysts for deep hydrodesulfurization: Effect of support Si/Al ratio. Appl Catal A 2008; 335: 159-171.

Koriakin A, Muruganandam Ponvel K, Lee C. Denitrogenation of raw diesel fuel by lithium-modified mesoporous silica. Chem Eng J 2010; 162: 649–655.

Krivtsov EB, Golovko AK. The kinetics of oxidative desulfurization of diesel fraction with a hydrogen peroxide-formic acid mixture. Pet Chem 2014; 54: 51–57.

Kropp PJ, Breton GW, Fields JD, Tung JC, Loomis BR. Surface-Mediated Reactions. 8. Oxidation of Sulfides and Sulfoxides with tert-Butyl Hydroperoxide and OXONE1. J Amer Chem Soc 2000; 122: 4280-4285.

Kumar D, Schumacher K, von Hohenesche CD, Grün M, Unger KK. MCM-41, MCM-48 and related mesoporous adsorbents: their synthesis and characterisation. Colloids Surf A Physicochem Eng Asp 2001; 187: 109-116.

Kumar S, Srivastava VC, Badoni RP. Oxidative desulfurization by chromium promoted sulfated zirconia, Fuel Process Technol 2012; 93: 8-25.

Kumar S, Srivastava VC, Badoni RP. Studies on adsorptive desulfurization by zirconia based adsorbents. Fuel 2011; 90: 3209–3216.

Kurnia KA, Quental MV, Santos LM, Freire MG, Coutinho JA. Mutual solubilities between water and non-aromatic sulfonium-, ammonium-and phosphonium-hydrophobic ionic liquids. Phys Chem Chem Phys 2015; 17: 4569-4577.

Kwak C, Lee JJ, Bae JS, Moon SH. Poisoning effect of nitrogen compounds on the performance of $CoMoS/Al_2O_3$ catalyst in the hydrodesulfurization of dibenzothiophene, 4-methyldibenzothiophene, and 4, 6-dimethyldibenzothiophene. Appl Catal B Environ 2001; 35: 59-68.

Kwong CW, Chao CYH, Hui KS, Wan MP. Removal of VOCs from indoor environment by ozonation over different porous materials. Atmos Environ 2008; 42: 2300–2311.

Labana S, Pandey G, Jain RK. Desulphurization of dibenzothiophene and diesel oils by bacteria. Lett Appl Microbiol 2005; 40: 159-63.

Laredo GC, Likhanova NV, Lijanova IV, Rodriguez-Heredia B, Castillo JJ, Perez-Romo P. Synthesis of ionic liquids and their use for extracting nitrogen compounds from gas oil feeds towards diesel fuel production. Fuel Process Technol 2015; 130: 38-45.

Laredo GC, Vega-Merino PM, Trejo-Zárraga F, Castillo J. Denitrogenation of middle distillates using adsorbent materials towards ULSD production: a review. Fuel process technol 2013; 106: 21-32.

Le Borgne S, Ayala M. Microorganisms utilizing sulfur-containing hydrocarbons. In: Timmis KN, editor. Handbook of hydrocarbon and lipid microbiology. Germany: Springer-Verlag Berlin Heidelberg, 2010: 2129–2141.

Le Bui TT, Van Ho S, Nguyen BT, Uong HT. Synthesis, characterization and application of some non-halogen ionic liquids as green solvents for deep desulfurization of diesel oil. Fuel 2017; 191: 54-61.

Ledesma BC, Martínez ML, Beltramone AR. Iridium-supported SBA-15 modified with Ga and Al as a highly active catalyst in the hydrodenitrogenation of quinoline. Cataly Today 2018

Lee YK, Oyama ST. Sulfur resistant nature of Ni_2P catalyst in deep hydrodesulfurization. Appl Catal A 2017; 548: 103-113.

Lee YK, Shu Y, Oyama ST. Active phase of a nickel phosphide (Ni_2P) catalyst supported on KUSY zeolite for the hydrodesulfurization of 4, 6-DMDBT. Appl Catal A 2007; 322: 191-204.

Leng K, Sun Y, Zhang X, Yu M, Xu W. Ti-modified hierarchical mordenite as highly active catalyst for oxidative desulfurization of dibenzothiophene. Fuel 2016; 174: 9–16.

Lewandowski M. Hydrotreating activity of bulk NiB alloy in model reaction of hydrodenitrogenation of carbazole. Appl Catal B Environ 2015; 168: 322-332.

Li B, Ma W, Liu J, Han C, Zuo S, Li X. Synthesis of the well-ordered hexagonal mesoporous silicate incorporated with phosphotungstic acid through a novel method and its catalytic performance on the oxidative desulfurization reaction. Catal Commun 2011; 13: 101–105.

Li FL, Xu P, Ma CQ, Luo LL, Wang XS. Deep desulfurization of hydrodesulfurization-treated diesel oil by a facultative thermophilic bacterium *Mycobacterium* sp. X7B. FEMS Microbiol Lett 2003; 223: 301-307.

Li H, Zhang D, Han X, Xing B. Adsorption of antibiotic ciprofloxacin on carbon nanotubes: pH dependence and thermodynamics. Chemosphere 2014; 95: 150-155.

Li SW, Li JR, Gao Y, Liang LL, Zhang RL, Zhao JS. Metal modified heteropolyacid incorporated into porous materials for a highly oxidative desulfurization of DBT under molecular oxygen. Fuel 2017; 197: 551-561.

Li YG, Li WL, Huang JX, Xiong XC, Gao HS, Xing JM, Liu HZ. Biodegradation of carbazole in oil/water biphasic system by a newly isolated bacterium *Klebsiella* sp. LSSE-H2. Biochem Eng J 2008; 41: 166-170.

Li YG, Ma J, Zhang QQ, Wang CS, Chen Q. Sulfur-selective desulfurization of dibenzothiophene and diesel oil by newly isolated *rhodococcus erythropolis* NCC-1. Chin J Chem 2007; 25: 400-405.

Li YH, Tan P, Liu XQ, Zu DD, Huang CL, Sun LB. Facile fabrication of AgCl nanoparticles and their application in adsorptive desulfurization. J Nanosci Nanotechnol 2015; 15: 4373–4379.

Li Z, Jin S, Zhang R, Shao X, Zhang S, Jiang N, Jin M, Meng T, Mu Y. Adsorption of thiophene, dibenzothiophene, and 4, 6-dimethyl dibenzothiophene on activated carbons. Adsorpt Sci Technol 2016; 34: 227-243.

Lin Q, Jianlong W. Biodegradation characteristics of quinoline by *Pseudomonas putida*. Bioresour Technol 2010; 101: 7683-7686.

Liu F, Xu S, Cao L, Chi Y, Zhang T, Xue D. A comparison of $NiMo/Al_2O_3$ catalysts prepared by impregnation and coprecipitation methods for hydrodesulfurization of dibenzothiophene. J Phys Chem C 2007; 111: 7396-402.

Liu H, Liu C, Yin C, Chai Y, Li Y, Liu D, Liu B, Li X, Wang Y, Li X. Preparation of highly active unsupported nickel-zinc-molybdenum catalysts for the hydrodesulfurization of dibenzothiophene. Appl Catal B 2015; 174: 264-276.

Liu S, Wang B, Cui B, Sun L. Deep desulfurization of diesel oil oxidized by Fe (VI) systems. Fuel 2008; 87: 422–428.

Liu W, Jiang W, Zhu W, Zhu W, Li H, Guo T, Zhu W, Li H. Oxidative desulfurization of fuels promoted by choline chloride-based deep eutectic solvents. J Mol Catal A Chem 2016; 424: 261-268.

Liu X, Li X, Yan Z. Facile route to prepare bimodal mesoporous γ-Al_2O_3 as support for highly active como-based hydrodesulfurization catalyst. Appl Catal B 2012; 121:50-56.

Lü H, Gao J, Jiang Z, Yang Y, Song B, Li C. Oxidative desulfurization of dibenzothiophene with molecular oxygen using emulsion catalysis. Chem Commun 2007; 2: 150–152.

Luo MF, Xing JM, Gou ZX, Li S, Liu HZ, Chen JY. Desulfurization of dibenzothiophene by lyophilized cells of *Pseudomonas delafieldii* R-8 in the presence of dodecane. Biochem Eng J 2003; 13: 1-6.

Ma CQ, Feng JH, Zeng YY, Cai XF, Sun BP, Zhang ZB, Xu P. Methods for the preparation of a biodesulfurization biocatalyst using *Rhodococcus* sp. Chemosphere 2006; 65: 165-169.

Ma X, Sun L, Song C. A new approach to deep desulfurization of gasoline, diesel fuel and jet fuel by selective adsorption for ultra-clean fuels and for fuel cell applications. Catal Today 2002; 77: 107-116.

Ma X, Zhou A, Song C. A novel method for oxidative desulfurization of liquid hydrocarbon fuels based on catalytic oxidation using molecular oxygen coupled with selective adsorption. Catal Today 2007; 123: 276–284.

Maghsoudi S, Vossoughi M, Kheirolomoom A, Tanaka E, Katoh S. Biodesulfurization of hydrocarbons and diesel fuels by *Rhodococcus* sp. strain P32C1. Biochem Eng J 2001; 8: 151-156.

Mambrini RV, Maia CZ, Ardisson JD, de Souza PP, Moura FC. Fe/C and FeMo/C hybrid materials for the biphasic oxidation of fuel contaminants. New J Chem 2017; 41: 142-150.

Manirethan V, Raval K, Rajan R, Thaira H, Balakrishnan RM. Kinetic and thermodynamic studies on the adsorption of heavy metals from aqueous solution by melanin nanopigment obtained from marine source: Pseudomonas stutzeri. J Environ Manage 2018; 214: 315-324.

Mendoza-Nieto JA, Vera-Vallejo O, Escobar-Alarcón L, Solís-Casados D, Klimova T. Development of new trimetallic NiMoW catalysts supported on SBA-15 for deep hydrodesulfurization. Fuel 2013; 110: 268-277.

Menzel R, Iruretagoyena D, Wang Y, Bawaked SM, Mokhtar M, Al-Thabaiti SA, Basahel SN, Shaffer MS. Graphene oxide/ mixed metal oxide hybrid materials for enhanced adsorption desulfurization of liquid hydrocarbon fuels. Fuel 2016; 181: 531–536.

Miller JT, Hineman MF. Non-first-order hydrodenitrogenation kinetics of quinoline. J Catal 1984; 85: 117-126.

Ministry of petroleum and Natural gas, Government of India. Auto fuel vision and policy 2025. 2014 (Available from: http://petroleum.nic.in/docs/autopol.pdf).

Misran H, Singh R, Begum S, Yarmo MA. Processing of mesoporous silica materials (MCM-41) from coal fly ash. J Mater Process Technol 2007; 186: 8-13.

Mohammadian M, Ahmadi M, Khosravi-Nikou MR. Adsorptive desulfurization and denitrogenation of model fuel by mesoporous adsorbents (MSU-S and CoO-MSU-S). Petrol Sci Technol. 2017; 35: 608-614.

Mohebali G, Ball AS. Biodesulfurization of diesel fuels-Past, present and future perspectives. Int Biodeterior Biodegrad 2016; 110: 163-180.

Mokhtar WN, Bakar WA, Ali R, Kadir AA. Catalytic oxidative desulfurization of diesel oil by Co/Mn/Al_2O_3 catalysts –tert-butyl hydroperoxide (TBHP) system: preparation, characterization, reaction, and mechanism. Clean Technol Environ Policy 2015; 17: 1487–1497.

Mokhtar WN, Bakar WA, Ali R, Kadir AA. Deep desulfurization of model diesel by extraction with N, N-dimethylformamide: optimization by Box-Behnken design. J Taiwan Inst Chem Eng 2014; 45: 1542–1548.

Mokhtar WN, Bakar WA, Ali R, Kadir AA. Development of bimetallic and trimetallic oxides doped on molybdenum oxide based material on oxidative desulfurization of diesel. Arab J Chem 2018; 11: 1201-1208.

Monticello DJ. Biodesulfurization and the upgrading of petroleum distillates. Curr Opin Biotechnol 2000; 11: 540-546.

Morales-Ortuño JC, Klimova TE. Development of new hydrodesulfurization NiMo catalysts supported on Al_2O_3-TiSBA-15 hybrid materials. Fuel 2017; 198: 99-109.

Morales-Ortuño JC, Ortega-Domínguez RA, Hernández-Hipólito P, Bokhimi X, Klimova TE. HDS performance of NiMo catalysts supported on nanostructured materials containing titania. Catal Today 2016; 271: 127-139.

Mouli KC, Soni K, Dalai AK, Adjaye J. Effect of pore diameter of Ni-Mo/Al-SBA-15 catalysts on the hydrotreating of heavy gas oil. Appl Catal A 2011; 404: 21-29.

Nair S, Tatarchuk BJ. Supported silver adsorbents for selective removal of sulfur species from hydrocarbon fuels. Fuel 2010; 89: 3218–3225.

Naito M, Kawamoto T, Fujino K, Kobayashi M, Maruhashi K, Tanaka A. Long-term repeated biodesulfurization by immobilized Rhodococcus erythropolis KA2-5-1 cells. Appl Microbiol Biotechnol 2001; 55: 374-378.

Nashine AL, Tembhurkar AR. Equilibrium, kinetic and thermodynamic studies for adsorption of As (III) on coconut (Cocos nucifera L.) fiber. J Environ Chem Eng 2016; 4: 3267-3273.

Nejad NF, Shams E, Amini MK, Bennett JC. Ordered mesoporous carbon CMK-5 as a potential sorbent for fuel desulfurization: application to the removal of dibenzothiophene and comparison with CMK-3. Microporous Mesoporous Mater 2013; 168: 239–246.

Nekodzuka S, Nakajima-Kambe T, Nomura N, Jie L, Nakahara T. Specific desulfurization of dibenzothiophene by *Mycobacterium* sp. strain G3. Biocatal Biotransform 1997; 15: 17-27.

Ngamcharussrivichai C, Chatratananon C, Nuntang S, Prasassarakich P. Adsorptive removal of thiophene and benzothiophene over zeolites from Mae Moh coal fly ash. Fuel 2008; 87: 2347–2351.

Nogueira LS, Ribeiro S, Granadeiro CM, Pereira E, Feio G, Cunha-Silva L, Balula SS. Novel polyoxometalate silica nano-sized spheres: efficient catalysts for olefin oxidation and the deep desulfurization process. Dalton Trans 2014; 43: 9518–9528.

Nunthaprechachan T, Pengpanich S, Hunsom M. Adsorptive desulfurization of dibenzothiophene by sewage sludge-derived activated carbon. Chem Eng J 2013; 228: 263–271.

Ogunlaja AS, Abdul-quadir MS, Kleyi PE, Ferg EE, Watts P, Tshentu ZR. Towards oxidative denitrogenation of fuel oils: Vanadium oxide-catalysed oxidation of quinoline and adsorptive removal of quinoline-N-oxide using 2, 6-pyridine-polybenzimidazole nanofibers. Arabian J Chem 2017.

Ogunlaja AS, Alade OS. Catalysed oxidation of quinoline in model fuel and the selective extraction of quinoline-N-oxide with imidazoline-based ionic liquids. Egypt J Pet 2018; 27: 159-168.

Ohshiro T, Izumi Y. Microbial desulfurization of organic sulfur compounds in petroleum. Biosci Biotechonol Biochem 1999; 6: 1-9.

Okamoto Y, Ochiai K, Kawano M, Kobayashi M, Kubota T. Effects of support on the activity of Co-Mo sulfide model catalysts. Appl Catal A 2002; 226: 115.

Oldfield C, Pogrebinsky O, Simmonds J, Olson ES, Kulpa CF. Elucidation of the ametabolic pathway for dibenzothiophene desulphurization by *Rhodococcus* sp. strain IGTS8 (ATCC 53968). Microbiology 1997; 143: 2961-2973.

Olgun A, Atar N. Removal of copper and cobalt from aqueous solution onto waste containing boron impurity. Chem Eng J 2011; 167: 140-147.

Önal Y, Akmil-Başar C, Eren D, Sarıcı-Özdemir Ç, Depci T. Adsorption kinetics of malachite green onto activated carbon prepared from Tunçbilek lignite. J Hazard Mater 2006; 128: 150-157.

Otsuki S, Nonaka T, Qian W, Ishihara A, Kabe T. Oxidative desulfurization of middle distillate. J Jpn Petrol Inst 2001; 44: 18-24.

Otsuki S, Nonaka T, Qian W, Ishihara A, Kabe T. Oxidative desulfurization of middle distillate using ozone. J Jpn Pet Inst 1999; 42: 315–320.

Otsuki S, Nonaka T, Takashima N, Qian W, Ishihara A, Imai T, Kabe T. Oxidative desulfurization of light gas oil and vacuum gas oil by oxidation and solvent extraction. Energy Fuels 2000; 14: 1232–1239.

Ouchiyama N, Zhang Y, Omori T, Kodama T. Biodegradation of carbazole by *Pseudomonas* spp. CA06 and CA10. Biosci. Biotechnol. Biochem 1993; 57: 455-460.

Palcheva R, Dimitrov L, Tyuliev G, Spojakina A, Jiratova K. TiO_2 nanotubes supported NiW hydrodesulphurization catalysts: characterization and activity. Appl Surf Sci 2013; 265: 309-316.

Palomino JM, Tran DT, Hauser JL, Dong H, Oliver SR. Mesoporous silica nanoparticles for high capacity adsorptive desulfurization. J Mater Chem A 2014; 2: 14890-14895.

Palomino JM, Tran DT, Kareh AR, Miller CA, Gardner JM, Dong H, Oliver SR. Zirconia-silica based mesoporous desulfurization adsorbents. J Power Sources 2015; 278: 141–148.

Papadopoulou C, Vakros J, Matralis HK, Kordulis C, Lycourghiotis A. On the relationship between the preparation method and the physicochemical and catalytic properties of the CoMo/γ -Al_2O_3 hydrodesulfurization catalysts. J Colloid Interface Sci 2003; 261: 146-153.

Parashar K, Ballav N, Debnath S, Pillay K, Maity A. Rapid and Efficient Removal af Fluoride Ions From Aqueous Solution Using a Polypyrrole Coated Hydrous Tin Oxide Nanocomposite. J Colloid Interface Sci 2016; 476: 103-118.

Pawelec B, Fierro JL, Montesinos A, Zepeda TA. Influence of the acidity of nanostructured CoMo/P/Ti-HMS catalysts on the HDS of 4, 6-DMDBT reaction pathways. Appl Catal B 2008; 80: 1-4.

Pawelec B, Navarro RM, Campos-Martin JM, Fierro JL. Towards near zero-sulfur liquid fuels: a perspective review. Catal Sci Technol 2011; 1: 23-42.

Pecoraro TA, Chianelli RR. Hydrodesulfurization catalysis by transition metal sulfides. J Catal 1981; 67: 430-445.

Petkov P, Tasheva J, Stratiev D. Extraction approach for desulphurization and dearomatization of middle distillates. Petrol Coal 2004; 46: 13-18.

Petzold FG, Jasinski J, Clark EL, Kim JH, Absher J, Toufar H, Sunkara MK. Nickel supported on zinc oxide nanowires as advanced hydrodesulfurization catalysts. Catal Today 2012; 198: 219-227.

Pradhan BK, Sandle NK. Effect of different oxidizing agent treatments on the surface properties of activated carbons. Carbon 1999; 37: 1323-1332.

Prahas D, Kartika Y, Indraswati N, Ismadji S. Activated Carbon from Jackfruit Peel Waste by H_3PO_4 Chemical Activation: Pore Structure and Surface Chemistry Characterization. Chem Eng J 2008; 140: 32–42.

Prasad VVDN, Jeong KE, Chae HJ, Kim CU, Jeong SY. Oxidative desulfurization of 4,6-dimethyl dibenzothiophene and light cycle oil over supported molybdenum oxide catalysts. Catal Commun 2008; 9: 1966–1969.

Qiu L, Cheng Y, Yang C, Zeng G, Long Z, Wei S, Luo L. Oxidative desulfurization of dibenzothiophene using a catalyst of molybdenum supported on modified medicinal stone. RSC Adv 2016; 6: 17036–17045.

Qu D, Feng X, Li N, Ma X, Shang C, Chen XD. Adsorption of heterocyclic sulfur and nitrogen compounds in liquid hydrocarbons on activated carbons modified by oxidation: capacity, selectivity and mechanism. RSC Adv 2016; 6: 41982-41990.

Rabarihoela-Rakotovao V, Brunet S, Berhault G, Perot G, Diehl F. Effect of acridine and of octahydroacridine on the HDS of 4, 6-dimethyldibenzothiophene catalyzed by sulfided NiMoP/Al_2O_3. Appl Catal A Gen 2004; 267: 17-25.

Rahma WS, Mjalli FS, Al-Wahaibi T, Al-Hashmi AA. Polymeric-based deep eutectic solvents for effective extractive desulfurization of liquid fuel at ambient conditions. Chem Eng Res Des 2017; 120: 271-283.

Rakesh-Kumar D, Srivastava VC. Studies on Adsorptive Desulphurization by Activated Carbon. CLEAN – Soil Air Water 2012; 40: 545-550.

Rameshraja D, Srivastava VC, Kushwaha JP, Mall ID. Quinoline adsorption onto granular activated carbon and bagasse fly ash. Chem Eng J 2012; 181: 343-351.

Rashidi S, Nikou MR, Anvaripour B. Adsorptive desulfurization and denitrogenation of model fuel using HPW and NiO-HPW modified aluminosilicate mesostructures. Microporous Mesoporous Mater 2015; 211: 134-141.

Rashtchi M, Mohebali GH, Akbarnejad MM, Towfighi J, Rasekh B, Keytash, A. Analysis of biodesulfurization of model oil system by the bacterium, strain RIPI-22. Biochem Eng J 2006; 29: 169-173.

Rhee SK, Chang JH, Chan YK, Chang HN. Desulfurization of dibenzothiophene and diesel oils by a newly isolated strain, *Gordona* CYKS1. Appl Environ Microbiol 1998; 64: 2327-2331.

Ribeiro S, Barbosa ADS, Gomes AC, Pillinger M, Goncalves IS, Cunha-Silva L, Balula SS. Catalytic oxidative desulfurization systems based on Keggin phosphotungstate and metal-organic framework MIL-101. Fuel Process Technol 2013; 116: 350–357.

Ribeiro SO, Juliao D, Cunha-Silva L, Domingues VF, Valença R, Ribeiro JC, de Castro B, Balula SS. Catalytic oxidative/extractive desulfurization of model and untreated diesel using hybrid based zinc-substituted polyoxometalates. Fuel 2016; 166: 268–275.

Ristovski ZD, Jayaratne ER, Lim M, Ayoko GA, Morawska L. Influence of diesel fuel sulfur on nanoparticle emissions from city buses. Environ Sci Technol 2006; 40: 1314-1320.

Ruthven DM, editor. Principles of Adsorption and Adsorption Processes, Ist ed., New York, USA: Wiley, 1984.

Safa M, Mokhtarani B, Mortaheb HR. Deep extractive desulfurization ofdibenzothiophene with imidazolium orpyridinium-based ionic liquids. Chem Eng Res Des 2016; 111: 323-331.

Safa MA, Ma X. Oxidation kinetics of dibenzothiophenes using cumene hydroperoxide as an oxidant over MoO_3/Al_2O_3 catalyst. Fuel 2016; 171: 238–246.

Saleh TA, Danmaliki GI. Influence of acidic and basic treatments of activated carbon derived from waste rubber tires on adsorptive desulfurization of thiophenes. J Taiwan Inst Chem Eng 2016; 60: 460–468.

Saleh TA, editor. Applying Nanotechnology to the desulfurization process in petroleum engineering, Pennsylvania, USA: IGI Global, 2015.

Saleh TA, Sulaiman KO, AL-Hammadi SA, Dafalla H, Danmaliki GI. Adsorptive desulfurization of thiophene, benzothiophene and dibenzothiophene over activated carbon manganese oxide nanocomposite: with column system evaluation. J Clean Prod 2017; 154: 401-412.

Salleh MZ, Hadj-Kali MK, Hizaddin HF, Hashim MA. Extraction of nitrogen compounds from model fuel using 1-ethyl-3-methylimidazolium methanesulfonate. Sep Purif Technol 2018; 196: 61-70.

Samadi-Maybodi A, Teymouri M, Vahid A, Miranbeigi A. In situ incorporation of nickel nanoparticles into the mesopores of MCM-41 by manipulation of solvent-solute

interaction and its activity toward adsorptive desulfurization of gas oil. J Hazard Mater 2011; 192: 1667–1674.

Sampanthar JT, Xiao H, Dou J, Nah TY, Rong X, Kwan WP. A noveloxidative desulfurization process to remove refractory sulfur compounds from diesel fuel. Appl Catal B 2006; 63: 85–93.

Sano Y, Choi KH, Korai Y, Mochida I. Adsorptive removal of sulfur and nitrogen species from a straight run gas oil over activated carbons for its deep hydrodesulfurization. Appl Catal B Environ 2004; 49: 219-225.

Santos AL, Reis RA, Rossa V, Reis MM, Costa AL, Veloso CO, Henriques CA, Zotin FM, Paredes ML, Silveira EB, Chiaro SS. Silica–alumina impregnated with cerium, nickel, and molybdenum oxides for adsorption of sulfur and nitrogen compounds from diesel. Mater Lett 2012; 83: 158-160.

Sarda KK, Bhandari A, Pant KK, Jain S. Deep desulfurization of diesel fuel by selective adsorption over Ni/Al_2O_3 and Ni/ZSM-5 extrudates. Fuel 2012; 93: 86-91.

Sarkar M, Majumdar P. Application of response surface methodology for optimization of heavy metal biosorption using surfactant modified chitosan bead. Chem Eng J 2011;175: 376-387.

Sarker M, Song JY, Jeong AR, Min KS, Jhung SH. Adsorptive removal of indole and quinoline from model fuel using adenine-grafted metal-organic frameworks. J hazard mater 2018; 344: 593-601.

Seki Y, Yurdakoç K. Adsorption of Promethazine Hydrochloride with KSF Montmorillonite. Adsorption 2006; 12: 89-100.

Sentorun-Shalaby C, Saha SK, Ma X, Song C. Mesoporous-molecular-sieve-supported nickel sorbents for adsorptive desulfurization of commercial ultra-low-sulfur diesel fuel. Appl Catal B 2011; 101: 718-726.

Shah SS, Ahmad I, Ahmad W, Ishaq M, Khan H. Deep desulphurization study of liquid fuels using acid treated activated charcoal as adsorbent. Energy Fuels 2017; 31: 7867–7873.

Shah SS, Ahmad I, Ahmad W. Adsorptive desulphurization study of liquid fuels using Tin (Sn) impregnated activated charcoal. J Hazard Mater 2016; 304: 205–213.

Shan GB, Xing JM, Zhang HY, Liu HZ, 2005. Biodesulfurization of dibenzothiophene by microbial cells coated with magnetite nanoparticles. Appl Environ Microbiol 2005; 71: 4497-4502.

Shao X, Zhang X, Yu W, Wu Y, Qin Y, Sun Z, Song L. Effects of surface acidities of MCM-41 modified with MoO_3 on adsorptive desulfurization of gasoline. Appl Surf Sci 2012; 15: 263: 1–7.

Sharma VK. Potassium ferrate(VI): an environmentally friendly oxidant. Adv Environ Res 2002; 6: 143–156.

Shetty M, Murugappan K, Prasomsri T, Green WH, Roman-Leshkov Y. Reactivity and stability investigation of supported molybdenum oxide catalysts for the hydrodeoxygenation (HDO) of m-cresol. J Catal 2015; 331: 86-97.

Shi Y, Zhang X, Liu G. Activated carbons derived from hydrothermally carbonized sucrose: remarkable adsorbents for adsorptive desulfurization. ACS Sustainable Chem Eng 2015; 3: 2237-2246..

Shiraishi Y, Naito T, Hirai T. Vanadosilicate molecular sieve as a catalyst for oxidative desulfurization of light oil. Ind eng chem res 2003; 42: 6034-6039.

Shu Y, Shao Y, Wei X, Wang X, Sun Q, Zhang Q, Li L. Synthesis and characterization of Ni-MCM-41 for methyl blue adsorption, Microporus Mesoporous Mater 2015; 214: 88-94.

Shukla OP, Kaul SM. Microbiological transformation of pyridine N-oxide and pyridine by Nocardia sp. Can J of Microbiol 1986; 32 :330-341.

Sikarwar P, Kumar UA, Gosu V, Subbaramaiah V. An overview of conventional and alternative technologies for the production of ultra-low-sulfur fuels. Rev Chem Eng 2018a (DOI: https://doi.org/10.1515/revce-2017-0082).

Sikarwar P, Kumar UA, Gosu V, Subbaramaiah V. Catalytic oxidative desulfurization of DBT using green catalyst (Mo/MCM-41) derived from coal fly ash. J Environ Chem Eng 2018b; 6: 1736-1744.

Singh GB, Gupta S, Gupta N. Carbazole degradation and biosurfactant production by newly isolated *Pseudomonas* sp. strain GBS. 5. Int Biodeterior Biodegradation 2013; 84: 35-43.

Singh R, Kunzru D, Sivakumar S. Monodispersed ultrasmall NiMo metal oxide nanoclusters as hydrodesulfurization catalyst. Appl Catal B 2016; 185: 163-173.

Solar JM, Derbyshire FJ, De Beer VH, Radovic LR. Effects of surface and structural properties of carbons on the behavior of carbon-supported molybdenum catalysts. J Catal 1991; 129: 330-342.

Solís-Casados DA, Escobar-Alarcón L, Klimova T, Escobar-Aguilar J, Rodríguez-Castellón E, Cecilia JA, Morales-Ramírez C. Catalytic performance of CoMo/Al_2O_3-MgO-Li(x) formulations in DBT hydrodesulfurization. Catal Today 2016; 271: 35-44.

Song C, Ma X. New design approaches to ultra-clean diesel fuels by deep desulfurization and deep dearomatization. Appl Catal 2003; 41: 207–238.

Srivastav A, Srivastava VC. Adsorptive desulfurization by activated alumina. J Hazard Mater 2009; 170: 1133–1140.

Srivastava VC. An evaluation of desulfurization technologies for sulfur removal from liquid fuels, RSC Adv 2012; 2: 759-783.

Stanislaus A, Marafi A, Rana MS. Recent advances in the science and technology of ultra low sulfur diesel (ULSD) production. Catal Today 2010; 153: 1-68.

Subbaramaiah V, Srivastava VC, Mall ID. Catalytic activity of Cu/SBA-15 for peroxidation of pyridine bearing wastewater at atmospheric condition. AIChE J 2013; 59: 2577-2586.

Subhan F, Aslam S, Yan ZF, Ikram M, Rehman S. Enhanced desulfurization characteristics of Cu-KIT-6 for thiophene. Microporous Mesoporous Mater 2014; 199: 108–116.

Subhan F, Liu BS. Acidic sites and deep desulfurization performance of nickel supported mesoporous AlMCM-41 sorbents. Chem Eng J 2011; 178: 69–77.

Sun Q, Bai Y, Zhao C, Xiao Y, Wen D, Tang X. Aerobic biodegradation characteristics and metabolic products of quinoline by a *Pseudomonas* strain. Bioresour Technol 2009; 100: 5030-5036.

Tam PS, Kittrell JR, Eldridge JW. Desulfurization of fuel oil by oxidation and extraction. 1. Enhancement of extraction oil yield. Ind Eng Chem Res 1990a; 29: 321–324.

Tam PS, Kittrell JR, Eldridge JW. Desulfurization of fuel oil by oxidation and extraction. 2. Kinetic modeling of oxidation reaction. Ind Eng Chem Res 1990b; 29: 324–329.

Tang K, Hong X. Preparation and characterization of Co–MCM-41 and its adsorption removing basic nitrogen compounds from fluidized catalytic cracking diesel oil, Energy Fuels 2016; 30: 619-624.

Tang K, Song LJ, Duan LH, Li XQ, Gui JZ, Sun ZL. Deep desulfurization by selective adsorption on a heteroatoms zeolite prepared by secondary synthesis. Fuel Process Technol 2008; 89: 1–6..

Tang N, Zhao X, Jiang Z, Li C. Oxidation of dibenzothiophene using oxygen and a vanadophosphate catalyst for ultra-deep desulfurization of diesels. Chin J Catal 2014; 35: 1433–1437.

Teymouri M, Samadi-Maybodi A, Vahid A, Miranbeigi A. Adsorptive desulfurization of low sulfur diesel fuel using palladium containing mesoporous silica synthesized via a novel in-situ approach. Fuel Process Technol 2013; 116: 257–264.

Thaligari SK, Gupta S, Srivastava, VC, Prasad B. Simultaneous desulfurization and denitrogenation of liquid fuel by nickel-modified granular activated carbon. Energy Fuels 2016b; 30: 6161-6168.

Thaligari SK, Srivastava VC, Prasad B. Adsorptive desulfurization by zinc-impregnated activated carbon: characterization, kinetics, isotherms, and thermodynamic modeling. Clean Technol Envir 2016a; 18: 1021–1030.

Thaligari SK, Srivastava VC, Prasad B. Simultaneous adsorptive desulfurization and denitrogenation by zinc loaded activated carbon: optimization of parameters. Pet Sci Technol 2015; 33: 1667–1675.

Tong DS, Wu CW, Adebajo MO, Jin GC, Yu WH, Ji SF, Zhou CH. Adsorption of methylene blue from aqueous solution onto porous cellulose-derived carbon/montmorillonite nanocomposites. Appl Clay Sci 2018; 161: 256-264.

Toteva V, Topalova L, Manolova P. Extractive dearomatization and desulphur- ization of a distillate gasoil cut with dimethylformamide. J Univ Chem Technol Metall 2007; 42: 17-20.

Trejo F, Rana MS, Ancheyta J. CoMo/MgO-Al_2O_3 supported catalysts: an alternative approach to prepare HDS catalysts. Catal Today 2008; 130: 327-336

Triantafyllidis KS, Deliyanni EA. Desulfurization of diesel fuels : Adsorption of 4, 6-DMDBT on different origin and surface chemistry nanoporous activated carbons. Chem Eng J 2014; 236: 406-414.

Tuo BH, Yan JB, Fan BA, Yang ZH, Liu JZ. Biodegradation characteristics and bioaugmentation potential of a novel quinoline-degrading strain of Bacillus sp. isolated from petroleum-contaminated soil. Bioresour technol 2012; 107: 55-60.

Uma TS, Sandhya S, Sathyanarayana S, Kaul SN. Biodegradation of pyradine from pharmaceutical wastewater using *bacilus consortia* J IAEM 2002; 29: 76-80.

Vafaei F, Torkaman R, Moosavian MA, Zaheri P. Optimization of extraction conditions using central composite design for the removal of Co (II) from chloride solution by supported liquid membrane. Chem Eng Res Des 2018; 133:126-136.

Van de Voorde B, Boulhout M, Vermoortele F, Horcajada P, Cunha D, Lee JS, Chang JS, Gibson E, Daturi M, Lavalley JC, Vimont A. N/S-heterocyclic contaminant removal from fuels by the mesoporous metal–organic framework MIL-100: The role of the metal ion. J Am Chem Soc 2013; 135: 9849-9856.

Vázquez-Garrido I, López-Benítez A, Berhault G, Guevara-Lara A. Effect of support on the acidity of NiMo/Al_2O_3-MgO and NiMo/TiO_2-Al2O_3 catalysts and on the resulting competitive hydrodesulfurization/hydrodenitrogenation reactions. Fuel 2019; 236: 55-64.

Vijayaraghavan K, Padmesh TV, Palanivelu K, Velan M. Biosorption of nickel (II) ions onto Sargassum wightii: application of two-parameter and three-parameter isotherm models. J hazard mater 2006; 133: 304-308.

Wajnert A, Wojciechowska M, Pietrowski M, Przystajko W. Novel supported catalyst for hydrodesulfurization reaction. Catal Commun 2008; 9: 1493-1496.

Wan Y, Zhao DY. On the controllable soft-templating approach to mesoporous silicates. Chem Rev 2007; 107: 2821–2860.

Wang D, Liu N, Zhang J, Zhao X, Zhang W, Zhang M. Oxidative desulfurization using ordered mesoporous silicas as catalysts. J Mol Catal A Chem 2014b; 393: 47–55.

Wang D, Qian EW, Amano H, Okata K, Ishihara A, Kabe T. Oxidative desulfurization of fuel oil: part I. Oxidation of dibenzothiophenes using tert-butyl hydroperoxide. Appl Catal A 2003; 253: 91–99.

Wang D, Qian W, Ishihara A, Kabe T. Elucidation of Sulfidation State and Hydrodesulfurization Mechanism on TiO_2 Catalysts Using 35S Radioisotope Tracer Methods. J Catal 2001; 203: 322-328.

Wang H, Xie C, Yu S, Liu F. Denitrification of simulated oil by extraction with H_2PO_4-based ionic liquids. Chem Eng J 2014a; 237: 286–290.

Wang J, Liu H, Yang H, Qiao C, Li Q. Competition adsorption, equilibrium, kinetic, and thermodynamic studied over La (III)-loaded active carbons for dibenzothiophene removal. J Chem Eng Data 2016; 61: 3533-3541.

Wang X, Zhao Z, Zheng P, Chen Z, Duan A, Xu C, Jiao J, Zhang H, Cao Z, Ge B. Synthesis of NiMo catalysts supported on mesoporous Al_2O_3 with different crystal forms and superior catalytic performance for the hydrodesulfurization of dibenzothiophene and 4,6-dimethyldibenzothiophene. J Catal 2016; 344: 680-691.

Wang Y, Geder J, Schubert JM, Dahl R, Pasel J, Peters R. Optimization of adsorptive desulfurization process of jet fuels for application in fuel cell systems. Fuel Process Technol 2012; 95: 144-153.

Wang Y, Sun Z, Wang A, Ruan L, Lu M, Ren J, Li X, Li C, Hu Y, Yao P. Kinetics of hydrodesulfurization of dibenzothiophene catalyzed by sulfided Co− Mo/MCM-41. Ind Eng Chem Res 2004; 43: 2324-2329.

Wang Y, Sun Z, Wang A, Ruan L, Lu M, Ren J, Li X, Li C, Hu Y, Yao P. Kinetics of hydrodesulfurization of dibenzothiophene catalyzed by sulfided Co− Mo/MCM-41, Ind. Eng. Chem. Res. 43 (2004) 2324-23249.

Wang Y, Yang RT, Heinzel JM. Desulfurization of jet fuel by π-complexation adsorption with metal halides supported on MCM-41 and SBA-15 mesoporous materials. Chem Eng Sci 2008 63: 356–365.

Wen J, Han X, Lin H, Zheng Y, Chu W. A critical study on the adsorption of heterocyclic sulfur and nitrogen compounds by activated carbon: equilibrium, kinetics and thermodynamics. Chem Eng J 2010; 164: 29-36.

Won DB, Park SJ, Han KJ, Kim CJ. Liquid–liquid equilibria for methanol+ hexadecane+ heterocyclic nitrogen-containing compounds at 298.15 K. Fluid Ph. Equilibria 2002; 193: 217-27.

Xia Y, Yang P, Sun Y, Wu Y, Mayers B, Gates B, Yin Y, Kim F, Yan H. One-dimensional nanostructures: synthesis, characterization, and applications. Adv Mater 2003; 15: 353.

Xie D, He Q, Su Y, Wang T, Xu R, Hu B. Oxidative desulfurization of dibenzothiophene catalyzed by peroxotungstate on functionalized MCM-41 materials using hydrogen peroxide as oxidant. Chin J Catal 2015; 36: 1205–1213.

Xie LL, Favre-Reguillon A, Pellet-Rostaing S, Wang XX, Fu X, Estager J, Vrinat M, Lemaire M. Selective extraction and identification of neutral nitrogen compounds contained in straight-run diesel feed using chloride based ionic liquid. Ind Eng Chem Res 2008; 47: 8801–8807.

Xin H, Ke T. Preparation and adsorption denitrogenation from model fuel or diesel oil of heteroatoms mesoporous molecular sieve Co-MCM-41. Energy Sources, Part A: Recovery, Utilization, and Environmental Effects. 2016 Sep 1;38(17):2560-7.

Xiong L, Chen FX, Yan XM, Mei P. The adsorption of dibenzothiophene using activated carbon loaded with cerium. J Porous Mater 2012; 19: 713–719.

Xiong L, Yan XM, Mei P. Synthesis and characterization of a ZrO_2/AC composite as a novel adsorbent for dibenzothiophene. Adsorpt Sci Technol 2010; 28: 341–350.

Xu K, Li Y, Xu X, Zhou C, Liu Z, Yang F, Zhang L, Wang G, Gao J, Xu C.Single-walled carbon nanotubes supported Ni–Y as catalyst for ultra-deep hydrodesulfurization of gasoline and diesel. Fuel 2015; 160: 291–296.

Yan XM, Mei P, Lei J, Mi Y, Xiong L, Guo L. Synthesis and characterization of mesoporous phosphotungstic acid/TiO_2 nanocomposite as a novel oxidative desulfurization catalyst. J Mol Catal A Chem 2009; 304: 52–57.

Yang C, Zhao K, Cheng Y, Zeng G, Zhang M, Shao J, Lu L. Catalytic oxidative desulfurization of BT and DBT from n-octane using cyclohexanone peroxide and catalyst of molybdenum supported on 4A molecular sieve. Sep Purif Technol 2016; 163: 153–161.

Yang H, Jiang B, Sun Y, Hao L, Huang Z, Zhang L. Synthesis and oxidative desulfurization of novel lactam-based Brønsted-Lewis acidic ionic liquids. Chem Eng J 2016; 306: 131–138.

Yang RT, Hernandez-Maldonaldo AJ, Yang FH. Desulfurization of transportation fuels with zeolites under ambient conditions. Science 2003; 301: 79–81.

Yoosuk B, Song C, Kim JH, Ngamcharussrivichai C, Prasassarakich P. Effects of preparation conditions in hydrothermal synthesis of highly active unsupported NiMo sulfide catalysts for simultaneous hydrodesulfurization of dibenzothiophene and 4, 6-dimethyldibenzothiophene. Catal Today 2010; 149: 52-61.

Yu F, Liu C, Yuan B, Xie P, Xie C , Yu S. Energy-efficient extractive desulfurization of gasoline by polyether-based ionic liquids. Fuel 2016; 177: 39-45.

Yu M, Li Z, Xia Q, Xi H, Wang S. Desorption activation energy of dibenzothiophene on the activated carbons modified by different metal salt solutions. Chem Eng J 2007; 132: 233–239.

Zhang H, Song H. Study of adsorptive denitrogenation of diesel fuel over mesoporous molecular sieves based on breakthrough curves. Ind Eng Chem Res 2012; 51: 16059-16065.

Zhang J, Bai X, Li X, Wang A, Ma X. Preparation of MoO_3-CeO_2-SiO_2 oxidative desulfurization catalysts by a sol-gel procedure. Chinese J Catal 2009; 30: 1017–1021.

Zhang J, Wang A, Li X, Ma X. Oxidative desulfurization of dibenzothiophene and diesel over $[Bmim]_3PMo_{12}O_{40}$. J Catal 2011; 279: 269-275.

Zhang L, Fu W, Ke Q, Zhang S, Jin H, Hu J, Wang S. Study of hydrodesulfurization of 4, 6-DMDBT over Pd supported on mesoporous USY zeolite. Appl Catal A 2012; 433: 251-257.

Zhang MH, Fan JY, Chi K, Duan AJ, Zhao Z, Meng XL, Zhang HL. Synthesis, characterization, and catalytic performance of NiMo catalysts supported on different crystal alumina materials in the hydrodesulfurization of diesel. Fuel Process Technol 2017; 156: 446-453.

Zhang S, Zhang Q, Zhang ZC. Extractive desulfurization and denitrogenation of fuels using ionic liquids. Ind Eng Chem Res 2004; 43: 614-622.

Zhang S, Zhang ZC. Novel properties of ionic liquids in selective sulfur removal from fuels at room temperature. Green Chem 2002; 4: 376-379.

Zhang ZY, Shi TB, Jia CZ, Ji WJ, Chen Y, He MY. Adsorptive removal of aromatic organosulfur compounds over the modified na-y zeolites. Appl Catal B Environ 2008; 82: 1-10.

Zhao C, Zhang Y, Li X, Wen D, Tang X. Biodegradation of carbazole by the seven *Pseudomonas* sp. strains and their denitrification potential. J hazard mater 2011; 190: 253-259.

Zhao DS, Sun ZM, Li FT, Shan HD. Optimization of oxidative desulfurization of dibenzothiophene using acidic ionic liquid as catalytic solvent. J Fuel Chem Technol 2009; 37: 194–198.

Zheng D, Zhu W, Xun S, Zhou M, Zhang M, Jiang W, Qin Y, Li H. Deep oxidative desulfurization of dibenzothiophene using low-temperature-mediated titanium dioxide catalyst in ionic liquids. Fuel 2015; 159: 446-453.

Zheng J, Chu W, Zhang H, Jiang C, Dai X. CO oxidation Over Co_3O_4/Sio_2 catalysts: Effects of porous structure of silica and catalyst calcination temperature. J Nat Gas Chem 2010; 19: 583-588.

Zhou C, Gao Q, Luo W, Zhou Q, Wang H, Yan C, Duan P. Preparation characterization and adsorption evaluation of spherical mesoporous Al-MCM-41 from coal fly ash. J Taiwan Inst Chem Eng 2015; 52: 147-157.

Zhou X, Zhao C, Yang J, Zhang S. Catalytic oxidation of dibenzothiophene using cyclohexanone peroxide. Energy Fuels 2007; 21: 7–10.

Zhou XR, Hong Ma, Fu XM, Yao CB, Xiao JQ. Catalytic oxidation of carbazole using t-butyl hydroperoxide over molybdenum catalysts. J Fuel Chem Technol 2010; 38: 75-79.

Zhu W, Zhu G, Li H, Chao Y, Zhang M, Du D, Wang Q, Zhao Z. Catalytic kinetics of oxidative desulfurization with surfactant-type polyoxometalatebased ionic liquids, Fuel Process Technol 2013; 106: 70–76.

Zhuang H, Han H, Xu P, Hou B, Jia S, Wang D, Li K. Biodegradation of quinoline by *Streptomyces* sp. N01 immobilized on bamboo carbon supported Fe_3O_4 nanoparticles. Biochem Eng J 2015; 99:44-47.

BRIEF BIODATA

Mrs. Prerana Sikarwar is a Research scholar in Department of Chemical Engineering, Malaviya National Institute of Technology (MNIT), Jaipur. She has received her B.E degree in Chemical Engineering from Madhav Institute of Science and Technology (MITS), Gwalior. She has completed her Master's degree in Chemical Engineering with specialization in Computer Aided Process Plant Design at the Indian Institute of Technology Roorkee, Roorkee. She has joined Ph.D. program under the supervision of Dr. V. Subbaramaiah, Department of Chemical Engineering, MNIT, Jaipur. During her research work, she has published three research papers (2 SCI indexed and 1 Scopus indexed). Her current research interest includes desulfurization & denitrogenation of liquid fuels, catalysis, material characterization, and adsorption. She has received MHRD scholarship during her master's and Ph.D., and also qualified GATE (Chemical Engineering) in 2011 and 2012.